MODELLING PRESENT AND FUTURE CLIMATES OVER SOUTHERN AFRICA

Alec Michael Joubert

University of the Witwatersrand, Johannesburg
Department of Geography and Environmental Studies

Thesis submitted to the Faculty of Science
for the Degree of Doctor of Philosophy

ABSTRACT

The representation of contemporary southern African climate by a wide range of general circulation models used in climate studies is evaluated. In addition, projections of regional climate change by the models are interpreted in terms of their present climate performance. Projections of regional climate change by two different types of climate models are considered. First, projections of the equilibrium response to an instantaneous doubling of atmospheric carbon dioxide using atmospheric models linked to simple mixed-layer oceans are assessed. Second, projections of the transient response to gradually-increasing anthropogenic forcing by fully-coupled ocean-atmosphere general circulation models are considered.

All of the mixed-layer models considered have been developed since 1990 and are more recent and generally higher-resolution versions of the models considered previously for southern Africa. The improved resolution and model physics result in a general improvement in the representation of several features of circulation around southern Africa. Specifically, these include the meridional pressure gradient, the zonal wind profile, the intensity and seasonal location of the circumpolar trough and the subtropical anticyclones, as well as planetary wave structure at 500 hPa. Atmospheric models forced by observed sea-surface temperatures simulate the large-scale circulation adjustments around southern Africa known to accompany periods of above- and below-average rainfall over the subcontinent. Fully-coupled models simulate the observed features of intra- and inter-annual variability in mean sea-level pressure, although the simulated variability is weaker than observed. Summer rainfall totals throughout southern Africa are over-estimated by all of the models, although the pattern of rainfall seasonality over the subcontinent as a whole is well-reproduced. The inclusion of sulphate aerosols in addition to greenhouse gases does not result in a statistically significant improvement in the simulation of contemporary temperature variability over southern Africa.

Warming projected by fully-coupled models is smaller than projections by mixed-layer models due to the fact that the transient response of the fully-coupled system and not an equilibrium response of an atmospheric model linked to a mixed-layer ocean is simulated. The inclusion of sulphate aerosols results in a reduction in the magnitude and rate of warming over southern Africa. Projected changes in the diurnal temperature range are seasonally-dependent, with increases in summer and autumn and decreases in winter. Simulated changes in mean sea-level pressure are small but similar in magnitude to observed anomalies associated with extended wet and dry spells over the subcontinent. No change in rainfall seasonality over southern Africa is expected. Nonetheless, little confidence exists in projected changes in total rainfall. While both types of model simulate a 10-15% decrease in summer rainfall on average, projected changes are smaller than the simulation errors and little inter-model consensus in terms of the sign of projected changes exists. No change in the location or intensity of anticyclonic circulation and divergence at 700 hPa in winter is expected. While fully-coupled models provide a more comprehensive treatment of the global climate system and the process of climate change, there is no evidence to conclude that current fully-coupled models should be used to the exclusion of mixed-layer models when developing regional climate change scenarios for southern Africa.

I declare that this thesis is my own, unaided work,
and that it has not been submitted previously
as a dissertation or thesis for any degree
at any other University

Signed: ....

Alec Michael Joubert
January 1997

University of the Witwatersrand, 1997

To my mom

and to my dad

PREFACE

Changes in mean climate and climate variability since the industrial revolution suggest that human activity is impacting on global climate and resulting in anthropogenically-induced climate changes. The Second Scientific Assessment Report of the Intergovernmental Panel of Climate Change (IPCC) concludes that "the balance of evidence suggests that there is a discernible human influence on global climate" (IPCC, 1995, p5). Climate models have been developed in response to a need to project the possible impacts of anthropogenically-induced climate change. The first models used in climate change experiments used an atmospheric general circulation model linked to a simple, non-dynamic mixed-layer ocean (mixed-layer models) and simulated the equilibrium response of the climate system to an instantaneous doubling of atmospheric carbon dioxide. More recently, fully-coupled models of the ocean and atmosphere (fully-coupled models) have been developed which simulate the transient response of the climate system to gradually-increasing concentrations of greenhouse gases and (more recently) sulphate aerosols.

On global and hemispheric scales, climate models reproduce the features of contemporary climate realistically and projections of *global* climate change are considered robust. However, climate models involve the representation of several important physical processes and feedbacks which occur at sub-grid-scales by means of parameterisations. The uncertainties introduced by such parameterisations are most keenly felt at regional and local scales. Climate models are consequently least reliable at these scales. Given the fact that the possible impacts of global climate change will be experience at these (and finer) spatial scales, an important component of assessing the impact of future climate change is the need to provide realistic projections of *regional* climate change.

The ability of a wide range of both mixed-layer and fully-coupled general circulation models (GCMs) to reproduce the features of mean climate and variability over the southern African region will be assessed. The ability of the models to reproduce the features of contemporary regional climate is used as the basis for developing scenarios of future regional climate change. The mixed-layer models that will be used in the thesis have all been developed since 1990 and are of higher-spatial resolution in comparison to earlier versions considered by previous evaluations. Mixed-layer model projections of the equilibrium response over southern Africa to a doubling of CO_2 represent a comprehensive update of previous simulations. No previous analyses of the ability of fully-coupled models to simulate features of regional climate, or of the transient response to increasing anthropogenic forcing of climate over southern Africa have been performed.

The aim of the thesis is to provide a critical assessment of projections of regional climate change over southern Africa by a range of different climate models. Specifically, the objectives of the study are to:

(i) evaluate the present climate performance of a range of both mixed-layer and fully-coupled climate models over the southern African region;

(ii) determine the best contemporary models for use in southern Africa;

(iii) provide updated simulations of possible future regional climate change based on both equilibrium and transient climate change scenarios; and

(iii) define the levels of confidence associated with the simulations of future conditions over southern Africa.

The thesis is divided into 4 sections with 9 chapters. **Section 1** is an introductory section containing the first three chapters. In **Chapter 1** a background to the phenomenon of anthropogenically-induced climate change is provided. The development and use of general circulation models is discussed, with emphasis on developments in the ability to model the global climate system which have occurred since approximately 1990. Chief among these is the representation of transient climate change by fully-coupled atmosphere-ocean general circulation models. The review of climate modelling concentrates first on the representation of features of southern hemisphere circulation and subsequently on existing analyses of model performance over southern Africa and existing scenarios of regional climate change derived from climate models. **Chapter 2** contains a description of the sources of both climate model and observational data used in the thesis. The statistical methods and techniques used in the thesis are defined in **Chapter 3**.

In **Section II**, the present climate performance of a range of climate models is assessed. In **Chapter 4**, simulated features of observed climate and circulation over southern Africa during the 1979-1988 period by atmospheric general circulation models forced by observed sea-surface temperatures is assessed. All of the models considered are participants in the Atmospheric Model Intercomparison Project. The representation of contemporary regional climate by a selection of mixed-layer and fully-coupled models (used later to derived regional climate change scenarios) is assessed in **Chapter 5**. Included in the chapter is an evaluation of the effect of including sulphate aerosol in addition to greenhouse gas forcing on the ability of a fully-coupled model to simulate observed temperature variability observed over recent decades. The ability of two fully-coupled models to represent the observed features of intra- and inter-annual variability in mean sea-level pressure around southern Africa is discussed in **Chapter 6**.

Projections of regional climate change are provided in **Section III**. Projections from a range of mixed-layer and fully-coupled models (evaluated in Chapter 5) are described in **Chapter 7**. Recent projections of transient climate change by two fully-coupled models are presented in **Chapter 8**. Estimated changes in regional temperatures due to the inclusion of both greenhouse gases and sulphate aerosols are discussed. Also included is an assessment of possible future changes in circulation variability around southern Africa and anticyclonic circulation over the subcontinent. The final section **(Section IV)** includes **Chapter 9** and presents a summary of the results.

Sections of the thesis have been published or accepted for publication in the *International Journal of Climatology, Progress in Physical Geography* and the *South African Journal of Science*. Other sections are being considered for publication by the *Journal of Climate*. Parts of the research have also been presented at the *Regional Conference of the International Geosphere-Biosphere Programme. Global Environmental Change: Implications for Southern Africa* (Pretoria, South Africa, 24-26 April 1995), the *GAIM First Science Conference* (Garmische-Partenkirchen, Germany, 25-29 September

1995) as well as the South African Society for the Atmospheric Sciences annual conferences in 1995 and 1996.

Observed southern African temperature and rainfall records were obtained through the Climate Impacts LINK Project (UK Department of the Environment Contract PECD7/12/96) on behalf of the Climatic Research Unit (CRU) of the University of East Anglia, with the assistance Dr M. Hulme. Surface and tropospheric circulation data were obtained from the Australian operational analyses of the Australian Bureau of Meteorology Research Centre with the assistance of Dr. W. Drosdowski. Atmospheric Model Intercomparison Project (AMIP) output were obtained through Diagnostic Subproject No. 20 with acknowledgement to Dr L. Gates and Dr. M. Fiorino. A selection of mixed-layer and fully-coupled model output was obtained with permission from several modelling groups from the Commonwealth Scientific and Industrial Research Organisation (CSIRO) Division of Atmospheric Research and with the kind assistance of Dr. P. Whetton and Dr X. Wu. Two transient integrations using the Second Hadley Centre fully-coupled ocean-atmosphere model were obtained from Dr D. Viner through the Climate Impacts LINK Project (UK Department of the Environment Contract PECD7/12/96) on behalf of the Climatic Research Unit (CRU) of the University of East Anglia. A transient climate change integration using the CSIRO fully-coupled model was obtained through the CSIRO Division of Atmospheric Research and with the assistance of Dr. H. Gordon and Dr. S. O'Farrell.

Research that lead to the completion of this thesis was funded by the Technology Research and Investigations Division of the Technology Group of Eskom. My thanks and acknowledgement to Mr C. Turner and Mr G. Tosen. The support and patience of Fiona, my wife, as well as all of the members of my family, friends and colleagues is acknowledge with much gratitude. Mr P. Sticker and Mrs W. Job are thanked for their assistance with the diagrams. In addition, the assistance of Mrs. R. Kotsiovos, Mr P. Pearson (among many others) of the University of the Witwatersrand Computer and Networking Services, as well as Ms S. Bunge, Mr A. Osborne and Mr V. Prinsloo is acknowledged with thanks. Lastly, the support, encouragement and supervision of Professor P.D. Tyson is acknowledged with gratitude.

CONTENTS

CHAPTER

CHAPTER

CHAPTER

SECTION IV: SUMMARY AND CONCLUSIONS

APPENDICES

SECTION I

INTRODUCTION

CHAPTER ONE

BACKGROUND

Introduction

The global climate system exhibits natural variability on all time-scales. From hours to approximately ten days, the development, maturation and decay of weather systems in the atmosphere can be accurately forecasted using sophisticated numerical forecasting models. Beyond this theoretical limit, however, the non-linear chaotic dynamics which govern individual weather systems ensure that deterministic forecasts of their behaviour are impossible (Lorenz, 1963, 1984, 1990). Recent statistical developments in the field of ensemble forecasting ensure that probabilistic forecasts of the most likely state of the atmosphere can be provided on monthly and seasonal time-scales (Brankovic *et al.*, 1990; Palmer *et al.*, 1990; Palmer and Anderson, 1994). Forecasting the time-averaged behaviour of the climate system as a whole however, represents a different challenge.

The fundamental distinction between weather and climate is one of time-scale. Climate can be broadly defined as the average of weather considered over much longer time-scales from months to years, decades and centuries. The techniques required to model climate processes numerically must take into account all components of the global climate system (atmosphere, ocean, land, biosphere) and are therefore fundamentally different to those required for weather forecasting. Since the 1970s, general circulation models (GCMs) of the atmosphere and ocean have been continually developed to model the global climate system. For this reason, they are often referred to as climate models.

There is increasing evidence of a human-induced, or *anthropogenic* influence on climate, resulting in climate changes which cannot be explained in terms of the observed natural variability of the climate system alone. To a large extent, GCMs have been developed in response to a need to project the possible impacts of anthropogenically-induced climate change. Considerable progress has been made over the last decade in the understanding and prediction of climate change on a global scale using climate models. Such progress is best summarised by the Intergovernmental Panel on Climate Change (IPCC), established in 1988 to provide scientific assessments of climate change (IPCC, 1990, 1992, 1995). However, the impacts of climate change are likely to be encountered most keenly at regional and local scales. To date, climate models have displayed considerably less skill in simulating regional climate processes. An overall objective of this thesis is to investigate the ability of GCMs developed since 1990 to provide reliable simulations of present climate, and reasonable estimates of future conditions over the southern African region.

The Global Climate System and Climate Change

The Global Climate System

The atmosphere, hydrosphere, biosphere and geosphere are all components of the climate system, which is defined largely by the interactions which occur between these various components (Fig. 1.1). The system is driven by both external and internal factors. External factors include variations in the input of solar energy to the system (for instance in the form of the 11-year sunspot cycle), long-term variations associated with changes in the Earth's orbit (the Milankovich cycles), and other physical factors such as topography and the distribution of land and sea. However, natural climate variations also occur due to alterations in the interaction between the internal components of the system. By far the best known of such interactions involves the coupling of the atmosphere and ocean in the tropical Pacific Ocean known as El Niño-Southern Oscillation (ENSO) events.

The sole source of energy for the climate system is the Sun. Of the total amount of incident solar radiation at the top of the atmosphere, only approximately 31 % (approximately 1370 Wm^{-2}) reaches the Earth's surface, the rest being scattered or reflected back to space by molecules, microscopic airborne particles (aerosols) and clouds.

Radiation is absorbed at the Earth's surface and re-emitted as longwave radiation. While the atmosphere is essentially transparent to incoming shortwave solar radiation, it is heated from below by longwave radiation in the infrared spectrum. Due to the spherical shape of the globe, an excess of incoming solar radiation is received in the tropics and must be redistributed poleward. This meridional energy imbalance and the need to transport heat poleward give rise to the general circulation of the globe, with a broad band of westerlies in the extra-tropics of both hemispheres and an embedded jet stream. The wave-like structure of these systems aids in the process of poleward heat transport.

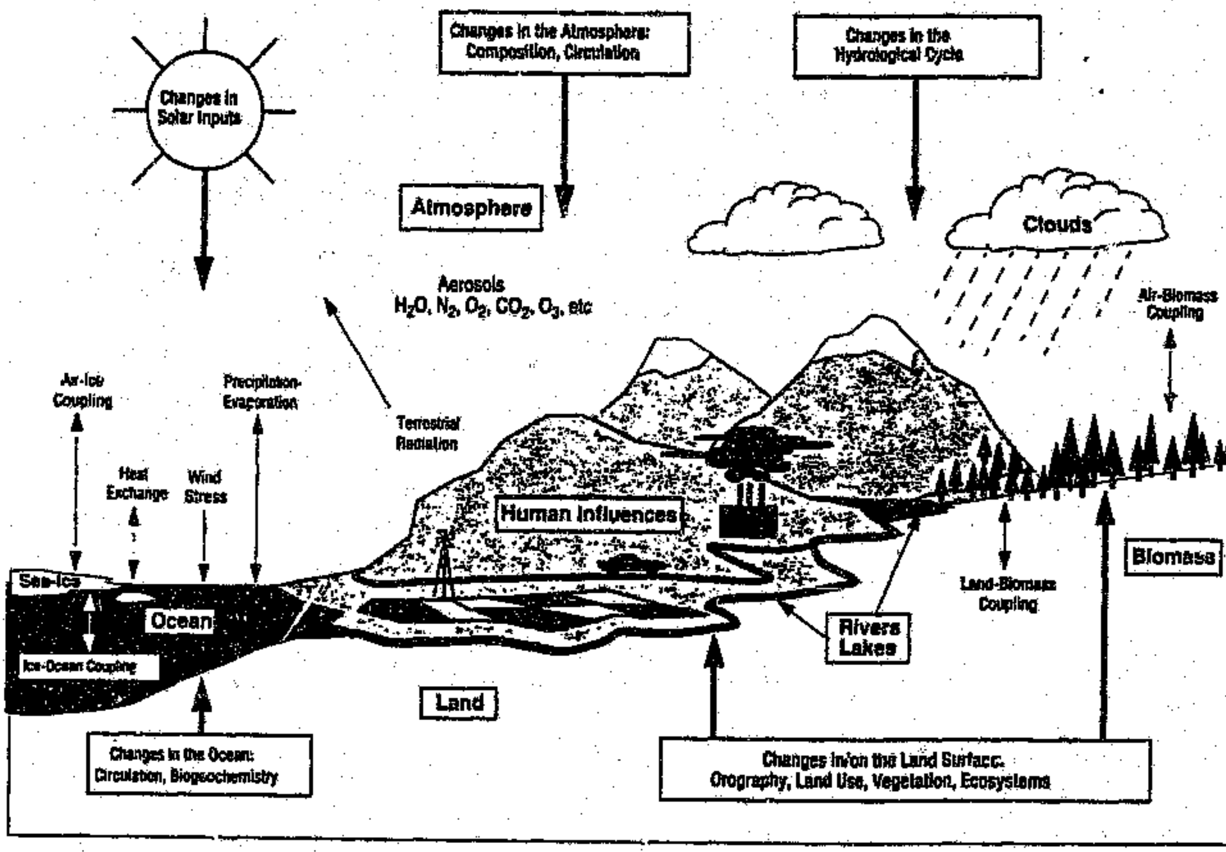

Figure 1.1. Schematic view of the components of the global climate system (bold), their processes and interactions (thin arrows) and some aspects that may change (bold arrows) (after IPCC, 1995).

The bulk of outgoing longwave terrestrial radiation is absorbed and re-emitted upwards and downwards in the atmosphere by a group of radiatively active gases known as the *greenhouse gases* (while oxygen and nitrogen make up 99% of the volume of the atmosphere these gases are transparent to infrared radiation). By definition, any process which acts to modify the amount the energy available to the climate system is termed a *radiative forcing* (IPCC, 1990). Most important of the greenhouse gases are water vapour (H_2O) which makes up as much as 2% of the volume of the atmosphere, and carbon dioxide (CO_2) but other greenhouse gases include methane (CH_4), nitrous oxide (N_2O), halocarbons and halogenated compounds (CFCs and HCFCs) and ozone (O_3). By absorbing and re-emitting infrared radiation, these gases exert a radiative forcing which serves to warm the atmosphere and are the reason that the global average temperature is approximately 288 K (15°C). The process is known as the natural *greenhouse effect*.

Other important atmospheric constituents which exert a radiative forcing are stratospheric and tropospheric aerosols. The presence of very small particles and droplets of both natural and human origin in the atmosphere exerts both a direct (by scattering and absorbing radiation) and indirect (by modifying the optical properties, amount and lifetime of clouds) influence on the global radiation balance. Aerosols tend to be washed out of the atmosphere due to precipitation and are therefore relatively short-lived in the atmosphere. In comparison to the greenhouse gases which exert a radiative forcing globally and may be resident in the atmosphere for years, aerosols tend to be concentrated near their source region. However, radiative forcing by tropospheric aerosols tends to cool climate locally whereas the effect of greenhouse gases is to warm climate globally (Taylor and Penner, 1994).

Anthropogenic Influences on Climate Change

Any change in the distribution or concentration of greenhouse gases and tropospheric aerosols must by definition, exert an additional radiative forcing on the climate system. Recent evidence suggests that the concentration of greenhouse gases and aerosols is increasing as a result of human activity (IPCC, 1995). In the case of CO_2, concentrations have increased from pre-industrial levels of about 280 ppmv to 358 ppmv in 1994 (Fig.

1.2). This phenomenon gives rise to the so-called *enhanced* greenhouse effect. The existence of an anthropogenic influence on climate change requires a careful definition of the term *climate change*. In accordance with the United Nations Convention on Climate Change, climate change is defined as "a change of climate which is attributed directly or indirectly to human activity that alters the composition of the global atmosphere and which is in addition to natural climate variability observed over comparable time periods".

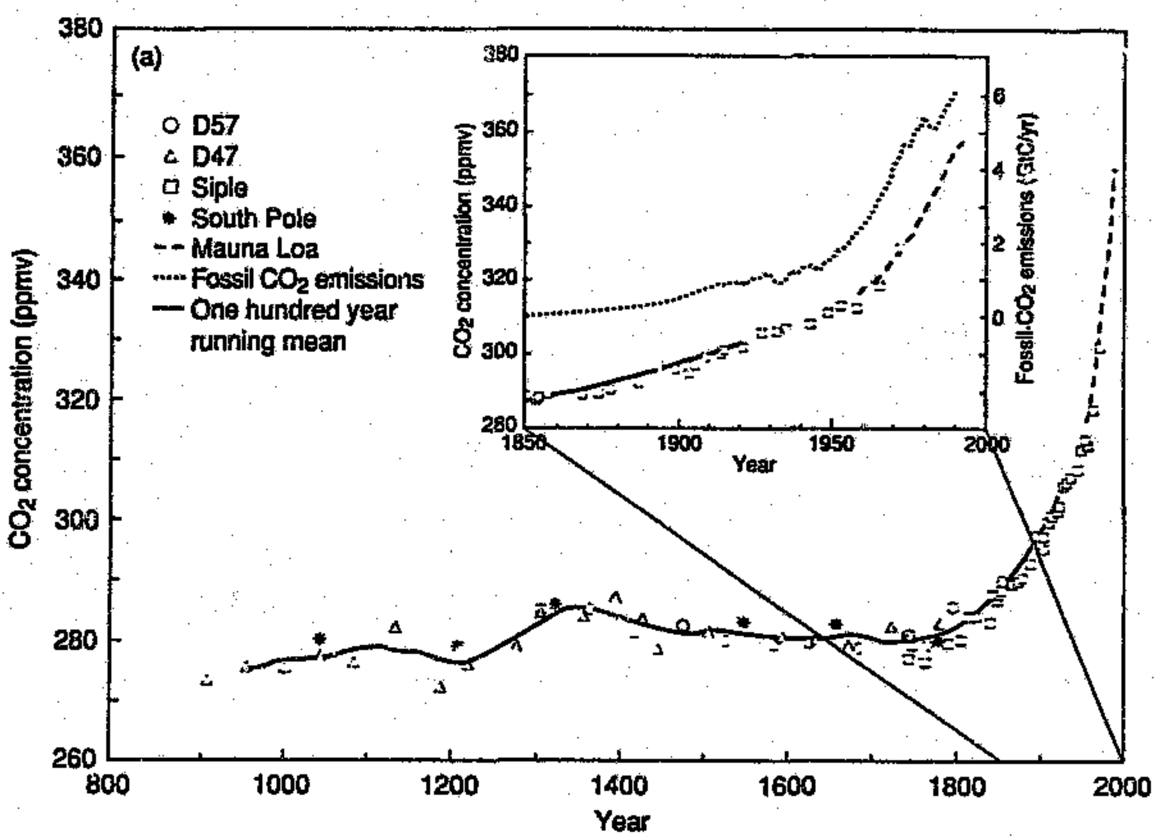

Figure 1.2. CO_2 concentrations over the past 1000 years from ice core records (D47, D57, Siple and South Pole) and (since 1958) from Mauna Loa, Hawaii (dashed line). The smooth curve is based on a hundred year running mean. From 1850 onwards (inset) CO_2 concentration has increased rapidly and has closely followed the increase in fossil fuel emissions (dotted line) (modified after IPCC, 1995).

Importantly, the impact on the climate system as a whole of any anthropogenically-induced change in radiative forcing depends largely on the present understanding, and representation in climate models of the processes, interactions and feedbacks between it's components. Feedbacks can both amplify (a positive feedback) and dampen (a negative feedback) the response to a change in radiative forcing. Possibly the greatest area of uncertainty in terms of the projection of future climate change relates to the parameterisation of physical processes and feedbacks in climate models.

An anthropogenically-induced climate change will be superimposed on the naturally-occurring climate variability. The task of detecting an anthropogenic climate change signal involves demonstrating that an observed change in climate is highly unusual in a statistical sense (IPCC, 1995). This task is complicated by both the relatively short period of instrumental records (not much greater than the last 100 years), and the relative paucity of reliable palaeoclimatic records. For this reason, improving the understanding of, and ability to model the known climate system and it's natural variability has been a long-standing aim of the IPCC. However, the secondary aim of attribution, which involves attributing an observed change to a particular cause and effect link (IPCC, 1995), is further complicated by the large number of interactions and feedbacks which can be invoked to explain any observed globally-averaged change. Nonetheless, the latest report of Working Group I of the IPCC (IPCC, 1995) suggests that considerable advances have been made since the first IPCC Report (IPCC, 1990) in the search for an identifiable human-induced effect on climate. One of it's primary findings therefore, is that "the balance of evidence suggests that there is a discernible human influence on global climate" (IPCC, 1995, p5).

Climate Modelling

Introduction

GCMs are based on numerical solutions of the mathematical equations representing the physical laws which describe the global climate system. Integrations are provided in three dimensions and often over long time-scales to account for the time evolution of the climate system. Developments in the present understanding of the global climate system, and in the ability to project future climates are largely the result of the development of global climate models. While GCMs demonstrate significant skill at the continental and hemispheric spatial scales and incorporate a large proportion of the complexity of the global system, they are inherently unable to represent local sub-grid-scale features and dynamics. Typical spatial resolution of current climate models is ~250 km horizontally and ~1 km vertically (IPCC, 1995). Due to this coarse resolution, many physical processes are not explicitly treated in the models but their effects are incorporated by means of parameterisations that are physically-based. Parameterisation of for example, convective cloud processes (which are sub-grid scale and yet a primary producer of precipitation) are a significant source of uncertainty in climate models (Wilson and Mitchell, 1987; Cess *et al.*, 1989, Cess *et al.*, 1990; Harrison *et al.*, 1990; Senior and Mitchell, 1993).

Available computing resources and the costs associated with integrations using supercomputing facilities impose a physical constraint on the sophistication with which the global climate system is represented in climate models. Until the late 1980s, the use of GCMs in climate change studies was limited to determining the time-independent or *equilibrium* response of the climate system to increased forcing (by instantaneously doubling atmospheric CO_2 concentrations and allowing an equilibrium to be re-established in the model). The magnitude of the equilibrium response was determined by the nature and sign of a variety of climate feedback mechanisms. In general, equilibrium climate change experiments are performed using fairly coarse-resolution atmospheric GCMs linked to simple mixed-layer slab oceans (referred to below as mixed-layer models) (cf. IPCC, 1990, 1992).

Fully-coupled models

The most sophisticated climate models include both atmospheric and oceanic GCMs, and represent all the physical processes shown in Figure 1.1, including those involving interactions between the atmosphere and ocean, as well as land-surface processes. Such models are known as fully-coupled global ocean-atmosphere GCMs (referred to below as fully-coupled models). Reviews of the development of fully-coupled models are provided by IPCC (1992, 1995) and Meehl (1990, 1995).

Fully-coupled models provide a more comprehensive treatment of the process of climate change by incorporating the effects of the thermal inertia of the oceans, allowing mixing to greater depths in the oceans and by representing ocean dynamics explicitly. In particular, fully-coupled models linking the atmosphere and ocean are required in order to simulate the time-dependent, or *transient* response of the climate system to increasing anthropogenic forcing of climate (Meehl *et al.*, 1994; Murphy, 1995). Several current fully-coupled model simulations now also include the direct effects of sulphate aerosols on the radiative forcing of global climate (e.g. Hasselmann *et al.*, 1995; Mitchell *et al.*, 1995a; Mitchell and Johns, 1996). Fully-coupled models also demonstrate significantly different predictions of transient climate change when compared to equilibrium climate change estimates. Most notable of these is a much-reduced warming in high latitudes of the southern hemisphere (Bryan and Spelman, 1985; Bryan *et al.*, 1988; Stouffer *et al.*, 1989; Washington and Meehl, 1989, 1991; Manabe *et al.*, 1991, 1992; Cubasch *et al.*, 1992; Gregory, 1993; Meehl *et al.*, 1993a; Manabe and Stouffer, 1994; Murphy, 1995; Murphy and Mitchell, 1995; Tett, 1995; Gordon and O'Farrell, 1996; Mitchell and Johns, 1996).

On inter-annual and longer time-scales, variability in climate model dynamics is largely a function of the manner in which the coupling of the climate system components is represented (Campbell *et al.*, 1995). Given the importance of ocean dynamics in determining inter-annual and longer-term variability (cf. Wigley and Raper, 1990), their representation (or not) in a climate model is an important constraint on the simulated atmospheric variability. Hence, atmospheric general circulation models linked to non-dynamic mixed-layer oceans (mixed-layer models) are incapable of reproducing variability associated with El Niño / Southern Oscillation (ENSO) forcing in the tropical Pacific (Campbell *et al.*, 1995) unless forced by observed sea-surface temperatures.

The large-scale dynamics of current ocean GCMs appear realistic but have not been fully validated as yet. For example, the response of the thermohaline circulation to increased inputs of fresh water at high latitudes is unknown (Manabe and Stouffer, 1988). The atmosphere and ocean interact via fluxes of heat, momentum and fresh water. However, whilst the atmosphere operates on time-scales of weeks, certain ocean processes operate on time-scales of thousands of years. In order to provide coupled integrations, the separate oceanic and atmospheric components of a fully-coupled model are allowed to "spin-up" before coupling (cf. Meehl, 1995). During spin-up, the ocean models are generally forced with specified fluxes and therefore arrive at an unrealistic state in the absence of atmosphere-ocean feedbacks. The inconsistencies between the surface fluxes in the atmospheric and oceanic components of the coupled model result in a drift away from a realistic climate when they are coupled (a phenomenon known as climate drift). To prevent this from occurring, flux adjustments can be applied at the atmosphere-ocean interface (Manabe and Stouffer, 1988; Sausen *et al.*, 1988). While flux adjustments can prevent climate drift, they also mask the coupled model's response in terms of feedbacks between the atmosphere and ocean to transient climate change.

In general, coupled models are capable of reproducing variability on inter-monthly and inter-annual time-scales which is similar (although of lower amplitude) to the observed system, and there is evidence to suggest that the mechanisms responsible for the variability are operating in both the natural system and the coupled model (Meehl *et al.*, 1994). This observation is applicable to most fully-coupled models, and is most apparent for the case of ENSO variability in the tropics, where simulated variability is generally half the amplitude of that observed (Meehl *et al.*, 1993a, 1993b; Meehl *et al.*, 1994; Meehl, 1995; Campbell *et al.*, 1995; Tett, 1995; Gordon and O'Farrell, 1996). Some reservations must be expressed, however, in terms of coupled model simulations of ENSO-related variability, due in part to the coarse resolution of most current fully-coupled models (IPCC, 1995).

Uncertainties

Most of the uncertainties associated with climate models relate to the representation of physical processes in the models. Uncertainties relating to the adequate inclusion of physical processes, interactions and feebacks directly affect the ability of climate models to simulate present climate and influence the simulated response to an increase in radiative forcing of climate (IPCC, 1995). For a given change in radiative forcing, current climate models project global temperature increases which vary by a factor of two (IPCC, 1995). The major cause of this uncertainty is the representation of cloud processes and their interactions with the hydrological cycle and radiation in the models. Other important sources of uncertainty in climate model projections are related to the representation of oceanic and land-surface processes. While each of these areas have seen substantial development since the first IPCC Report (IPCC, 1990), they are still largely parameterised processes as opposed to being explicitly solved in terms of the model physics. For regional-scale climate predictions they are thus still substantial sources of error, particularly at sub-grid scales.

Cloud processes

Feedbacks associated with the distribution, height, type and optical properties of clouds, as well as their interaction with the Earth's radiation budget and cloud aerosols are all sources of uncertainty in climate models (Wilson and Mitchell, 1987; Cess *et al.*, 1989; Cess *et al.*, 1990; Harrison *et al.*, 1990; Senior and Mitchell, 1993). Results from the Earth Radiation Budget Experiment (ERBE) indicated that on a global and annual mean, the net effect of clouds is a negative feedback which tends to cool present climate (Ramanathan *et al.*, 1989). However, low clouds such as marine stratocumulus may act to warm climate (Slingo, 1990). In climate change experiments, the amount of high clouds in the tropics increases, enhancing the greenhouse effect resulting in a positive feedback (Wetherald and Manabe, 1988; Mitchell and Ingram, 1992). Earlier cloud parameterisation schemes based on assumed relationships between cloud amount and relative humidity (e.g. Wilson and Mitchell, 1987) have been replaced by a newer scheme based on prognostic cloud water variables that explicitly determine the amount of cloud liquid water in each grid cell (e.g. Roeckner *et al.*, 1990; Smith, 1990; Del Genio *et al.*, 1995). The prognostic cloud water content parameterisation allows for different feedbacks associated with changes in cloud-water content and phase and has lead to improved simulations of the Earth's radiation budget (Senior and Mitchell, 1993; Del Genio *et al.*, 1995; Fowler and Randall, 1996). In a recent update, Cess *et al.* (1996) show that the substantial changes that have occurred in cloud parameterisation since 1990 have resulted in smaller differences in net cloud feedback between models (Fig. 1.3). However, this result may indicate that current models may simply be producing similar errors, and does not necessarily indicate an improved accuracy in the parameterisation of cloud feedback processes.

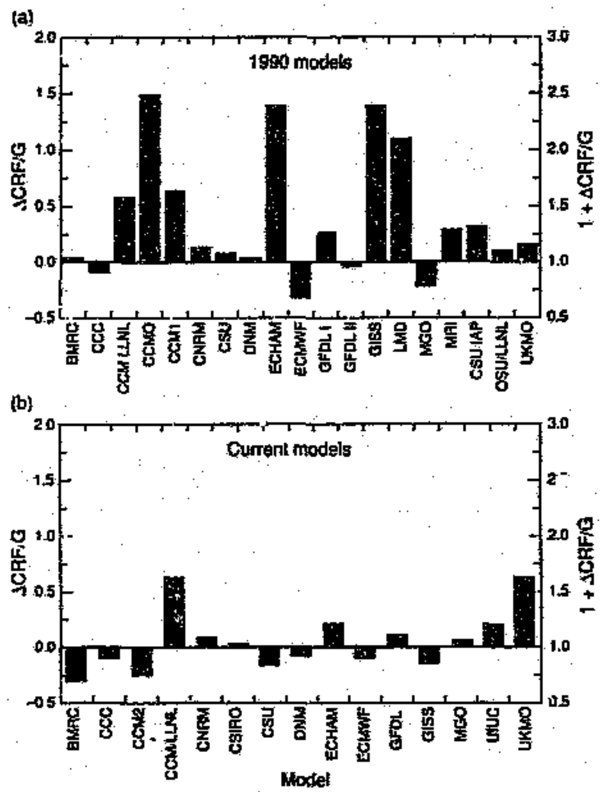

Figure 1.3. (a) The cloud feedback parameter, Δ CRF/G, as produced by the 19 atmospheric GCMs used in the Cess *et al.* (1990) study, where Δ CRF is the cloud radiative forcing in Wm^{-2} due to cloud changes and G is the overall Wm^{-2} change, both as a result of prescribed sea-surface temperature change. (b) The same as (a) but for the Cess *et al.* (1996) study (after IPCC, 1995).

Oceanic processes

Several uncertainties are associated with the ocean component of fully-coupled models. These include uncertainties in the representation of the thermohaline circulation, fluxes of energy, momentum and water between the ocean and atmosphere, parameterisation of sub-grid-scale processes such as near-surface mixing and deep ocean convection, sea-ice albedo feedback and ENSO-related variability (IPCC, 1995).

The response of the thermohaline circulation to changes in the inputs of fresh water at high latitudes induced by increased radiative forcing is currently unknown. Under doubled-CO_2 conditions, a recent coupled transient experiment indicated that the thermohaline circulation in the North Atlantic Ocean weakened and then returned, but under 4 x CO_2 it collapsed completely (Manabe and Stouffer, 1994). The fluxes of heat, momentum and fresh water between the atmosphere and ocean are dependent for example on the parameterisation of clouds, and hence may be a significant source of error. Most ocean GCMs use fairly crude parameterisations of sub-grid-scale processes such as mixing and ocean convection. In particular, mixing processes associated with meso-scale eddies are poorly resolved. Recent analyses suggest that south of 50°S the ocean models in many contemporary fully-coupled models sequester heat from the atmosphere too rapidly and significantly over-estimate vertical mixing and convective overturning (England, 1995; England *et al.*, 1994). The role of sea-ice albedo feedback is an important element in the response of a climate model to a transient increase in radiative forcing because it modulates the exchange of energy between the ocean and atmosphere. For example, as climate warms and sea-ice decreases at high latitudes, low clouds and hence cloud albedo increase. However, this may be more than compensated for by a decrease in surface albedo due to the melting of sea-ice, resulting in a net decrease of planetary albedo at high latitudes and relatively high climate sensitivity in the model (cf. Washington and Meehl, 1996). In general, sea-ice-albedo feedback remains poorly understood and treated in current ocean models.

Land-surface processes

Land surface processes are important determinants of near-surface climate, surface temperature and soil moisture and are an important influence on the hydrological cycle. Current uncertainties in the surface energy balance and radiation and water budgets are a significant source of error in regional climate simulations. Earlier climate models treated land surface processes using bucket models (IPCC, 1995). Newer treatments include several sub-grid-scale processes, but the relative importance of these processes is yet to be determined. The various processes operating on a wide range of scales which govern runoff are not yet comprehensively treated. More recent models now simulate a more heterogeneous land surface, allowing for a wider range of responses from land surface processes. For example, more sophisticated soil-vegetation-atmosphere transfer schemes are now included in several models which allow for a more realistic transfer of moisture from the surface to the atmosphere, by means of transpiration through the canopy (Henderson-Sellers *et al.*, 1995; Pollard and Thompson, 1995).

Evaluating Model Performance and Projecting Future Climate

A primary use of climate models has been to predict the future state of the climate system resulting from increased anthropogenic forcing of climate change. Given the uncertainties associated with the parameterisation of physical processes and feedbacks in the model, an important aspect of both model development and scenario development is the assessment of model performance. Both of these issues are central to the development of regional climate change scenarios and are central to the analyses presented in this thesis.

According to the definition provided by IPCC (1995), the goal in assessing climate model performance is to define the extent to which they simulate the real world they seek to represent (cf. Oreskes *et al.*, 1994). The Report uses the term *evaluation* to describe this process as opposed to *validation* used in earlier IPCC Reports (IPCC, 1990, 1992) and in the modelling literature. The aim here is to describe the ability of a range of different types of climate models to simulate southern African climate and not specifically model development. This process is best described according to IPCC (1995) as model evaluation.

The IPCC (1995) Report also distinguishes between *projections* and *predictions* of future climate. All climate model simulations of future climate are based on a given forcing scenario (for example the IS92 scenarios defined in IPCC, 1992 and IPCC, 1994). Consequently simulated changes in climate are dependent on the forcing scenario used in the model. The resulting climate change scenarios are an attempt to estimate and understand the responses of the climate system to that forcing scenario, and not an attempt to predict the most likely state of future climate. As such, the term *projections* of future climate will be used throughout this thesis.

Modelling Regional Climate

Introduction

While GCMs demonstrate significant skill at the global and hemispheric spatial scales and incorporate a large proportion of the complexity of the global system, simulations of regional climate and climate change are considerable less reliable (IPCC, 1995). Given the disparity in performance on global and regional scales, GCM projections of regional climate change are strongly dependent on their ability to simulate present regional climate (Mitchell, *et al.*, 1987). However, when considering the *impacts* of global climate change the focus is primarily on societal responses to the local and regional consequences of large-scale changes. The conflict between GCM performance at regional spatial scales and the needs of regional-scale impact assessment is largely related to model resolution. Model grid resolution (usually no better than 2° of latitude by 4° of longitude) is substantially removed from model *skill* resolution. Skill resolution may be defined as the spatial scale of aggregation at which the temporal and spatial information from the model approaches that of observational data (Hewitson, *personal communication*). In GCMs this may well only be achieved at aggregated scales of 7 or more grid cells (Grotch and MacCracken, 1991; von Storch *et al.*, 1993). Furthermore, these issues pertain only to the model's ability to represent regional climates, and are separate from the issue of the model's ability to *project* correctly the system response to the changing atmospheric composition. For these reasons, evaluation of GCM regional-scale performance is an important pre-requisite for developing climate change scenarios.

The deterioration in model performance on regional spatial scales requires that particular attention be placed on assessments of regional climate simulations, particularly when the goal is to provide reasonable projections of regional climate change. The region of interest in the present analysis includes the southern African subcontinent and adjacent oceans and will be referred to below as the southern African region. However, features of the general climate and circulation of the southern hemisphere as a whole influence climate over the southern African region. As a consequence, a discussion of approaches to regional climate studies and a review of climate model studies performed to date over the southern African region is preceded by a discussion of model performance for the southern hemisphere as a whole.

Model Performance in the Southern Hemisphere

Tropospheric circulation exerts a dominant control on surface weather and regional climate. As a consequence, the accuracy with which circulation features throughout the southern hemisphere are simulated directly influences the ability of the GCMs to simulate southern African climate. There have been notably fewer attempts, however, to evaluate the present climate performance of GCMs in the southern than in the northern hemisphere (Meehl, 1996; Whetton *et al.*, 1996a). In addition, there are considerable differences between the dominant climatic influences in the two hemispheres. Thus it is not sufficient to rely on evaluations of GCM performance for the northern hemisphere when considering the policy implications of climate change and variability for countries and regions in the southern hemisphere (Giambelluca and Henderson-Sellers, 1996).

The differing distributions of land, sea and ice between the northern and southern hemispheres have important implications for the dominant climatic forcing in each hemisphere. There is almost uninterrupted ocean between 35°S and 70°S in the southern hemisphere, whereas in the northern hemisphere these latitudes are almost completely covered by land. In addition, the Antarctic continent has a permanent elevated ice sheet and is surrounded by extensive sea-ice which ensures that equator-pole temperature gradients are much stronger in the southern than in the northern hemispheres. As a consequence, mid-latitude westerlies in the southern hemisphere are approximately 40% stronger than in the northern hemisphere, a phenomenon which contributes to the greater relative importance of the zonal motion (Adler, 1975) and the dominance of zonal standing waves 1 and 2 (van Loon and Jenne, 1972) at higher latitudes. The stronger westerlies cause the subtropical high pressure belt to be located further equatorward than in the northern hemisphere, and may account for the observed asymmetry in the Inter-Tropical Convergence Zone (Flohn, 1969).

Recent higher-resolution GCM simulations provide a generally-improved simulation of the large-scale circulation in the southern hemisphere over earlier lower-resolution models. The improvement is illustrated with reference to simulations of zonally-averaged mean sea-level pressures in Figure 1.4. Performance is notably better with regard to the simulated position and intensity of the circumpolar trough (Boville, 1991; Boer *et al.*, 1992a; Parrish *et al.*, 1994). Improvement is also noted in the intensity of tropical convection which directly influences simulated meridional temperature gradients and hence the strength of the mid-latitude westerlies (Hack *et al.*, 1994; Meehl and Albrecht, 1988, 1991). Models with higher spatial resolution also simulate stronger subtropical and high-latitude jets as well as the double jet-structure in the region of Australia and New Zealand (Kinter *et al.*, 1988; Kitoh *et al.*, 1990; Kitoh, 1994; Mullan and McAvaney, 1995).

In contrast, current models display several persistent difficulties in simulating other key features of southern hemisphere circulation. For example, GCMs under-estimate the intensity of the stationary eddies and hence the standing wave structure at middle and high latitudes (Malone *et al.*, 1984; Xu *et al.*, 1990; Yang and Gutowski, 1994; Mullan and McAvaney, 1995). GCMs also show a significant over-prediction of mid-latitude cyclone frequency, although the general hemispheric-scale positioning of the cyclones is not unrealistic (Murray and Simmonds, 1991; König *et al.*, 1993). However, there is considerably greater variability of cyclone positions than is found in observed data. The models further display a persistent inability to simulate both ENSO-related variability and the semi-annual oscillation (SAO) at middle and high latitudes (Xu *et al.*, 1990; Mullan and McAvaney, 1995).

Approaches to Regional Climate Studies

Approaches and techniques for regional climate studies and their application to the southern African region have been discussed by Joubert and Hewitson (1996). Uncertainties associated with climate model simulations are accentuated at regional spatial scales, due largely to the disparity between model resolution and skill resolution. Hence, while GCM accuracy decreases at increasingly finer spatial scales, the needs of impacts researchers conversely increase with higher resolution.

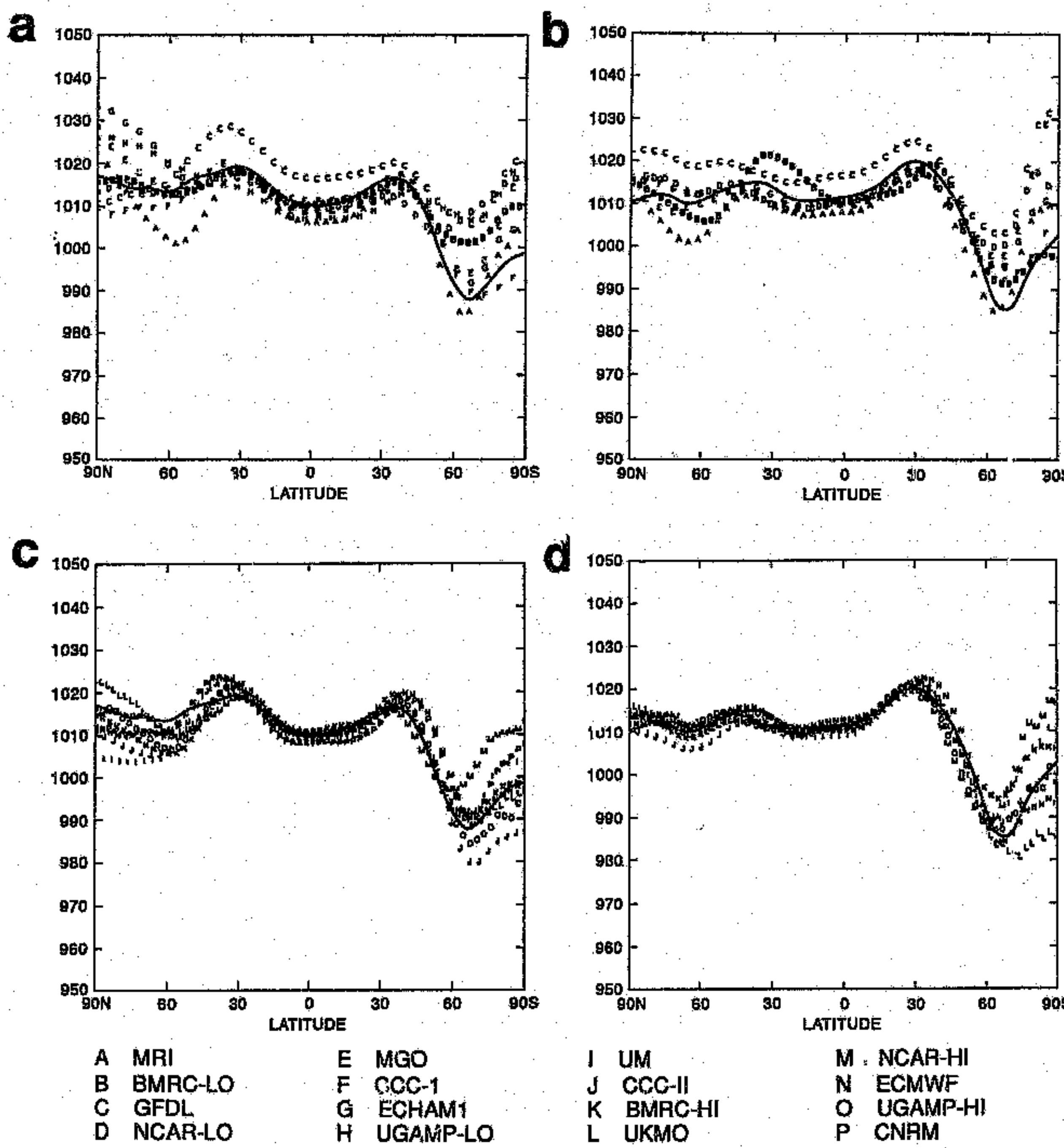

Figure 1.4. Zonally-averaged summer (December-February, a,c) and winter (June-August, b,d) mean sea-level pressure as simulated by various atmospheric GCMs (symbols, see legend) and based on observations (solid curve) (modified after Boer *et al.*, 1992a). The models are separated into lower (a,b) and higher (c,d) resolution categories.

Evaluation of GCM output against observed regional climate is a necessary first step towards developing regional climate change scenarios. Simulation of circulation dynamics (at least) must be reasonable at the synoptic and regional scales before any given model can be used to develop scenarios. Model evaluation serves two purposes. Firstly, it is of diagnostic value to climate modellers in the process of model development. Secondly, by using only those models which agree best with observations on both the temporal and spatial scales under investigation provides some (but not complete) confidence in the reliability of the projected changes (Mitchell, *et al.*, 1987). Several approaches can be adopted to address the need for regionally-specific information and can be classified into two categories: process based techniques, involving the explicit solving of the physical dynamics of the system, and empirical techniques that use identified system relationships derived from observational data. Either approach may be adopted for developing regional climate change information, and both have advantages and shortcomings (Hewitson and Crane, 1996).

Historically, many evaluations of regional climate performance have used direct grid-cell output from GCMs at the grid-scale resolution and have been interpreted in terms of the ability of the models to simulate the large-scale circulation features throughout the hemisphere. These have typically involved comparing multiple simulations of regional climate (e.g. Grotch and MacCracken, 1991; Portman *et al.*, 1992) in order to identify those models which agree best with observations, and also to identify consensus between those models which simulate regional climate reliably. The approach is essentially process-based in that the models' ability to simulate the regionally-important physical climate is assessed and the technique has been widely applied in southern Africa (Joubert, 1994, 1995, 1996; Joubert and Tyson, 1996). As present generation GCMs demonstrate an ability to represent synoptic scale circulation realistically, this would seem a reasonable approach, and further evaluation of the performance of GCMs over southern Africa through this approach is discussed below.

An alternative approach to using GCM grid cell data in regional scale climate prediction is downscaling, which relates local and regional scale climate variables to the larger scale atmospheric forcing (Wigley *et al.*, 1990; Hewitson and Crane, 1992, 1996).

Two broad classes of downscaling approaches exist. The first is a nested modelling approach which typically involves driving a nested regional dynamic model at mesoscale or finer resolutions with boundary conditions drawn from a GCM simulation (Giorgi and Mearns, 1991). This has been applied with relative success to numerous regions of the northern hemisphere including North America and western Europe (Giorgi *et al.*, 1990, Giorgi *et al.*, 1994; Jones *et al.*, 1995; Jenkins and Baron, 1996). However, a number of technical difficulties are still being addressed. For example, the implications of different physics between the nested and global models, and the formulation of boundary conditions for the fine resolution model which have consequent edge effects transmitted to the nested domain. While nested modelling is likely to be the most informative approach to deriving regional information in the long term, constraints such as the limited southern African computing infrastructure suitable for such studies make such an approach difficult to implement locally at present (Joubert and Hewitson, 1996).

A second, less computationally-demanding approach is empirical downscaling. In this approach, the atmospheric circulation is related to the local climate through means of a statistical or direct quantitative transfer function (Hewitson and Crane, 1996). For example, over southern Africa, Hewitson and Crane (1996) derive a direct mathematical relationship between the observed circulation and observed local precipitation using Artificial Neural Networks (ANNs) (Hewitson and Crane, 1994). The transfer function determined in this manner is then applied to the GCM present circulation (or circulation under enhanced greenhouse conditions) to derive local-scale information (or predictions) consistent with the synoptic-scale forcing of the GCM.

Simulations of Southern African Climate

Existing assessments of GCM performance in the southern hemisphere have generally been of a regional nature, focusing on model performance over the major land masses. Regional analyses have been performed over Australia (Whetton and Pittock, 1991; Whetton *et al.*, 1994), New Zealand (Mullan and Renwick, 1990), South America (Burgos, *et al.*, 1991) and southern Africa (Joubert, 1995, 1996; Hewitson and Crane, 1996). A review of GCM performance throughout the hemisphere is provided by Whetton *et al.* (1996a) and specifically for the southern African region by Joubert and Hewitson (1996).

Present climate simulations

Some early attempts to provide regional climate change scenarios for southern Africa derived from GCMs did not include any assessment of the present climate performance of the models considered (Tyson, 1990, 1991, 1993). Subsequently, considerable emphasis has been placed on the need to perform evaluation studies before GCMs can be used with confidence to derive climate change predictions. Southern Africa is influcnced by systems of both tropical and mid-latitude origin and the interaction between them is an important control on the region's climate (Harrison, 1986; Tyson, 1986). Furthermore, the region's orography is characterised by coastal plains and high altitude plateau; areas of strong topographical forcing, and regions with very sharp topographic and climatic boundaries. These produce considerable local variability in precipitation and present a particularly challenging environment for GCMs (Joubert *et al.*, 1996; Mason and Joubert, 1996).

Assessments of the present climate performance of a range of GCMs have generally been made using equilibrium climate change experiments with mixed-layer models, and have been performed at fairly coarse spatial resolution. An initial validation study which examined the performance of six pre-1990 mixed-layer models for simulations of surface variables including observed surface air temperature, mean sea-level pressure and precipitation, found that errors in the simulation of a particular variable could be related to uncertainties in the representation of physical processes by means of parameterisations in the models (Joubert, 1995). For example, large errors were identified in simulations of convective precipitation, a process strongly dependent on model resolution and cumulus parameterisation (IPCC, 1990, 1992). While the models were shown to reproduce the annual cycle of rainfall over several regions of the subcontinent, substantial errors existed in the simulation of actual rainfall amounts (Fig. 1.5). However, the models were able to reproduce the pattern of rainfall seasonality reliably. The successful simulation of the pattern of rainfall seasonality is related to substantial changes in radiation associated with the annual cycle and suggests that some confidence can be placed in simulated rainfall changes associated with the relatively smaller changes in radiation resulting from a doubling of atmospheric CO_2 (Whetton and Pittock, 1991).

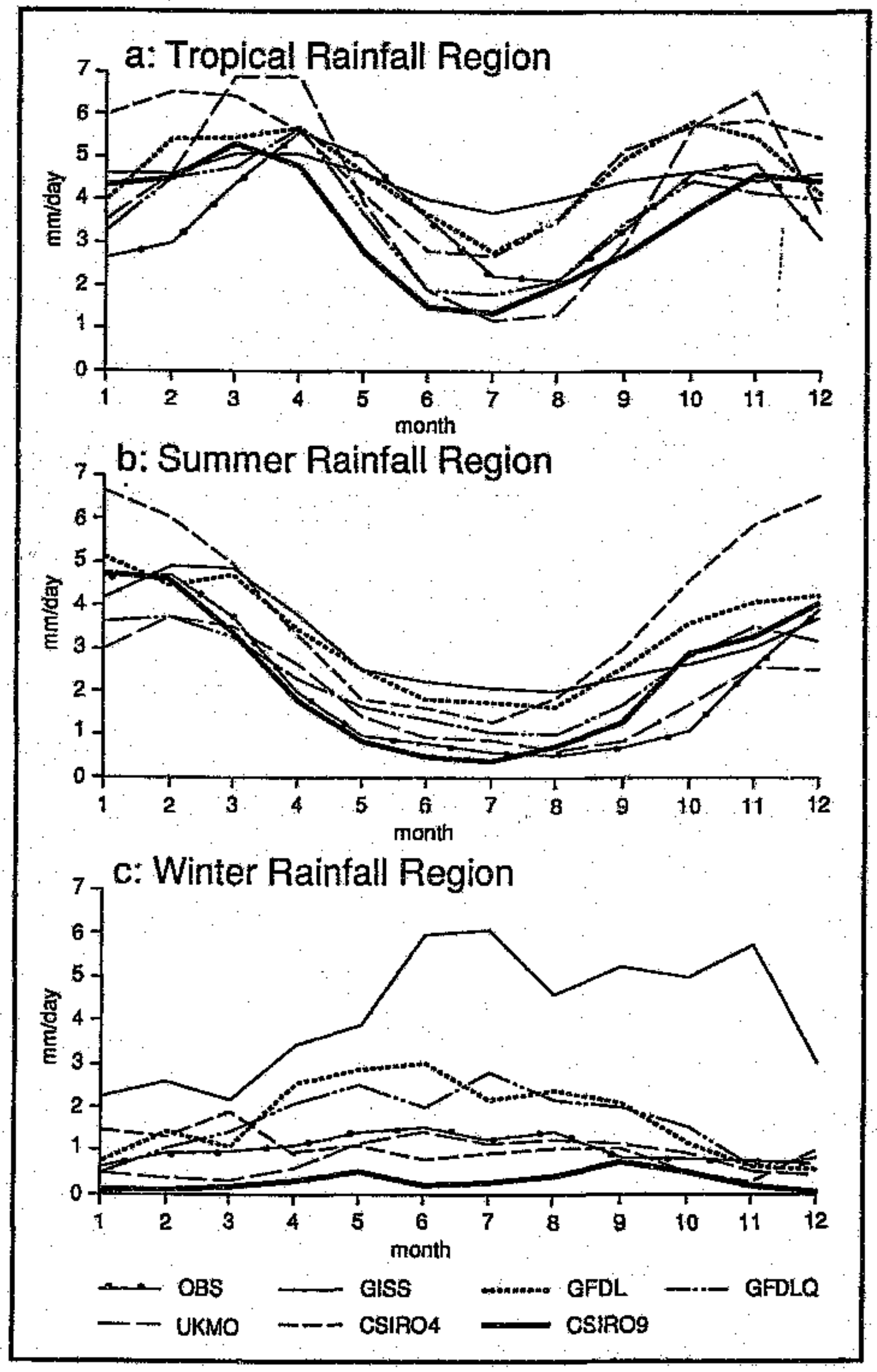

Figure 1.5. Comparison of observed and simulated monthly average precipitation rates for the tropical (a), summer (b) and winter (c) rainfall regions (mm.day^{-1}) (after Joubert, 1995). All of the models are atmospheric GCMs linked to mixed-layer oceans. The three regions are defined in Joubert (1995).

There is a need to investigate more recent, higher resolution models which incorporate more sophisticated representations of physical processes such as cloud feedback and cumulus convection than those previously considered for southern Africa. One such opportunity arises with the Atmospheric Model Intercomparison Project (AMIP) (Gates, 1992). The AMIP project involves an extensive range of current (generally high resolution) simulations and aims specifically to identify systematic regional errors in the models. The project is unique in that all participating modelling groups provide simulations of global climate between 1979 and 1988 using boundary conditions and observed sea-surface temperatures which are common to the whole project. As a result, complications in comparing the regional performance of different models across different regions caused by differences in experimental design are removed. An AMIP diagnostic subproject was formed in 1994 (Diagnostic Subproject No. 20) to investigate AMIP simulations of circulation variability for the southern African region. In addition, assessments of AMIP model performance considers the ability of atmospheric GCMs linked to mixed-layer oceans to simulate climate variability in addition to mean climate in the southern African region.

Lastly, the development of fully-coupled model represents probably the most important advance in climate modelling technology since 1990. There is an important need to assess the ability of such models to simulate present and future climate for the southern African region.

Projections of future regional climate

Given the uncertainties associated with modelling regional climate change using GCMs, it is important to define the level of confidence with which a given projection of future climate can be interpreted. Accurate simulation of present climate is one important means of establishing confidence in a projection. Another is to determine the level of consensus between a range of models in terms of the nature of projected regional climate change (assuming the models' ability to represent observed circulation dynamics adequately has been demonstrated). Due to the variety of parameterisation schemes used in individual models, it is often the case that particular models perform better in regions where the dominant physical processes are best captured by the particular parameterisation scheme used in that model. Hence, the aim of developing reliable projections of regional climate may be best served by considering predictions from a range models (Whetton *et al.*, 1993).

Early estimates of regional climate change over southern Africa were based on coarse-resolution equilibrium climate change experiments with GCMs linked to mixed-layer oceans (Tyson, 1990, 1991; Joubert, 1994). Warming projected by these models over the southern African region is within the range of globally-averaged estimates, and a general southward shift of tropical, subtropical and mid-latitude circulation systems is indicated. (Joubert, 1994). Much less confidence exists in projected changes in precipitation, however, due largely to the significant control simulation errors in these models (e.g. Joubert, 1995). While acknowledging these problems, the mixed-layer models project broad-scale increases in rainfall, both within the tropics and over the summer rainfall region of the central interior in summer. In addition, the models project a decrease in winter rainfall over the south-western parts of the subcontinent (a winter rainfall region). Such changes are consistent with the projected changes in circulation.

It is important to note, that relatively small changes in mean rainfall may be accompanied by much larger changes in the frequency and intensity of both wet and dry years (Mearns *et al.*, 1984; Katz and Brown, 1992; Katz and Acero, 1994), and have magnified effects in surface hydrology. Given both the agricultural and socio-economic vulnerability of the southern African region to droughts and floods (Vogel, 1994), possible changes in the frequency and intensity of such extremes under enhanced greenhouse conditions are of concern. GCMs have been used to assess the possible impacts of changes in extreme rainfall events for several other regions (e.g. Mearns *et al.*, 1990; Gordon *et al.*, 1992; Whetton *et al.*, 1993; Hennessey *et al.*, 1995) and similar studies have been performed for southern Africa. The Commonwealth Scientific and Industrial Research Organisation (CSIRO) 9-level model, most reliable of a range of mixed-layer models considered by Joubert (1995), has been used to investigate possible changes in extreme rainfall over southern Africa (Mason and Joubert, 1996). As with the Australian region (Gordon *et al.*, 1992; Whetton *et al.*, 1993), simulated increases in rainfall intensity provide a spatially coherent and an apparently less regionally-dependent signal of climate change than changes in mean rainfall or the number of rain days. Simulated increases in the frequency and intensity of extreme daily rainfall events are widespread over much of the subcontinent, particularly over the winter rainfall region of the Western Cape province (Fig. 1.6). Increases are most severe in the lowest frequency floods, and are also evident when changes in prolonged heavy rainfall events are considered.

A similar analysis has examined possible changes in drought frequency and intensity over southern Africa (Joubert *et al.*, 1996). The CSIRO 9-level model simulates an increase in the probability of dry years in the tropics, to the south-west of the subcontinent as well as over the western and eastern parts of South Africa and southern Mozambique, where largest percentage increases in the most intense dry spells are expected. The frequency of dry spells is expected to decrease over much of the remainder of the subcontinent south of 10°S, and in these regions the most severe droughts occur less often. The predicted changes in both droughts and floods suggest a shift in the frequency distribution of daily rainfall events in the model (cf. Fig. 1.6). Such a change may have further implications for the frequency of mid-summer droughts during the summer rainfall region. Over eastern Mpumalanga (formerly the Transvaal Lowveld region), where mid-summer droughts occur frequently, the model simulates an increase in frequency. The model displays considerable skill in simulating the frequency of occurrence of mid-summer droughts over the eastern Free State, where few mid-summer droughts occur. The model projects little change in this region. Over the Kalahari region, where drought frequencies are expected to decrease, the frequency of occurrence of mid-summer droughts is also projected to decrease.

In general, the projections of future climate change for the southern African region to date have been provided almost exclusively using mixed-layer models. Given the advances in climate modelling, scenarios based on these early-generation GCMs require updating to consider, for example, the changes in model sensitivity resulting from increased spatial resolution of models and the impact of improved parameterisation of, for example, cloud feedback processes. Most important is the need to develop regional climate change scenarios based on fully-coupled models and to assess their reliability in comparison to scenarios provided by mixed-layer models. In addition, the impact of incorporating the direct forcing effects of sulphate aerosols in addition to greenhouse gases remains to be assessed for the southern African region.

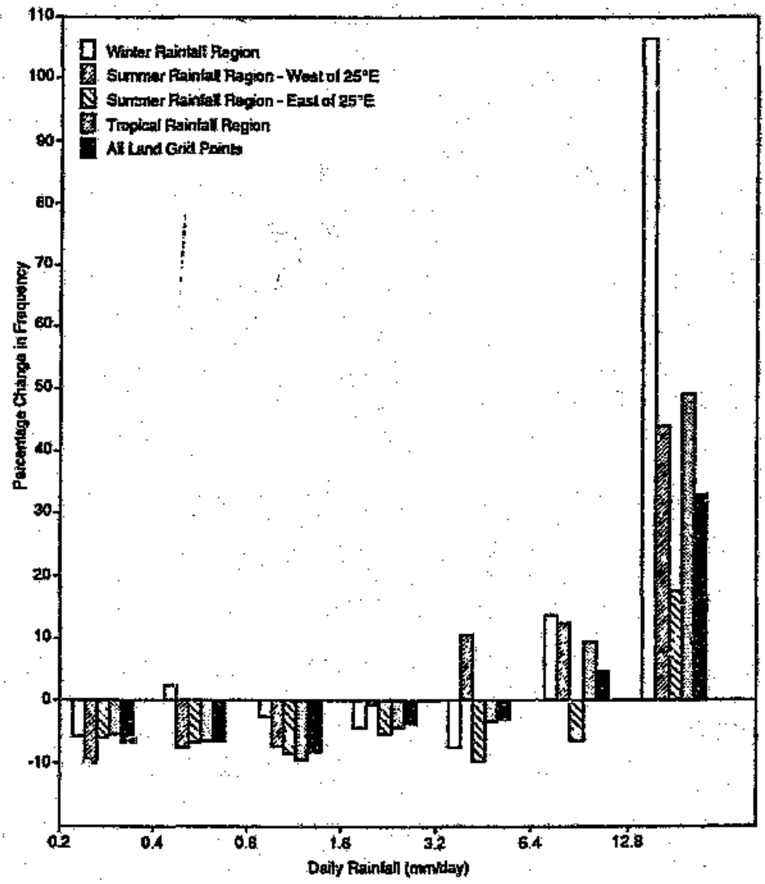

Figure 1.6. Percentage changes in the frequency of simulated daily rainfall (for raindays > 0.2 mm) totals for various rainfall classes. Results are illustrated for four regions over the southern African subcontinent (defined in Joubert, 1995), as well as for all land grid points (after Joubert *et al.*, 1996).

Hypotheses

The overall aim of this thesis is to provide a critical assessment of the representation of present climate and projections of future climate over the southern African region using general circulation models. The research expands on previous studies by considering a wider range of more recent models. The models considered have all been developed subsequent to 1990. Both atmospheric GCMs linked to simple, non-dynamic mixed-layer

-s (mixed-layer models) and fully-coupled ocean-atmosphere GCMs (fully-coupled models) are considered. While the mixed-layer models simulated an equilibrium response to an instantaneous doubling of atmospheric CO_2, the fully-coupled models simulate the transient response of the global climate system to gradually-increasing concentrations of greenhouse gases. Unlike previous studies, the representation of both mean climate and regional climate variability will be assessed. Projected changes in regional climate variability will also be examined. Finally, an updated set of regional climate change scenarios based on increasing concentrations of both greenhouse gases and sulphate aerosols will be assessed.

In terms of the representation of present climate over the southern African region, the hypotheses to be tested are:

(i) that both fully-coupled and mixed-layer models are capable of reproducing the important features of present mean climate for the southern African region;

(ii) that improved spatial resolution (both horizontal and vertical) of a climate model results in an improved representation of regional climate over southern Africa;

(iii) that the inclusion of sulphate aerosol in addition to greenhouse gas forcing of climate results in an improved simulation of the observed record of temperatures over southern Africa;

(iv) that atmospheric GCMs forced by observed sea-surface temperatures are capable of reproducing the observed features of southern African climate and inter-annual variability over the 1979-1988 decade;

(v) that fully-coupled ocean-atmosphere models are capable of representing the principal modes of circulation variability over southern Africa and the surrounding oceans; and lastly

(vi) that it is possible on the basis of evaluations of present climate performance to identify those models which best reproduce contemporary southern Africa climate and hence are most reliable for use in deriving scenarios of regional climate change.

In terms of projections of the future climate of southern Africa, the hypotheses to be tested are;

(i) that reliable estimates of regional climate change can be derived from both mixed-layer and fully-coupled models; however,

(ii) that important regional differences exist between estimates of the equilibrium and transient response to increased anthropogenic forcing and must be considered when developing scenarios;

(iii) that measures of inter-model consensus in terms of the nature of projected changes can be used in conjunction with similar measures of present climate performance to provide greater confidence in projections of regional climate change;

(iv) that fully-coupled models do not simulate any significant change in the principal modes of inter-annual circulation variability over southern Africa and the surrounding oceans;

(v) that the inclusion of sulphate aerosols in addition to greenhouse gas forcing of climate change results in a decrease in both the magnitude and rate of projected warming over southern Africa; and

(vi) that changes in wintertime anticyclonic circulation responsible for extended periods of fine weather are indicated which could have significant impacts on the transport of aerosols and trace gases from the southern African region in future.

****

The use of general circulation models to simulate present and future climate both globally and regionally has been discussed. Several recent advances in terms of the resolution of climate model simulations, as well as in the representation of climate processes and climate change by climate models have been discussed. The hypotheses outlined above will be tested using both mixed-layer and fully-coupled models, and will consider both regional climate means and variability. The sources of both observational and climate model data, and the methodologies to be used in this thesis are described in the following two chapters.

CHAPTER TWO

DATA

Introduction

Climate model output from a wide range of mixed-layer models and fully-coupled models will be utilised. The availability and reliability of suitable observational datasets is an important limitation imposed on all model evaluation and validation studies. In some cases, the data required to assess the representation of particular physical processes or feedbacks are simply unavailable. As a result, this problem is recognised as a priority issue by the IPCC (IPCC, 1995). The observational data used here to evaluate the current climate performance of the models originate from a number of sources. The reliability of all data has been carefully assessed and they have been widely used in the climatological field. The majority of variables considered describe atmospheric circulation. These include mean sea-level pressure, geopotential heights and u- and v-wind components at several levels throughout the troposphere. Other variables considered include surface air temperature and rainfall.

Climate Model Data

Climate model output from both mixed-layer models linked to simple, non-dynamic oceans and fully-coupled ocean-atmosphere GCMs have been obtained from several international modelling groups. Results from mixed-layer models include mean fields from individual modelling groups as well 10-year simulations from the Atmospheric Model Intercomparison Project (AMIP). Climate means from five fully-coupled model experiments are utilised. The specifications of the CSIRO and Hadley Centre fully-coupled models are described in greater detail as longer-term (century-scale) simulations are available for these models.

Mixed-Layer Models

The Atmospheric Model Intercomparison Project

Evaluations of general circulation models used in climate modelling have historically been hampered by differences in experimental and model design, as well as by the availability of reliable observational data against which to assess model performance. The Atmospheric Model Intercomparison Project (AMIP) was established to address the need for a comprehensive assessment of model performance (Gates, 1992). Through diagnostic and validation studies, AMIP aims to document and compare the performance of a wide range of atmospheric general circulation models (GCMs) and to identify systematic model errors (Gates, 1992, 1995). As a consequence, the AMIP results can be used as a benchmark against which future model versions can be evaluated (Gates, 1995).

Modelling groups participating in AMIP provide a simulation of global climate between 1979 and 1988 during which observed sea-surface temperatures and sea-ice distributions are used as surface boundary conditions. A standard output of monthly means for a range of output variables have been made available for diagnostic studies. Such studies have been co-ordinated as a range of AMIP diagnostic subprograms. In addition, a standard set of validation data were to be made available to all diagnostic subprojects. A selection of AMIP runs from seven climate modelling groups are assessed here. Monthly means of precipitation, mean sea level pressure, geopotential height and u- and v-wind components are compared with observations. While the total number of modelling groups exceeds 30, many simulations are based on models used most often for numerical weather prediction (e.g. the European Centre for Medium-Range Weather Forecasts, ECMWF). Many of these models are successful in simulating the global climate between 1979 and 1988 (Gates, 1995). Given the focus here on climate models, only those models used routinely in climate change experiments are considered.

The models considered include those of the Australian Bureau of Meteorology Research Centre (BMRC), the Canadian Climate Centre (CCC), the Commonwealth Scientific and Industrial Research Organisation (CSIRO), the Geophysical Fluid Dynamics Laboratory (GFDL), the Max Planck Institüt Für Meteorologie (MPI), the National Centre for Atmospheric Research (NCAR) and the United Kingdom Meteorological Office (UKMO). Comprehensive documentation on the AMIP runs for each group is available (Phillips, 1994) and is described briefly in Table 2.1.

Table 2.1. Details of AMIP model simulations (after Philips, 1994). Horizontal resolution is indicated by either the spectral wave number of truncation ('R' for rhomboidal and 'T' for triangular truncation) or latitude by longitude grid-cell resolution. Vertical resolution is indicated by the symbol 'L' and defines the number of levels in the model atmosphere.

Model	Primary Reference	Resolution
BMRC	McAvaney and Colman (1993)	R31 L9
CCC	Boer *et al.* (1992b)	T32 L10
CSIRO	McGregor *et al.* (1993)	R21 L9
GFDL	Wetherald *et al.* (1991)	R30 L14
MPI	DKRZ (1992)	T42 L19
NCAR	Hack *et al.*, (1994)	T42 L18
UKMO	Cullan (1993)	2.5° x 3.75° L19

A wide range of horizontal resolutions ranging from R21 (~3.2° latitude by ~5.6° longitude) to T42 (~2.8° latitude by ~2.8° longitude) exists among the models (Table 2.1). For the purposes of validation and comparison all models must be interpolated to a common horizontal resolution before analysis. So as not to fabricate information where no information exists, all models have been interpolated to approximately the lowest model resolution. In this case, that is the spectral R21 resolution of the CSIRO model. Interpolation is based on an inverse squares method (following Willmott *et al.*, 1985) and allows interpolation of points onto a spherical surface. So as not to favour the CSIRO model, *all* models have been interpolated to a regular 3.2° latitude by 5.6° longitude grid. The interpolation method is described in Chapter 3.

Equilibrium climate change experiments

Results of equilibrium climate change experiments from the modelling centres of the CSIRO, BMRC, UKMO, GFDL, CCC and MPI are calculated as changes in summer, September-November (SON) and December-February (DJF), as well as winter, March-May (MAM) and June-August (JJA) seasonal means are calculated. Five mixed-layer models (BMRC, CCC, CSIRO, GFDLH and UKHI) are considered. Details of the enhanced greenhouse experiments are provided in Table 2.2. The selection of experiments has been made in order to allow comparison of results for the southern African region with similar results for the rest of the globe and specifically for the Australian region (Whetton *et al.*, 1996b). As far as possible, output from modelling groups considered in Joubert (1995) are used again, although for more recent versions of the models. All of the mixed-layer models use a simple slab ocean with no ocean currents, in which the prescribed heat flux ('Q-flux') within the ocean compensates for the absence of currents under present climate conditions. All seasonal means are based on at least ten years of data post-equilibrium under both 1 x CO_2 and 2 x CO_2 conditions.

Fully-Coupled Models

Transient climate change experiments

Seasonal mean (DJF, MAM, JJA and SON) changes centred around the time of CO_2-doubling from a total of six fully-coupled models (CSIROC, GFDLC, MPIOC, MPILC, UKTR) are compared with the set of five mixed-layer models described above. Details of the transient climate change experiments are provided in Table 2.3.

All of the fully-coupled models use an atmospheric model fully-coupled to a full ocean model, incorporating a flux correction to reduce climate drift. A fully-coupled model simulation from NCAR (Washington and Meehl, 1991) has been excluded because it does not incorporate a flux correction. Coupled models which do not incorporate such a correction exhibit a marked drift away from realistic simulations of present climate (Meehl, 1995). Inclusion of such models is likely to introduce unrealistic bias into the interpretation of results (cf. Whetton *et al.*, 1996b). Where possible, 30 years of data centred around the time of CO_2 doubling are used and compared with a corresponding 30 year period from the control run.

Table 2.2. Details of the mixed-layer model experiments used.

Experiment	Reference	Horizontal Resolution (Number of waves or lat. x lon.)	Number of years used for 1 x CO_2 and 2 x CO_2 means	Global average warming (°C)
BMRC	Colman *et al.* (1994)	R21	14	2.1 [(1)]
CCC	Boer *et al.* (1992b)	T32	20	3.5
CSIRO	Watterson *et al.* (1996)	R21	30	4.3
GFDLH	IPCC (1[illegible])	R30	10	4.0
UKHI	Gregory and Mitchell (1995)	2.5° x 3.75°	10	3.5

(1) Colman *(personal communication)*

The CSIRO fully-coupled model

The CSIRO fully-coupled model contains atmospheric, oceanic, sea-ice and biospheric submodels. The atmospheric model has 9 vertical levels with R21 spectral resolution and is based on the version described in McGregor *et al.* (1993). The ocean model is the GFDL grid point ocean model with 12 vertical levels (Bryan, 1969, Cox, 1984). The model uses flux corrections to couple the atmosphere and ocean components following the method described by Sausen *et al.* (1988). The coupled model and it's components, as well as the spin-up and flux correction procedures are described in detail in Gordon and O'Farrell (1996).

In the coupled model control integration, CO_2 amount is set at 330ppm. In total, 300 years of the control integration are considered. The control run showed only a small global mean surface temperature drift over the 105 year period (Gordon and O'Farrell, 1996), and this remains small throughout the control integration (O'Farrell, *personal communication*). The transient experiment is started after 30 years of the control integration and allows CO_2 concentration to increase at a rate of 1% per annum (compounded). Using this scenario, CO_2-doubling occurs after 70 years. This is probably unrealistically high, and may be compared to the IPCC IS92a emission scenario which gives a doubling of equivalent CO_2 after 95 years (IPCC, 1995). Mean sea-level pressure and surface air temperature data for the 300-year control integration and 270 years of the transient experiment are considered.

Table 2.3. Details of the fully-coupled model experiments used. All models simulate a linear 1 % per annum (compounded) increase in CO_2 concentration in their enhanced greenhouse runs.

Experiment	Reference	Horizontal Resolution (Number of waves or lat. x lon.)	Number of years used for 2 x CO_2 means	Number of years used for 1 x CO_2 means	Global average warming at the time of CO_2 doubling (°C)
CSIROC	Gordon and O'Farrell (1996)	R21	30 (1)	30 (3)	2.1
GFDLC	Manabe *et al.* (1991)	R15	20 (2)	100 (4)	2.3
MPILC	Cubasch *et al.* (1993)	T21	10 (2)	10 (4)	1.4 (5)
MPIOC	Lunkeit *et al.* (1994)	T21	10 (2)	10 (4)	1.4 (5)
UKTR	Murphy, (1995), Murphy and Mitchell (1995)	2.5° x 3.75°	10 (2)	10 (4)	1.7

(1) centred 10 years before CO_2 doubling
(2) centred at doubling
(3) corresponding years of control run
(4) full control run
(5) Lunkeit (*personal communication*)

The Second Hadley Centre fully-coupled model

Output from the control integration and two transient climate change experiments from the Hadley Centre for Climate Prediction and Research model has been used (Mitchell *et al.*, 1995a; Mitchell and Johns, 1996). The horizontal resolution of both the atmospheric and oceanic components is 2.5° of latitude by 3.75° of longitude. The atmospheric model is a version of the unified numerical weather prediction/climate model of the UKMO (Cullen, 1993) with 19 vertical levels. The ocean model is derived from Cox (1984) with a vertical resolution of 20 levels. The model is also flux-corrected to reduce errors in the present climate simulation, following Murphy (1995). These include fluxes of heat and water but exclude the explicit sea-ice adjustments used by Murphy (1995). As a result, there is no perceptible drift in global mean surface air temperature in the control simulation (Mitchell and Johns, 1996).

CO_2 concentration is held constant in the control integration. In both transient climate change experiments, the standard CO_2 concentration for the period 1960-1990 in the model is increased to represent the change in forcing due to all greenhouse gases (effective CO_2 concentration). The first transient climate change experiment (GHG), is forced by increasing concentrations of greenhouse gases only. After 1990, the CO_2 concentration is increased by 1% per annum (compounded) up to 2100. The second experiment (SUL) includes increases in both CO_2 and direct sulphate aerosol forcing (by scattering). As the model's radiation scheme does not allow explicitly for scattering of radiation by atmospheric aerosols, their effect has been represented by an increase in surface albedo over certain regions of the globe, including southern Africa (Mitchell *et al.*, 1995a). The pattern of aerosol loading to 1990 is based on the calculated annual mean distribution (seasonal variation is ignored) for the 1980s (Langner and Rodhe, 1991) and scaled by the estimated annual mean sulphate emissions (Dignon and Hameed, 1989; Hammed and Dignon, 1992). A sulphate distribution for 2050 (cf. Mitchell *et al.*, 1995a) was obtained using a sulphur-cycle model (Langner and Rodhe, 1991). Between 1990 and 2050, the loading pattern was interpolated, with the field scaled to give the global loading for IPCC scenario IS92a (Fig. 2.1). Output considered below include mean, maximum and minimum surface air temperature, mean sea-level pressure, as well as geopotential height and u- and v-wind components at 500 and 700 hPa.

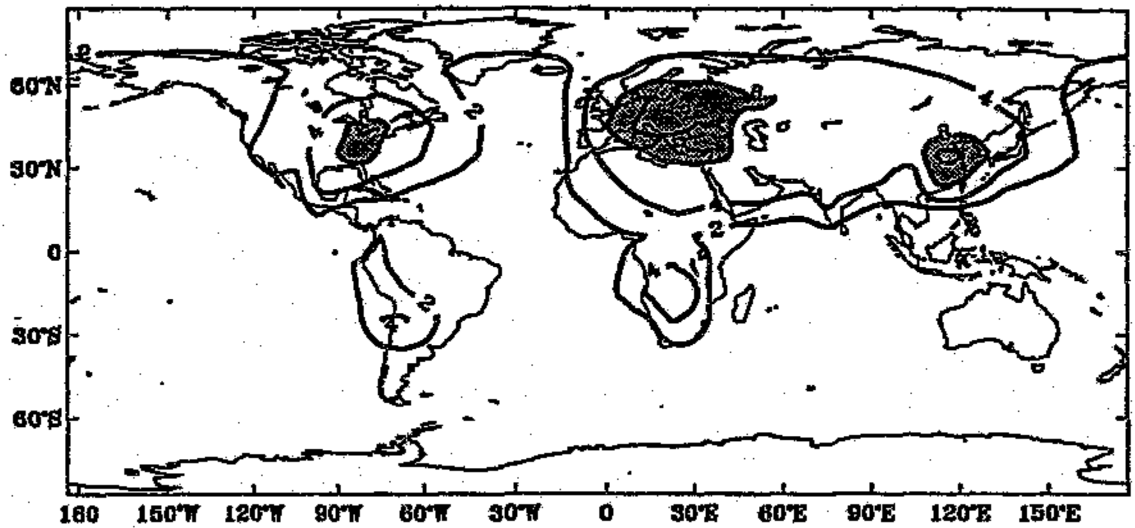

Figure 2.1. Mass loading of sulphate aerosol due to human activity derived from the sulphur cycle model of Langer and Rodhe (1991) (after Mitchell and Johns, 1996). Contours at 2, 4, 8 and 12 mg m^{-2} and shaded above 8 mg m^{-2}.

Observational Data

Atmospheric Circulation Data

Australian Meteorological Bureau operational analyses

Observed atmospheric variables extracted from the Australian Bureau of Meteorology operational analyses include mean sea-level pressures, geopotential heights and u- and v-wind components. These data have been widely used for studies of southern hemisphere meteorology (Trenberth, 1979, 1980, 1981; Le Marshall *et al.*, 1985; Karoly and Oort, 1987; van Loon *et al.*, 1993; Hurrel and van Loon, 1994). Once daily (0000 GMT) data are available from May 1972 and twice daily (0000 and 1200 GMT) from April 1973. The data-set was discontinued in December 1992. The quality of the data has been assessed in several studies (Trenberth, 1979; Swanson and Trenberth, 1981; Le Marshall *et al.*, 1985). In general, there is some question over the reliability of data over the high southern latitudes south of 50°S, due largely to the sparse network of observing points used as the basis for the operational analyses. The 0000 GMT maps have been more carefully analysed, and the monthly mean fields have few flaws (van Loon, 1980) and are used in the current study.

Long-term mean sea-level pressure data

In order to analyse fully-coupled model simulations of inter-annual circulation variability, it is necessary to consider a longer dataset than the approximately twenty years available from the Australian Meteorological Bureau operational analyses. For this reason, observed mean sea-level pressure data for the period 1911-1985 were obtained from the reconstructed dataset of Jones (1991). The data are available on a staggered (diamond-shaped) grid extending from 20°W to 100°E and from 15°S to 60°S. The data were interpolated onto a regular 5°x5° grid extending from 10°W to 90°E and from 15°S to 60°S prior to analysis. The recontructions are best near continental areas and data are unreliable over oceanic areas between 1911 and 1951 (Jones, 1991) but are considered reliable for the period 1951-1985.

Surface Air Temperature and Rainfall

CRU baseline climatology for southern Africa

A new baseline climatology for southern Africa for the period 1961-1990 is available at a resolution of 0.5° latitude by 0.5° longitude (Hulme *et al.*, 1996). The climatology has been developed at the Climate Research Unit (CRU) of the University of East Anglia. Variables utilised from the climatology include long-term mean monthly values for mean, maximum and minimum surface air temperature and rainfall as well as monthly temperature and rainfall anomalies for the 1961-1990 period. The climatology is based on observations supplied by the meteorological agencies of the region (Hulme *et al.*, 1996). The interpolation of the 1961-1990 averages accounts for elevation as well as longitude and latitude as predictor variables. On this basis, three climate surfaces representing 'minimum', mean and 'maximum' elevation within each 0.5° cell are constructed. Interpolation of the 1961-1990 anomaly fields does not consider elevation (Hulme *et al.*, 1996). Gridded anomalies of monthly mean temperature (Jones, 1994) and rainfall (Hulme, 1994) were interpolated using a distance weighting scheme from coarser resolutions of 5° latitude / longitude and 2.5° latitude by 3.75° longitude, respectively.

While more observing sites are available for rainfall (over 900) than any other variable, reliability of the interpolated values is still problematic. Mean absolute errors (relative to selected validation sites) in the wet season are approximately 15 % (~20 mm) but rise to 40 % (~8 mm) in the dry season (Hulme *et al.*, 1996) and are higher, for example, than similar regions in Europe (Hulme *et al.*, 1995). Mean absolute errors for mean temperature are below 1°C for minimum and maximum temperatures, although seasonal differences occur in the accuracy of the temperature surface. The CRU rainfall climatology compares well with other gridded climatologies (e.g. Legates and Willmott, 1990), except in regions of sharp topographic gradients in the southern Cape region (Hulme *et al.*, 1996). Given the use of three elevation surfaces, the CRU climatology may be considered more accurate under such conditions.

****

The sources and preparation of both climate model and observational data to be used in this thesis have been described. The methodologies and statistical procedures used in the thesis are described in the following chapter.

CHAPTER THREE

STATISTICAL METHODS

Interpolation

Observational data are often recorded for individual stations. For comparison with output from climate models, these data require interpolation to a regular latitude by longitude grid. In addition, interpolation procedures are required when observations on a regular grid are to be compared to model output, or where output from several models at differing resolutions are to be compared. However, comparison between models is complicated by the fact that GCM output is provided on an areal grid cell basis, not grid points, and the comparison of several GCMs requires the interpolation of the models grid cell fields to a common grid. The choice of interpolation scheme may affect results, as cells from different GCMs may straddle climate and coastal boundaries in different ways. More importantly, the use of different interpolation schemes in separate studies further complicates finding a basis for comparison between studies (Joubert and Hewitson, 1996).

The interpolation scheme used below to interpolate both observations and climate model output to a common resolution is based on an inverse squares method following Shepard's (1968) local search method, and allows interpolation of points onto a spherical surface (Willmott *et al.*, 1985). Shepard's (1968) interpolation function estimates a value at each node of a predetermined lattice from a small number of nearby original data-points. The contribution of the nearby points to the estimated value of the point at each node is determined by weighting the data points according to their distance from the node. To allow for the curvature of the earth, the distance between all original data-points and nodes is calculated in spherical co-ordinates (Willmott *et al.*, 1985). The algorithm therefore explicitly accounts for the reduction in surface area enclosed by a given grid box that occurs closer to the poles. The policy adopted below is to interpolate both observations and simulations to a common resolutio ch approximates the lowest common resolution among the data.

Measures of Consensus

The uncertainties associated with the representation of physical processes in climate models often severely limit the extent to which projections of future climate from such models can be interpreted with confidence. One valuable means of increasing the level of confidence with which a projection of future climate can be interpreted is to define the level of agreement, or *consensus*, which exists amongst a range of climate models. An important reason for the growing confidence with which climate models are used to project climate change on global and hemispheric scales is the level of consensus which exists amongst the models (IPCC, 1995). Hence, considerable confidence exists in projections that global mean surface air temperature will increase by about 2°C by 2100 relative to 1990 (IPCC, 1995; given IPCC emission scenario IS92a, assuming the "best estimate" value of climate sensitivity, and including the effects of future increases in aerosols). Measures of inter-model consensus are being increasingly utilised (cf. Henderson-Sellers and Hanson, 1995, Whetton *et al.*, 1996b).

A measure of consensus for projected changes in climate over southern Africa is calculated based on the number of models which project a positive increase in the variable in question at each grid point. This method readily allows spatial patterns of agreement within a group of models to be identified. Greater confidence in the sign of projected changes may be expressed in regions where consensus between models is greatest. Greatest confidence exists in regions where models of a different type (for example, mixed-layer and fully-coupled models) also display agreement.

Consensus between models in terms of projected changes in climate does not, of itself, indicate sufficient confidence in the projection for it to be interpreted without reservation. An important additional component is to consider the level of consensus which exists between simulated and observed climate. Confidence in projected changes in climate from any model is greater when the model is capable of simulating present climate realistically. Once again, this is a necessary but not sufficient pre-requisite for interpreting projections of regional climate change (Wilson and Mitchell, 1987). As stated above, the uncertainties implicit in all climate models must be stated and understood clearly when interpreting projected climate change, particularly on regional spatial scales. To improve (although not guarantee) the level of confidence in projected changes over southern Africa, a second measure of consensus between models for simulations of present climate is defined. Those models which display *both* good agreement with observed climate *and* consensus in projections of future climate are most reliable.

A measure of consensus for present climate simulations which defines both model-observed and model-model agreement uses a counter, x_{ij} defined by

$$x_{ij} = \begin{cases} 1 \\ 0 \end{cases} \tag{3.1}$$

where $x_{ij} = 1$ if the simulated mean value at the i^{th} grid point for the j^{th} model falls within one standard deviation of the observed mean, and $x_{ij} = 0$ otherwise. It is then possible to calculate

$$N_i = \sum_{j=1}^{n} x_{ij} \tag{3.2}$$

where n represents the total number of models (n=7) and N_i the number of models at the i^{th} grid point which simulate a value of a given variable within one standard deviation of the observed mean. Values of N_i range from zero, indicating no agreement between models and very poor agreement with observations (no model within one observed standard deviation) to N_i = 7, indicating perfect inter-model and good agreement between the model and observations. A secondary issues relates to the reliability of the observations used to evaluate model performance. A weakness of the present measure of consensus is that it does not incorporate an indication of the uncertainty which surrounds the observed value. For the present analysis, the assumption is made that all observed quantities are reliable and therefore can be used for the purposes of model evaluation.

Harmonic Analysis

Harmonic analysis allows the description of the spatial and temporal variation of climatological series by defining periodic behaviour in the form of oscillations about a mean value (Jenkins and Watts, 1968; Rayner, 1971). Harmonic analysis has been used to describe variations in time series of most atmospheric variables including rainfall, sea-level pressures, geopotential heights, winds and temperatures (McGee and Hastenrath, 1966; van Loon, 1967; van Loon *et al.*, 1968; van Loon, 1972; Trenberth, 1983; Ropelewski and Halpert, 1986; Lindesay, 1988; Hurrell and van Loon, 1994). The importance of zonal standing waves in the southern hemisphere has been extensively studied using zonal harmonic analysis (Taljaard *et al.*, 1969; van Loon and Jenne, 1972; Trenberth, 1979, 1980; Wallace, 1983; Mo and van Loon, 1984; van Loon *et al.*, 1993). Zonal harmonic analysis has also been used to assess the simulation of standing waves in the southern hemisphere by climate models (Xu *et al.*, 1990; Mullan and McAvaney, 1995).

Given an oscillation around a mean of A_0, over a finite distance, X, with an amplitude A and frequency (wave number) f, the observed value at any point x, will be

$$y_x = A_0 + A\cos\left(\frac{2\pi f x}{X} - \phi\right) \tag{3.3}$$

where ϕ represents the phase angle, from an arbitrary starting point x.

Equation 3.3 can be expanded to allow for more than one oscillation to be present in the series. Hence the series can be seen as the sum of all frequencies f_j with corresponding amplitudes A_j and phase angles ϕ_j, giving a Fourier series:

$$y_x = \int_0^\infty A_j \cos\left(\frac{2\pi f_j x}{X} - \phi_j\right) dj \tag{3.4}$$

The amplitude and phase angle of each harmonic can be obtained from

$$A_j = \sqrt{a_j^2 + b_j^2} \tag{3.5}$$

and

$$\phi_j = \tan^{-1}\left(\frac{b_j}{a_j}\right) \tag{3.6}$$

where

$$a_k = \frac{2}{n}\sum_{i=1}^{n} y_i \cos\left(\frac{2\pi ki}{n}\right) \tag{3.7}$$

and

$$b_k = \frac{2}{n}\sum_{i=1}^{n} y_i \sin\left(\frac{2\pi ki}{n}\right) \tag{3.8}$$

The maximum number of harmonics that can be defined for a series of length N is $N/2$. In the case of monthly mean time-series, this would be six. The phase angle in this case would indicate the time of year that the maximum (a) occurs on that harmonic. In terms of zonal harmonics analysis, the phase angle represents the longitudinal position (in degrees) of the first ridge of the wave associated with harmonic *j*.

Spectral Analysis

Harmonic analysis assumes that time series are deterministic and hence that amplitudes, frequencies and phases of harmonics are fixed (Jenkins and Watts, 1968). In cases where it is of interest to investigate inter-annual variability in a climatological time series, this assumption is violated and hence the approach is inappropriate. Using spectral analysis, the problem is avoided by defining quasi-continuous oscillations of arbitrary length which are unrelated to the total length of the series and calculating the spectral power across those defined wave bands. Jenkinson's (1977) method of spectral analysis is used here. The time series is defined in terms of oscillations with arbitrary period, λ_j and frequency $f_j = \lambda_j^{-1}$.

For discrete data, equation 3.4 becomes

$$y_i = \sum_{j=0} A_j \cos\left(\frac{2\pi f_j i}{n} - \phi_j\right) \tag{3.9}$$

where $f_j = 0.5e^{-kj}$, thus giving a set of geometrically increasing wavelengths. The tuning parameter k can be defined to determine the resolution at which the spectral ordinates are calculated. As with harmonic analysis, equation 3.9 can be broken into separate sine and cosine components, and the parameters A_j and ϕ_j calculated as in equations 3.5 and 3.6.

Sampling errors can result in the identification of spurious quasi-periodicities and so it is necessary to test the significance of the spectral peaks. The X^2 contribution to the total variance of each wave length is

$$X^2 = v_j H_j \tag{3.10}$$

where $_j$ represents the degrees of freedom associated with wave j and H_j represents its standardised variance.

Principal Components Analysis

Temporal variability across a spatial field of $i = 1, ...n$ observations is usually represented at a particular point by $j = 1, ...m$ time series, x_j. Meteorological variables often covary across a spatial field and therefore it is useful to describe $k = 1, ...m$ new variables ξ_k, or principal components, which describe variability over the field as a whole (Overall and Klett, 1972; Richman, 1986). Often, variability within the field can be explained by only a few principal components. The principal components can be defined by a linear combination of the original variables and a different weighting α_{kj}, associated with each principal component such that

$$\xi_{ki} = \alpha_{k1} x_{1i} + \alpha_{k2} x_{1i} + \ldots \alpha_{km} x_{mi} \tag{3.11}$$

or, expressed in vector notation,

$$\mathbf{Z} = \mathbf{F}\mathbf{A}^{\mathrm{T}} \tag{3.12}$$

where **Z** is the original data matrix, **F** the matrix of principal components or principal component scores, and **A** the matrix of component loadings.

By convention, the loadings **A** are transformed under two constraints. Firstly, they are transformed to maximise the proportion of variance explained by each successive component ξ_k, so that the variance in the data field is explained by as few components as possible. This is achieved by normalising the coefficients by requiring that the squares elements of the vector of coefficients $\mathbf{a}_k$ sum to unity i.e.

$$\mathbf{a}_k \mathbf{a}_k^T = \sum_{j=1}^{m} \alpha_{kj}^2 = 1.0 \tag{3.13}$$

A second constraint is that the principal components are orthogonal and therefore that the correlations between the principal components are by definition, zero i.e.

$$\xi_i \xi_j^T = 0.0 \qquad i \neq j \tag{3.14}$$

The variance of each principal component, λ_k, or eigenvalue, is given by

$$\lambda_k = \mathrm{var}(\xi_k) = \xi_k \xi_k^T \tag{3.15}$$

The sum of eigenvalues represents the total variance in the data field. Hence, the proportion of variance explained by each principal component $\mathrm{var}(\xi)$ is estimated using

$$\mathrm{var}(\xi_i) = \frac{\lambda_i}{\sum_{k=1}^{m} \lambda_k} \tag{3.16}$$

The matrix of component loadings can be rotated using, for example, the VARIMAX criteria (Richman, 1986) in order to reduce the number of original variables with non-zero loadings on the principal components and to increase the weights of the original variables with large loadings. The rotation is achieved without changing the variances of the unrotated principal components and retaining their orthogonality. The rotation of principal component loadings is affected by the number of principal components which are retained (Richman, 1986). While no theoretical guidelines exist for deciding how many principal components to retain, an arbitrary cut-off point of 5 % of the total variance has been adopted (following Mason, 1995). In the case of the analysis presented in Chapter 6 only observed principal component loadings are rotated in this manner, however. A specific rotation is applied to the matrices of simulated loadings in order to transform them into a matrix as much as possible like the matrix of observed loadings.

Procrustes Target Rotation

Unrotated principal component loadings of simulated mean sea-level pressures are rotated to fit, as closely as possible, the matrix of observed principal component loadings using Procrustes target rotation (Green, 1952; Hurley and Cattel, 1962; Schönemann, 1966;

Richman, 1986; Richman and Easterling, 1988). The method is described diagramatically in Figure 3.1. The purpose of Procrustes Target Rotation is to maximise the agreement between the two matrices by finding a transformation matrix which provides the optimal least-squares fit between the target (observed) and simulated matrix, using a linear combination of principal components (Richman, 1986). Procrustes target rotation is used to test explicitly the ability of the climate models to simulate the principal modes of observed variability in mean sea-level pressures.

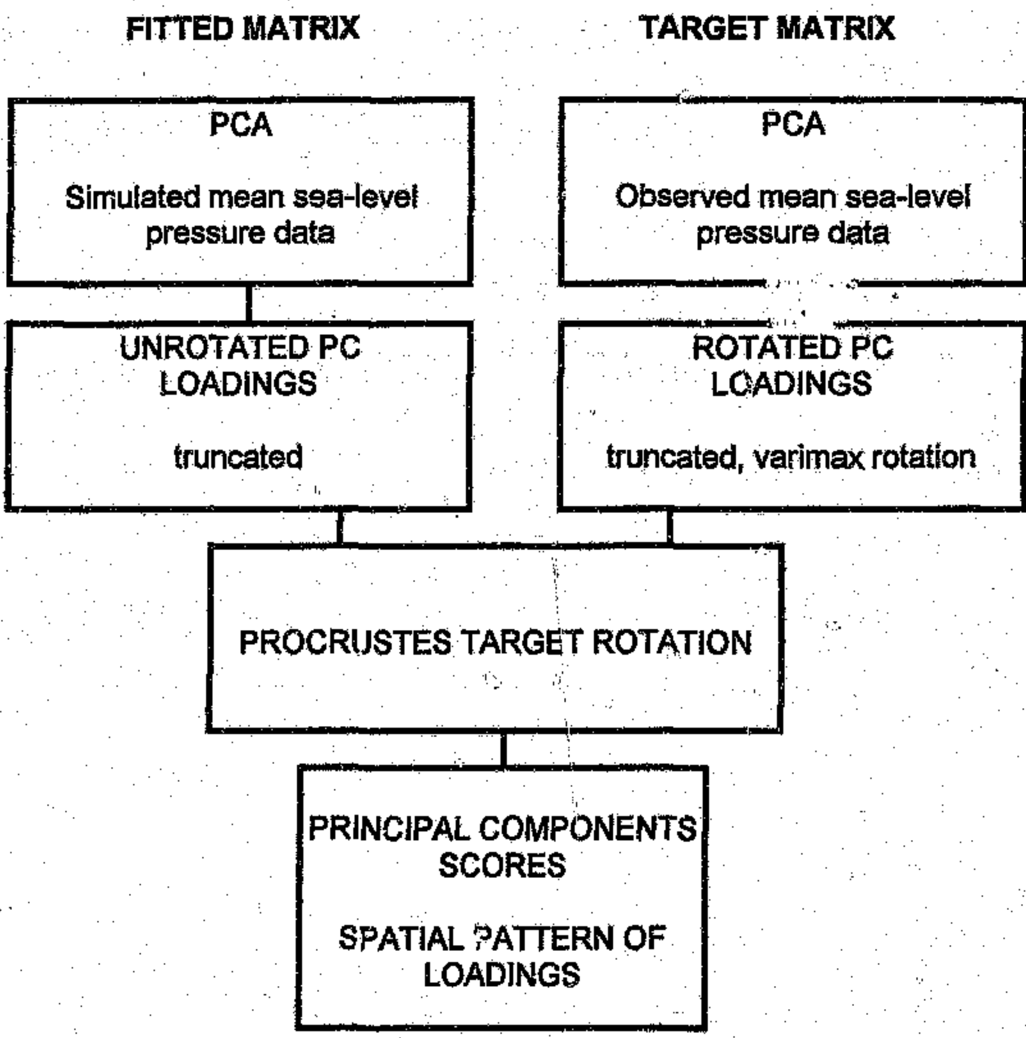

Figure 3.1 Flow diagram describing the calculation of observed principal components and the use of Procrustes Target Rotation on the unrotated simulated principal component scores.

The Procrustes equation (Richman, 1986) is

$$\mathbf{B} = \mathbf{AT} + \mathbf{E} \tag{3.17}$$

where $\mathbf{B}$ is the n x r target matrix, $\mathbf{A}$ is the n x r principal component unrotated loading matrix, $\mathbf{T}$ is the r x r transformation matrix and $\mathbf{E}$ is the n x r matrix of discrepancies or residuals. The objective is to find a transformation matrix $\mathbf{T}$ such that

$$\mathrm{trace}\left(\mathbf{E}^{\mathrm{T}}\mathbf{E}\right) = \mathrm{trace}(\mathbf{B} - \mathbf{AT})^{\mathrm{T}}(\mathbf{B} - \mathbf{AT}) \quad \text{is a minimum} \tag{3.18}$$

Two-Way Analysis of Variance

Two-way analysis of variance (ANOVA) is used to test the statistical significance of differences between several trials. It is applied to time series of simulated and observed surface air temperatures with the objective of determining whether or not the models simulate temperature variability which is statistically significantly different from that which is observed. ANOVA is based on distinguishing between two systematic sources of variation; variation between the samples and random variation within each sample (e.g. Clarke and Cooke, 1983).

Given observations y_{ij} (i = 1,2, ...k; j = 1,2, ...n_i) from k samples or treatments and n_i observations within each treatment. The mean of observations within each sample $\overline{y}$ is given by the sample mean

$$\overline{y}_i = \frac{1}{n_i}\Sigma_j y_{ij} \tag{3.19}$$

and the mean of all values is given by the grand mean

$$\overline{y} = \frac{\Sigma_{ij} y_{ij}}{\Sigma_i n_i} = \frac{\Sigma_i n_i \overline{y}_i}{\Sigma_i n_i} \tag{3.20}$$

The total square deviation of each data value from the corresponding mean is given by the sample sum of squares

$$s_i^2 = \Sigma\left(y_{ij} - \overline{y}_i\right)^2 \tag{3.21}$$

The statistical model assumes that the overall variation in the data is defined by two components representing the deviation between the treatments and random deviation between the observations within each treatment (known as the residual). The deviation due to treatment i is defined as the difference between the mean of treatment i the grand mean,

$$\overline{y}_i - \overline{y} \tag{3.22}$$

The residual is given by difference between each observation in treatment i and the mean of each treatment i,

$$y_{ij} - \overline{y}_i \tag{3.23}$$

Therefore, any observations y_{ij} can be written as the sum of the grand mean, the deviation due to treatment and the residual, i.e.

$$y_{ij} = \overline{y} + \left(\overline{y}_i - \overline{y}\right) + \left(y_{ij} - \overline{y}_i\right) \tag{3.24}$$

The overall difference due to differences in treatment are measured by calculating the treatment sum of squares (TSS) so that

$$\text{TSS} = \sum\left(\overline{y}_i - \overline{y}\right)^2 \tag{3.25}$$

Similarly, the variation due to random errors within each treatment is given by the sum of squares of the residuals or error sum of squares (ESS)

$$\mathrm{ESS} = \sum \left(y_{ij} - \bar{y}_i \right)^2 \tag{3.26}$$

and the total sum of squares is given by TSS + ESS.

Under the null hypothesis that the differences between treatments (samples) are due to random sampling errors and that all samples considered arise from the same statistical population, an F-statistic can be calculated so that

$$\mathrm{F} = \frac{\mathrm{TSS}/(k-1)}{\mathrm{ESS}/(n-k)} \tag{3.27}$$

where k represents the number of treatments and $n = \sum_{i=1}^{k} n_i$, or the sum of all observations on all treatments.

****

The statistical methods used in the processing and analysis of data in this thesis have been described. The representation of present mean climate and climate variability by a range of models is assessed in Section II.

SECTION II

SIMULATIONS OF PRESENT CLIMATE

CHAPTER FOUR

AMIP SIMULATIONS OF PRESENT CLIMATE

Introduction

Several features of the circulation of the southern hemisphere are unique. The differing distributions of land, sea and ice between the northern and southern hemispheres have important implications for the dominant climatic forcing in each hemisphere. The almost uninterrupted ocean between 35° and 70°S and the permanent Antarctic ice sheet result in steep meridional temperature and pressure gradients. As a consequence, mid-latitude westerlies in the southern hemisphere are stronger than in the northern hemisphere, flow throughout the troposphere is more zonal (Adler, 1975) and zonal standing waves 1 and 2 dominate at higher latitudes (van Loon and Jenne, 1972). Given the differences in mean circulation patterns between the two hemispheres, evaluations of climate model performance must consider simulations of the southern hemisphere separately from the northern hemisphere. Adequate representation of circulation in the northern hemisphere cannot be used as a proxy for climate studies in the southern hemisphere.

Relatively few attempts have been made to assess GCM performance throughout the southern hemisphere (e.g. Xu *et al.*, 1990) and all have been hampered by the availability and reliability of observational data. Several well-documented errors (chief among them an inability to simulate the strength of the mid-latitude westerlies) can be related to the coarse spatial resolution of most early atmospheric models (Meehl and Albrecht, 1991; Boer *et al.*, 1992a). Higher-resolution models (of the order of T42, or ~2.8° latitude by ~2.8° longitude and 18 or more vertical levels) generally provide improved simulations of the meridional pressure gradient and hence strength of the mid-latitude westerlies (Boer *et al.*, 1992a; Hack *et al.*, 1994). Earlier systematic errors in the representation of the intensity of southern hemisphere circulation have been related to both the spatial resolution of the models as well as the representation of tropical convection. Improvements in the representation of tropical convection result in proportionally greater transports of heat and moisture higher into the troposphere, which have the effect of improving the simulation of extratropical climate and the response in the extratropics to imposed sea-surface temperature anomalies (Meehl and Albrecht, 1988, 1991). Another consequence of improved spatial resolution is a better representation of Antarctic topography. As the zonal asymmetry of standing wave 1 at 500 hPa as well as the circumpolar trough is essentially a response to the shape of the Antarctic continent (van Loon, 1967; van Loon and Jenne, 1972), improved representation of the continent results in an improved representation of the intensity and seasonal location of the circumpolar trough (Boville, 1991, Parrish *et al.*, 1994). Similarly, stronger and better-defined subtropical and polar jet streams also result from increased spatial resolution (Kinter *et al.*, 1988; Kitoh *et al.*, 1990; Kitoh, 1994; Mullan and McAvaney, 1995).

Tropospheric circulation in the vicinity of southern Africa is known to undergo significant adjustment in association with inter-annual rainfall variability over the subcontinent (Harrison, 1986; Tyson, 1986). These have been related to hemisphere-wide circulation adjustments in the Walker circulation in response to ENSO events in the tropical Pacific Ocean (Lindesay, 1988). Evaluations of GCM simulations of circulation in the southern African region have largely considered early (pre-1990) coarse-resolution mixed-layer models (e.g. Joubert, 1995). Almost none of the existing studies provide a comprehensive assessment of model performance throughout the depth of the troposphere nor the representation of inter-annual variability over southern Africa by atmospheric GCMs.

The Atmospheric Model Intercomparison Project (AMIP) involves an extensive range of current (generally high resolution) atmospheric GCM simulations and aims to identify systematic regional errors in the models (Gates, 1992). Assessments of the simulation of mean climate by a selection of AMIP simulations will serve to update the evaluation of pre-1990 (coarse resolution) models provided by Joubert (1995). In addition, the atmospheric GCMs are forced by observed sea-surface temperatures for the 1979-1988 decade. This enables the simulation of known atmospheric variations during that period to be assessed as a model sensitivity study. The 1980s were a period of marked inter-annual variability in the climate of southern Africa. Much of southern Africa experienced prolonged drought conditions in the early 1980s as a consequence of the 1982/83 ENSO event (Schulze, 1984). In contrast, the summer of 1987/88 was considerably wetter than average, and severe flooding occurred (Triegaardt *et al.*, 1988; Lindesay and Jury, 1991). The ability of the AMIP models to simulate such events and the large-scale adjustments in circulation known to have accompanied marked inter-annual rainfall variability during the AMIP decade will be examined.

Mean Climate

Surface Circulation

Mean sea-level pressure

Characteristic features of the mean sea-level pressure distribution in the vicinity of southern Africa are illustrated in Figure 4.1. These include lower pressures over the tropical subcontinent (indicating the southerly extension of the ITC) in summer (January), two well-defined oceanic anticyclones adjacent to the subcontinent, and a strong meridional pressure gradient (Fig. 4.1). During July, the oceanic anticyclones intensify and shift northward, with a concomitant deepening of the circumpolar trough (Fig. 4.1b).

A selection of four AMIP simulations of mean sea-level pressure is shown in Figures 4.2 and 4.3 for January and July respectively. All of the AMIP models provide an improved simulation of the mean sea-level pressure distribution when compared to earlier simulations (e.g. Joubert, 1995), reproducing the broad zonal patterns and the seasonal migration of circulation systems accurately. In January (Fig. 4.2), the relative position of the oceanic anticyclones and the strength of the westerlies are well captured, although the pressure gradient simulated by the lower-resolution CSIRO model is weaker than observed. While the simulated distribution is accurate (see the pattern correlation statistics in Table 4.1), the models both over- and under-estimate the amplitude of this pattern, expressed as the ratio of the simulated and observed spatial variances. For example, the

CCC, GFDL, NCAR and UKMO models all over-estimate the observed spatial variability, simulating larger pressure gradients between regions of high and low pressure than observed (Table 4.1). In the tropics and subtropics, there is a general tendency to over-estimate pressures over the tropical oceans and under-estimate pressures over the land (although this result is likely to be a result of the elevation of the central plateau region). Over the region as a whole, all models simulate a positive anomaly in mean sea-level pressure (Table 4.1). The anomaly is smallest in the UKMO simulation, and notably largest in the GFDL simulation, which exhibits a large positive anomaly globally throughout the year.

Table 4.1. Comparative statistics for simulated and observed mean sea-level pressure, for January and July. Statistics include a pattern correlation coefficient (r), ratio of simulated and observed spatial variances, and the difference between simulated and observed spatial means. All pattern correlations are significant at the 5 % significance level.

	JANUARY			JULY		
Model	Pattern Correlation	Ratio of spatial variance	Difference between spatial means	Pattern Correlation	Ratio of spatial variance	Difference between spatial means
BMRC	0.84	0.72	1.29	0.34	0.65	0.92
CCC	0.87	1.19	1.03	0.53	0.96	0.52
CSIRO	0.82	0.76	1.55	0.46	0.85	0.72
GFDL	0.79	1.10	5.99	0.67	0.85	7.06
MPI	0.83	0.87	1.91	0.45	1.02	1.40
NCAR	0.93	1.38	1.26	0.57	1.44	0.80
UKMO	0.90	1.35	0.16	0.58	1.42	1.50

In July, all models simulate a northward shift and intensification of the anticyclones, as well as stronger westerlies associated with the deeper circumpolar trough (Fig. 4.3). Most models do not simulate a sufficiently large meridional shift in the position of the anticyclones and pattern correlations are lower than in January as a result (Table 4.1). Both the amplitude of the simulated pattern of mean sea-level pressure, as well as the simulated magnitude of observed July pressures are improved with respect to January (Table 4.1). The UKMO simulation does not perform consistently well throughout the year, performing worse during winter than during summer. In July, the CSIRO and MPI models provide better overall simulations of mean sea-level pressure. In their analysis of zonally-averaged mean sea-level pressure simulations, Mullan and McAvaney (1995) have also shown that model performance is seasonally-dependent.

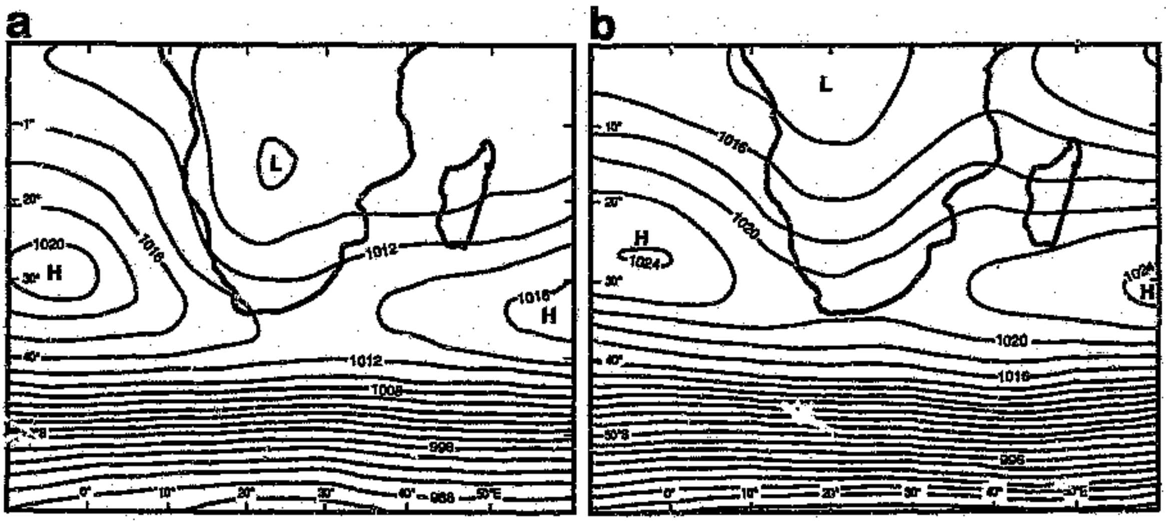

Figure 4.1. Observed mean sea-level pressure in a) January and b) July (in hPa).

The two semi-stationary oceanic anticyclones intensify during winter and undergo pronounced longitudinal shifts in position (Tyson, 1986). Accurate simulation of the seasonal changes in these systems represents an important test of the ability of the AMIP models to simulate the annual cycle of southern African circulation. Changes in the position and intensity of the high pressure systems between January and July are illustrated in Figure 4.4 by plotting the maximum pressure at any grid point for each line of longitude between 20^{0}W and 65^{0}E. In January, the models tend to over-estimate maximum pressures in both the South Atlantic and South Indian high pressure systems, with the pressure bias in the GFDL model again clearly visible (Fig. 4.4a). The centre of the simulated high pressure cells tends to be west of observations in the South Atlantic high pressure cell. During July (Fig. 4.4b), the CSIRO, CCC, BMRC and MPI models simulate maximum pressures (particularly in the South Atlantic Ocean) which are close to observations, although the GFDL, UKMO and NCAR models simulate maximum pressures which are too high. While the common (approximately R21) resolution is too coarse to allow a detailed analysis, it appears that most models simulate maximum mean sea-level pressures further north than observed in January (not shown). The latitudinal position of maximum sea-level pressure is better simulated in July, with the exception of the BMRC and CCC models, which simulate the centre of the high pressure systems further north than observed.

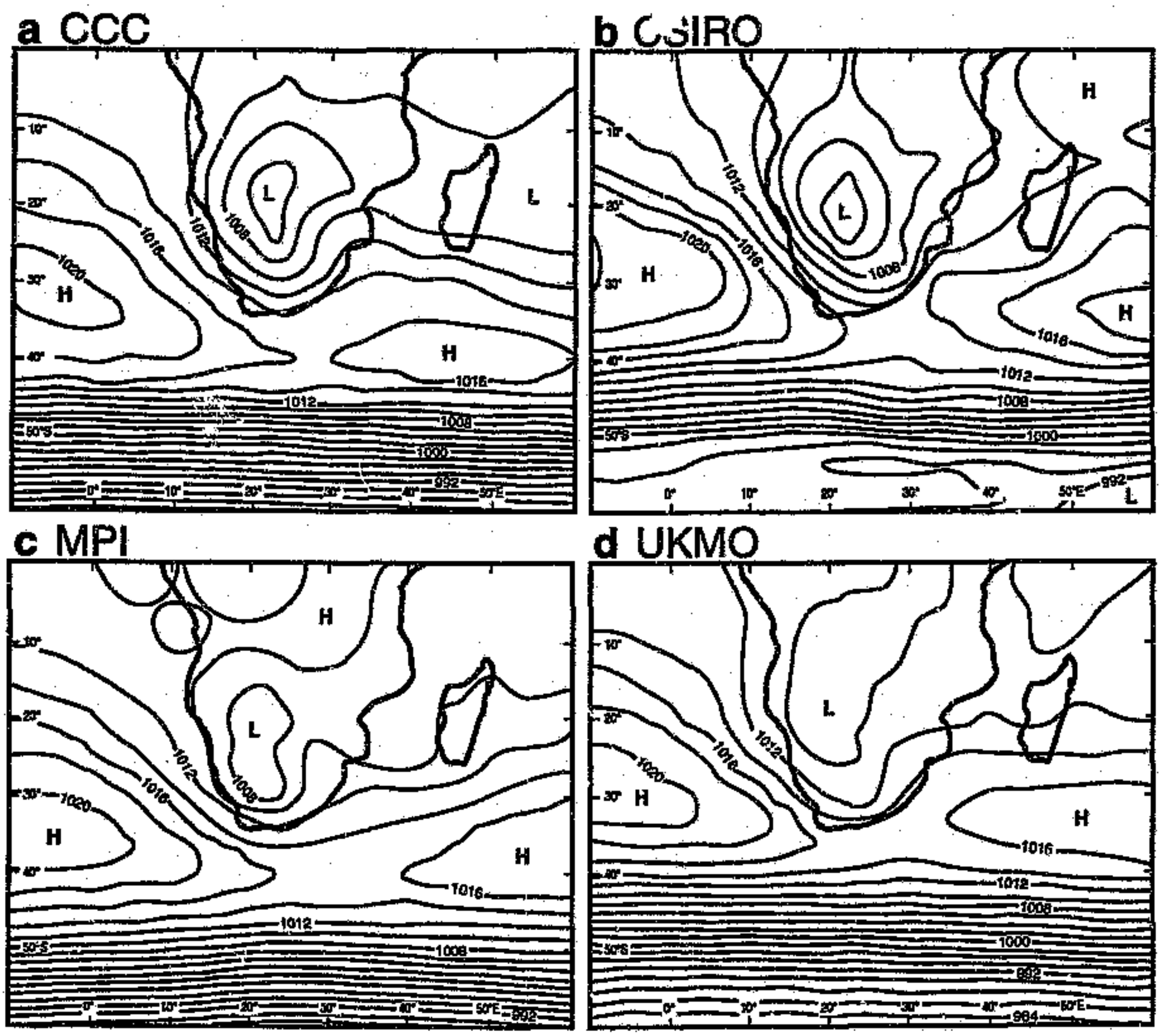

Figure 4 2. January mean sea-level pressure simulated by the a) CCC, b) CSIRO, c) MPI and d) UKMO models (in hPa).

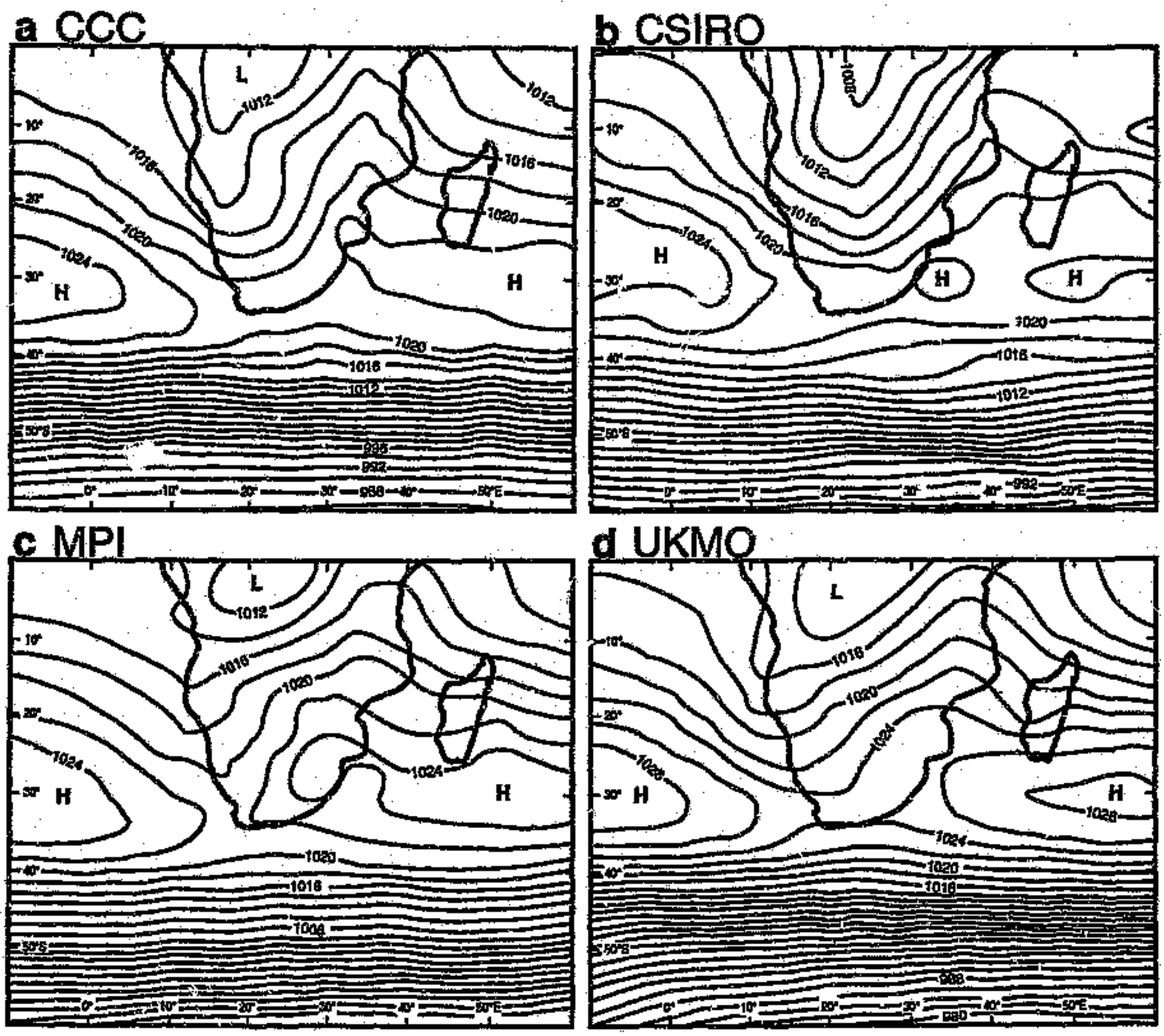

Figure 4.3. As Figure 2, but for July.

The range of model-observation agreement for simulated mean sea-level pressure is shown in Figure 4.5. Over the subcontinent, the AMIP models are not successful in simulating observed mean sea level pressures in either January (Fig. 4.5a) or July (Fig. 4.5b). The poor simulation of mean sea-level pressures over southern Africa during summer has been observed previously and attributed to a systematic error associated with the parameterisation of convection in the models (Joubert, 1995). The error may also reflect the fact that much of the subcontinent is more than 1000m above sea-level, and as a consequence, estimates of mean-sea level pressure over the interior plateau may not be a suitable measure of model performance. Agreement with observed values is better over the oceanic areas, and improves notably over the mid-latitude Indian Ocean in July (Fig. 4.5b). The higher levels of model-observed agreement in the mid-latitudes may be misleading.

Inter-annual variability in mean sea-level pressures in the subtropics and mid-latitudes is higher over the Indian Ocean than at similar latitudes in the Atlantic Ocean (Dyer, 1981; Physick, 1981) and the standard deviation of values around the observed mean may be expected to be large. The relatively good agreement statistics may be indicative of a larger range of acceptable values (a larger observed standard deviation), rather than better model performance.

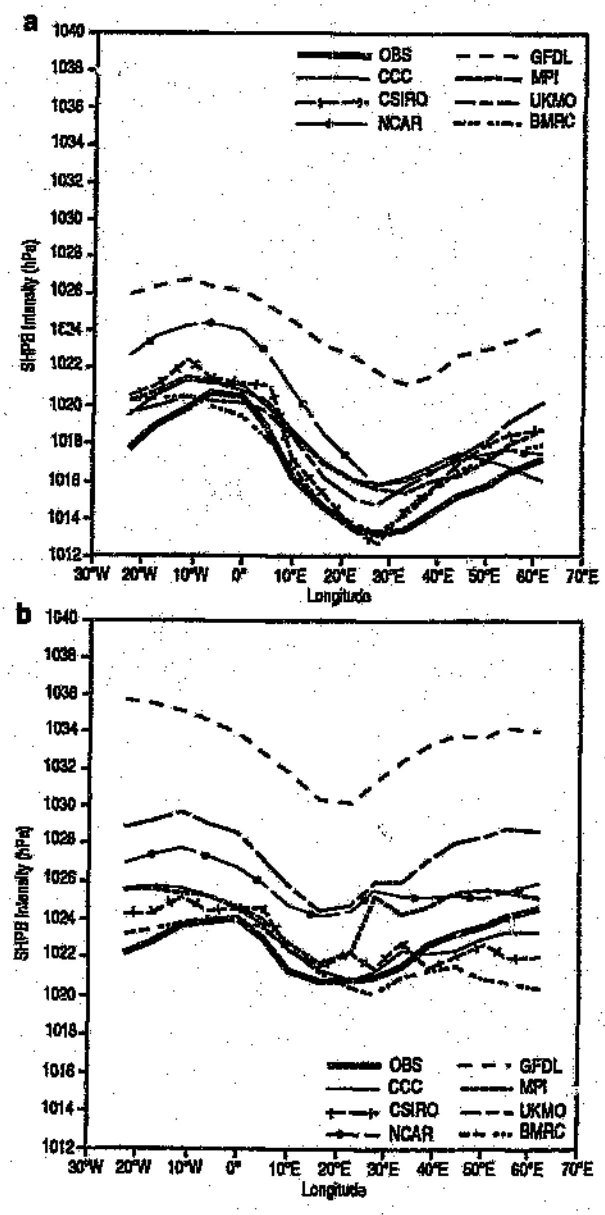

Figure 4.4. Maximum intensity of sea level pressure at each longitude between 20^0W and 65^0E during a) January, and b) July (in hPa).

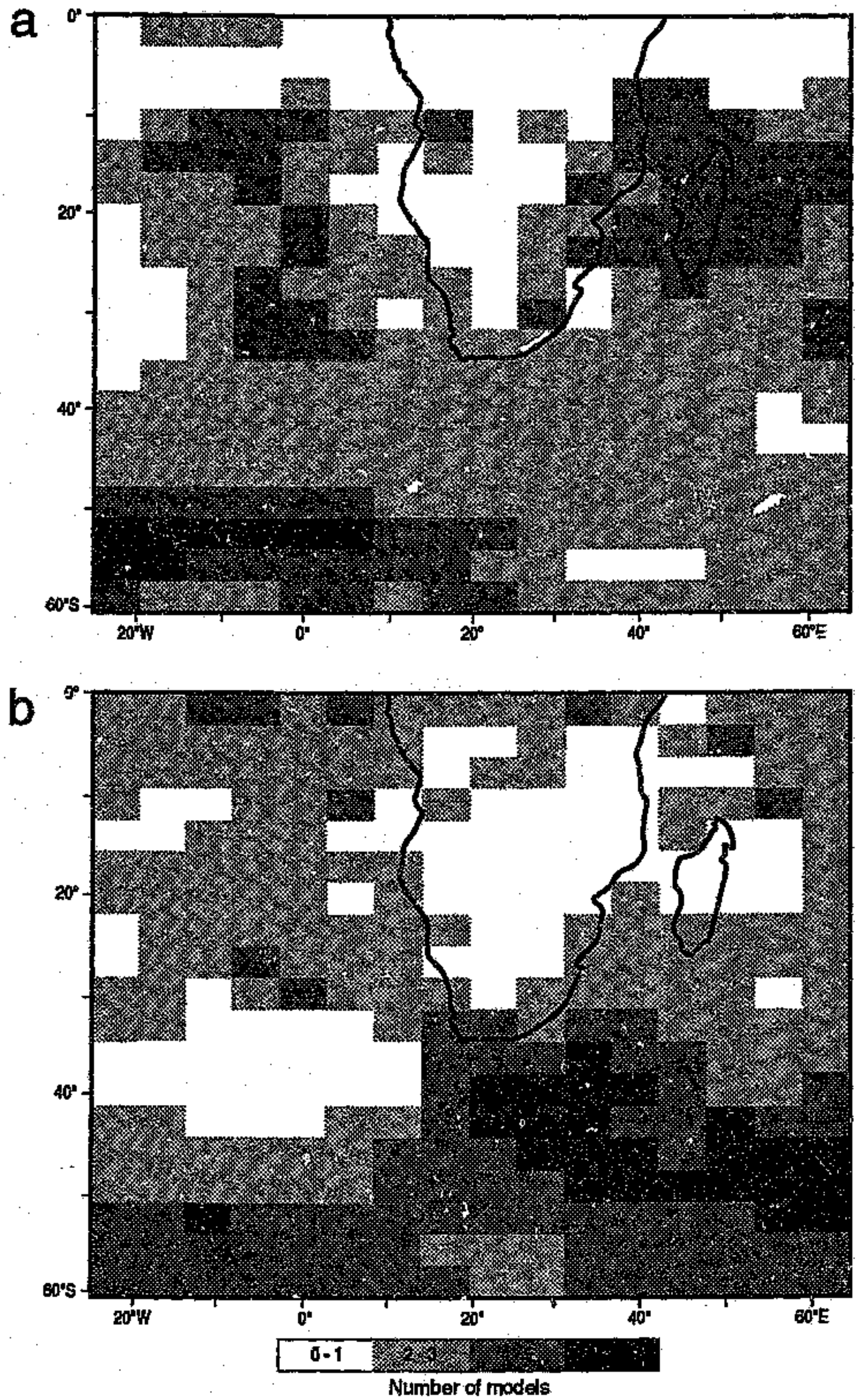

Figure 4.5. The number of models at each grid point which simulate mean sea-level pressure within one observed standard deviation a) in January and b) in July. The total number of models is 7.

Zonal winds

The increased spatial resolution and representation of tropical convection in many post-1990 atmospheric GCMs has resulted in an improved simulation of equator-pole temperature and pressure gradients at the surface and in the troposphere, thereby producing more realistic mid-latitude westerlies than simulated by the coarse resolution pre-1990 models (Boer *et al.*, 1992a; Hack *et al.*, 1994). All of the AMIP models used in the present study have spatial resolutions of R21 or higher (Table 4.1). By comparison, R21 is the highest resolution of the models considered in a previous analysis for southern Africa (Joubert, 1995). The surface (850 hPa) zonal wind profile, averaged over longitudes 25°W to 65°E, is illustrated in Figure 4.6. All models simulate the zonal wind profile well, with mean easterly flow north of 25°S, and strong westerly flow in the mid-latitudes. In January (Fig. 4.6a), the models tend to exaggerate the strength of the westerly wind maximum in the mid-latitudes slightly, locating the maximum further south than observed. This is most notable in the CCC and MPI models, which position the maximum at approximately 55°S, as opposed to the observed 45°S. Similar results have also been observed in the zonally-averaged analyses of Mullan and McAvaney (1995). During July (Fig. 4.6b), the observed strengthening and northward shift in the mean wind field is well captured, except by the lower resolution CSIRO model. In addition, the UKMO and GFDL models simulate the westerly wind maximum too far north, at approximately 40°S. The increased resolution of most of these models results in an improved simulation of mean zonal flow near the surface in the southern hemisphere mid-latitudes.

Tropospheric Circulation

Tropospheric circulation in the southern hemisphere is marked by a well-defined standing wave structure (van Loon and Jenne, 1972; Wallace, 1983). Semi-stationary forced waves predominate in the southern hemisphere, exhibiting an equivalent barotropic structure and maintaining a similar amplitude and location throughout the year (Trenberth, 1980). Zonal harmonic analysis of 500 hPa geopotential heights has shown that standing waves 1 and 3 together account for most of the variability in the annual mean pattern (Taljaard, *et al.*, 1969; van Loon and Jenne, 1972; Trenberth, 1979), with some studies indicating that the percentage of variance explained by the semi-stationary waves may exceed 99 per cent (van Loon and Jenne, 1972). A characteristic failing of pre-1990 GCMs has been an inability to reproduce the well-defined planetary wave structure and intensity of stationary eddies (Xu *et al.*, 1990; Yang and Gutowski, 1994). A consequence of this is that the zonal asymmetries (which define the standing wave structure) are generally not well reproduced (Xu *et al.*, 1990). The ability of the AMIP simulations to reproduce these tropospheric circulation features is assessed below.

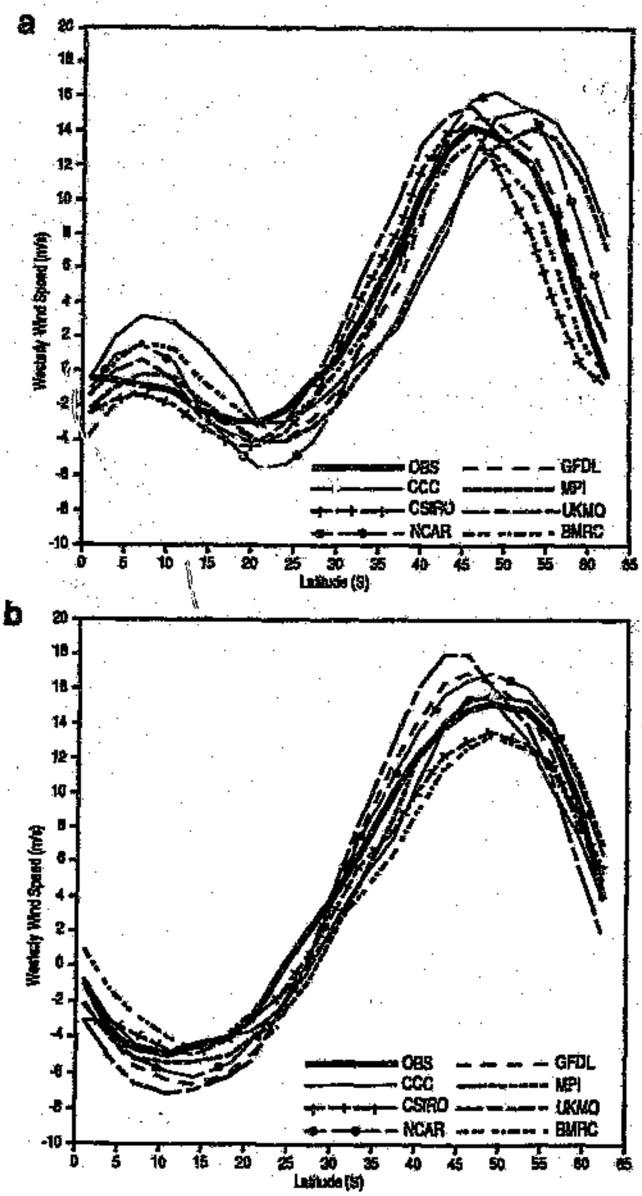

Figure 4.6. Observed and simulated zonal averages (for 20°W to 65°E) of 850 hPa zonal wind speed ($m.s^{-1}$). (a) January and (b) July.

Zonally asymmetric flow at 500 hPa

Zonal-asymmetries in 500 hPa geopotential heights are shown in Figures 4.7 and 4.8, for January and July, respectively. As shown in Figures 4.7a and 4.8a, highest values occur south of New Zealand and lowest values in the South Indian Ocean, at 50°S. The pattern is reversed at 30°S with the result of that a broad band of westerlies is located in the southern Indian Ocean, and a split jet stream structure (strongest in winter) occurs in the region of New Zealand (see Trenberth, 1980).

The three simulations shown in Figures 4.7 and 4.8 are more successful in capturing the intensified winter (July) pattern than the January pattern (cf. Mullan and McAvaney, 1995). The juxtaposition of positive and negative zonal anomalies at 30°S and 50°S in January is best captured by the UKMO model. At 50°S, all models simulate negative anomalies in the South Indian Ocean as well as positive anomalies in the region of New Zealand. The BMRC and CCC models simulate weaker zonal asymmetries than observed, indicating a weaker wave structure in the mid-latitudes. While the magnitude of zonal asymmetries in the UKMO simulation is close to observed, the positive zonal anomaly in the region of New Zealand is displaced approximately 30°E of it's observed position, indicating that the split jet structure and associated blocking in that region may not be well reproduced. In July, all the models simulate the intensification in the pattern of zonal asymmetries, although again the pattern and magnitude of the anomalies is best captured by the UKMO simulation (Figure 4.8d). Over southern Africa, the location of a ridge at 30°S and a trough at 50°S is responsible for the strong westerlies to the south of the subcontinent. The pattern is present in all of the models, although best reproduced by the UKMO model in January and the UKMO and BMRC models in July.

Standing wave structure

The most stationary component of southern hemisphere wave structure, associated with standing wave 1 is analysed using Fourier analysis. The observed and simulated position of the ridge, amplitude, and percentage of variance explained by wave 1 at 500 hPa are shown in Figures 4.9 and 4.10, for January and July respectively. From 40°S to 70°S, the ridge of wave one is located in the southern Pacific Ocean (150°W to 120°W), with a sharp discontinuity at about 40°S. Equatorward of this region, the ridge occurs between

10°W and 50°E (van Loon and Jenne, 1972). The percentage of variance explained by wave 1 displays maxima in phase with the maxima in the amplitude of the wave at subtropical, mid-latitude and subpolar latitudes.

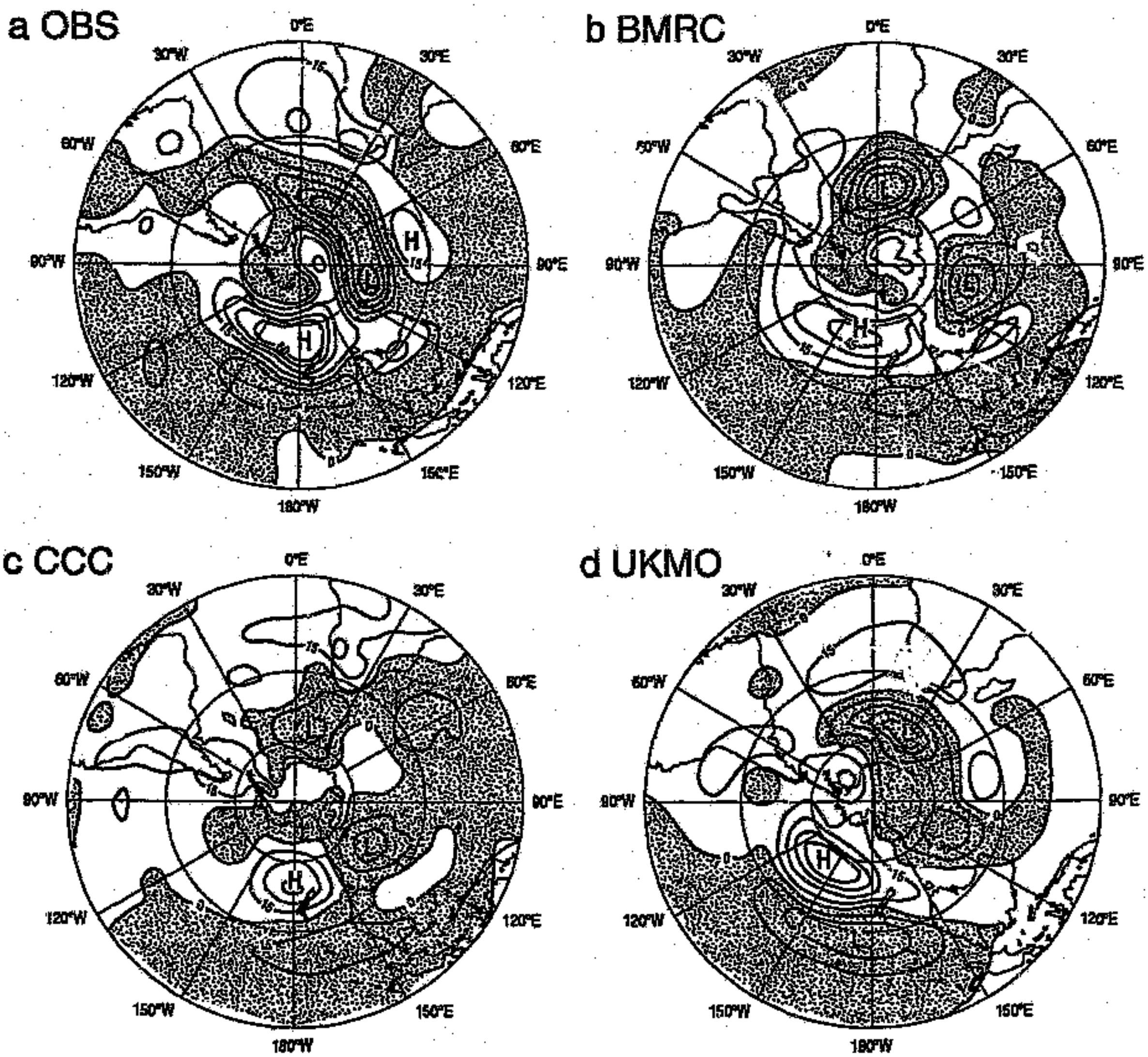

Figure 4.7. Zonally asymmetric component of the flow at 500 hPa during January, a) observed, and simulated by b) BMRC, c) CCC and d) UKMO models. Contour units are 15 gpm. Negative anomalies are shaded.

All of the models simulate the phase of zonal wave 1 at subpolar latitudes realistically, locating the ridge in the southern Pacific Ocean. These results represent an improvement over those demonstrated for a range of four spectral GCMs by Xu *et al.* (1990). The improvement may be due, in part, to the increased spatial resolution of most of these models over earlier versions, as zonal standing wave 1 in the southern hemisphere reflects the topography of Antarctica (van Loon and Jenne, 1972). The increased resolution of these models implies an improved representation of the Antarctic continent, and hence an improved simulation of the position of the ridge of standing wave 1. By comparison, the lower-resolution CSIRO model is least successful in simulating the phase of standing wave 1 in the mid-latitudes during January (Fig 4.9). All simulations display a marked improvement during July (Fig. 4.10). The seasonal variation in performance has been observed before (Mullan and McAvaney, 1995), as the simulated phase of standing wave 1 improves during the winter months, when the stationary waves are stronger (Fig. 4.10).

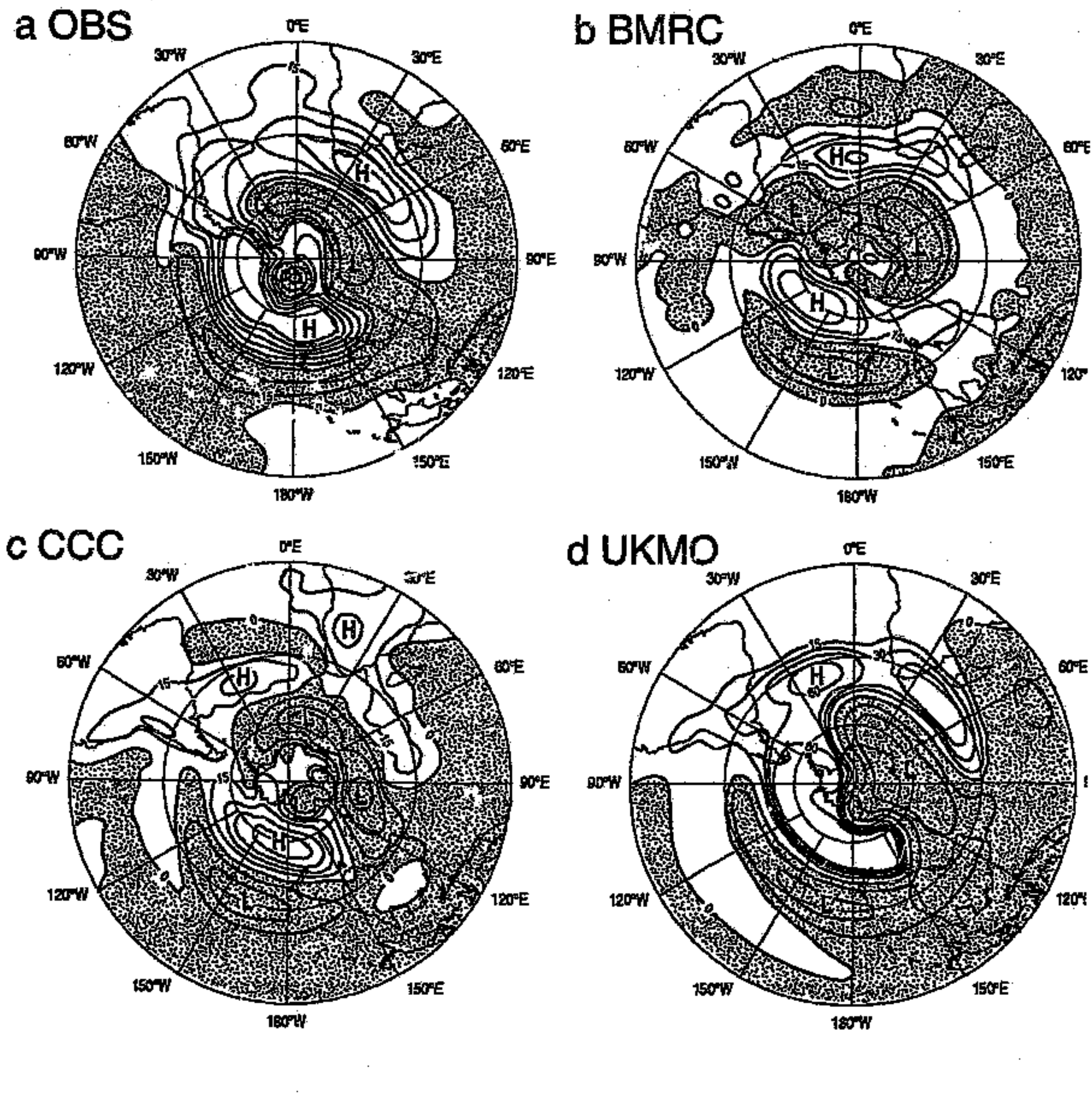

Figure 4.8. As Figure 7, but for July.

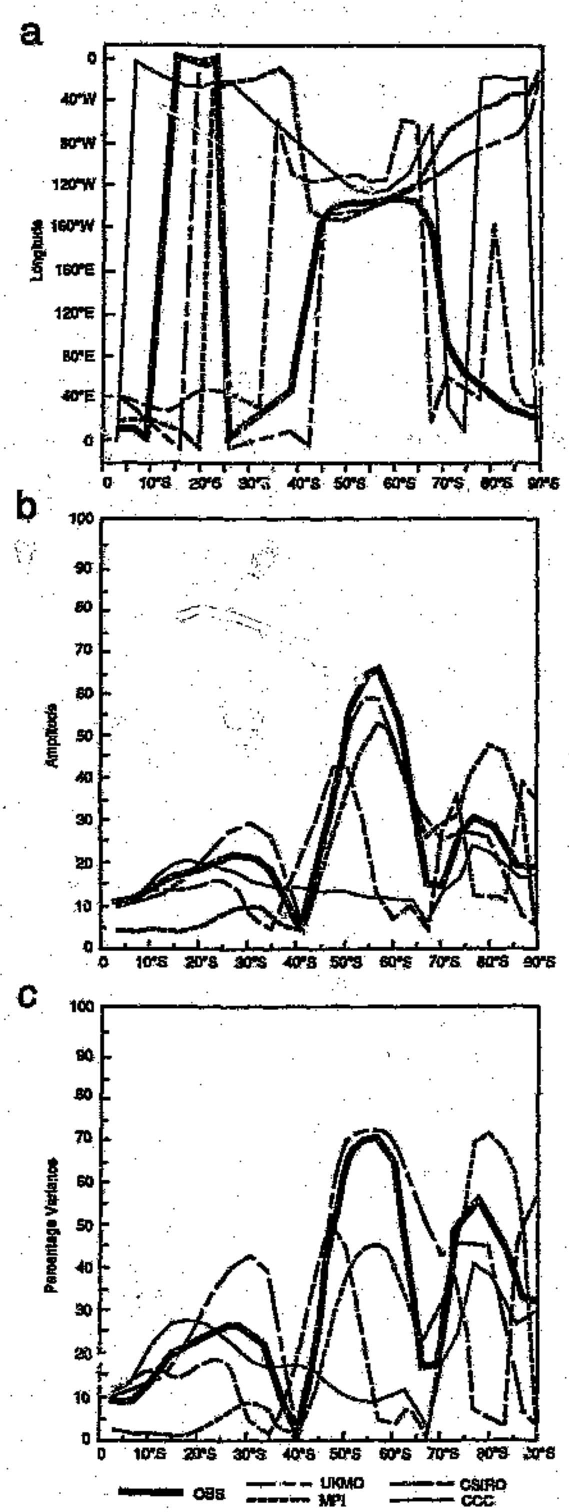

Figure 4.9. January a) longitudinal position of the ridge, b) amplitude (in gpm) and c) percentage of variance explained by zonal standing wave 1 at 500 hPa, for observations, and simulated by the CCC, CSIRO, MPI and UKMO models.

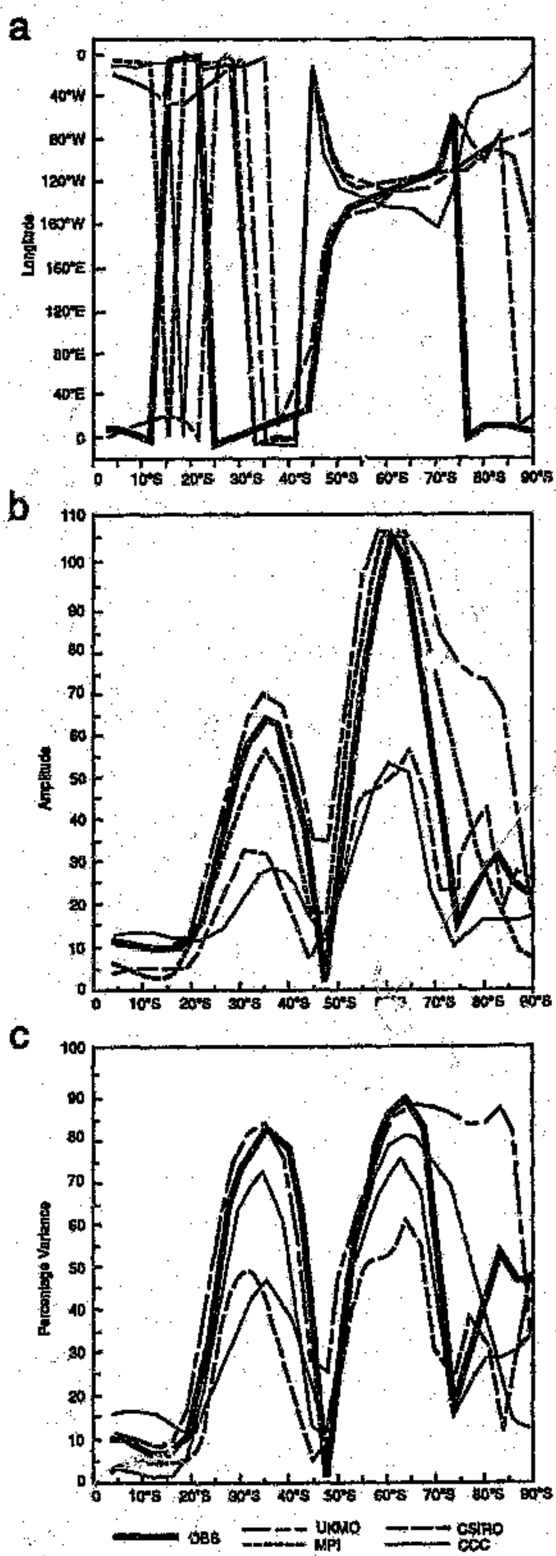

Figure 4.10. As Figure 4.9, but for July.

The MPI and UKMO models best simulate the amplitude of standing wave 1 (Figs. 4.9b and 4.10b). These two models perform better than any of the other models, including the CCC and CSIRO models shown in the figures. The increased amplitude of zonal wave 1 during July is well captured by both these models. Errors are smaller during July, although both the CCC and CSIRO models consistently under-estimate the observed amplitude. This is most serious in the CCC model in January when the maximum at subpolar latitudes is absent, while the CSIRO model consistently locates the maximum some 10 degrees north of its observed location. Similar conclusions may be drawn for simulation of the percentage of variance explained by zonal wave 1. Both the UKMO and MPI simulations are closest to observed values, with the UKMO model providing the best simulation of both the subtropical and subpolar maxima, although performing worse at polar latitudes (Figs. 4.9c and 4.10c). There is a marked seasonality in the performance of CCC model, which fails completely to simulate the January maximum, but accounts for almost 80 per cent of the observed variance in July. CSIRO consistently under-estimates the percentage variance accounted for by standing wave 1, locating the maxima in January again some 10 degrees north of their observed location. A distinction on the basis of horizontal resolution is apparent in these results. The higher resolution MPI (T42) and UKMO (2.75° x 3.75°), and to a lesser extent, the CCC (T32) model are more successful in capturing the amplitude and percentage of variance explained by standing wave 1 than the coarser-resolution CSIRO (R21) model. While simulations of standing waves 2 and 3 are not shown here, similar broad conclusions, with model performance dependent on horizontal resolution may be drawn.

Summer Rainfall over the Central Subcontinent

Due to the coarse resolution and simplistic parameterisation of convective processes in many GCMs, rainfall totals in regions where rainfall is of convective origin, such as central southern Africa, are characteristically poorly simulated (Joubert, 1995). Nonetheless, it is important to assess whether the generally higher resolutions and improved physical parameterisations inherent in the AMIP simulations result in an improvement in the simulation of summer rainfall over southern Africa. Area-averaged rainfall totals for a window over the summer rainfall region extending from 22.5°E to 33.75°E and from

20.71°S to 27.08°S are presented in Figure 4.11. All seven models simulate a clearly-defined annual rainfall cycle, with a strong summer maximum. Equally, however, all models over-estimate rainfall totals during the summer season (October-March). The MPI model over-estimates total rainfall most seriously, simulating rainfall totals during the summer which are almost three times those observed. No clear improvement in the simulation of rainfall totals by the AMIP models over the earlier atmospheric GCMs considered by Joubert (1995) is evident. The systematic error inherent in the grid-point simulation of convective rainfall totals does not indicate that the models are generally unreliable. The AMIP models have all demonstrated considerable accuracy in simulating the broad-scale features of mean circulation over southern Africa. In terms of circulation, performance is largely better than the earlier coarse-resolution atmospheric GCMs considered by Joubert (1995).

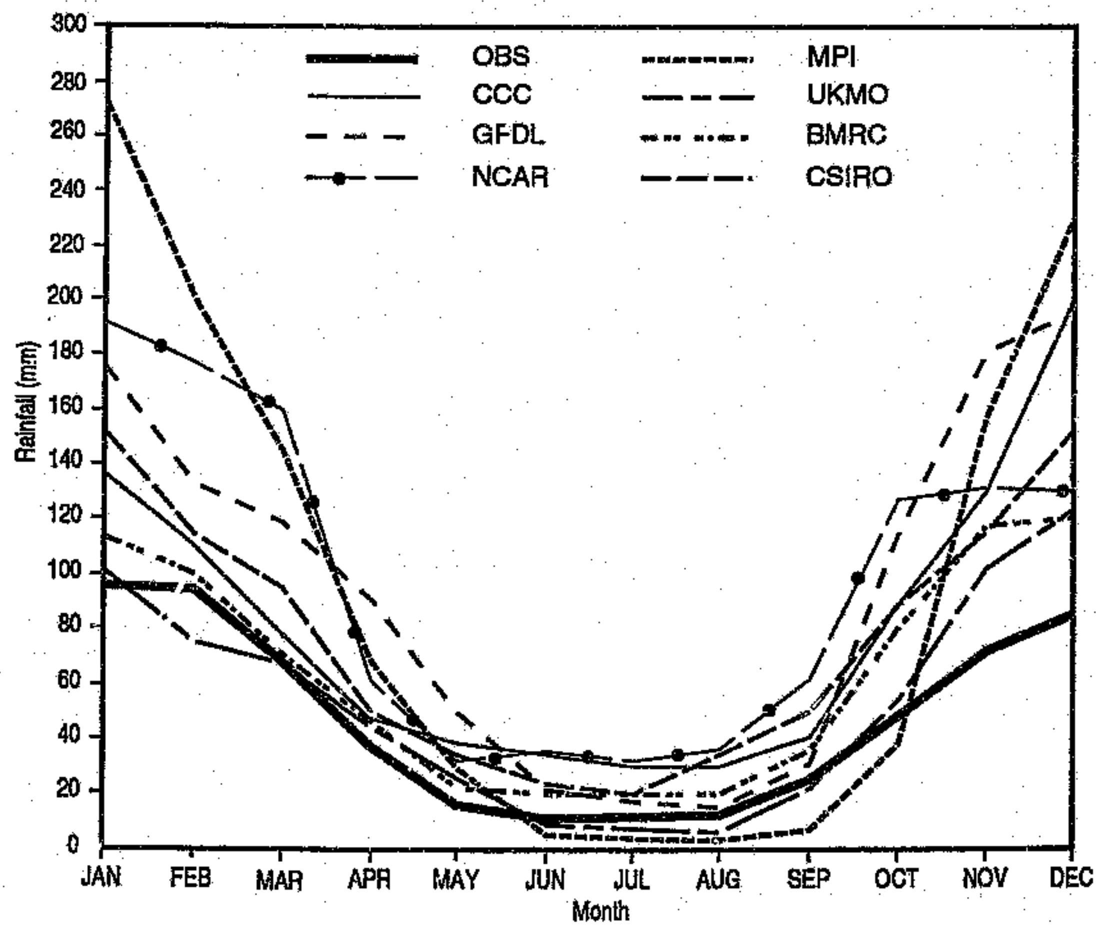

Figure 4.11. The annual cycle in simulated and observed area-averaged rainfall totals (in mm) over the central subcontinent. Rainfall totals are averaged over a window extending from 22.5°E to 33.75°E and from 20.71°S to 27.08°S.

Inter-Annual Variability

A climate model's ability to reproduce features of inter-annual variability is of equal importance to it's representation of mean climate. Each of the AMIP simulations is forced by known sea-surface temperature and sea-ice distributions for the 1979-1988 decade. The simulated features of inter-annual variability in, for example, precipitation and tropospheric circulation can therefore be assessed against the known (observed) variability. Like extended range weather forecasts, climate forecasts on inter-annual time scales have an inherent uncertainty associated with the internal variability of the model (e.g. Barnett *et al.*, 1994; Brankovic *et al.*, 1994; Barnett, 1995). This problem directly affects the AMIP integrations and strongly suggests that single model forecasts forced by observed sea-surface temperatures are inadequate for forecasting and sensitivity studies (Barnett, 1995). One means of overcoming the problem is to provide forecasts within a probabilistic framework using ensemble techniques and providing the actual forecast in terms of the moments of the ensemble (e.g. Palmer, 1993). This approach has been increasingly applied in the analysis of the AMIP results (Barnett, 1995; Ferranti *et al.*, 1995; Zwiers, 1995). While an assessment of simulated inter-annual variability using an ensemble approach is beyond the scope of the present study, it must be recognised that the single AMIP integrations considered below may not be representative of the models' true response to the imposed forcing.

Inter-Annual Rainfall Variability

The analysis of simulated inter-annual rainfall variability during the 1979-1988 decade is focused on the January-March (JFM) second half of the summer rainfall season. Area-averaged rainfall totals for the JFM season during the AMIP decade indicate two anomalously dry periods associated with the two ENSO events (JFM 1983 and 1987), and two wetter periods (JFM 1981 and 1988), although neither wetter period is classified as a La Niña event. As is demonstrated with reference to the UKMO, CSIRO and BMRC models, all of the AMIP results indicate generally weaker inter-annual variability in rainfall than observed (Fig. 4.12). The UKMO, CSIRO and BMRC models display a tendency to simulate wetter than normal JFM seasonal rainfall totals during 1981, 1984 and 1988 (Fig.

4.12), although the response is not clearly defined. The dry conditions of JFM 1982, 1983 and also 1986 and 1987 are also not clearly reproduced by the models. For example, the models appear to capture the reduction in rainfall over southern Africa during the 1987 ENSO event better than the much more severe 1982/1983 event.

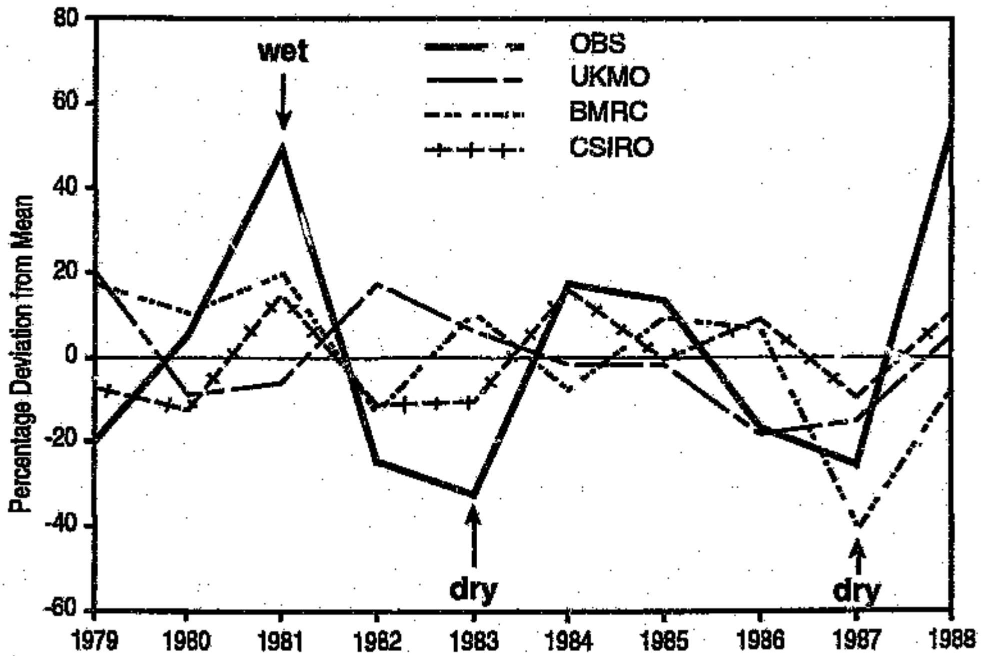

Figure 4.12. January-March (JFM) departures from area-averaged rainfall over the window defined in Figure 14, for the period 1979-1988. Observed and simulated (BMRC, CSIRO and UKMO) rainfall departures are expressed as percentage departures from the individual observed or simulated 1979-1988 means.

The simulated response in area-averaged rainfall over subtropical southern Africa is generally weak. However, the result may not indicate a serious failure in the models. It is widely recognised that the atmospheric GCM response (in terms of both precipitation and circulation) to imposed ENSO-related sea-surface temperature forcing is strongest and most realistic within the tropics (e.g. WMO, 1988). In addition, while ENSO-related variability is recognised as the single most important influence on inter-annual variability in summer rainfall over much of southern African (Tyson, 1986), the relationship accounts for only approximately 30% of the total inter-annual variability in South African rainfall (Lindesay, 1988). Given the additional problems in the representation of regional rainfall totals identified above, the poor representation of observed rainfall variations during the

AMIP decade is not unexpected. The representation of large-scale circulation adjustments associated with inter-annual rainfall variability may provide a more realistic test of the ability of the AMIP simulations to simulate inter-annual variability over southern Africa.

Inter-Annual Circulation Variability

The potential for predictability of the atmospheric response to ENSO on seasonal and inter-annual time scale is greatest within the tropics, where the coupling between the atmospheric and ocean is direct (e.g. Livezey, 1990). The simulated adjustments in tropical circulation during the 1982/83 ENSO are likely to be attributable to ENSO, although no attempt is made here to define the proportion of variability over southern Africa which is associated with sea-surface temperature forcing from the tropical Pacific Ocean. Adjustments in mid-latitude circulation in the vicinity southern Africa are not directly attributable to, although have been associated with (e.g. Harrison, 1986) ENSO variability in the tropical Pacific Ocean, given the inherent chaotic instability of the extratropical atmosphere (Palmer and Anderson, 1994). The large-scale systematic adjustments in extratropical circulation associated with periods of above- and below-normal rainfall over the subcontinent are generally consistent and have been observed over several decades (Tyson, 1986). It is the ability of the AMIP atmospheric GCMs to reproduce these features which is tested below. No attempt is made to attribute the extratropical atmospheric response in the vicinity of southern Africa to ENSO.

Adjustments in the westerlies in the mid-latitudes

Extended periods of above average rains over southern Africa are associated with a southward shift of the mid-latitude westerly storm tracks, and stronger storms, implying a more intense westerly circulation Harrison (1986). Dry periods, by contrast, are associated with a northward shift in the position of the storm track and an effectively less-intense westerly circulation. The extent to which the AMIP simulations reproduce the observed latitudinal shift in the region of maximum westerlies is illustrated in Figure 4.13. With the exception of the NCAR simulation, all of the models simulate a northward shift in the latitudinal position of the westerly wind maximum under dry conditions, regardless of the ability of each individual model to locate the maximum at the latitude of the observed maximum. The shift is best illustrated with reference to the strong ENSO event of JFM 1983, although it is also evident during JFM 1987. During wetter periods such as JFM 1981, there is less consensus amongst the models for a southward shift in the maximum westerlies. Simulated adjustments in the westerlies are in agreement with observed changes during both wet and dry periods over the subcontinent.

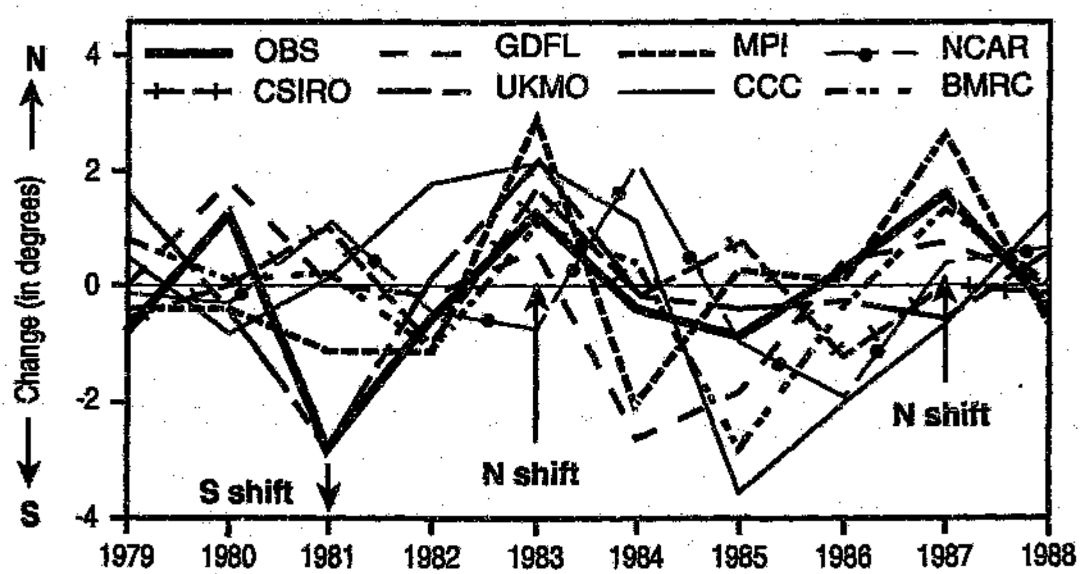

Figure 4.13. January-March observed and simulated latitudinal shifts in the region of maximum 850 hPa westerly wind speeds, for the period 1979-1988. Results are based on zonally-averaged windspeeds over four longitudes between 22.5^{0}E and 39.4^{0}E. Latitudinal shifts are expressed in degrees relative to the latitude of the zonally-averaged maximum of each model, and hence do not account for the ability of the models to locate the maximum correctly.

Mean sea-level pressure anomalies

Mean sea-level pressure anomalies for the JFM 1981 and JFM 1983 seasons (expressed relative to the 1979-1988 mean) are given for three AMIP simulations in Figure 4.14. Observations show that when rainfall is above average over the subcontinent (JFM 1981), pressures are anomalously positive over Gough Island and negative over the subcontinent (Fig. 4.14a). The AMIP simulations display various degrees of accuracy in reproducing the observed anomalies. The UKMO model (Fig. 4.14d) simulates a ridge of higher pressure throughout the mid-latitudes which is of similar magnitude to that observed, although the centre of the anomaly is located further east than observed. The MPI model (Fig. 4.14c), as well as the BMRC and CCC integrations (not shown) simulate weaker ridges in the mid-latitudes and negative pressure anomalies over parts of the subcontinent. In contrast, the CSIRO model (Fig. 4.14b) simulates an inverted pattern of anomalies, with negative pressure anomalies throughout the mid-latitudes and positive anomalies over much of the subcontinent. The NCAR and GFDL anomalies (not shown) are also unlike observations, with a strong trough in the NCAR integration near Marion Island, and weak positive anomalies throughout the region in the GFDL integration.

Under drier than normal conditions (JFM 1983), pressures are anomalously low over the mid-latitudes south of southern Africa, and anomalously positive over the subcontinent (Fig. 4.14e). All three of the integrations shown in Figure 4.14 are more successful in reproducing the pattern of pressure anomalies during the dry 1982/83 ENSO event. The pattern of negative pressure anomalies south of the subcontinent and positive anomalies throughout the subtropics is possible best captured by the UKMO integration (Fig. 4.14h). The observed pattern of circulation anomalies is also found in the BMRC and CCC simulations, although the magnitude of the anomalies is weaker than observed (not shown). The GFDL and NCAR anomaly patterns (also not shown) are less accurate, indicating ridging throughout the region.

500 hPa geopotential height anomalies

Systematic adjustments in large-scale circulation are also observed at 500 hPa (Tyson, 1981; Miron and Tyson, 1984; Tyson, 1986). During above-average rainfall seasons (e.g. JFM 1981), ridging again occurs in vicinity of Gough Island (indicating the presence of a larger-amplitude westerly wave off the west coast), with negative height departures over the subcontinent (Fig. 4.15a). Most models successfully reproduce the negative height anomalies throughout the subtropics, but display a wider range of accuracy reproducing the extratropical anomalies. The UKMO integration again accurately reproduces the pattern of 500 hPa geopotential height anomalies during JFM 1981 (Fig. 4.15d). The pattern is less-well reproduced by the MPI model (Fig. 4.15e), but the model does simulate ridging in the vicinity Marion Island (e.g. Tyson, 1984). The pattern of geopotential height anomalies is less well reproduced in the CSIRO (Fig. 4.15b) model, as well as in the BMRC, CCC, GFDL and NCAR simulations (not shown).

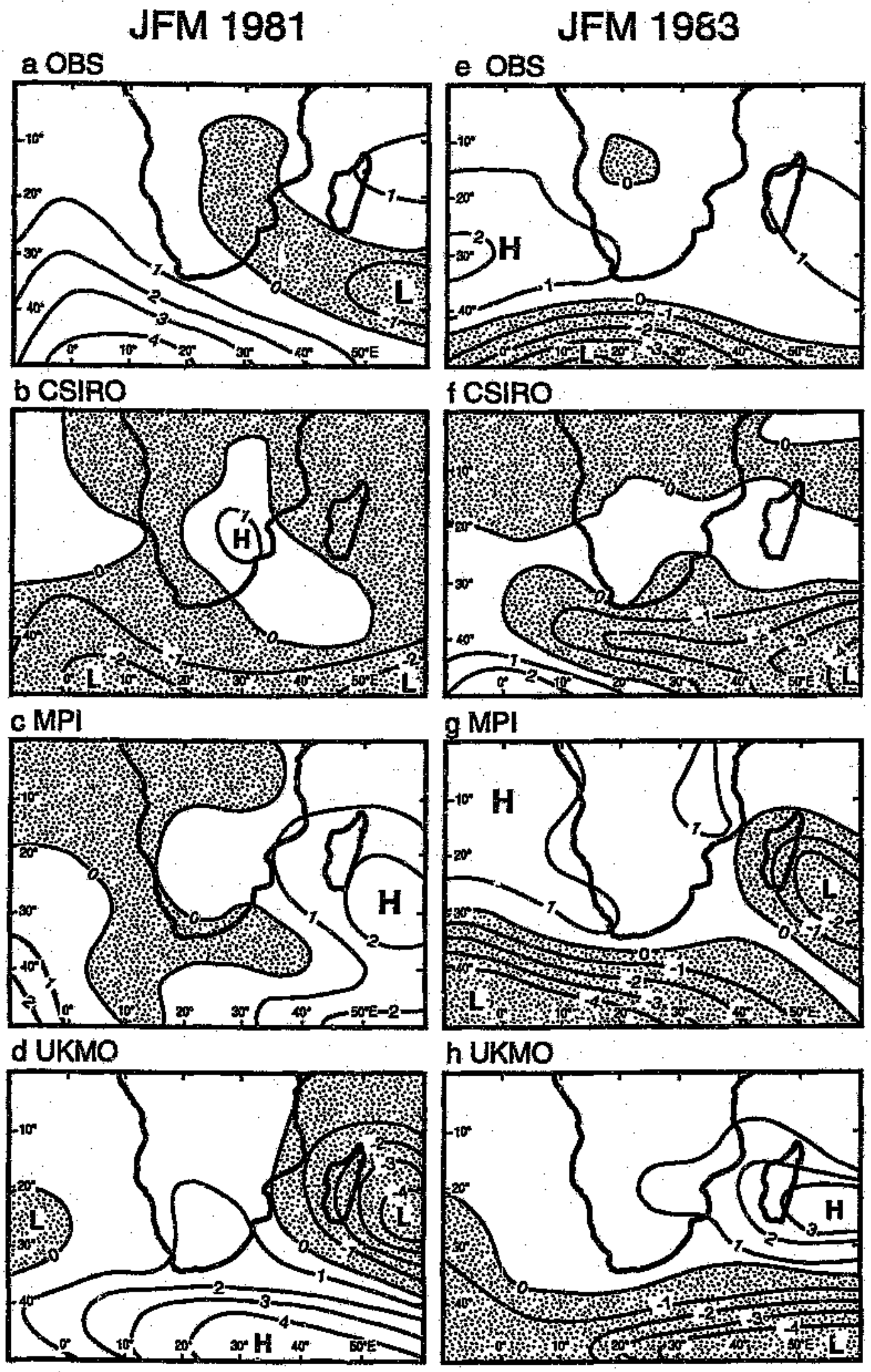

Figure 4.14. January-March (JFM) 1981 (a-d) and JFM 1983 (e-h) mean sea-level pressure anomalies (expressed relative to the 1979-1988 mean), in hPa. Anomalies are shown for observations (a,e) as well as the CSIRO (b,f), MPI (c,g) and UKMO (d,h) models. Contours are every 1 hPa and shading indicates negative anomalies.

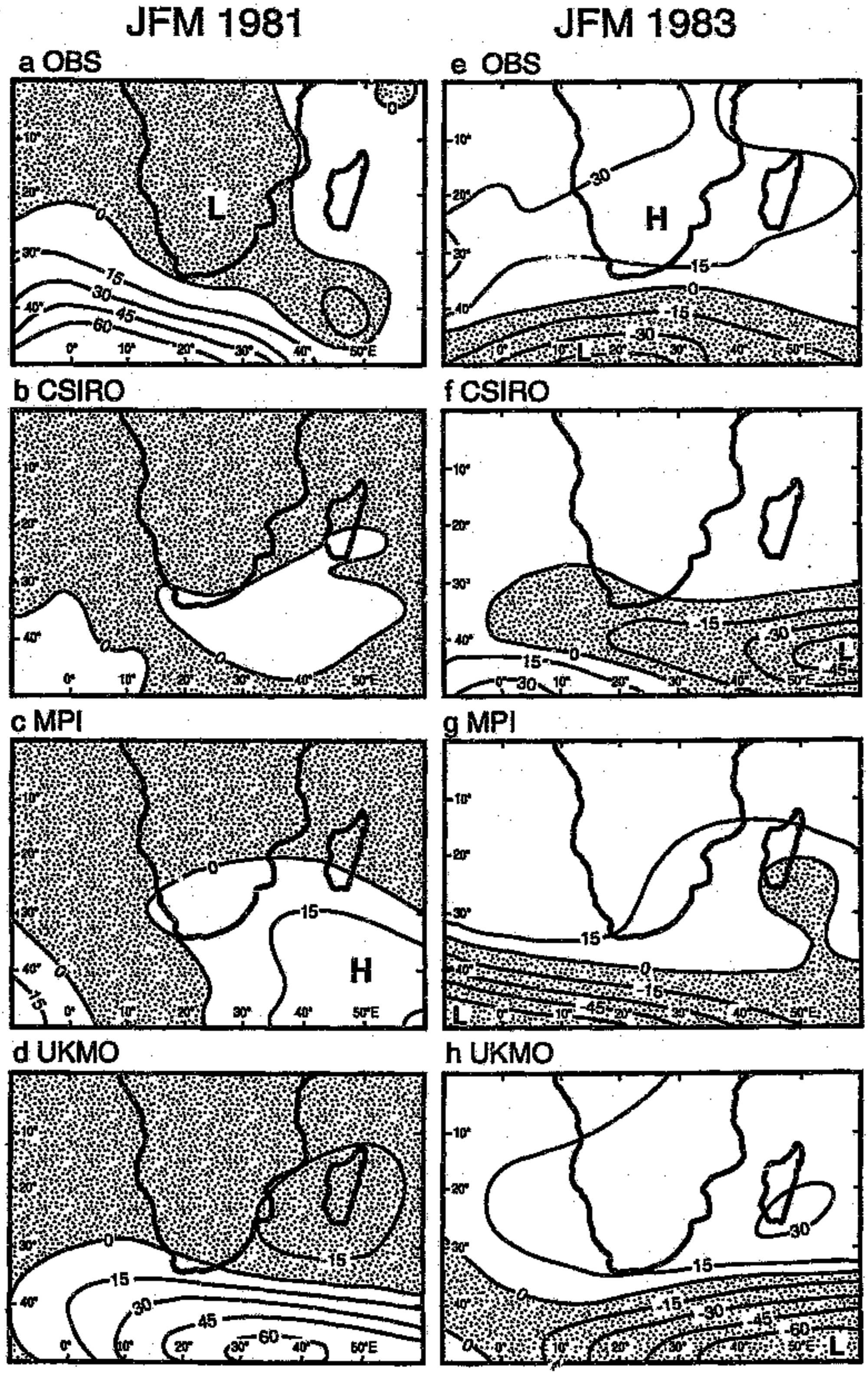

Figure 4.15. January-March (JFM) 1981 (a-d) and JFM 1983 (e-h) 500 hPa geopotential height anomalies (expressed relative to the 1979-1988 mean), in gpm. The same models as shown in Fig. 15 are used. Contours are every 15 gpm and shading indicates negative anomalies.

The pattern of height departures reverses during above-average rainfall years; with negative height departures in the mid-latitudes and positive anomalies throughout the subtropics (Fig. 4.15b, Tyson, 1986). Both the MPI and UKMO models (Fig. 4.15g,h) successfully reproduce the pattern of 500 hPa geopotential height anomalies. A similar (weaker) pattern of ridging is indicated by the CSIRO model (Fig. 4.15b), as well as the BMRC, CCC, CSIRO and GFDL simulations. The NCAR integration is least accurate, simulating weak positive height anomalies throughout the region (also not shown).

Adjustments in planetary wave structure

Planetary waves in the vicinity of southern Africa play an important role in modulating inter-annual rainfall variability over the subcontinent (Harrison, 1986). The leading edge of the upper level trough of the semi-stationary planetary wave (planetary wave 3 or 4) marks the position of the cloud band, which acts as a important channel for the poleward transfer of energy and momentum. Cloud bands are recognised as the single most important rainfall-producing system over southern Africa in summer (Harrison, 1986). According to the observational model developed by Harrison (1986), the upper level trough of the Atlantic wave is located preferentially over southern African during normal and above average rainfall years, and displaced further east during low rainfall years associated with ENSO events. Simulated adjustments in the position of standing wave 3 during anomalously wet and dry years should, therefore, provide further indication of the ability of the AMIP models to simulate ENSO-related circulation variability.

Adjustments in the phase of standing wave 3 in January-March average 500 hPa geopotential heights, relative to its mean position, for both the wet (JFM 1981) and dry (JFM 1983) case studies, are shown in Figure 4.16. As suggested by Harrison (1986), the ridge of standing wave 3 during the dry case study is located east of its mean position in the region of southern Africa (20°S to 35°S). As a result, another ridge of standing wave 3 is located over southern Africa, subsidence occurring over the subcontinent (Fig. 4.16a). During the JFM 1981 season, when conditions were wetter, standing wave 3 is located west of it's mean position throughout the subtropics and mid-latitudes, with the trough located over the central interior (Fig. 4.16b). The UKMO model is most successful in capturing the phase shifts in standing wave 3 under wetter and drier conditions. While the

MPI model successfully reproduces the westward shift during the JFM 1981 wet case study, it fails to reproduce the eastward shift in the region of southern Africa, simulating a large westward shift south of the subcontinent. The inability of the lower-resolution CCC and CSIRO models to simulate adjustments in the position of standing wave 3 accurately is related to their poorer simulations of southern hemisphere planetary wave structure in general.

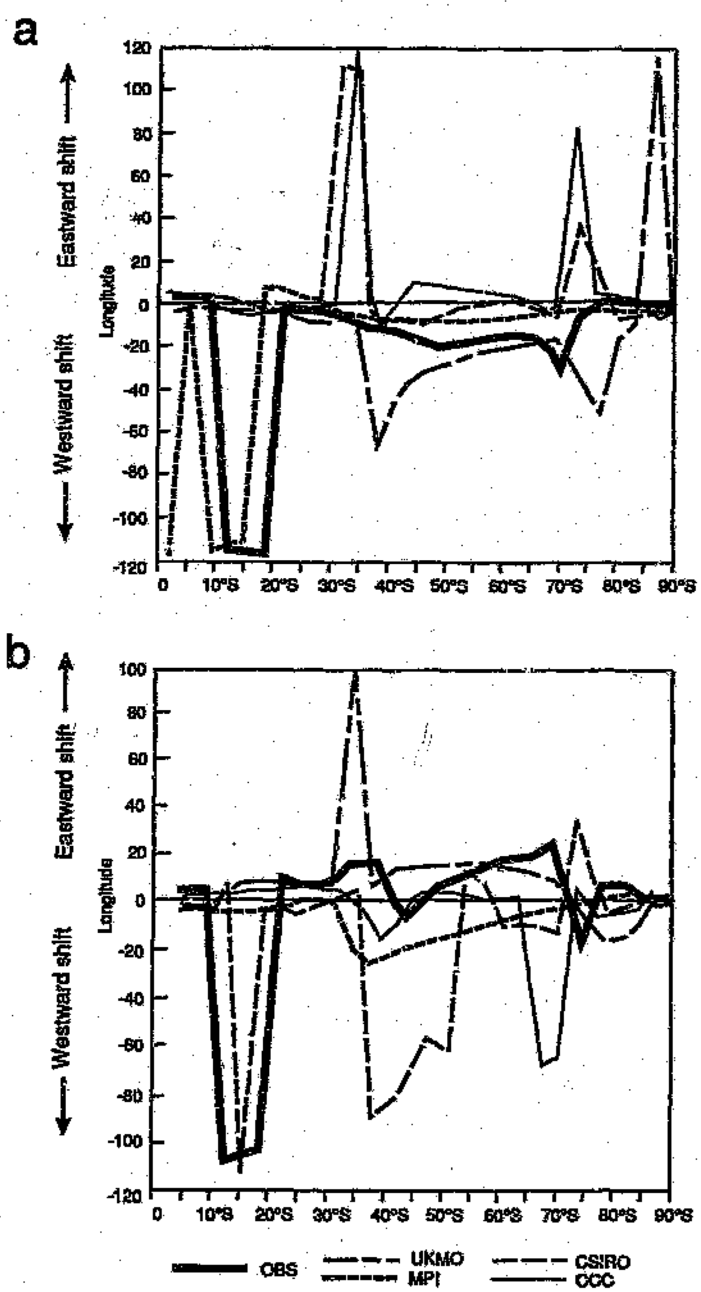

Figure 4.16. Observed and simulated adjustments in the phase of standing wave 3 in January-March average 500 hPa geopotential heights, relative to its mean position, for a) JFM 1981 and b) JFM 1983

Synthesis

The representation of southern African climate by seven AMIP models has been assessed. The models are all atmospheric GCMs used in climate studies and are forced with observed sea-surface temperatures and sea-ice distributions over the 1979-1988 period. The representation of both the mean regional and hemispheric circulation features, as well as the simulation of inter-annual circulation variations during the AMIP decade has been assessed.

Most features of the surface circulation around southern Africa are simulated well by the AMIP models and the simulations represent a general improvement over earlier-generation atmospheric GCMs (Joubert, 1995). Improvements have been noted in the simulated intensity and position of the subtropical anticyclones and the circumpolar trough as well as the meridional pressure gradient and zonal wind profile. These improvements are the result of increased spatial resolution in most of the AMIP models over the earlier GCMs considered by Joubert (1995), as well as improved parameterisation of tropical convection implicit in the models (e.g. M[illegible] and Albrecht, 1988, 1991; Boer *et al.*; 1992a, Hack *et al.*, 1994).

Within the troposphere, representation of the zonally-asymmetric component of the flow, as well as standing wave 1 are also dependent on model resolution. Standing wave 1 reflects the topography and shape of Antarctic (van Loon and Jenne, 1972) and consequently the improved representation of the continent that is possible with increased horizontal and vertical resolution may be expected to result in an improved simulation of the feature (e.g. Parrish *et al.*, 1994). For this reason, the higher resolution UKMO, MPI, and to a lesser extent CCC models perform better than the CSIRO model in simulating the phase, amplitude and intensity of zonal standing wave 1 at 500 hPa.

Overall, no single model simulates all features of southern African circulation accurately. Similar conclusions were drawn in the hemispheric analyses of Mullan and McAvaney (1995). Model performance is shown to be strongly seasonally-dependent. For example, while the UKMO best reproduces the mean sea-level distribution in summer, it performs poorly in winter in comparison to the BMRC and CCC simulations. A measure of model-observation consensus for mean sea-level pressure has been defined. A model is said to agree with observations at a grid point if the simulated value falls within one observed standard deviation of the observed mean. Model agreement with observations is poor over much of the subcontinent. Improved agreement observed over the mid-latitude oceans may reflect the larger inter-annual variability in mean sea-level pressure and may not be indicative of an improvement in model performance.

Southern Africa experienced anomalously dry conditions during 1982, 1983 and 1987, and anomalously wet conditions during 1981 and late 1988. Each of the three dry periods are associated with ENSO events (Lindesay, 1988). While the simulated sensitivity to ENSO-related variability in the tropical Pacific Ocean is an important component of AMIP, no attempt has been made here to assign the proportion of inter-annual variability observed in the models over southern Africa to ENSO. The ENSO signal may, however, be expected to be strongest within the tropics, and weakest (if present at all) in the extratropics. Systematic circulation adjustments in the subtropics and mid-latitudes are associated with extended wet and dry spells over the subcontinent, including those which occurred during the AMIP decade (Tyson, 1986). The present analysis has evaluated the ability of the AMIP models to simulate the inter-annual circulation adjustments over the southern African region which are known to have accompanied inter-annual variability in rainfall over the subcontinent between 1987 and 1988.

The AMIP models all simulate weaker inter-annual variability in summer rainfall and circulation over southern Africa than observed. Given the problems associated with the representation of precipitation in atmospheric GCMs, it is more instructive to consider simulated inter-annual variability in circulation. The present analysis does not consider ensembles of AMIP predictions. Ensemble forecasts are required to account for the uncertainty associated with the predicted response to sea-surface temperatures by single integrations from an atmospheric GCM (e.g. Barnett, 1995). Conclusions drawn here concerning the representation of large-scale circulation adjustments around southern Africa between 1979 and 1988 should be considered indicative of model performance, although not conclusive. The simulated circulation departures at the surface and 500 hPa are well reproduced by the UKMO, and to a lesser extent, the MPI, BMRC and CCC integration. While the CSIRO model has lower horizontal as well as vertical resolution than the other models, the generally poor representation of circulation by the NCAR and GFDL integrations suggests that no clear distinction on the basis of spatial resolution *alone* can be drawn.

The assessment of the simulation of inter-annual variability over southern Africa between 1979 and 1988 is somewhat hampered by the availability of single integrations from each of the atmospheric GCMs. Considerable uncertainty exists concerning the simulated response to imposed sea-surface temperature forcing from single integrations of an atmospheric GCM (e.g. WMO, 1988). A similar problem has been demonstrated to affect the simulated response to imposed sea-surface temperatures in the AMIP integrations (Barnett, 1995). As a consequence, greater emphasis is now placed on the use of ensemble approaches to define a stable prediction from the models (Barnett, 1995; Ferranti *et al.*, 1995; Zwiers, 1995). For this reason, no definitive conclusions can be drawn from the present study about the AMIP models to simulate inter-annual variability over southern Africa associated with forcing imposed by global sea-surface temperature anomalies. For this, ensemble approaches will have to be adopted.

The analyses presented in this Chapter have demonstrated that current atmospheric GCMs forced by observed sea-surface temperatures provide an accurate representation of present mean circulation over southern Africa. In addition simulated inter-annual variability appears to be robust in several of the higher-resolution models, if weaker than observed. Sensitivity to sea-surface temperature variability is a necessary requirement for using atmospheric GCMs in climate change experiments (Druyan *et al.*, 1995). A realistic representation of the response to sea-surface temperature forcing does not necessarily guarantee a realistic response to changes in greenhouse gas forcing, unless it is assumed that the feedbacks between atmosphere and ocean in the model are accurate. The evaluations of present climate performance presented in this chapter are valuable indicators *only* of a reliable response to increasing anthropogenic forcing of climate.

****

Seven AMIP simulations of mean climate and inter-annual variability over southern Africa during the 1979-1988 decade have been evaluated. In general, the AMIP integrations provide an improved simulation of mean circulation around southern Africa when compared to earlier atmospheric general circulation models. The AMIP models generally simulate weaker than observed inter-annual variability in both summer rainfall and circulation. Nonetheless the simulated patterns of inter-annual variability in circulation appear to be robust. Ensemble approaches are required to provide a more comprehensive assessment of the simulated response to imposed forcing. The present climate performance of mixed-layer and fully-coupled models used in Section III to derive estimates of future regional climate over southern Africa is evaluated in Chapter 5.

CHAPTER FIVE

COMPARATIVE PERFORMANCE OF MIXED-LAYER AND FULLY-COUPLED MODELS

Introduction

Global and hemispheric performance of most current climate models may now be considered reliable and physically consistent estimates of future climate change are available. At regional scales, deficiencies in model resolution and uncertainties associated with the parameterisation of physical processes result in an increased discrepancy between the need for reliable estimates of change and the ability of the models to provide them. Evaluations of the regional performance of climate models for present-day conditions establishes confidence in the ability of the models to simulate features of regional climate and regional climate processes. Greater confidence can be placed in estimates of possible future regional climate if the model is known to simulate present climate realistically. The ability of a range of both mixed-layer and fully-coupled models to simulate monthly mean sea-level pressures, surface air temperatures and rainfall over the southern African region will be assessed in this chapter.

Mean Sea-Level Pressure

December-February (DJF)

Mean sea-level pressures for the December-February (DJF) season are illustrated in Figures 5.1 and 5.2 for mixed-layer and fully-coupled models respectively. The observed distribution is repeated for reference as the first frame of each figure. During DJF, the central pressure in the South Atlantic Anticyclone is above 1020 hPa (Fig. 5.1a). The centre of the South Indian Anticyclone is located east of 60°E, and pressures between longitudes 40°E and 60°E within the anticyclone are 4-6 hPa lower than in the South Atlantic ocean (e.g. Taljaard, 1972). The South Indian Anticyclone is located slightly further south than the South Atlantic Anticyclone (Fig. 5.1a). Other features of the mean sea-level pressure distribution shown in Figure 5.1a include pressures below 1010 hPa over the tropical subcontinent, indicating the southernmost location of the Inter-Tropical Convergence (ITC) and a well-defined meridional pressure gradient.

The mixed-layer models (Fig. 5.1) capture the features of the observed mean sea-level pressure distribution over the tropics and subtropics well (Table 5.1). All models under-estimate pressures in the ITC and both over- and under-estimate the intensity of the high pressure cells. The relative position of the high pressure cells as well as the meridional pressure gradient are well-reproduced by the BMRC, CSIRO and UKHI models. The BMRC and UKHI simulations best capture the pattern of mean sea-level pressures and simulate spatial variability (expressed as the ratio of simulated to observed variability) which most closely match the observed variability (Table 5.1). The spatial variability simulated by the CSIRO model is weaker than observed. The CCC model simulates a deeper than observed circumpolar trough and the GFDLH over-estimates the intensity of the high pressure cells. The result for both models is that the meridional pressure gradient is exaggerated and simulated spatial variability approaches twice that observed (Table 5.1). The tendency of the GFDLH model to over-estimate pressures over the entire field is reflected in a root mean square error (a measure of the simulation error at individual grid points) in excess of 5 hPa (Table 5.1).

The fully-coupled models (Fig. 5.2) are all of lower resolution than the mixed-layer models and simulate a weaker than observed meridional pressure gradient and a circumpolar trough that is not sufficiently intense. The UKTR fully-coupled model simulates more intense high pressures that the mixed-layer version of the model (UKHI), but both models display a negative pressure bias over the field as a whole (Table 5.1). Similarly, both MPI fully-coupled models simulate weaker than observed pressures. Like it's mixed-layer version, a positive pressure bias of almost 5 hPa is present in the GFDLC simulation. There is almost no difference between the performance of the CSIRO mixed-layer and fully-coupled models.

Table 5.1 December-February (DJF) statistical comparison of simulated and observed mean sea-level pressure for five mixed-layer and five fully-coupled models. All statistics are calculated for the region 15°S to 35°S and 10°W to 60°E. All pattern correlation coefficients (r) are significant at the 99 per cent significance level.

Model	Pattern Correlation (r)	Root Mean Square Error (hPa)	Overall Spatial Bias (hPa)	Ratio of Spatial Variances
Mixed-Layer Models				
BMRC	0.94	1.47	0.28	1.41
CCC	0.88	2.42	0.10	2.04
CSIRO	0.91	2.72	2.33	0.83
GFDLH	0.89	5.31	4.82	1.89
UKHI	0.93	2.81	-2.21	1.66
Fully-Coupled Models				
CSIROC	0.92	2.79	2.47	0.83
GFDLC	0.87	5.24	4.91	1.19
MPILC	0.93	3.14	-2.80	1.36
MPIOC	0.90	2.36	-1.75	1.14
UKTR	0.95	1.88	-0.86	1.75

June-August (JJA)

During the June-August (JJA) season, pressures intensify over much of the subtropics as both the South Atlantic and South Indian Anticyclones expand longitudinally and the ITC shifts northwards (Taljaard, 1972). Pressures in the circumpolar trough also deepen and consequently the meridional pressure gradient intensifies (Fig. 5.3a).

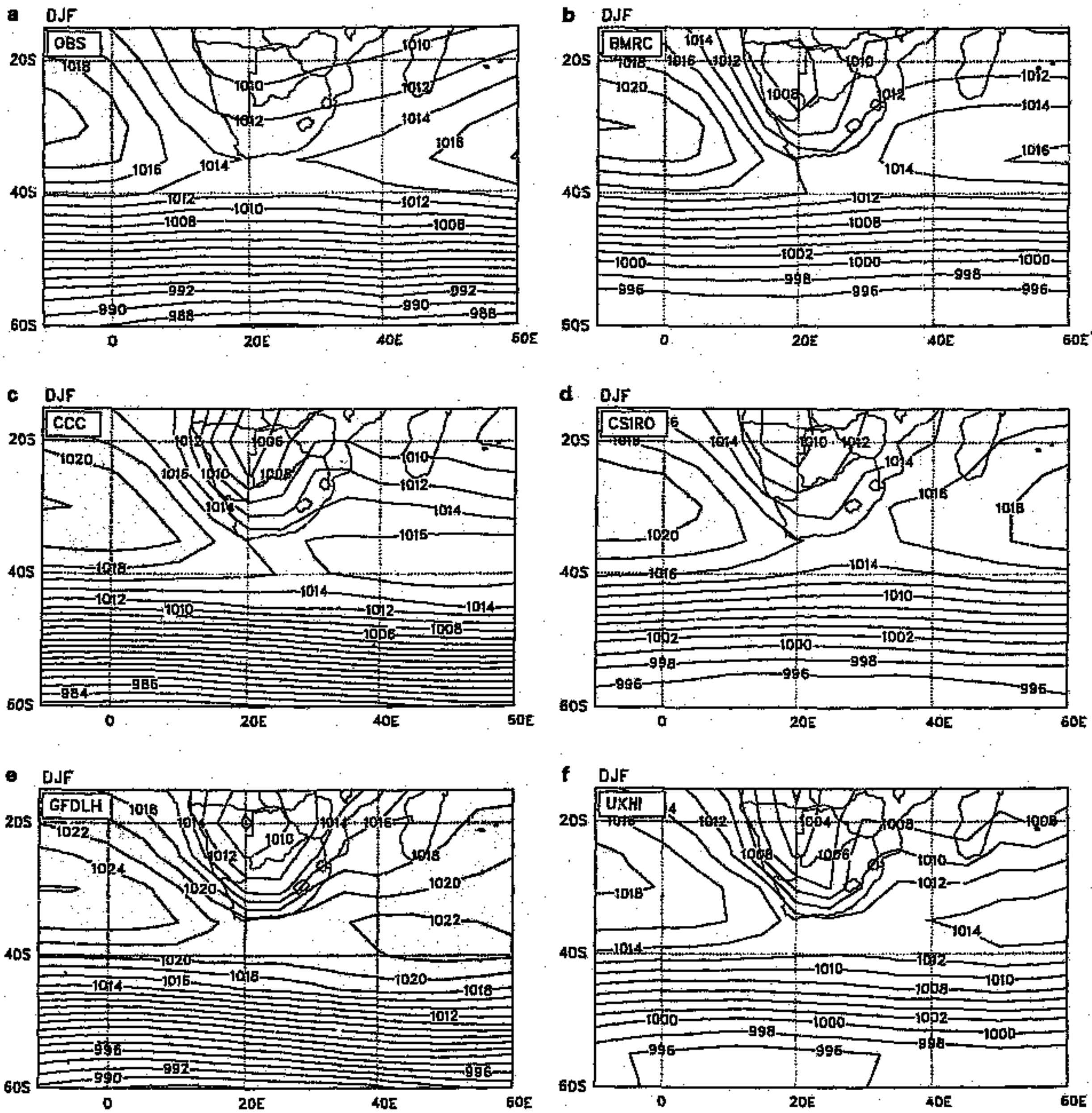

Figure 5.1. Observed (a) and simulated (b-f) mean sea-level pressures (in hPa) over southern Africa for the December-February (DJF) season. Contours are every 2 hPa and pressures above 1018 hPa are shaded. Mixed-layer models represented are the BMRC (b), CCC (c), CSIRO (d), GFDLH (e) and UKHI (f) models.

The mixed-layer models (Fig. 5.3) all simulate the intensification of pressures in the subtropics and the northward shift of the ITC in winter. Only the CSIRO model under-estimates pressures in the subtropics, while the other models (notably GFDLH) over-estimate pressures in the South Atlantic Anticyclone by approximately 2 hPa. The root mean square error and overall pressure bias in the UKHI and CSIRO models are the lowest of the five fully-coupled models and are better than the results for summer (Table 5.3). In contrast, the BMRC model (which performs well in summer) simulates are larger root mean square and over-estimates the observed spatial variability in winter.

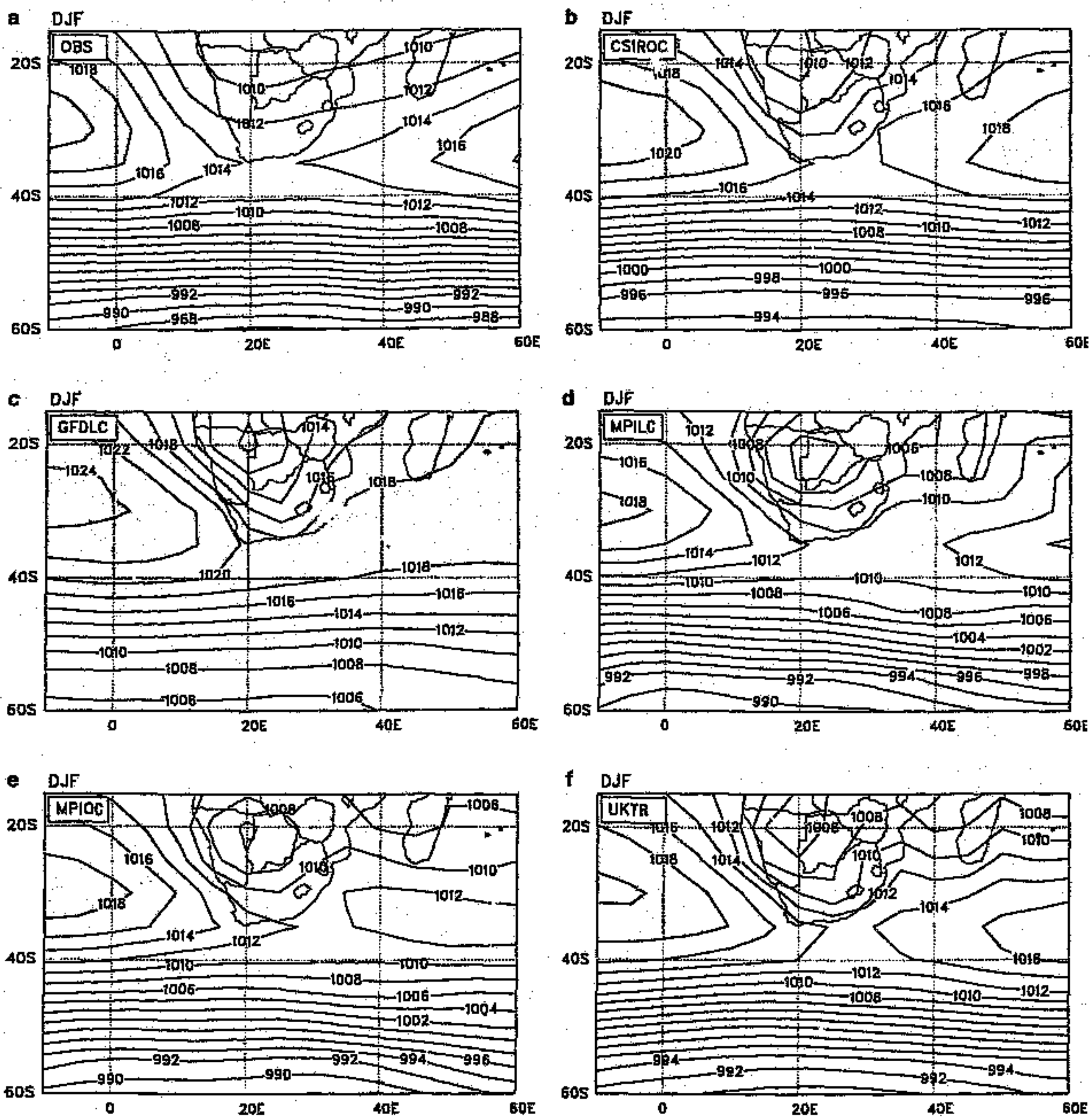

Figure 5.2. As for Figure 5.1, except for the fully-coupled models; CSIROC (b), GFDLC (c), MPILC (d), MPIOC (e) and UKTR (f). The observed mean sea-level pressure is repeated as (a).

Table 5.2 As for Table 5.1, except for June-August (JJA) seasonal means.

Model	Pattern Correlation (r)	Root Mean Square Error (hPa)	Overall Spatial Bias (hPa)	Ratio of Spatial Variances
Mixed-Layer Models				
BMRC	0.80	2.30	-0.80	2.23
CCC	0.90	1.66	0.89	1.69
CSIRO	0.80	1.71	0.86	0.90
GFDLH	0.90	7.47	7.28	2.03
UKHI	0.85	1.50	0.12	1.43
Fully-Coupled Models				
CSIROC	0.79	1.84	1.05	0.94
GFDLC	0.79	5.14	4.92	0.90
MPILC	0.65	3.29	-2.67	0.87
MPIOC	0.77	1.71	-0.70	0.79
UKTR	0.85	1.66	-0.26	1.67

The pattern of mean sea-level pressure within the tropics in winter is less well captured by the fully-coupled models (Table 5.2) than for any other group of models or season. With the exception of UKTR, all models simulate weaker than observed spatial variability, with smaller high pressure cells than observed (Fig. 5.4). While UKTR better represents the observed pressure distribution than the other models, the model still exhibits the negative pressure bias (Table 5.2) observed during summer and over-estimates the observed spatial variability in mean sea-level pressure. Both MPI fully-coupled models simulate smaller and weaker anticyclones than observed, although the feature is much better captured by the MPIOC than the MPILC simulation. Along with UKTR, the CSIRO and MPIOC fully-coupled models best represent the pattern of observed mean sea-level pressure in winter, with low root mean square errors (below 2 hPa) and simulated spatial variability which is close to observed (Table 5.2).

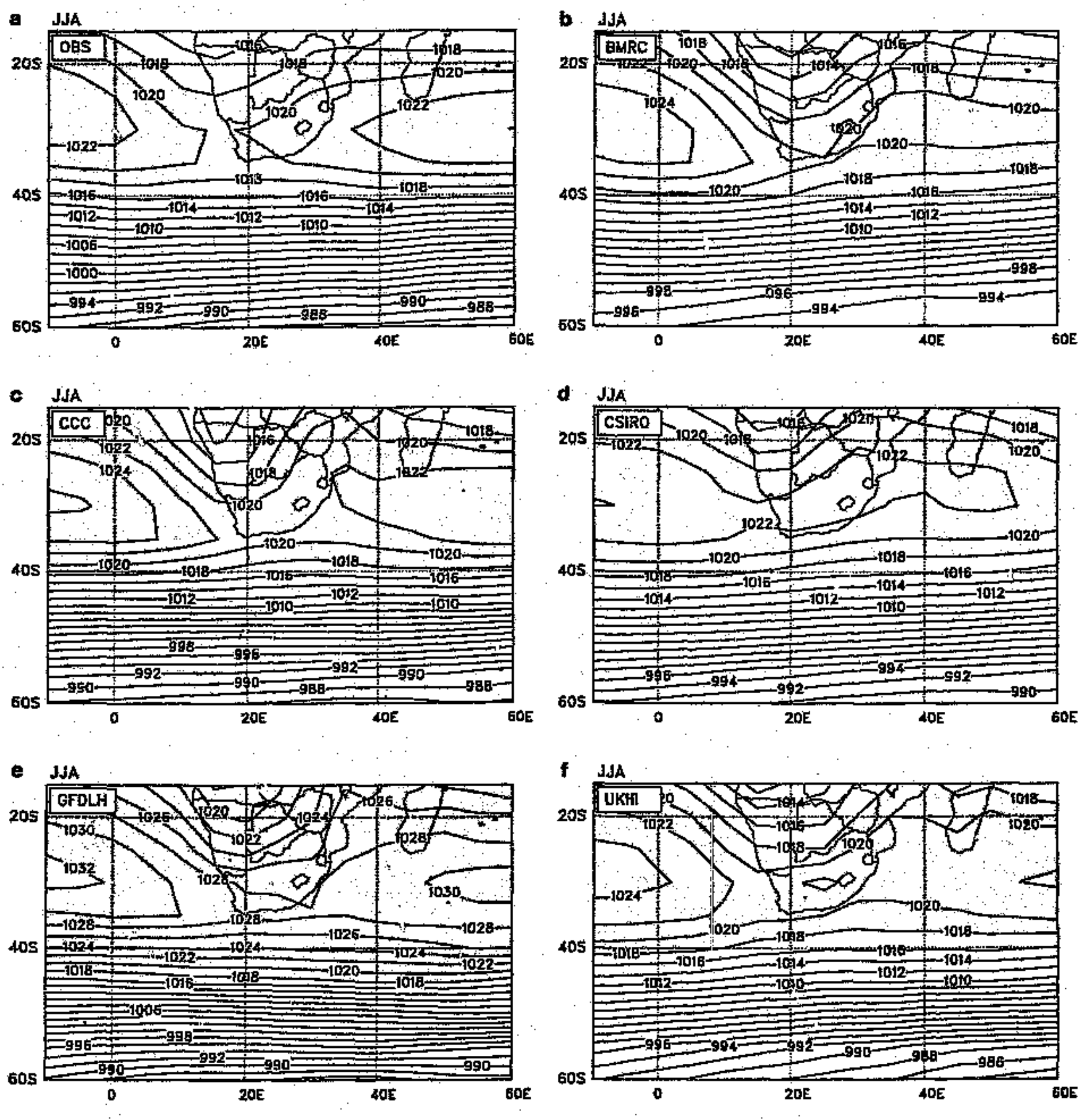

Figure 5.3. As for Figure 5.1, except for the June-August (JJA) season.

Model Agreement with Observations

Model agreement with observations is defined by calculating the number of models which simulate observed mean sea-level pressures within one standard deviation of the observed mean value at each grid point. In effect, simulations are said to agree with observations if they fall within 68 % of the distribution of observed values around the observed mean.

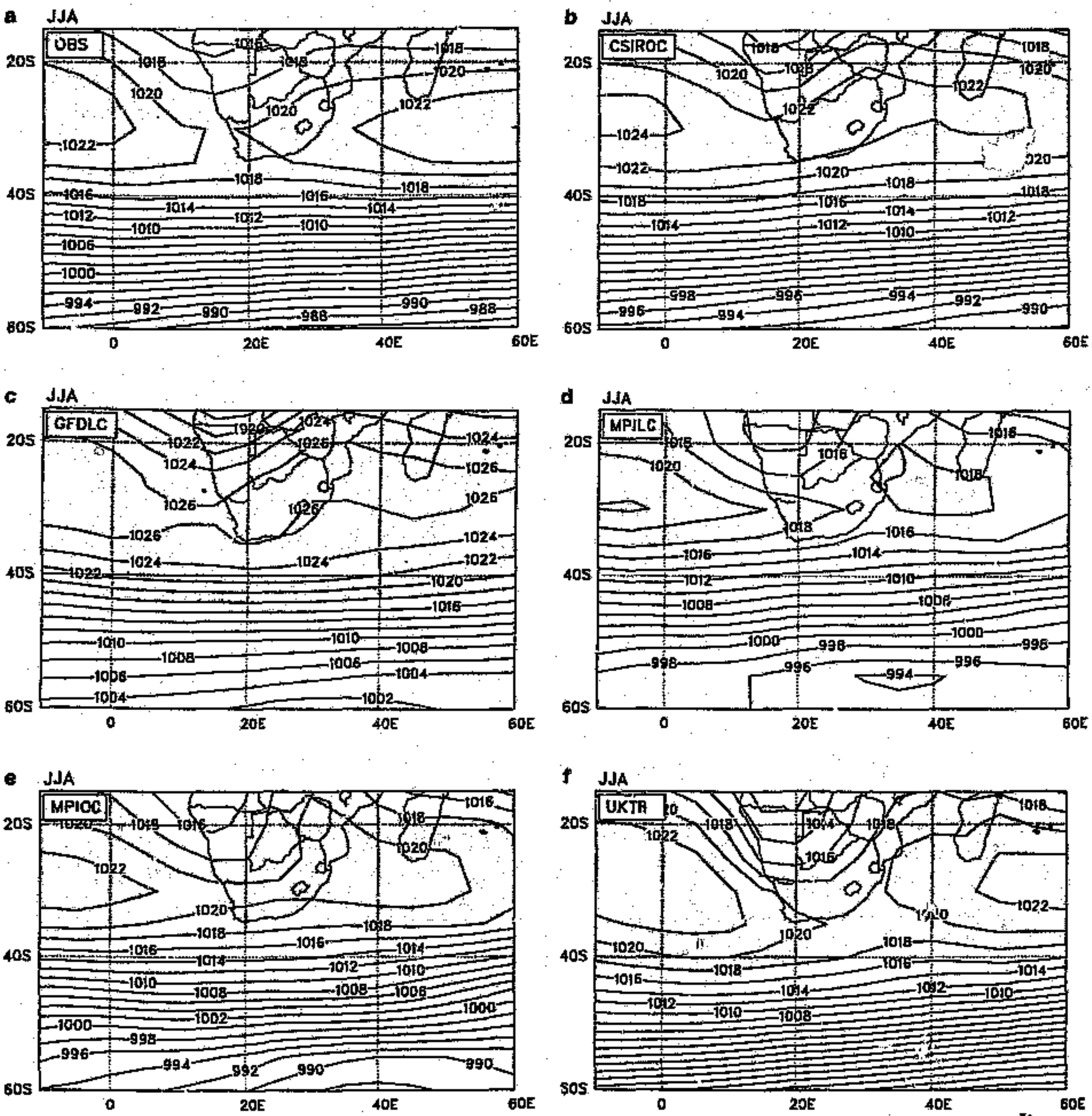

Figure 5.4. As for Figure 5.2, except for the June-August (JJA) season.

Throughout the tropics and subtropics and throughout the year, very few models simulate mean sea-level pressure within one standard deviation of the observed mean values. Around the subcontinent no more than two models display agreement with observations (Fig. 5.5). Where agreement is observed, it is limited spatially. While the models display some ability to reproduce the pattern and spatial variability of observed pressures, model errors at individual grid points are larger than the observed inter-annual variability. Model agreement with observations is greater over the southern oceans, around 45°S where slightly more than half of the total number of models simulate pressures within one observed standard deviation of the observed mean. The mixed-layer models which display agreement are the BMRC, CCC, CSIRO and UKHI models. The CSIRO, MPILC and UKTR models are the fully-coupled models which display agreement with observations at high latitudes. The higher levels of model-observed agreement in the mid-latitudes and high southern oceans may be misleading. These regions also exhibit the largest inter-annual and intra-annual variability in mean sea-level pressures (e.g. Dyer, 1981) and the standard deviation of values around the observed mean may be expected to be large. The relatively good agreement statistics may be indicative of a larger range of acceptable values, rather than better model performance.

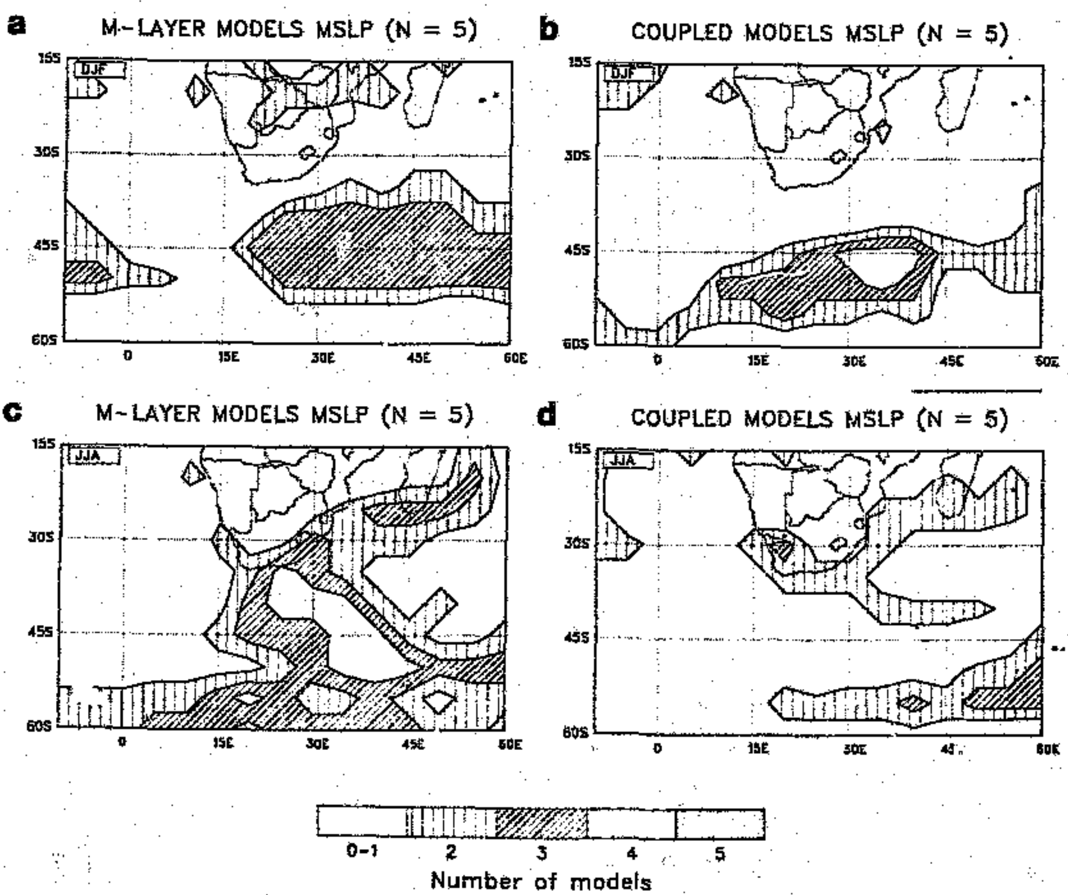

Figure 5.5. The number of models which simulate (a,b) December-February (DJF) and (c,d) June-August (JJA) mean sea-level pressures within one standard deviation above or below the observed mean at each grid point. (a,c) Mixed-layer models and (b,d) fully-coupled models. Shading is indicated in the legend.

Surface Air Temperature

Seasonal Mean Temperatures

The seasonal range in surface air temperatures between December-February (summer) and June-August (winter) is illustrated in Figure 5.6 for four climatically distinct locations over the tropics, the Kalahari Desert, the summer rainfall region (southern Zimbabwe) and the winter rainfall region (Western Cape province of South Africa).

Over the tropics (Fig. 5.6a,b) the observed annual temperature range is just over 3°C (indicated by dotted lines). Among the mixed layer models (Fig. 5.6a), both the CCC and CSIRO simulations simulate lower than observed temperatures during summer and winter. The GFDLH model simulates a smaller than observed annual temperature range, but with simulated winter temperatures similar to the observed summer temperatures. The annual temperature range simulated by UKHI is also smaller than observed, but falls within the observed range. There is almost no distinction in the BMRC model between summer and winter temperatures. Most of the fully-coupled models simulate a smaller than observed annual range in temperatures over the tropics (Fig. 5.6b). For both of the MPI models and the UKTR simulation, winter temperatures are higher than in summer indicating that the simulated seasonal cycle is the inverse of that observed. The annual temperature range simulated by the CSIROC model is of a similar magnitude to observations, although both summer and winter temperatures are lower than observed. Both the UKTR and GFDLC models simulate a small annual temperature range with temperatures that are higher than observed.

The observed annual temperature range over the summer rainfall region (Fig. 5.6c,d) is approximately 8°C. All mixed-layer models simulate an annual temperature range is slightly smaller than the observed range. Only the BMRC simulation is warmer than observed in summer, while the CCC and CSIRO models simulate lower than observed temperatures in winter (Fig. 5.6c). The fully-coupled models simulate a larger annual range in temperatures than the mixed-layer models over the summer rainfall region. The CSIRO and both MPI fully-coupled models simulate lower than observed winter temperatures, while both the GFDLC and UKTR models simulate warmer than observed summer temperatures (Fig. 5.6d).

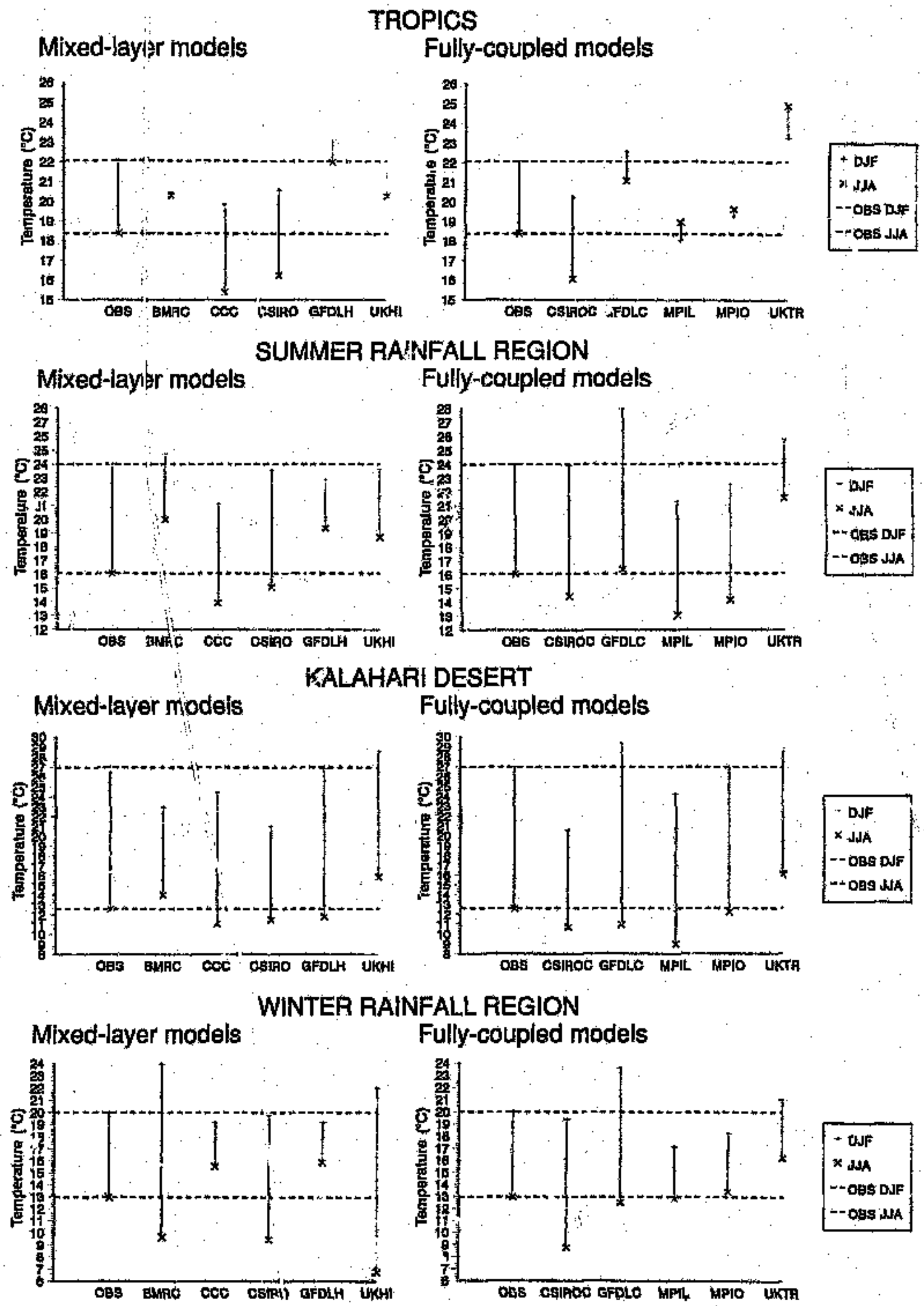

Figure 5.6. Observed and simulated December-February (DJF) and June-August (JJA) surface air temperatures (in °C) for four locations over the subcontinent (given in Figure 5.11f). The observed annual temperature range (DJF-JJA) is indicated by dashed lines on each graph. Graphs are presented for the mixed-layer and fully-coupled models separately.

The observed annual temperature range of more than 13°C over the dry Kalahari region is the largest for any region of the subcontinent. The large range in temperatures is well captured by the GFDLH and UKHI models, although the UKHI model simulates higher than observed temperatures in both summer and winter (Fig. 5.6e,f). The BMRC, CCC and CSIRO models simulate summer temperatures which are between 3° and 7°C lower than observed and hence the large observed range is not reproduced (Fig. 5.6e). Only the CSIRO fully-coupled model under-estimates the annual cycle over the Kalahari. The GFDLC, MPIOC, MPILC and UKTR models simulate an annual temperature range which is at least equivalent to the observations. Both the UKTR and GFDLC models simulate higher than observed summer temperatures, while the GFDLC and MPIL models simulate lower winter temperatures than observed.

The annual temperature range over the winter rainfall region is approximately 7°C (Fig. 5.6g,h). The CCC and GFDLH models (Fig. 5.6g) under-estimate this range, while the other three mixed-layer models all over-estimate the range. The UKHI and BMRC simulate annual temperature ranges which are more than twice that observed. Among the fully-coupled models (Fig. 5.6h), the MPI fully-coupled models and UKTR simulate a smaller than observed annual temperature range, although these fall within the observed range. The CSIRO and GFDLC fully-coupled models exaggerate the annual temperature range by up to 4°C.

Greenhouse Gas and Sulphate Aerosol Forcing of Present Climate

The reliability of most climate model estimates of anthropogenically-induced global warming is limited by the inability of the models to reproduce the observed variability in global climate realistically. Models forced by greenhouse gases only tend to produce a larger warming than has been observed over recent decades (IPCC, 1990, 1992). After greenhouse gases, sulphate aerosols exert the next most important anthropogenic forcing on global climate. The direct effect of sulphate aerosols introduces localised cooling in the regions where they are present (Taylor and Penner, 1994) and has recently been incorporated in climate model simulations (Hasselmann *et. al.*, 1995; Mitchell *et. al.*, 1995a; Mitchell and Johns, 1996). The inclusion of sulphate aerosols results in an improved simulation of observed *global* mean temperatures over the period of meteorological record (Mitchell *et al.*, 1995a; Mitchell and Johns, 1996; Santer *et al.*, 1995). The Hadley Centre fully-coupled model incorporates the direct effects of sulphate aerosol forcing over several regions of the globe, including much of tropical central southern Africa (cf. Fig. 2.1). The impact of including sulphate aerosol forcing on the ability of the Hadley Centre model to reproduce *regional* climate variability over southern Africa has not previously been assessed.

Annual mean temperature

Observed annual mean temperatures (Fig. 5.7) exhibit a statistically significant increasing trend between 1961 and 1990 of approximately 0.4°C (at the 1% confidence interval). Two Hadley Centre model experiments forced by greenhouse gases only and by combined greenhouse gas and sulphate aerosol forcing display considerable variability over the 1961-1990 period, although differences between the simulated and observed anomalies are not significant. Significance is assessed at the 5 per cent significance level, using a two-tailed paired sample t-test and assuming that differences between simulated and observed temperatures are random samples from a normal distribution. The assumption of normality and independence may be violated if temporal or spatial autocorrelation is present in the data. Given the fact that the statistics are calculated on spatial averages, spatial autocorrelation is accounted for. A Durbin-Watson test for normality fell within the indecision zone, suggesting that statistical significances may be slightly, although not seriously over-estimated.

Using two-way analysis of variance techniques, simulated temperature variability from both Hadley Centre experiments have been compared with observed variability between 1961 and 1990. Differences between observed and simulated variability for both experiments are not statistically significant at the 5 per cent level. In addition, multivariate regression analysis shows that neither the slope nor the intercept of the greenhouse gas only and sulphate aerosol curves are significantly different from the observed curve. The inclusion of sulphate aerosols has not resulted in an improved simulation of observed temperature variability over the southern African region when compared to the greenhouse gas only experiment.

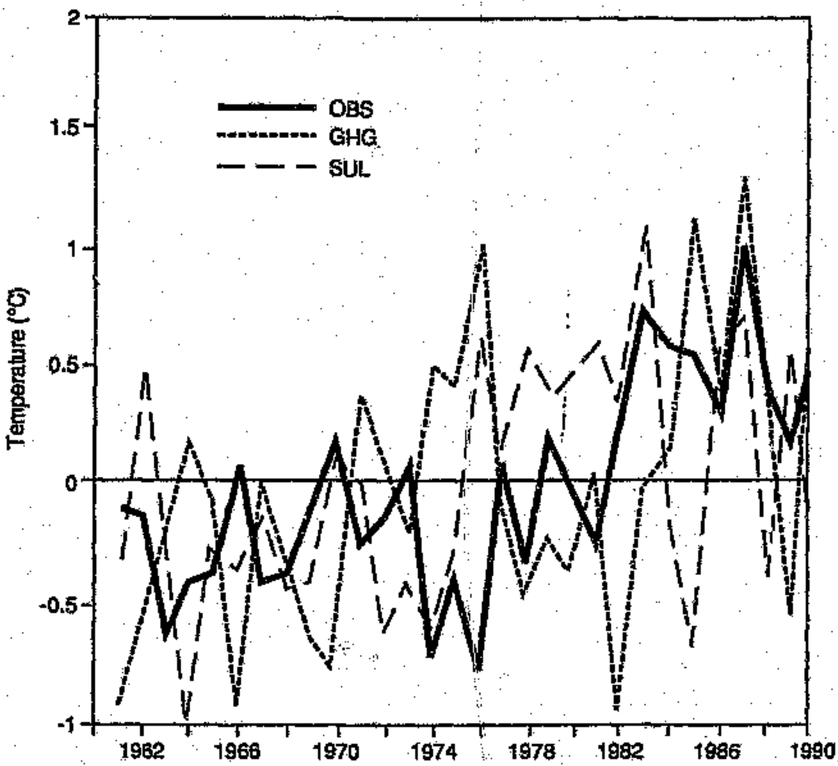

Figure 5.7. Changes in area-averaged annual mean surface air temperature, relative to the respective 1961-1990 means for observations (solid curve), GHG (dotted curve) and SUL (dashed curve). Area-averages are calculated for 18.75°E to 30°E and from 10°S to 30°S. Observed temperatures are extracted from the southern African climatology of Hulme *et al.* (1996).

Diurnal temperature range

The diurnal range of observed temperatures exceeds 14°C over much of the western half of the subcontinent, and is greater than 18°C over the central Kalahari Desert (Fig. 5.8). The range is ameliorated by the proximity of the oceans, with much smaller diurnal ranges along the coasts, falling below 5°C along the west coast. Over the tropics, diurnal temperature range is 10°-12°C.

Both the greenhouse gas only and combined greenhouse gas and sulphate aerosol experiments simulate the larger diurnal temperature range over the western half of the subcontinent, although both experiments simulate a range in temperatures which is approximately 2°C lower than observed (Fig. 5.8b,c). No discernible difference exists between the greenhouse gas only and sulphate aerosol maps, indicating that the inclusion of sulphate aerosol forcing does not influence the simulation of diurnal temperature ranges over the 1961-1990 period. Over the tropics, both the experiments reproduce the observed diurnal temperature range of approximately 10°C, with a slightly larger range in maximum and minimum temperatures over Tanzania and Kenya. The land-sea boundary and diminished diurnal range along the coast is pronounced in both experiments, with diurnal temperature range along the coast of below 2°C.

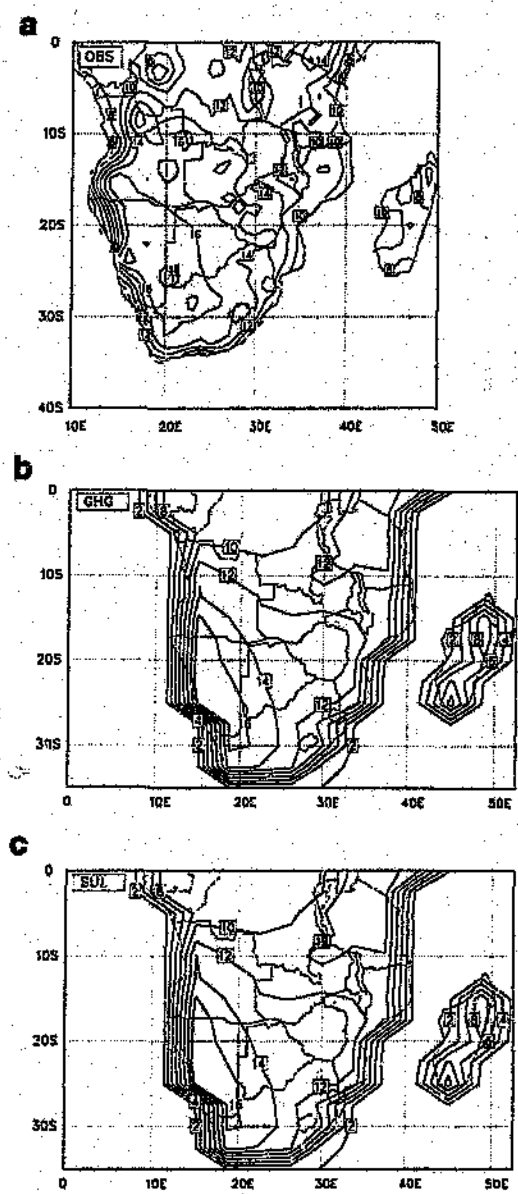

Figure 5.8. Diurnal range in annual mean temperatures (expressed as difference between maximum and minimum temperature) for observations (a), GHG (b) and SUL (c,, in°C. Contours are every 2°C and shading indicates regions where the diurnal range exceeds 14°C. Observed temperatures are extracted from the southern African climatology of Hulme *et al.* (1996).

Rainfall

Average Daily Rainfall

GCMs do not simulate regional-scale rainfall totals accurately due to their limited spatial resolution and simplistic parameterisation of rainfall-producing processes, especially convection (IPCC 1990, 1992, 1995). This systematic error affects the central southern African region as well, where the dominant mode of rainfall production is convective and simulated regional rainfall totals are known to be unreliable. The range of rainfall simulation errors at individual locations is illustrated for both mixed-layer and fully coupled models in Figure 5.9. Within the tropics, both mixed-layer and fully-coupled models tend to under-estimate average daily rainfall by as much as 30 per cent during the December-February season (Fig. 5.9a,b). During the rest of the year, observed average daily rainfall rates are both over- and under-estimated.

The range of errors in simulated daily rainfall is approximately 50 per cent over the summer rainfall region (Fig. 5.9c,d). Both the mixed-layer and fully-coupled models simulate the summer season rainfall maximum over this region, with insignificant rainfall occurring during the winter. During the summer (December-February) season, both the CSIRO and GFDL mixed-layer and fully-coupled models simulate higher than observed rainfall rates. The BMRC, CCC and UKHI mixed-layer models are more accurate, as is the UKTR fully-coupled model. Over the dry Kalahari Desert, average daily rainfall rates are most seriously over-estimated. During summer and autumn (March-May), rainfall rates simulated by the CSIRO, BMRC and GFDLH mixed-layer models are as much as five times larger than observed (Fig. 5.9e). A similar range of errors exists among the fully-coupled models with GFDL and CSIRO models exhibiting simulation errors of similar magnitude to their mixed-layer versions. Both the UKHI and UKTR models over-estimate rainfall rates although the error is smaller than among the other models. All of the models simulate higher average daily rainfall rates during the winter months over the winter rainfall region (Fig. 5.9g,h). Simulated average daily rainfall rates range between half and double the observed rate. Both the CSIRO and GFDLH mixed-layer models simulate maximum daily rainfall in March-May and not June-August as observed. The winter (June-

August) rainfall maximum is better reproduced by the fully-coupled models than by the mixed-layer models.

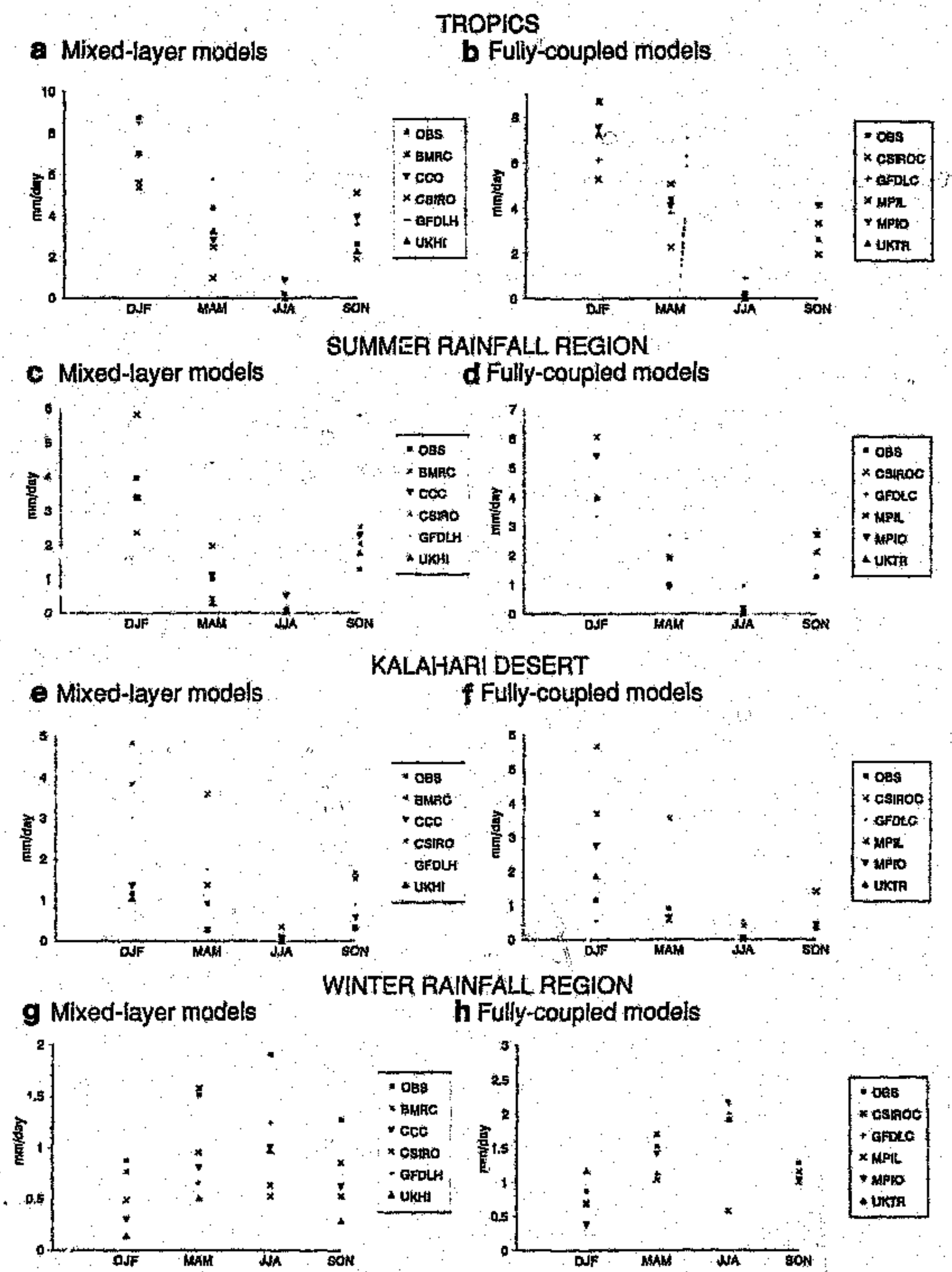

Figure 5.9. Daily rainfall rates (mm.day^{-1}) for the four locations shown in Figure 5.11f, for observations (Hulme *et al.*, 1996) and all mixed-layer and fully-coupled models.

Rainfall Seasonality

Given the inability of GCMs to simulate regional rainfall totals accurately, assessment of the ability of models to simulate rainfall seasonality is a fairer means of judging regional-scale performance (Whetton and Pittock, 1991). Accuracy in the simulated response in regional rainfall patterns to small changes in insolation associated with the annual cycle indicates that the model's response to larger changes in radiative forcing associated with an enhanced greenhouse effect may be reliable. Adequate simulation of the pattern of rainfall seasonality, though does not imply that reliable estimates of model grid-scale changes in rainfall can be obtained and caution must be exercised when interpreting projected changes in total rainfall.

Rainfall over the central interior of southern Africa is strongly seasonal with more than 70 per cent (shaded) of the annual rainfall total occurring during the summer months of September-November and December-February (Fig. 5.10). A winter rainfall maximum occurs over the Western Cape province of South Africa, with summer season rainfall totals accounting for only approximately 30 per cent of the annual rainfall total. The mixed-layer models (Fig. 5.10) all reproduce the strong summer rainfall maximum over the subcontinent, with a winter rainfall maximum towards the south-west of the subcontinent. Both the CSIRO and UKHI models simulate a summer rainfall maximum which does not extend sufficiently far west across the subcontinent. In contrast, the BMRC, CCC and GFDLH models simulate a stronger summer rainfall maximum over a larger area than observed. In all three models, the region for which summer rainfall accounts for more than 70 per cent of the annual total extends across to the west coast of the subcontinent near 20°S. Like it's mixed-layer version, the CSIRO fully-coupled model simulates a region of summer rainfall which does not extend as far west as observed (Fig. 5.11). The GFDL fully-coupled model most seriously misrepresents the pattern of rainfall seasonality, with a weaker-than observed summer rainfall maximum. The pattern of rainfall seasonality is better reproduced by the MPIO than by the MPIL fully-coupled model and closely resembles the observed distribution. Due to missing data, the UKTR fully-coupled model is not included.

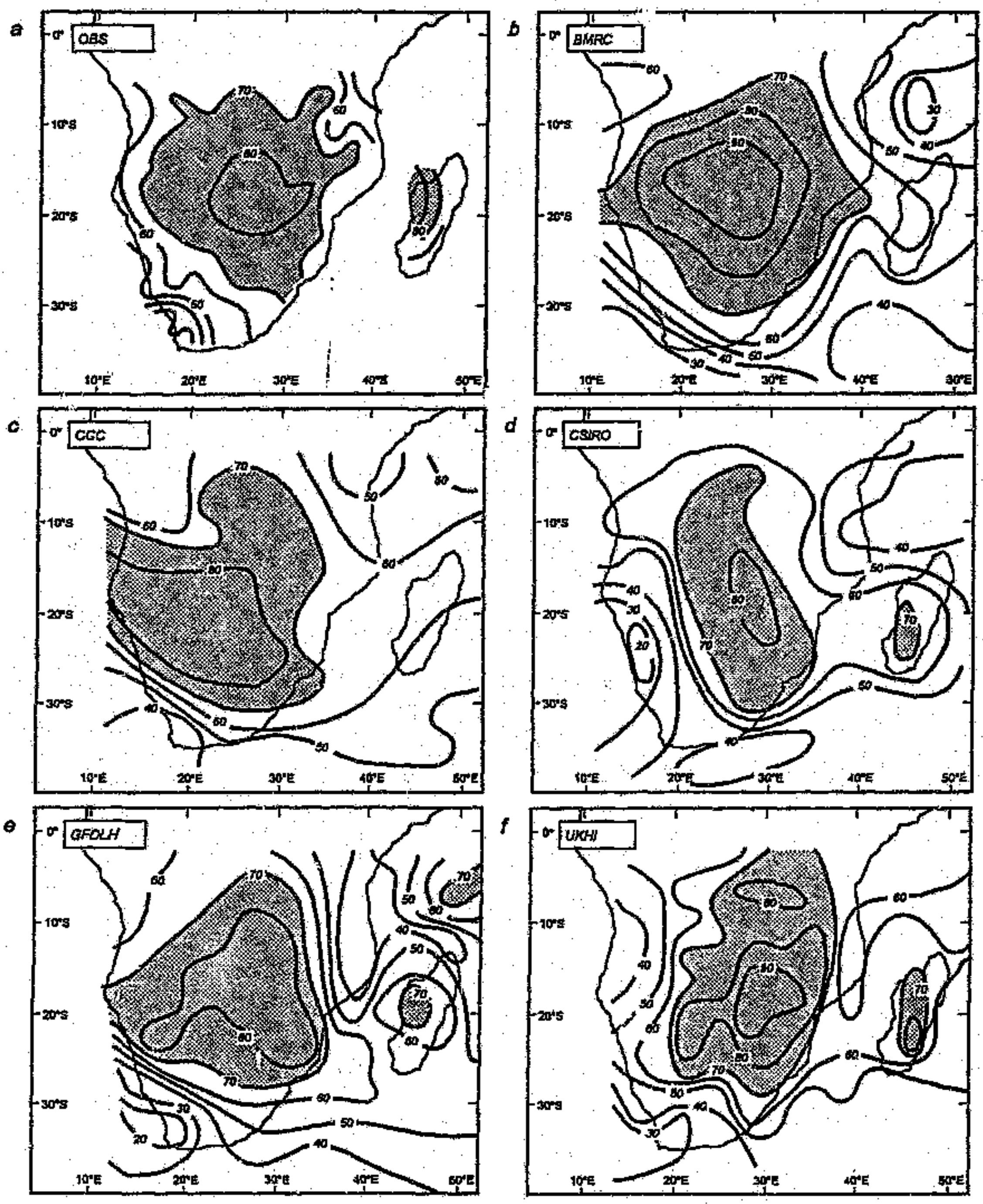

Figure 5.10. The percentage contribution of September-November (SON) and December-February (DJF) seasonal rainfall totals to the annual rainfall total. Observed rainfall totals (a) are taken from Hulme *et al.* (1996). The mixed-layer models are BMRC (b), CCC (c), CSIRO (d) GFDLH (e), and UKHI (f). Shading indicates regions where summer rainfall exceeds 70 per cent of the annual total.

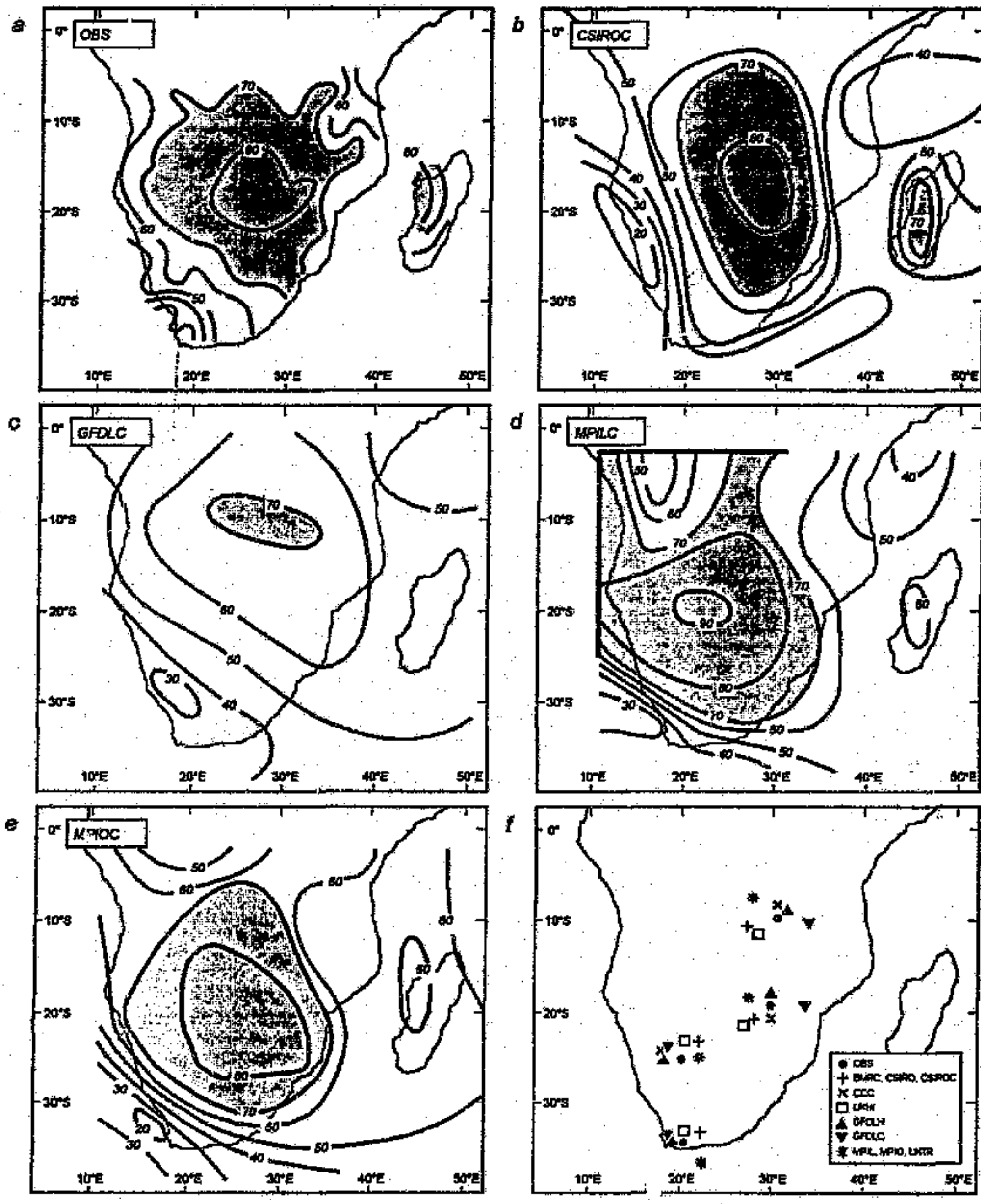

Figure 5.11. As for Figure 5.9 except for the fully-coupled models CSIROC (b), GFDLC (c), MPILC (d) and MPIOC (e). The UKTR simulation is not including due to missing data for the June-August (JJA) season (hence no annual rainfall total is calculated). The location of four sites over the tropics, the Kalahari Desert, summer rainfall region (southern Zimbabwe) and the winter rainfall region (Western Cape province of South Africa) is shown in (f).

Synthesis

Evaluation of the ability of a climate model to simulate the important features of observed regional climate is a necessary pre-requisite for developing regional climate change scenarios (e.g. Mitchell *et. al.*, 1987). Over southern Africa, evaluations of present climate performance of climate models have been limited to atmospheric GCMs linked to mixed-layer models (e.g. Joubert, 1995; Hewitson and Crane, 1996). The mean climate performance of a range of more recent (higher resolution) mixed-layer models as well as a range of fully-coupled models has been assessed in this chapter. The performance of both groups of models over southern Africa has not previously been assessed.

The mixed-layer and fully-coupled models all simulated the observed mean sea-level pressure distribution adequately. Features of the observed distribution which are well-reproduced include the Inter-Tropical Convergence over Angola in summer, the relative positions of the subtropical high pressure cells and their intensification in winter as well as the meridional pressure gradient south of the subcontinent. The mixed-layer models (with the exception of CSIRO) are all of higher spatial resolution than the fully-coupled models. The increased resolution is associated with better simulations of the intensity of the subtropical high pressures, the depth of the circumpolar trough and consequently in the strength of the meridional pressure gradient in the mid-latitudes. The BMRC, UKHI and CSIRO mixed-layer models best reproduce the observed mean sea-level pressure distribution. The UKTR fully-coupled model provides the best overall simulation of the fully-coupled models, although the MPIOC model performs well in winter. For both types of model, simulation errors at individual grid points throughout the tropics and subtropics are greater that the observed inter-annual variability and agreement with observations in terms of the magnitude of observed mean pressures is poor. In the mid-latitudes, inter-model agreement with observations is better, although this result is likely to reflect the larger observed inter-annual variability (and hence a larger range of acceptable values) rather than a real improvement in model performance.

The variation in annual temperature range over four climatically-distinct regions of the subcontinent is well captured by both the mixed-layer and fully-coupled models. In all four locations, however, individual models both over- and under-estimate observed summer and winter temperatures and no distinction on the basis of model type can be drawn. Comparisons of surface air temperature simulations are complicated by the fact that no standard field representing near-surface temperature is availa from all of the model models. In the case of the GFDL models, which display a tendency to over-estimate the observed annual temperature range over most regions, temperature at the lowest model level (0.99 sigma) have been used. By contrast, surface temperatures have been used for the CSIRO and UKMO models (for example). In each case, the fields which most closely represent screen height ten eratures have been used, but difference between models in terms of the simulation of observed annual temperature range do not necessarily represent differences in model performance.

In the Hadley Centre fully-coupled model, the inclusion of sulphate aerosol forcing in addition to forcing by greenhouse gases has not resulted in a statistically significant improvement in simulation of observed regional temperatures and temperature variability over recent decades. The absence of a clear distinction in performance due to the inclusion of sulphate aerosols over a region as small as southern Africa is r t unexpected given the high level of variability of temperature on small spatial scales (Mitchell *et al.*, 1995a). Differences between observed temperatures over the 1961 to 1990 period and both experiments are also not statistically significant. While no distinction can be drawn between the greenhouse gas and sulphate aerosol experiments, both represent observed temperatures over southern Africa accurately. Simulated diurnal temperature ranges also closely match observations, with largest diurnal ranges over the dry Kalahari Desert.

Simulation errors for average daily rainfall over the subcontinent are often considerably larger than the magnitude of the observed daily rainfall. The result is indicative of the unreliability of GCM estimates of regional rainfall totals observed in other regions (IPCC, 1990, 1992, 1995). No improvement in the present group of mixed-layer or fully-coupled models is observed over earlier mixed-layer model performance (Joubert, 1995). While the models display skill in terms of the representation of observed rainfall seasonality over the central interior, lit confidence can be placed in their ability to provide reliable estimates of grid-point changes in total rainfall in a future climate.

****

The present climate performance of both mixed-layer and fully-coupled models over southern Africa has been assessed. Regional climate performance from both types of models is largely resolution-dependent. For simulated mean sea-level pressure distributions, the mixed-layer models perform better than the coarser-resolution fully-coupled models. The inclusion of sulphate aerosol in addition to greenhouse gas forcing of regional climate in the Hadley Centre fully-coupled model integration does not result in a statistically significant improvement in the simulation of mean temperatures or temperature variability over recent decades, although both experiments accurately simulate observed temperatures over the region. Both mixed-layer and fully-coupled models simulate the observed pattern of rainfall seasonality over southern Africa well, but provide unreliable estimates of average daily rainfall at individual locations. The ability of two fully-coupled models to represent the features of intra- and inter-annual variability in mean sea-level pressure is considered in the next chapter.

****

The present climate performance of both mixed-layer and fully-coupled models over southern Africa has been assessed. Regional climate performance from both types of models is largely resolution-dependent. For simulated mean sea-level pressure distributions, the mixed-layer models perform better than the coarser-resolution fully-coupled models. The inclusion of sulphate aerosol in addition to greenhouse gas forcing of regional climate in the Hadley Centre fully-coupled model integration does not result in a statistically significant improvement in the simulation of mean temperatures or temperature variability over recent decades, although both experiments accurately simulate observed temperatures over the region. Both mixed-layer and fully-coupled models simulate the observed pattern of rainfall seasonality over southern Africa well, but provide unreliable estimates of average daily rainfall at individual locations. The ability of two fully-coupled models to represent the features of intra- and inter-annual variability in mean sea-level pressure is considered in the next chapter.

CHAPTER SIX

OBSERVED AND FULLY-COUPLED MODEL CIRCULATION VARIABILITY

Introduction

Fully-coupled ocean-atmosphere general circulation models are widely used to simulate the transient response of the climate system to increasing anthropogenic forcing of climate (IPCC, 1995). The extent to which a climate model reproduces observed features of variability largely determines the degree of realism with which changes in climate and climate variability due to increasing anthropogenic forcing can be predicted (Murphy, 1995). The representation of ocean dynamics in fully-coupled models means that important features of inter-annual variability associated with El Niño / Southern Oscillation (ENSO) forcing in the tropical Pacific Ocean can be directly simulated. By definition, atmospheric general circulation models linked to simple mixed-layer non-dynamic oceans are unable to represent ENSO-related variability unless forced by observed sea-surface temperatures (Campbell *et al.*, 1995). A comprehensive assessment of the response of the climate system as a whole to anthropogenic climate change, including possible changes in ENSO variability, requires the use of fully-coupled models (Murphy, 995; Murphy and Mitchell, 1995).

Fully-coupled models are capable of reproducing variability on inter-monthly and inter-annual time-scales which is similar, although of lower amplitude, to the observed variability (Meehl, 1995). There is evidence to suggest that the mechanisms responsible for the variability are operating in both the natural system and the coupled models (Meehl *et al.*, 1994). This observation is applicable to most fully-coupled models, and is most apparent for the case of ENSO-related inter-annual variability in the tropics, where simulated variability is generally half the amplitude of that observed (Meehl *et al.*, 1993a; Meehl *et al.*, 1993b; Meehl *et al.*, 1994; Tett, 1995; Campbell *et al.*, 1995).

Around southern Africa, atmospheric circulation varies on both intra- and inter-annual time-scales (McGee and Hastenrath, 1966; Harrison, 1986; Tyson, 1986). On intra-annual time-scales, the strong summer season (October-March) rainfall maximum over the interior region south of 20°S, is associated with the seasonal migration of the Inter-Tropical Convergence Zone, longitudinal shifts in the position of the subtropical high -pressure systems adjacent to the subcontinent (Vowinckel, 1955; McGee and Hastenrath, 1966; Tyson, 1981, Tyson, 1986) and associated variations in the mid-latitude storm track (van Loon, 1972). Systematic large-scale adjustment in circulation around southern Africa are related to inter-annual variability in summer rainfall over the subcontinent (Harrison, 1986; Tyson, 1986) and have been discussed in Chapter 4.

During dry conditions the centre of tropical convection over the subcontinent is displaced eastward, resulting in anomalously high pressures over the subcontinent (Miron and Tyson, 1984, Harrison, 1986). Changes in Hadley cell mass overturning and the zonal Walker circulation respond to changes in the longitudinal position of convection and have been related to ENSO variability in the tropical Pacific Ocean (Harrison, 1986; Lindesay, 1988). These changes are also associated with higher pressures in the region of Gough Island (Miron and Tyson, 1984), indicating a northward displaced of the temperate circulation and reflecting an eastward shift in the position of the trough of standing wave 3 and cloud bands linking tropical and temperate circulation systems (Harrison, 1986).

Most existing analyses of simulated circulation variability by fully-coupled models have focused on features of inter-annual variability such as ENSO and possible changes in ENSO variability in the tropical Pacific resulting from climate change (cf. Meehl *et al.*, 1993a; Meehl *et al.*, 1993b; Meehl *et al.*, 1994; Campbell *et al.*, 1995). The objective in this Chapter is to assess the ability of two fully-coupled models to simulate present-day mean sea-level pressure variability around southern Africa on both intra- and inter-annual time-scales. The approach adopted here differs from that of Campbell *et al.* (1995), for instance, in that the seasonal cycle in sea-level pressure is *not* removed prior to analysis.

Control climate integrations from the Commonwealth Scientific and Industrial Research Organisation (CSIROC CM8, Gordon and O'Farrell, 1996) and the Second Hadley Centre for Climate Prediction and Research (HADCM2 CON, Johns *et al.*, 1996; Tett *et al.*, 1996) fully-coupled models are utilised. Observed mean sea-level pressure variability is described using principal components analysis. Simulated principal components are rotated onto the observed matrix of loadings using Procrustes Target Rotation (Richman, 1986). The target rotation attempts to provide the closest possible fit (in a least squares sense) between a given matrix (simulated loadings) and the target matrix (observed loadings). This procedure ensures that the ability of the coupled models to reproduce the observed pattern of variability is tested formally.

Observed Circulation Variability

Examinations of observed circulation variability around southern Africa using principal components analysis have been performed previously. The analyses of Dyer (1981) describe features of inter-annual variability in mean sea-level pressure in the South Indian and South Atlantic Oceans. In addition, Tyson (1984) used principal components analysis to describe the relationship between geopotential height indices at 850 and 500 hPa and inter-annual rainfall over the subcontinent. In order to assess the fully-coupled model simulations of contemporary variability in mean sea-level pressure it is necessary to re-assess the features of observed variability. Features of both intra- and inter-annual variability are considered using 1951-1985 data. The region considered extends from 10°E to 90°E and from 15°S to 60°S.

Spatial Characteristics

Six principal components of observed mean sea-level pressure have been rotated. Each principal component accounts for more than 5 per cent of the total variance in the data. The loading patterns on each principal component indicate regions of cohesive spatial variance representing the principal modes of variability in the data. It is possible to ascribe some physical interpretation to these modes. Component loading patterns for the first six observed principal components are shown in Figure 6.1. The sign of all loadings is arbitrary. Collectively, the first six PCs account for more than 94 per cent of the total variance in the observed data (Table 6.1).

The region of highest loadings for PC 1 (Fig. 6.1a) is located in the mid-latitudes over a wide region extending from 10°E to 80°E and accounts for 39.3 per cent of the total variance (Table 6.1). The loading pattern represents variability associated with meridional shifts in the location of the mid-latitude storm-track on an annual cycle. It is likely that the loading pattern is the surface manifestation of variability associated with planetary wave activity. Planetary waves 1-3 in the southern hemisphere exhibit an equivalent barotropic structure, accounting for between 70 and 90 per cent of the variance in 500 hPa geopotential heights (van Loon and Jenne, 1972; Trenberth, 1979, 1980). The longitudinal position of PC 1 marks the location of the trough of standing wave 1 at subpolar latitudes, as well as the ridge of standing wave 3 (van Loon and Jenne, 1972; Trenberth, 1980).

Table 6.1. Rotated eigenvalues, variances and cumulative variances associated with the first six principal components of observed mean sea-level pressure for the southern African region. Mean sea-level pressure data include the annual cycle. Principal components are calculated using a correlation matrix and rotated using the varimax criteria.

Principal Component	Eigenvalues	Percentage of Total Variance	Cumulative Percentage of Total Variance
PC 1	82.6	39.3	39.3
PC 2	39.3	18.7	58.0
PC 3	23.1	11.0	69.0
PC 4	20.2	9.6	78.6
PC 5	18.6	8.8	87.4
PC 6	14.1	6.7	94.1

The loading patterns on PCs 2 and 3 represent variability in the South Indian and South Atlantic Anticyclones respectively (Figs. 6.1b and 6.1c). Longitudinal shifts in the position of the anticyclones during the year are larger than latitudinal shifts (McGee and Hastenrath, 1966; Tyson, 1986). The South Indian Anticyclone shifts 24° eastwards from

88°E in December to 64°E in July. This is larger than the shift in the South Atlantic Anticyclone which shifts 14° of longitude from 16°W in August to 2°W in December (Vowinckel, 1955; McGee and Hastenrath, 1966). Atmospheric variability over the subtropical Indian Ocean is consequently greater than over the South Atlantic Ocean on both intra-seasonal and inter-annual time-scales (Dyer, 1981). This feature is reflected in the principal components; PC 2 accounts for 18.7 per cent whereas PC 3 accounts for 11.0 per cent of total variance in mean sea-level pressures (Table 6.1).

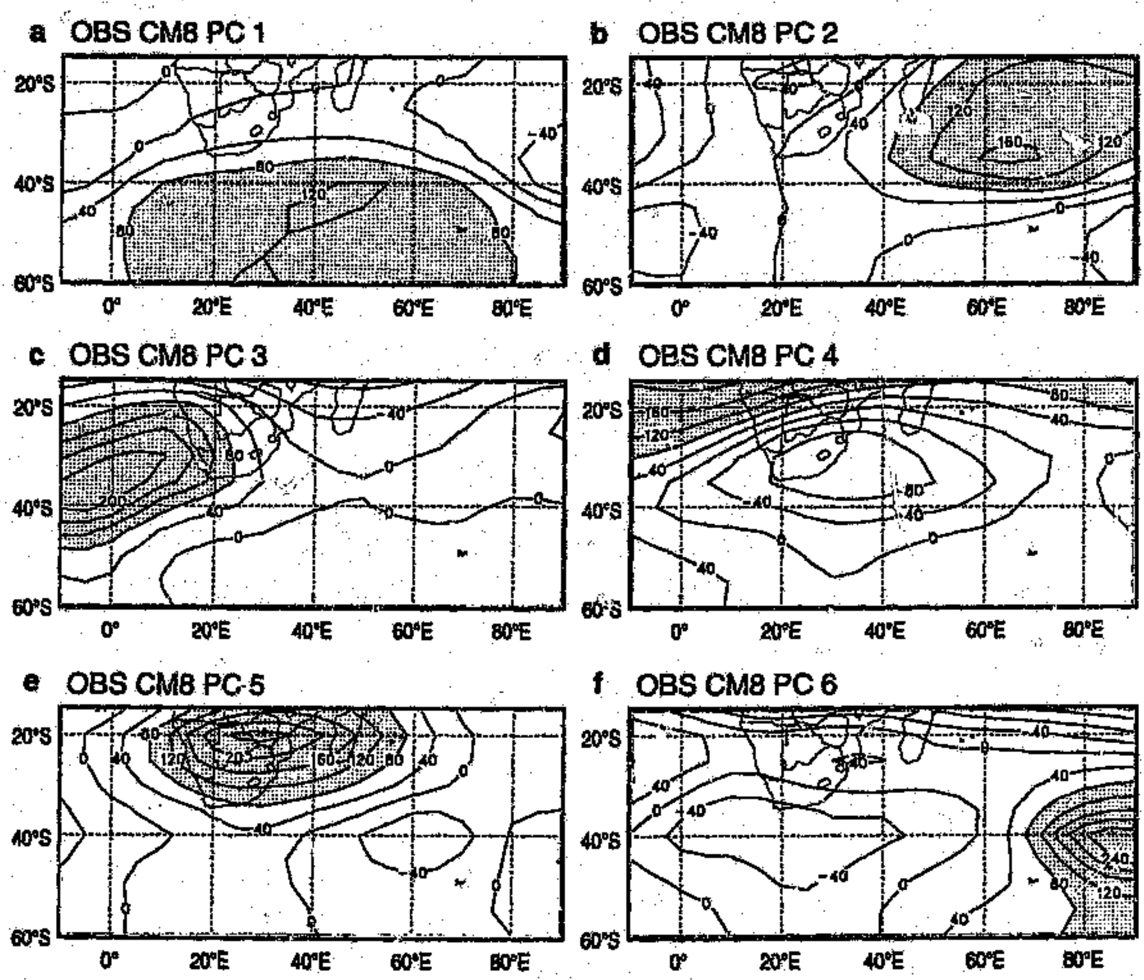

Figure 6.1. Observed mean sea-level pressure rotated principal component loading patterns for the first six principal components (a-f). Observed principal components are rotated using the varimax criteria.

The loading pattern on PC 4 is characterised by localised maxima throughout the tropics north of 20°S, and secondary maxima of the opposite sign located in the subtropics near 30°S (Fig. 6.1d). PC 4 accounts for 9.6 per cent of the total variance in mean sea-level pressures (Table 6.1). The pattern suggests an out of phase relationship between pressures over the tropics and subtropics which is approximately zonally uniform. The pattern suggests a coherent variation in circulation between the equator and approximately 30°S which may be related to inter-annual variability in Hadley cell mass overturning (Harrison, 1986; Lindesay, 1988).

PC 5 accounts for 8.8 per cent of the total variance in mean sea-level pressures (Table 6.1). The associated loading pattern has a maximum located over southern Africa, extending eastwards into the subtropical Indian Ocean (Fig 6.1e). The loading pattern represents variability associated with the annual cycle in mean sea-level pressures, which displays a maximum amplitude of greater than 4 hPa and accounts for 95 per cent of the total variance in that region (Taljaard *et al.*, 1969; van Loon, 1972).

The maximum loadings on PC 6 are located on the eastern boundary of the data window, and indicate a region of coherent spatial variance in the mid-latitudes of the Indian Ocean near Australia (Fig 6.1f). PC 6 accounts for 6.7 per cent of the total variance in mean sea-level pressure. The loading pattern is likely to be associated with blocking activity in the Australian region (Trenberth and Mo, 1985).

Temporal Characteristics

Observed mean sea-level pressures for the 1951-1985 period were not de-seasonalised before performing principal components analysis. This approach was adopted because circulation around southern Africa exhibits significant intra- and inter-annual variability (Tyson, 1986). Variations in synoptic-scale circulation can be associated with both the seasonal cycle of rainfall over southern Africa and with inter-annual rainfall variability (Harrison, 1986; Tyson, 1986). It is argued that any assessment of fully-coupled model variability over southern Africa must consider the models' ability to simulate the relative importance of both intra- and inter-annual circulation variability.

Intra-annual variability

The mean annual cycle of the first six principal component scores is described in terms of harmonic analysis. The percentage of variance in the mean annual cycle explained by each harmonic is illustrated for each of the first six principal components in Table 6.2. PC 1 exhibits a very strong annual cycle, with the first harmonic explaining 94 per cent of the total variance in PC scores. The first harmonic also accounts for more than 50 per cent of the total variance in PC 2, and more than 40 per cent of the total variance in PCs 5 and 6 (Table 6.2). The semi-annual cycle (PC 2) accounts more than 20 per cent of the total variance in PCs 2, 3 and 6. The annual and semi-annual cycles therefore explain in excess of 60 per cent of the total variance in PCs 1, 2, 3 and 6. Contributions from other harmonics only exceed the contribution of the first two harmonics on PC 4, where for example, the fifth harmonic accounts for 21.2 per cent of the total variance (Table 6.2).

Inter-annual variability

Conceptual models of atmospheric adjustments in the vicinity of southern Africa during wet and dry years have been established (Harrison, 1986; Tyson, 1986). The extent to which the principal component loading patterns and scores calculated here can be associated with inter-annual rainfall variability over the subcontinent is discussed below. The spectral characteristics of de-seasonalised PC scores on the six principal components of observed mean sea-level pressure are illustrated in Figure 6.2.

PC 1 exhibits small spectral peaks (~10 % of the normalised variance) at 7.6, 10.06 and 14.13 years (Fig. 6.2a). All of these peaks are significant at the 99 per cent significance level. The overwhelming importance of the annual cycle in PC 1 (Table 6.2) is evident from the absence of any peak at this wavelength in the de-seasonalised scores. There is no evidence to suggest a link between PC 1 and inter-annual rainfall variability over the subcontinent.

Table 6.2. Percentage of total variance explained by the first six harmonics on each observed principal component.

Principal Component	Harmonic					
	1	2	3	4	5	6
PC 1	94.1	2.0	1.1	1.0	1.0	0.7
PC 2	51.8	20.7	10.7	7.7	6.6	2.6
PC 3	34.7	26.6	17.3	9.7	8.7	3.0
PC 4	24.8	14.6	17.8	14.0	21.2	7.7
PC 5	44.5	14.4	12.6	13.5	9.9	5.0
PC 6	42.8	25.2	7.4	13.1	7.5	4.1

PC 2 exhibits spectral peaks significant at the 95 per cent level at 3.7, 5.6, 7.0 and 12.8 years (Fig. 6.2b). The spectral peaks between 3 and 7 years display some similarity to the Southern Oscillation, and similar spectral peaks have been observed in sea-surface temperatures in the tropical western Indian Ocean (Mason, 1995). The scores are strongest during the summer rainfall months of December, January and February (not shown) and therefore a possible link to inter-annual rainfall variability exists. De-seasonalised scores for PC 2 for the 1951-1985 period are shown in Figure 6.3a. There is some evidence to suggest that minima in PC 2 scores occur during dry years. Considered in conjunction with the loading pattern (Fig. 6.1b), this would suggest that a weaker South Indian Anticyclone occurs during dry years. In fact, during dry years the South Indian Anticyclone is typically weaker than normal, resulting in a diminished north-easterly inflow of moisture (an important source of moisture during summer) over the east coast (Jury and Pathack, 1993; D'Abreton and Lindesay, 1993, D'Abreton and Tyson, 1995).

Significant spectral peaks in PC 3 occur at 3.6, 4.2, 7.6 and 10.5 years (Fig. 6.2c). The peak at 10.5 years is the strongest observed on any PC, accounted for almost 35 per cent of the normalised variance of PC 3. The scores are strongest during the early winter months of May and June, although strong scores also occur during November and December. While clearly PC 3 does exhibit features of inter-annual variability, these cannot be clearly related to inter-annual rainfall variability over the summer rainfall region.

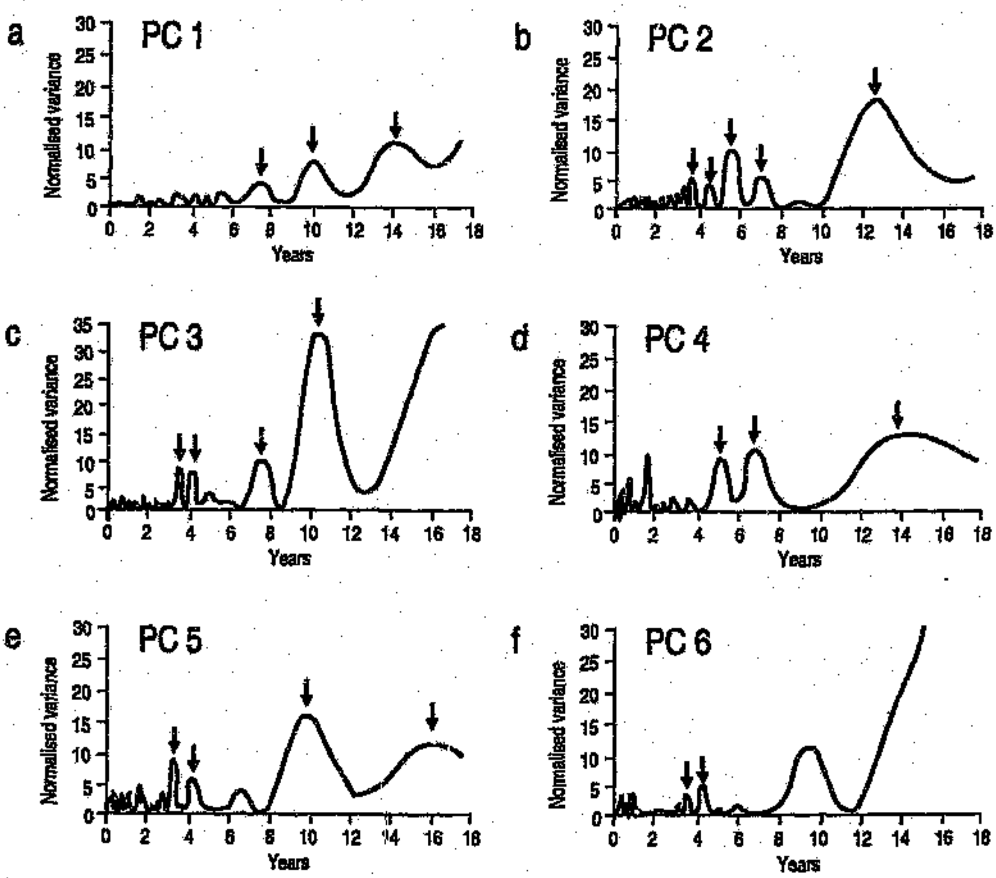

Figure 6.2. Results of spectral analysis on the first six principal component scores (a-f). Scores have been de-seasonalised. Spectral peaks indicated by an arrow are significant at the 99 per cent confidence level.

PC 4 exhibits significant spectral peaks at 1.4, 5.0, 6.7 and 14.1 years (Fig. 6.2d). De-seasonalised scores (Fig. 6.3b) reach minima during predominantly dry years. The loading pattern on PC 4 has been related to Hadley cell mass overturning (Fig. 6.1d). The Hadley circulation weakens during dry years over the subcontinent, and strengthens to the east of the subcontinent in association with longitudinal shifts of convection (Harrison, 1986; Lindesay, 1988) and strengthens during periods of increased rainfall. Strong scores occur during the late summer months of February and March, but are strongest during the winter months of July, August and September. During the late summer season, strong scores are predominantly negative (Fig. 6.3b), supporting a link between inter-annual variability in

Hadley cell mass overturning and inter-annual rainfall variability. During the late summer, variability in the Hadley circulation of tropical southern Africa has been linked to ENSO variability in the central Pacific Ocean and the Walker Circulation in the tropical Indian Ocean (Lindesay, 1988). A link between PC 4 and ENSO is supported by the significant spectral peaks between 5 and 7 years (Fig. 6.2d).

PC 5 exhibits significant spectral peaks at 3.2, 9.9 and 15.9 years (Fig 6.2e). Minima in de-seasonalised scores occur predominantly during wet years (Fig. 6.3c), suggesting that wet years over the subcontinent may be associated with negative pressure anomalies over the subcontinent (Miron and Tyson, 1984). This suggestion is strengthened by the fact that scores are strongest during the summer rainfall season (specifically during December, January and February).

Significant spectral peaks in PC 6 occur at 4.3 and 9.5 years (Fig. 6.2f). Given the location of the loading pattern in the vicinity of Australia, these do not appear to be related in any physically consistent way to inter-annual rainfall variability over the subcontinent.

An attempt has been made above to relate features of inter-annual variability in principal components of mean sea-level pressure to inter-annual variability in summer rainfall over the southern African subcontinent. However, several of the principal components exhibit significant spectral peaks at approximately 10 years. A 10-12 year rainfall oscillation accounts for over 30 per cent of the inter-annual rainfall variance over a very small region limited to extreme south coast of South Africa and is associated with year-round rainfall (Dyer, 1975, Tyson, 1986). The 10-12 year oscillation has been linked to changes in the position of standing wave 3 (Vines, 1980; Tyson, 1981). Several of the principal component loading patterns may be linked to planetary wave activity (PCs 1, 2, 3 and 6). Spectral peaks at approximately 10 years occur on each of these PCs (Fig. 6.2). Recent analyses of southern hemisphere circulation have identified a quasi decadal-scale variability in the circulation at high latitudes which has been linked to changes in standing wave activity (van Loon *et al.*, 1993; Hurrell and van Loon, 1994). Evidence suggests that the semi-annual component of the circulation weakened considerably and disappeared in the Pacific Ocean after the late 1970's; a change which was concurrent with an increase in the amplitude of standing wave 3 and decreases in the central pressures of the circumpolar trough and subtropical ridge (van Loon *et al.*, 1993). This may be expected to be reflected in the principal components of mean sea-level pressure which are associated with standing waves. Evidence for a decrease in the amplitude of the semi-annual component of principal component 3 after approximately 1977 is shown in Figure 6.4. While considerable inter-annual variability in the amplitude of the second harmonic exists between 1951 and 1985, the amplitude falls sharply after 1977 and does not recover by the end of the time series (Fig. 6.4).

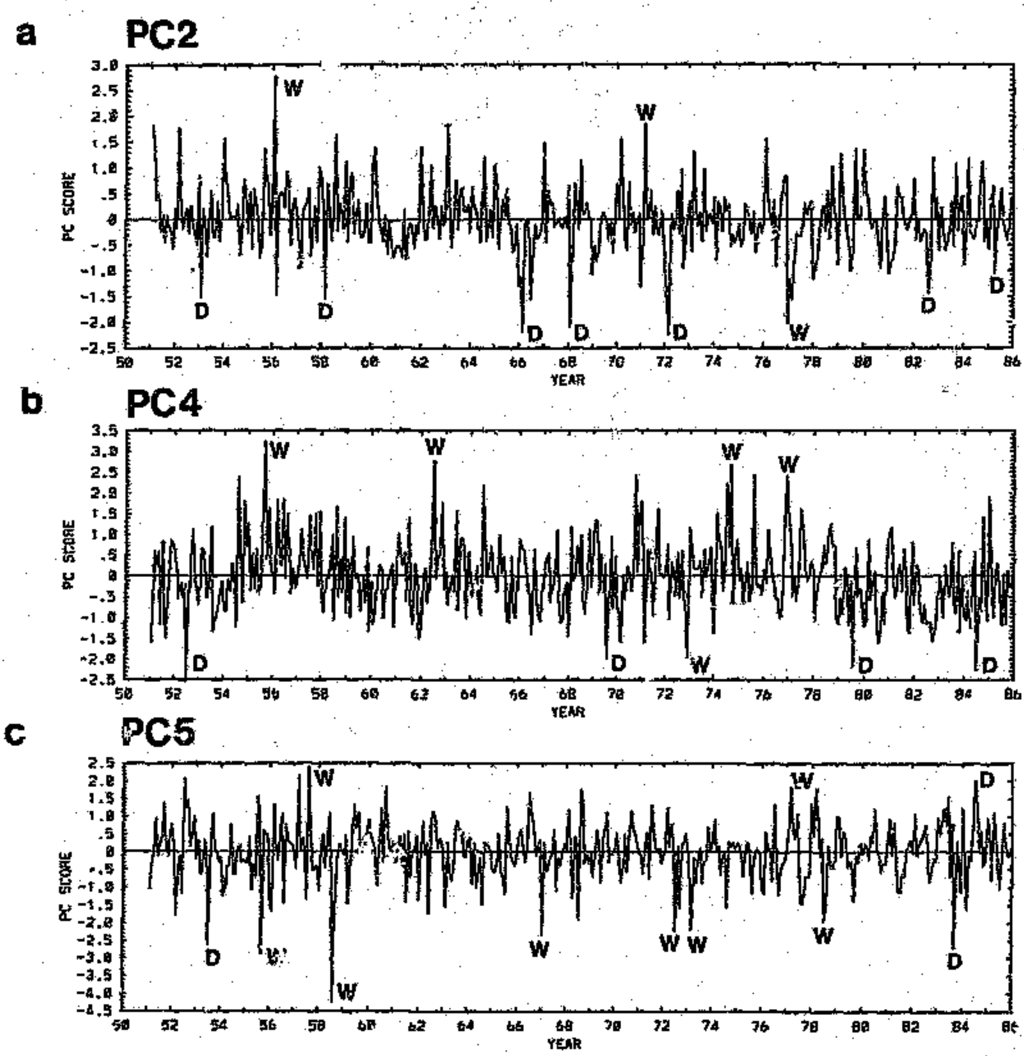

Figure 6.3. De-seasonalised principal component scores for the period 1951-1985 for observed PC 2 (a), PC 4 (b) and PC 5 (c). Predominantly dry years are indicated by the letter "D" and predominantly wet years by the letter "W".

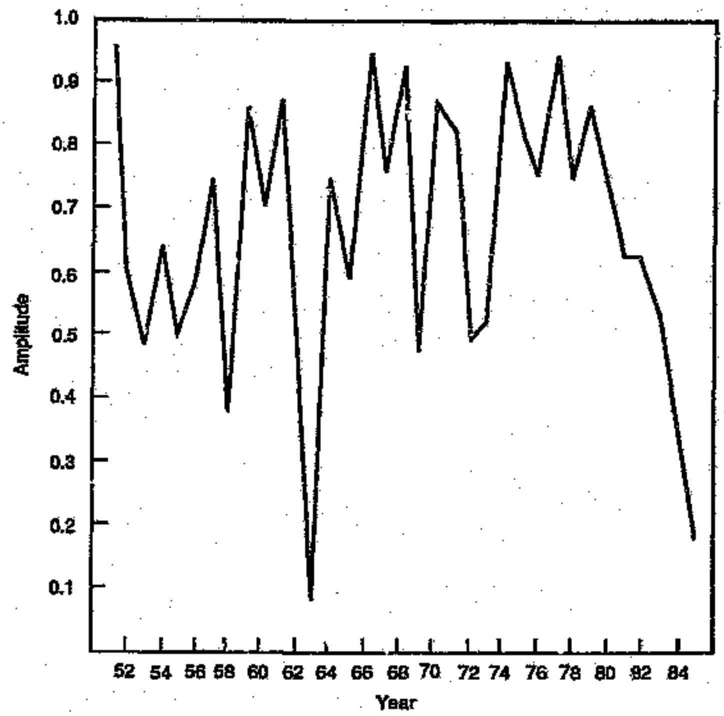

Figure 6.4. The amplitude of the second harmonic of observed PC 3 for the period 1951-1985.

Simulated Circulation Variability

Spatial Characteristics

The matrix of principal component loadings for both the CSIRO and Hadley Centre fully-coupled model control runs have been rotated using a Procrustes Target Rotation to provide the best possible agreement with the matrix of observed loadings. This procedure is used to test directly the ability of the models to represent the observed modes of mean sea-level pressure variability around southern Africa. The loading patterns for the first six principal components are shown in Figs. 6.5 and 6.6 for the CSIRO and Hadley Centre model control runs, respectively. The results of the principal components analyses for each model are summarised in Table 6.3.

The results summarised in Table 6.3 indicate that neither coupled model simulates as much variability in mean sea-level pressure as is observed in the region around southern

Africa (compare to Table 6.1). The first six PCs simulated by the CSIRO fully-coupled model account for only 64.7 per cent of the total variance accounted for by the first six observed principal components. The corresponding value for the Hadley Centre fully-coupled model is 72.5 per cent (Table 6.3). For the CSIRO model, PC 1 accounts for half of the variance of the first observed principal component. The cumulative percentage of total variance explained by all six CSIRO PCs is less than that accounted for by the first three observed PCs. The CSIRO model also does not represent the hierarchical contribution of each PC to the total variance. PC 4 accounts for less variability than any other PC, suggesting that the model does not reproduce the observed variability in Hadley cell mass overturning accurately. The first PC simulated by the HADCM2 CON model accounts for approximately 75 per cent of the variance explained by the first six observed PC (Table 6.3). While this is still a substantial under-estimate, it is considerably better than the performance of the CSIRO model. Like the CSIRO model, the Hadley Centre fully-model under-estimates variability in the Hadley Cell mode (PC 4) in particular, and assigns a greater proportion of the overall variance in mean sea-level pressure to PC 5.

Procrustes Target Rotation attempts to rotate a given matrix (of simulated loadings) to fit a target matrix (of observed loadings) as closely as possible. It is therefore expected that the loadings patterns on the first six PCs for both the CSIRO (Fig. 6.5) and Hadley Centre models (Fig. 6.6) closely resemble the observed loading patterns (Fig. 6.1). However, both of the models simulate a region of maximum loadings on PC 1 which extends further west and not as far east as observed (Figs. 6.5a and 6.6a). The region of maximum loadings over the subtropical Indian Ocean on PC 2 is better reproduced by the Hadley Centre (Fig. 6.6b) than the CSIRO model (Fig. 6.5b), which displaces the maximum loadings east of their observed location. Both models under-estimate the maximum loading on this PC. Observed loadings on PC 3 are also stronger than those simulated by either model (compare Fig. 6.1c to Figs. 6.5c and 6.6c). Weakest loadings are simulated by the CSIRO model (Fig. 6.5c). The location of the loading pattern is however well reproduced by both models. For PC 4 the approximately zonal symmetry in the juxtaposition of loadings of opposing sign between the tropics and subtropics is better reproduced in the Hadley Centre (Fig. 6.6d) than in the CSIRO (Fig. 6.5d) model. The CSIRO model also under-estimates the magnitude of the loadings more seriously than the

Hadley Centre model. The magnitude of loadings on simulated PCs 5 and 6 (Figs. 6.5e,f and 6.6e,f) is also weaker than observed. However, both models, and notably the Hadley Centre model (Fig. 6.6f) tend to locate a stronger than observed secondary loading maximum near 20°E, and some 20° further south than observed.

Table 6.3. Procrustes rotated eigenvalues, variances and cumulative variances associated with the first six principal components of mean sea-level pressure from the CSIRO and Hadley Centre fully-coupled model control runs over the southern African region. Mean sea-level pressure data include the annual cycle and principal components are calculated using a correlation matrix and rotated using Procrustes Target Rotation.

Principal Component	Eigenvalues	Percentage of Total Variance	Cumulative Percentage of Total Variance
CSIRO CM8			
PC 1	43.2	20.6	20.6
PC 2	31.0	14.8	35.4
PC 3	19.3	9.2	44.6
PC 4	10.3	4.9	49.5
PC 5	17.4	8.3	57.8
PC 6	14.4	6.9	64.7
HADCM2 CON			
PC 1	62.6	29.8	29.8
PC 2	24.2	11.5	41.3
PC 3	18.4	8.8	50.1
PC 4	11.6	5.5	55.6
PC 5	23.9	11.4	67.0
PC 6	11.5	5.5	72.5

Temporal Characteristics

Intra-annual variability

The contribution to the mean annual cycle of each harmonic on the first six PCs simulated by the CSIRO and Hadley Centre models is shown in Table 6.4 and may be compared to the observations in Table 6.2. Both models simulate a dominant annual cycle on PC 1 as observed, although the CSIRO model under-estimates it's contribution to the annual cycle by approximately 10 per cent. The first three observed harmonics on PC 2 account for more than 80 per cent of the total variance (Table 6.4). The annual cycle on PC 2 is over-estimated by the CSIRO model (70 %) and under-estimated by the HADCM2 model (40 %). As a consequence, the CSIRO model under-estimates the contribution of the semi-annual cycle on PC 2 to the total variance, and the Hadley Centre model exaggerates the contributions from PC 3 (Table 6.4).

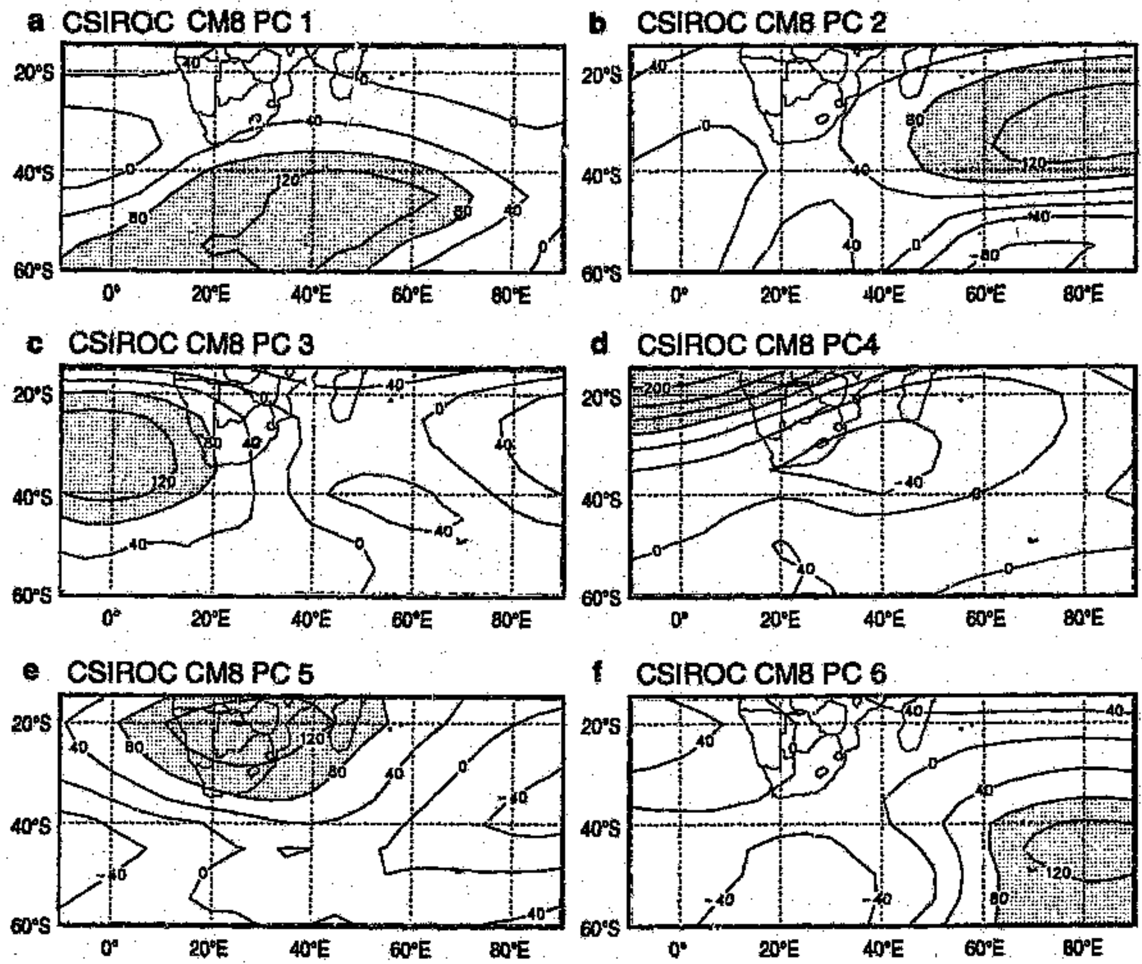

Figure 6.5. Loading patterns on the first six principal components (a-f) simulated by the CSIROC CM8 coupled model control run. Loadings on each PC have been rotated using Procrustes Target Rotation.

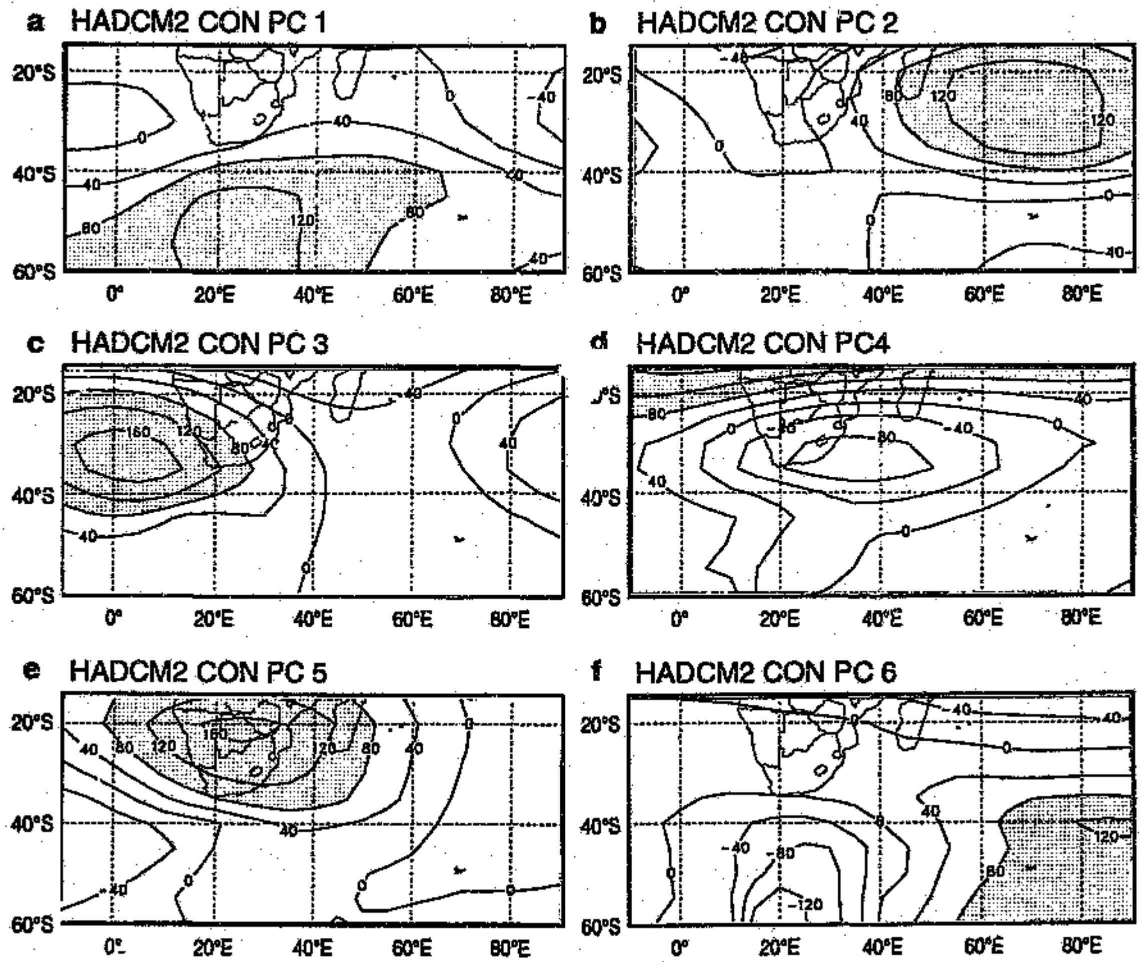

Figure 6.6. As for Figure 6.5, but for the HADCM2 CON coupled model control run.

As with PC 2, the first three harmonics on observed PC 3 account for almost 80 per cent of the total variance. The annual cycle on PC 3 is over-estimated by approximately 20 per cent in the CSIRO model, and slightly under-estimated by the Hadley Centre model. Both models fail to capture the contribution of the semi-annual cycle on PC 3, but both represent the contribution of harmonic 3 reasonably. While the first three harmonics in the Hadley Centre model account less of the total variance than both CSIRO and observed, their relative contributions to the total variance are more accurate than in the CSIRO simulation.

Table 6.4. Percentage of total variance explained by the first six harmonics on each principal component for CSIROC CM8 and HADCM2 CON integrations.

Principal Component	Harmonic					
	1	2	3	4	5	6
PC 1						
CSIROC CM8	84.0	3.5	4.2	3.7	3.4	1.1
HADCM2 CON	92.6	1.8	2.2	1.5	1.4	0.5
PC 2						
CSIROC CM8	69.5	10.2	6.4	5.9	5.4	2.6
HADCM2 CON	39.6	18.4	14.6	10.7	13.5	3.3
PC 3						
CSIROC CM8	53.6	9.9	13.4	8.5	9.3	5.4
HADCM2 CON	27.1	14.7	18.7	17.8	14.5	7.2
PC 4						
CSIROC CM8	33.5	16.6	14.6	16.5	11.8	7.0
HADCM2 CON	33.6	24.9	13.1	12.4	10.8	5.2
PC 5						
CSIROC CM8	46.8	13.2	13.3	11.1	11.0	4.7
HADCM2 CON	36.6	22.2	11.9	12.8	9.4	7.1
PC 6						
CSIROC CM8	37.3	28.9	13.5	8.0	9.4	2.9
HADCM2 CON	57.0	17.8	9.0	7.7	5.7	2.8

Harmonics 1 and 5 on observed PC 4 both account for more than 20 per cent of the annual cycle, with harmonics 2, 3 and 4 accounting for roughly 15 per cent each (Table 6.4). Both models represent contributions from the first five harmonics in excess of 10 per cent. However, both models exaggerate the contribution from the annual and semi-annual cycles (harmonics 1 and 2), and under-estimate the contribution from PC 5 by half.

The annual cycle in observed PC 5 accounts for almost 45 per cent of the total variance. The CSIRO model captures this feature well, although it is under-estimated in the Hadley Centre model (Table 6.1). The Hadley model also simulates a stronger than observed contribution to intra-annual variance from the semi-annual cycle. The annual and semi-annual cycle also dominate observed PC 6. While both models capture this feature, the CSIRO model under-estimates the contribution of the annual cycle by 6 per cent, and the Hadley Centre model over-estimates the contribution of the first harmonic by nearly 15 per cent (Table 6.1). The Hadley Centre model also simulates a weaker than observed semi-annual cycle, although this is well captured in the CSIRO model.

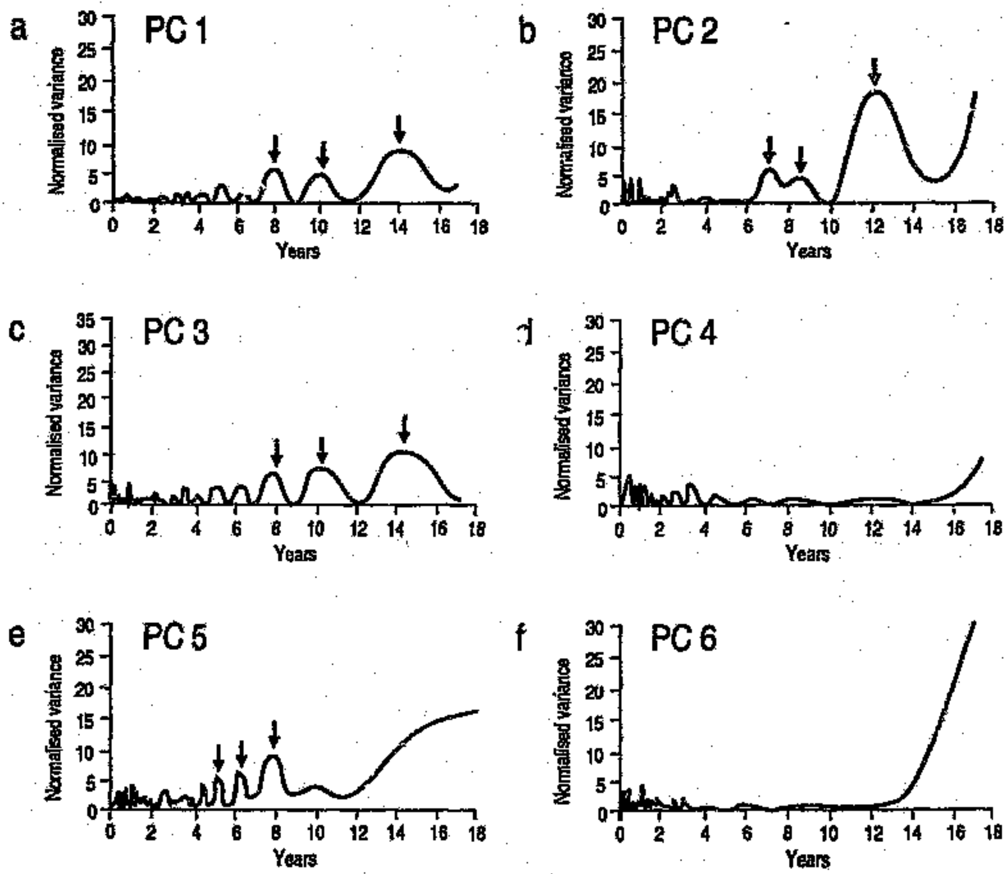

Figure 6.7. Results of spectral analysis on the first six principal component scores (a-f) for the CSIROC control integration. Scores have been de-seasonalised. Spectral peaks indicated by an arrow are significant at the 99 per cent confidence level.

Inter-annual variability

In general, both models under-estimate the amplitude of inter-annual variability over the southern African region (Figs. 6.7 and 6.8). The CSIRO model exhibits significant spectral on PC 1 at 7.9, 10.3 and 14.4 years (Fig. 6.7a). All three, coincide with similar peaks in the observed PC scores. Spectral peaks on PC 2 (Fig. 6.7b) occur at 7.2, 8.7 and 12.3 years and at 7.9, 10.3 and 14.7 years on PC 3 (Fig. 6.7c). While the spectral peaks at approximately 7 and 12 years on PC 2, are similar to observations, they account for less of the normalised variance than observed. While the peak at 10 years in observed PC 3 scores is present in the CSIRO model, it accounts for less than one third of the normalised variance accounted for by the observed s ral peak. No significant spectral peaks occur on PC 4 or PC 6 Figs. 6.7d,f), but very small peaks (accounting for less than 10 per cent of the normalised variance) occur at 5.2, 6.2 and 7.8 years on PC 5 (Fig. 6.7e). The significant peak at approximately 10 years in observed PC 5 is notably absent in the CSIRO model. Only the spectral peak at 12.3 years of PC 2 (Fig. 6.7b) accounts for more than 10 per cent of the normalised variance in CSIRO PC scores.

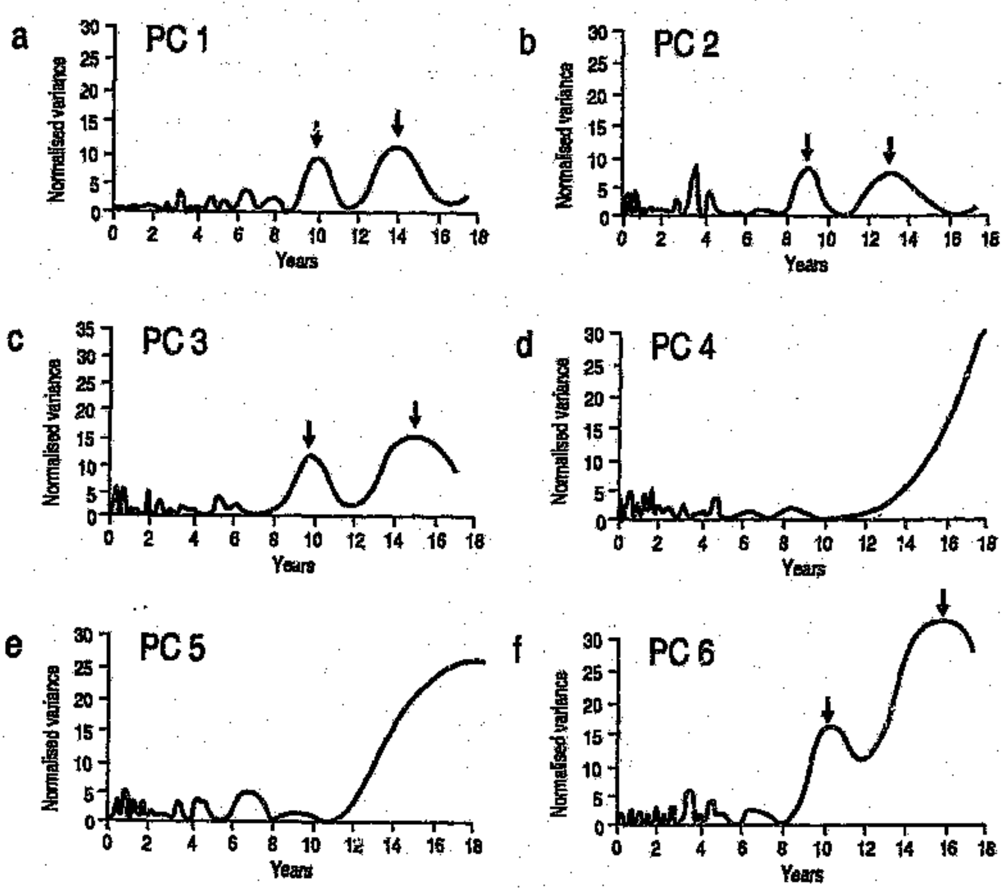

Figure 6.8. for Fig. 6.7, but for the HADCM2 control integration.

Results of spectral analysis for the Hadley Centre control integration are shown in Figure 6.8. In general, the Hadley Centre model performs slightly better than the CSIRO model in simulating the inter-annual variability captured by the first six principal components. The spectral peaks on PC 1 at 10.1 and 14.1 years (Fig. 6.8a) are similar to those observed, and account for roughly 10 per cent of the normalised variance on PC 1. Spectral peaks at 3.7 and 13.3 on PC 2 correspond to those observed, but the observed spectral peaks between 5 and 7 years associated with ENSO variability are absent in the Hadley Centre model, which simulates a peak at approximately 9 years (Fig. 6.8b). The spectral peak at approximately 10 years in PC 3 is captured by the Hadley Centre model (Fig. 6.2c), although like CSIRO, it accounts for little more than 30 per cent of the normalised variance accounted for the observed spectral peak. Again like CSIRO, significant spectral peaks on PC 4 (Fig. 6.8d) are absent. The spectrum of inter-annual variability on PC 5 (Fig. 6.8e) is also quite different to that observed. The spectral peak on PC 6 at approximately 10 years (Fig. 6.8f) accounts for more of the normalised variance in scores than observed, although this features is entirely absent in the CSIRO model.

Synthesis

Six coherent patterns of spatial variance in mean sea-level pressure around southern Africa have been identified using principal components analysis. Together, the first six observed principal components explain more than 94 per cent of the total variance over the region. Each of these are associated with specific synoptic-scale circulation systems or coherent features of intra- and inter-annual variability. PC 1 represents meridional shifts in the mid-latitude storm track on an annual cycle. Maximum loadings are located in the same region as the trough of standing wave 1 and the ridge of standing wave 3, suggesting that planetary wave activity is an important influence on this component.

PCs 2 and 3 are associated with variability in the South Indian and South Atlantic Anticyclones, respectively. Variability in the former is known to be greater than the latter, and hence is associated with PC 2. Spectral analysis of de-seasonal scores on PC 2 indicates spectral peaks which are similar to ENSO-like inter-annual variability. Peak scores also occur during the summer months, suggesting that variability in the South Indian Anticyclone is associated inter-annual rainfall variability. Accordingly, drier periods over the subcontinent are associated with weaker pressures in the south-west Indian Ocean (Jury and Pathack, 1993; D'Abreton and Lindesay, 1993, D'Abreton and Tyson, 1995). PC 3 exhibits statistically significant inter-annual variability at approximately decadal time-scales. Recent analyses of circulation in the high latitudes of the southern hemisphere have identified decadal scale variability in sea-level pressures and 500 hPa heights which are related changes in the amplitude of planetary wave 3 (van Loon *et al.*, 1993), and have been linked to a decrease in the strength of the semi-annual cycle (Hurrell and van Loon, 1994) after approximately 1977. The amplitude of the semi-annual cycle in PC 3 scores shows a similar decline after 1977, suggesting that variability in the South Atlantic Anticyclone can be associated with planetary wave activity.

PC 4 represents coherent variations of opposite sign between the tropics and subtropics throughout the region, suggesting variability in Hadley Cell mass overturning. Time-series of de-seasonalised scores show that lower pressures in the tropics and higher pressures in the subtropics, for example over the subcontinent occur during drier years. This pattern in PC scores occurs during the late summer months, suggesting a link between variability in the zonal Walker Circulation and ENSO and summer rainfall over the subcontinent (Lindesay, 1988). Strongest scores, however occur in mid-winter, suggesting that this is not the dominant mode of inter-annual variability on PC 4.

PC 5 is associated with the annual cycle in mean sea-level pressures, but does exhibit inter-annual variability suggesting a link between lower pressures over the subcontinent and wetter conditions (Miron and Tyson, 1984, Tyson, 1986). The location of PC 6 on the far eastern extreme of the region indicates that no link exists to inter-annual variability in rainfall over the subcontinent, although the PC is likely to be associated with blocking activity in the Australian region (Trenberth and Mo, 1985).

In general, the fully-coupled models are capable of reproducing, at least in qualitative terms, the principal models of variability associated with mean sea-level pressure around southern Africa. However, both the CSIRO and Hadley Centre fully-coupled models simulated weaker than observed variability over the region. The CSIRO model accounts for only 65 per cent of the observed variability over the region, while the Hadley model performs slightly better, accounting for 73 per cent of the total variance. Differences in the contribution of individual PCs to the observed cumulative total variance exist for both models. This is particularly evident on PCs 3 and 4, which account for less variability than observed in both models. As a consequence, PC 5 in both models accounts for more variability than observed. Harmonic analysis of de-seasonalised time-series of PC scores suggests that both models simulate a greater contribution to the overall variability in mean sea-level pressures from the annual cycle and semi-annual cycles. This is particularly so on PCs 2 and three (the South Indian and South Atlantic Anticyclones, and PC 4 associated with Hadley Cell mass overturning).

As a consequence, the models under-estimate the amplitude of inter-annual variability in mean sea-level pressure around southern Africa. Weak inter-annual variability on 5-7 year time-scales on PC 2 in the CSIRO control run may be associated with ENSO-related variability in the southern African region. However, due to the weaker than observed variability in Hadley cell mass overturning observed in both models, no inter-annual variability on ENSO time-scales is observed on simulated PC 4. The weak contribution to the overall variability from systems in the tropics (for example PC 4) is likely to be a result of the stronger variability generally in the extratropics (Campbell *et al.*, 1995). The models capture stronger decadal-scale variability on PCs 1 and 3 (CSIRO) and 1, 2, 3 and 6 (Hadley Centre), suggesting that inter-annual variability in hemispheric circulation features associated with planetary wave activity is more clearly represented in both models.

****

This chapter provides an updated assessment of the features of observed mean sea-level pressure variability around southern Africa using principal components analysis. In addition, simulations of intra- and inter-annual variability in mean sea-level pressure by two fully-coupled ocean-atmosphere models have been assessed. In general, the fully-coupled models are capable of simulating the principal modes of variability as observed. However, both models tend to over-estimate the contribution of the annual cycle and under-estimate the amplitude of inter-annual variability in mean sea-level pressure.

Evaluations of the representation of features of contemporary mean climate and climate variability by a range of mixed-layer and fully-coupled models (Section II) have been completed with this chapter. Section III provides a suite of regional climate change scenarios, including projected changes in mean climate and variability based on the mixed-layer and fully-coupled models assessed in Section II.

SECTION III

POSSIBLE FUTURE REGIONAL CLIMATES

CHAPTER SEVEN

EQUILIBRIUM AND FULLY-COUPLED MODEL PROJECTIONS OF FUTURE CLIMATE

Introduction

A distinction needs to be drawn between *predictions* and *projections* of climate change. All climate model integrations are based on a given scenario of future climate change, which includes assumptions about current and future anthropogenic emissions, of for example greenhouse gases, and allows for the cumulative impacts of emissions with time (IPCC, 1994). As such, all estimates of future climate derived from climate models are *projections* and not *predictions* of climate change. Projections of equilibrium climate change based on both atmospheric GCMs linked to simple mixed-layer models and transient climate change derived from fully-coupled ocean-atmosphere models are presented. With the exception of the CSIRO model, all mixed-layer model projections of climate change are based on more recent, generally higher-resolution models than those considered by Joubert (1994). No comprehensive assessment of regional climate change projections for southern Africa from fully-coupled models has been presented before. In this Chapter, the focus is on projected changes in mean climate, and the level of confidence that can be placed in those estimates.

Surface Air Temperature Changes

All of the mixed-layer and fully-coupled models considered project increased surface air temperatures under enhanced greenhouse conditions throughout the southern African region. There are however, notable differences between the two types of models in the magnitude of these increases. Average warming simulated by the fully-coupled models is smaller than that projected by the mixed-layer models. While this result holds throughout the southern African region, it is most obvious over the southern oceans south of 45°S, where average increases projected by the fully-coupled models are at least 3°C lower than the mixed-layer models in both DJF and JJA (Fig. 7.1). Warming projected by both types of models over the central subcontinent is larger than over the adjacent oceans and is also larger in mid-winter (JJA) than during mid-summer (DJF).

Differences in experimental design ensure that comparing magnitudes of projected warming (as in Fig. 7.1) from different types of GCMs can be misleading. Mixed-layer models simulate equilibrium climate change for an instantaneous doubling of CO_2. By simulating a transient increase in CO_2 (compounded by 1 per cent per annum), fully-coupled models are not at equilibrium when doubled CO_2 concentrations are reached, and are in fact seldom (if ever) run to equilibrium. By definition, the transient response to gradually-increasing anthropogenic forcing is lower than the equilibrium response to an instantaneous doubling of atmospheric CO_2. As a consequence, climate changes projected by fully-coupled models are smaller than mixed-layer models, even for comparable levels of radiative forcing. Hence projected changes in temperature at the time of CO_2 doubling are smaller in the fully-coupled than in the mixed-layer models. To compare the *pattern* of climate change (irrespective of the magnitude of the change) projected from both types of model over southern Africa, projected changes from both types of model are normalised to a global average warming of 1°C. This is achieved by dividing all projected warming by the respective global average warming (shown in Tables 2.2 and 2.3). The normalised patterns of climate change are averaged for all mixed-layer and fully-coupled models and shown in Figure 7.2. While the mixed-layer models project a greater magnitude of warming over the subcontinental land mass, the normalised warming is markedly less than from the fully-coupled models (Fig. 7.2). Over much of the subcontinent, the fully-coupled models simulate a pattern of normalised warming greater than the global annual average in both DJF and JJA. Over the southern oceans, the mixed-layer models project normalised warming which is greater than the global annual average. This pattern is almost completely absent in the fully-coupled model projections.

CHAPTER SEVEN

EQUILIBRIUM AND FULLY-COUPLED MODEL PROJECTIONS OF FUTURE CLIMATE

Introduction

A distinction needs to be drawn between *predictions* and *projections* of climate change. All climate model integrations are based on a given scenario of future climate change, which includes assumptions about current and future anthropogenic emissions, of for example greenhouse gases, and allows for the cumulative impacts of emissions with time (IPCC, 1994). As such, all estimates of future climate derived from climate models are *projections* and not *predictions* of climate change. Projections of equilibrium climate change based on both atmospheric GCMs linked to simple mixed-layer models and transient climate change derived from fully-coupled ocean-atmosphere models are presented. With the exception of the CSIRO model, all mixed-layer model projections of climate change are based on more recent, generally higher-resolution models than those considered by Joubert (1994). No comprehensive assessment of regional climate change projections for southern Africa from fully-coupled models has been presented before. In this Chapter, the focus is on projected changes in mean climate, and the level of confidence that can be placed in those estimates.

Surface Air Temperature Changes

All of the mixed-layer and fully-coupled models considered project increased surface air temperatures under enhanced greenhouse conditions throughout the southern African region. There are however, notable differences between the two types of models in the magnitude of these increases. Average warming simulated by the fully-coupled models is smaller than that projected by the mixed-layer models. While this result holds throughout the southern African region, it is most obvious over the southern oceans south of 45°S, where average increases projected by the fully-coupled models are at least 3°C lower than the mixed-layer models in both DJF and JJA (Fig. 7.1). Warming projected by both types of models over the central subcontinent is larger than over the adjacent oceans and is also larger in mid-winter (JJA) than during mid-summer (DJF).

Differences in experimental design ensure that comparing magnitudes of projected warming (as in Fig. 7.1) from different types of GCMs can be misleading. Mixed-layer models simulate equilibrium climate change for an instantaneous doubling of CO_2. By simulating a transient increase in CO_2 (compounded by 1 per cent per annum), fully-coupled models are not at equilibrium when doubled CO_2 concentrations are reached, and are in fact seldom (if ever) run to equilibrium. By definition, the transient response to gradually-increasing anthropogenic forcing is lower than the equilibrium response to an instantaneous doubling of atmospheric CO_2. As a consequence, climate changes projected by fully-coupled models are smaller than mixed-layer models, even for comparable levels of radiative forcing. Hence projected changes in temperature at the time of CO_2 doubling are smaller in the fully-coupled than in the mixed-layer models. To compare the *pattern* of climate change (irrespective of the magnitude of the change) projected from both types of model over southern Africa, projected changes from both types of model are normalised to a global average warming of 1°C. This is achieved by dividing all projected warming by the respective global average warming (shown in Tables 2.2 and 2.3). The normalised patterns of climate change are averaged for all mixed-layer and fully-coupled models and shown in Figure 7.2. While the mixed-layer models project a greater magnitude of warming over the subcontinental land mass, the normalised warming is markedly less than from the fully-coupled models (Fig. 7.2). Over much of the subcontinent, the fully-coupled models simulate a pattern of normalised warming greater than the global annual average in both DJF and JJA. Over the southern oceans, the mixed-layer models project normalised warming which is greater than the global annual average. This pattern is almost completely absent in the fully-coupled model projections.

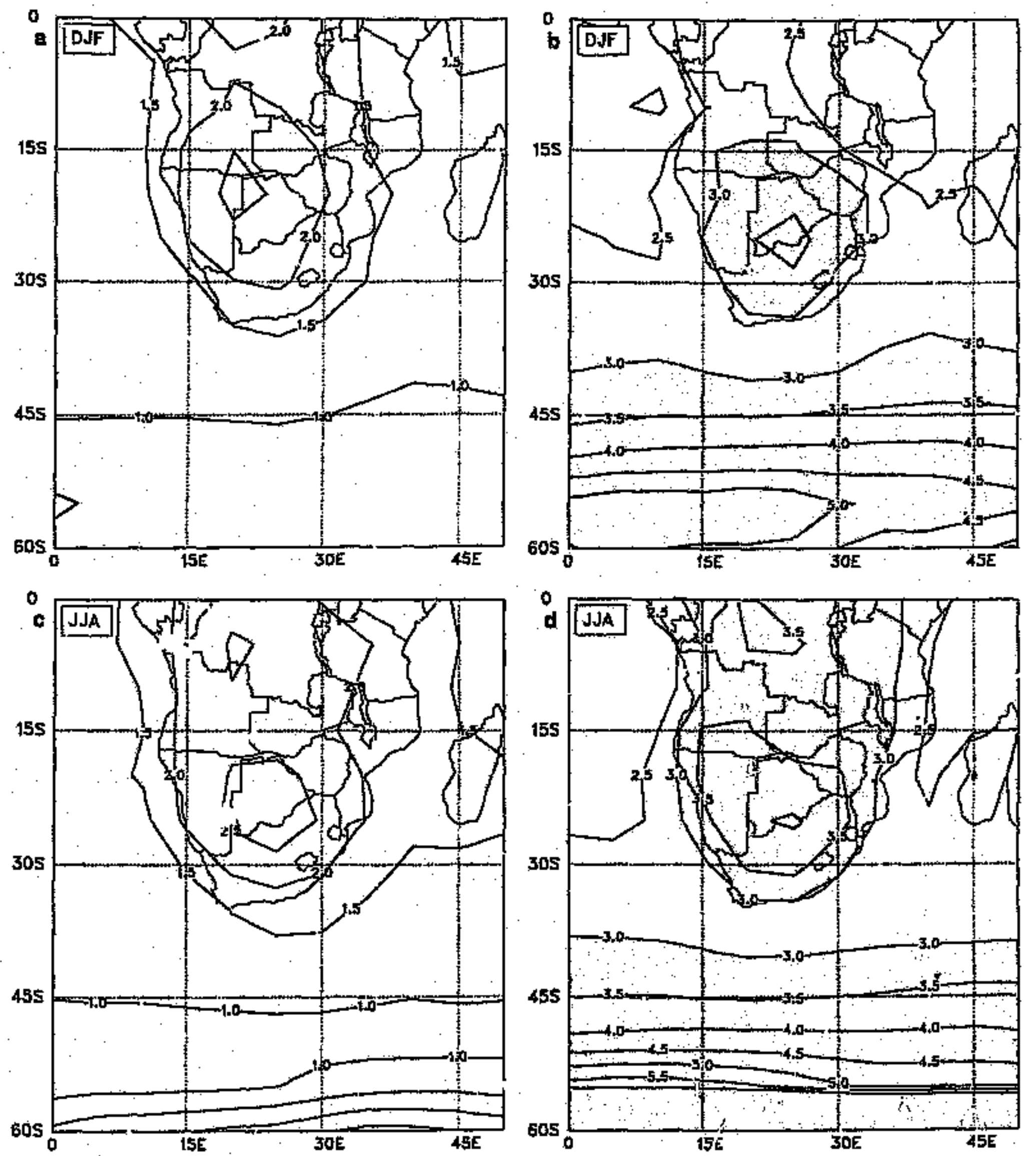

Figure 7.1. Average warming (°C) projected by all fully-coupled (*a,c*) and mixed-layer models (*b,d*) under enhanced greenhouse conditions. Averages are calculated for the December-February (DJF) (*a,b*) and June-August (JJA) seasons (*c,d*). Shading indicates regions of warming exceeding 3°C.

There are marked differences between the *magnitude* and *pattern* of temperatures changes over southern Africa which must be considered when comparing projections of change by mixed-layer and fully-coupled models. For the purposes of scenario development, it is useful to consider the range of absolute warming projected by different types of models. To this end, the maximum and minimum warming projected by any single model from each of the two groups are calculated at each grid point. Results for DJF and JJA are presented in Figures 7.3 and 7.4 respectively.

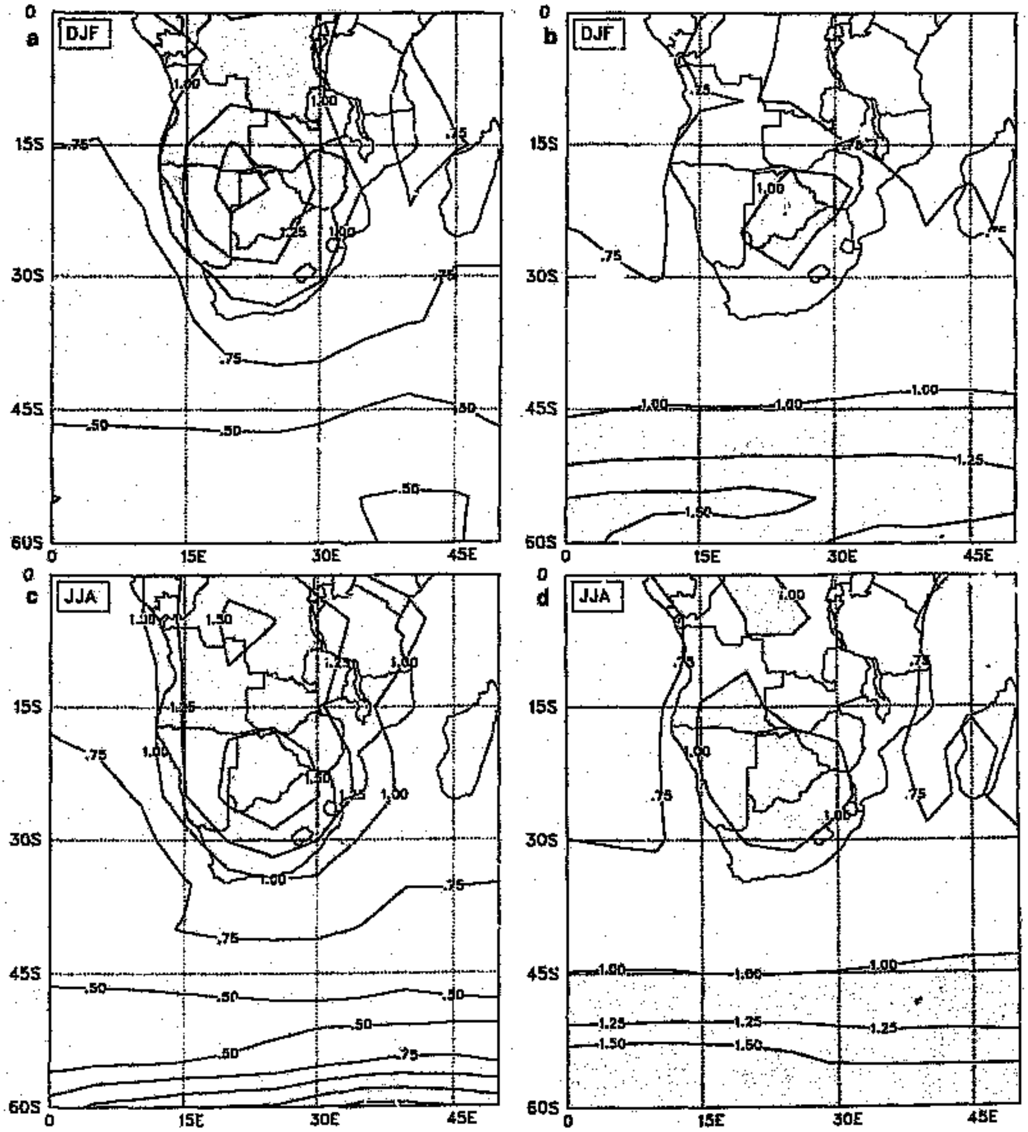

Figure 7.2. Average normalised warming (°C) projected by all fully-coupled (*a,c*) and mixed-layer models (*b,d*) under enhanced greenhouse conditions during both DJF ((*a,b*) and JJA (*c,d*). All warming is normalised relative to the global average warming of 1°C (see Tables 2.2 and 2.3) for each model. Shading indicates regions where normalised warming exceeds 1 °C.

The range of warming projected by the mixed-layer models is larger than the fully-coupled models in both DJF and JJA. For the fully-coupled models, warming over the subcontinent in excess 3.5°C is limited to the central subcontinent during both seasons. Over the southern oceans, maximum warming does not exceed 2°C in DJF and is lower than warming projected over the tropical oceans (Fig. 7.3a). Projected warming only exceeds 3°C south of 55°S during JJA (Fig. 7.4a). Lowest estimates of warming among the fully-coupled models indicate that almost no warming occurs in the southern oceans and warming of less than 2°C is expected over the subcontinent (Fig. 7.3b and 4b). For the mixed-layer models, maximum warming projected over the subcontinent exceeds 4.5°C during both DJF (Fig. 7.3c) and JJA (Fig. 7.4c) and exceeds 6°C in the southern oceans throughout the year. Minimum warming projected over the subcontinent in DJF (Fig. 7.3d) is similar to the average warming projected by the fully-coupled models (Fig. 7.1a). In addition, the minimum mixed-layer model projection in JJA (Fig. 7.4d) is very close to the maximum projection from the fully-coupled models (Fig. 7.4a).

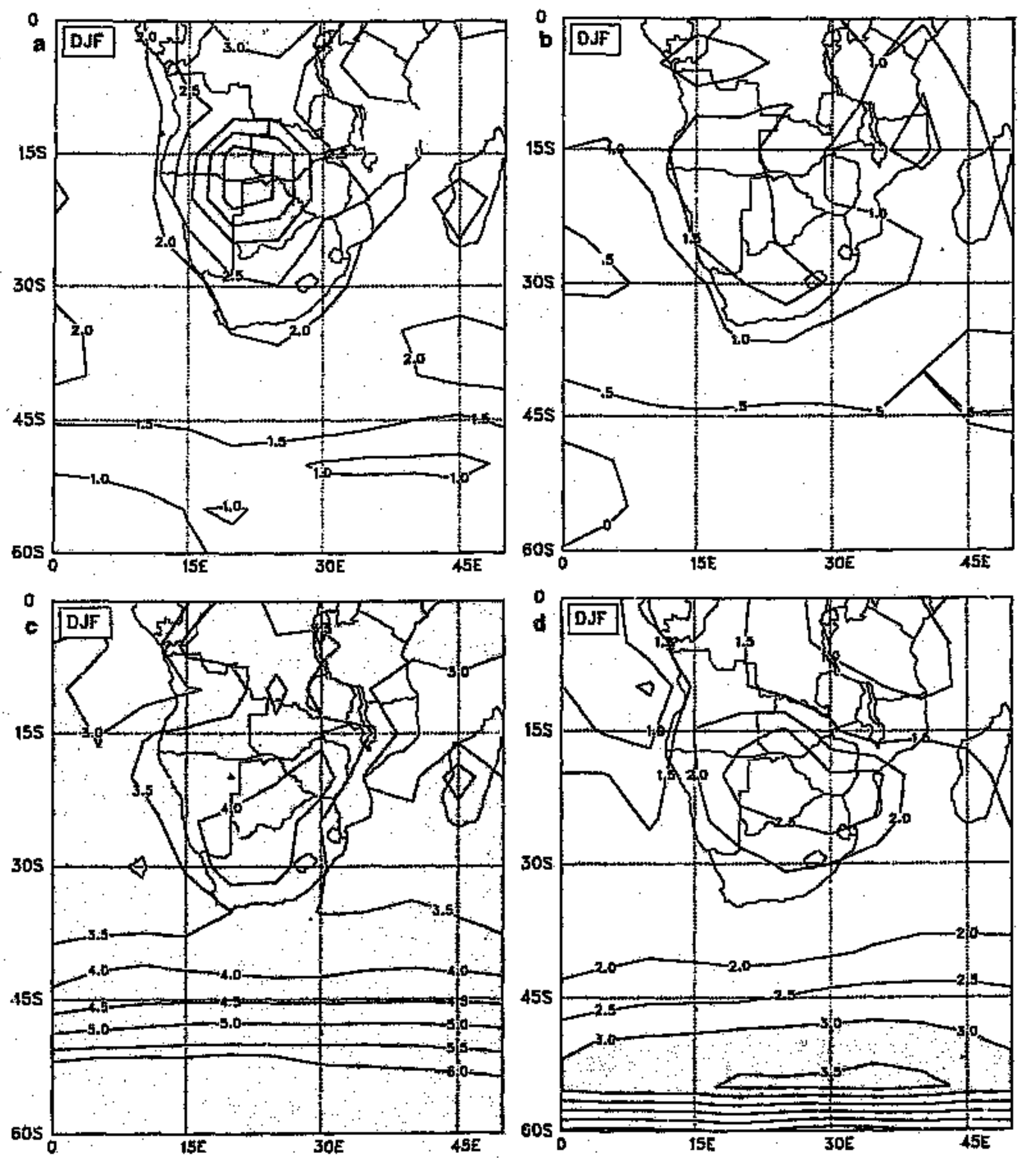

Figure 7.3. Maximum (*a,c*) and minimum (*b,d*) warming (°C) projected by any fully-coupled (*a,b*) or mixed-layer model (*c,d*) during DJF. Shading indicates regions of warming exceeding 3°C.

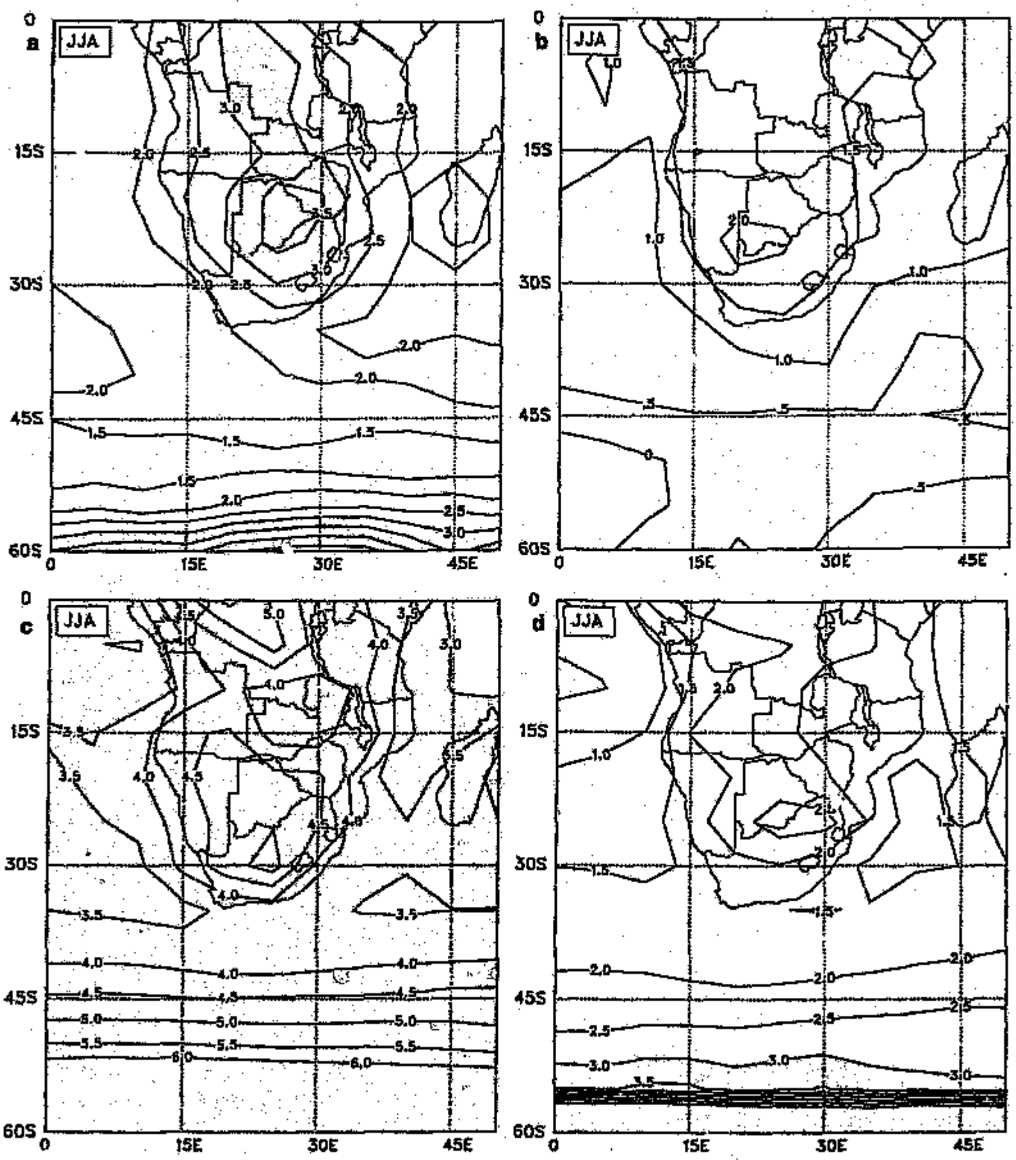

Figure 7.4. As for Figure 7.3 but for JJA.

Mean Sea-Level Pressure Changes

Over the oceanic regions, projected changes in mean sea-level pressure are indicative of systematic changes in circulation patterns. Over the subcontinent, changes in mean sea-level pressure may be misleading due to the altitude of the interior plateau. Caution must therefore be exercised when interpreting projected changes over the subcontinent.

Projected changes in seasonally-averaged mean sea-level pressure are illustrated in Figure 7. 5 for the two summer and two winter seasons (SON, DJF and MAM, JJA, respectively). On average, the fully-coupled models simulate widespread decreases in pressure throughout the year over the southern African subcontinent and adjacent oceans as far south as approximately 30°S (Fig. 7.5a-d). Over the subcontinent, it is only over the African rift valley (central eastern Africa) north of 20°S where the models simulate pressure increases. Another outstanding feature of the average changes projected by the fully-coupled models is an increase in pressure in the mid-latitudes, particularly in the southern Atlantic Ocean. In all cases, simulated changes in seasonally-averaged mean sea-level pressures are small, seldom reaching magnitudes greater than 1 hPa. Projected decreases in mean sea-level pressure by the fully-coupled models over the high latitudes of the southern oceans are on average greater than over the tropical or subtropical oceans. In addition, the range of projected changes (absolute difference between the largest and smallest projected changes from any fully-coupled model) is also largest south of 45°S (not shown).

In all seasons except DJF, the mixed-layer models simulate pressure decreases between the equator and 40°S (Fig. 7.5e,g,h). The mixed-layer models also project pressure increases over the southern oceans, but these are located further south than the increases projected by the fully-coupled models. In DJF, pressures are projected to increase over much of the tropical Atlantic Ocean, extending eastwards over much of tropical Africa (Fig 5f). Over the subcontinent, the mixed-layer models also simulate an increase in pressure during most seasons over the central eastern regions of the tropics, although these increases are restricted to regions north of 5°S. In contrast to the fully-coupled models, the mixed-layer models project generally small increases in pressure on average south of 45^0S throughout the (Fig. 7.5e-h). However, as with the fully-coupled models, the range of projected changes (maximum-minimum projection from any two mixed-layer models) in mean sea-level is also largest in the high latitudes (not shown). The range of projected changes by the mixed-layer models is generally larger than the range in projected changes by the fully-coupled models. In addition, the range in projected changes from both model types is smallest over the subcontinent and largest during the JJA season.

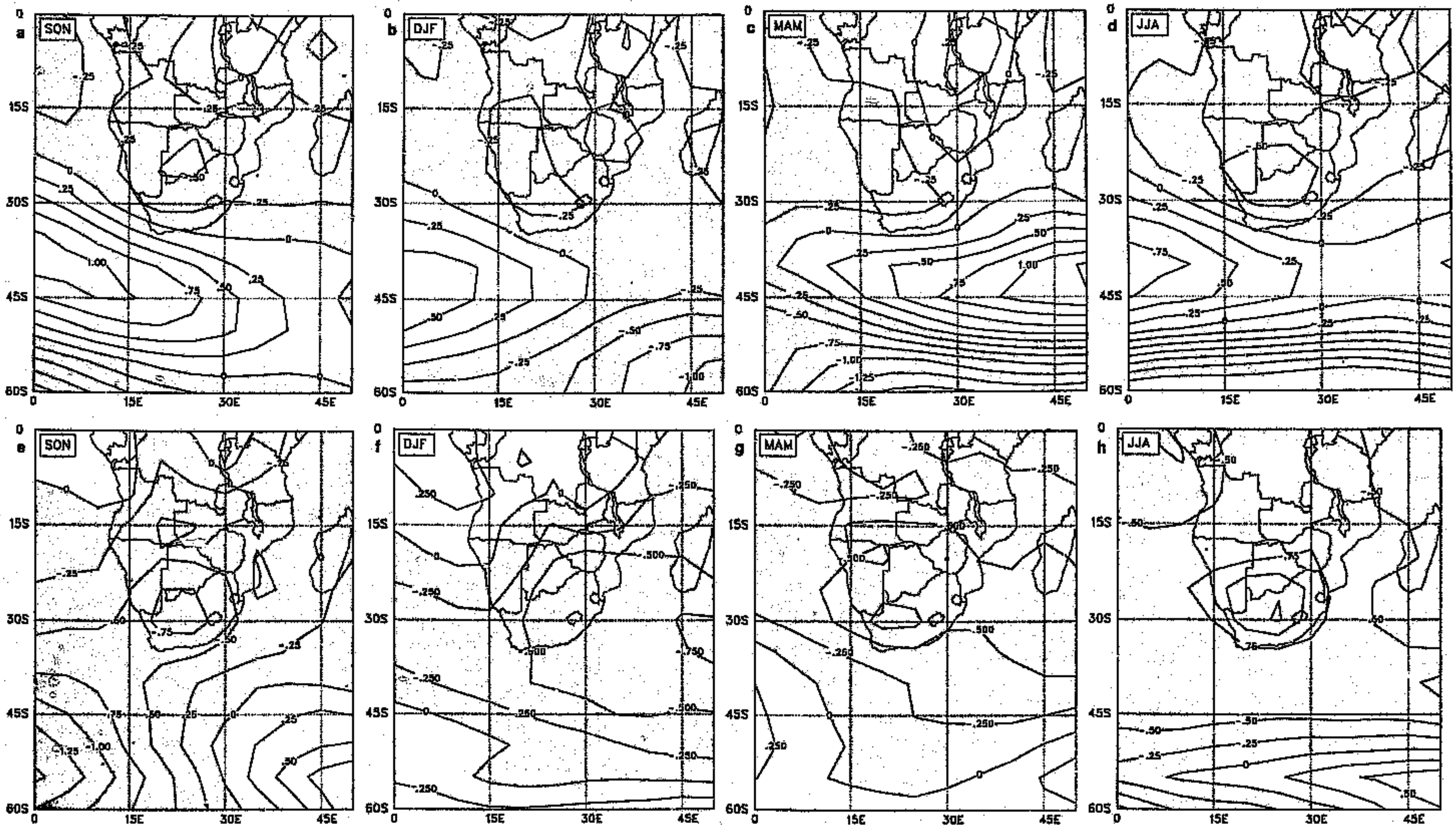

Figure 7.5. Average change in mean sea-level pressure (hPa) projected by all fully-coupled (*a-d*) and mixed-layer models (*e-h*) under enhanced greenhouse conditions. Results are calculated for the SON (*a,e*), DJF (*b,f*), MAM (*c,g*) and JJA seasons (*d,h*). Shading indicates regions of decreasing pressure.

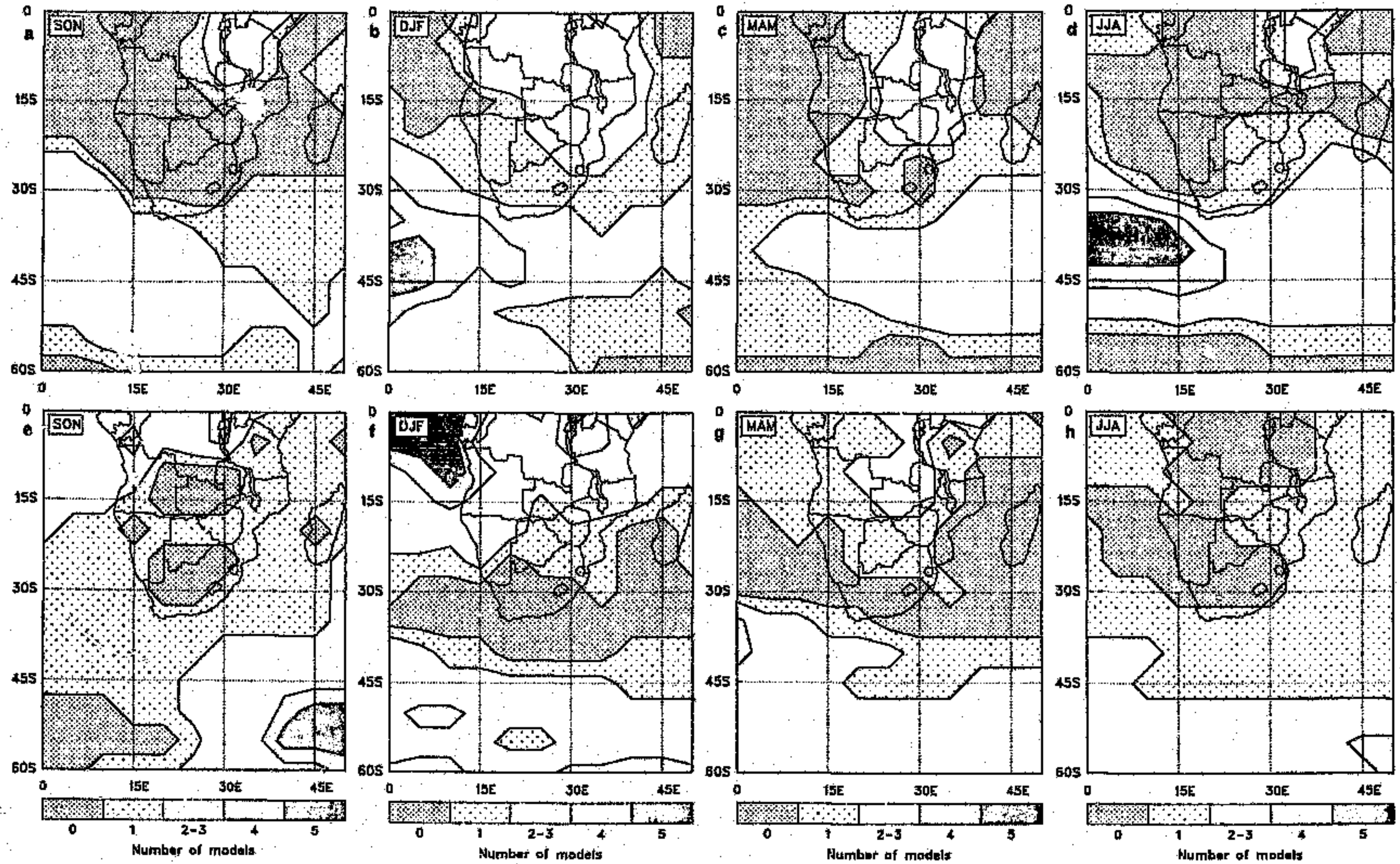

Figure 7.6. The number of fully-coupled (*a-d*) and mixed-layer models (*e-h*) at each grid point which simulate a pressure increase under enhanced greenhouse conditions. Hashes indicate agreement for a decrease, whereas shading indicates agreement for an increase in pressure. Regions where no agreement exists amongst models are clear. In MAM and SON, a total of three fully-coupled models are considered (*c,g*). For all other plots, the total number of models is five.

Confidence in the changes projected for a given region is greater when several models of the same type display agreement as to the nature of those changes. Even greater confidence may be expressed in projected changes when different types of models also display agreement for a given region. The number of both fully-coupled and mixed-layer models which simulate an increase in mean sea-level pressure at each grid point is shown in Figure 7.6. The total number of models of each type considered is five, except in MAM and SON, when only three fully-coupled models are available (missing data for the GFDLC and UKTR simulations). Regions are grey-shaded where good agreement between models exists for an increase (greater than four models), or are stippled where good agreement exists for a decrease (less than two models) in pressure, given a total of five models (Fig. 7.6). Good agreement exists amongst the fully-coupled models throughout the year for a decrease in pressure over much of the subcontinent and adjacent oceans between the equator and 30°S, as well as in the high latitude oceans south of 55°S (Fig. 7.6a-d). There is also good agreement that pressures will increase in the mid-latitude Atlantic Ocean during DJF and JJA (Fig. 7.6b,d). The region of greatest disagreement between the fully-coupled models is in the mid-latitude oceans south and south-east of the subcontinent, where no clear pattern of agreement in terms of an increase or decrease is apparent.

The mixed-layer models also agree broadly in terms of a decrease in pressure over the subcontinent south 15°S. Similarly, there is good agreement amongst the models for an increase in pressures during DJF (Fig 7.6f) in the tropical Atlantic ocean. Projected changes by the two types of models differ in this region. The mixed-layer models project an increase in pressure whereas the fully-coupled models display good agreement for a decrease in pressure. Agreement amongst the mixed-layer models is generally poorest over Africa north of 10°S and also over the mid-latitude oceans.

Rainfall Changes

Under present conditions, little rainfall occurs during the winter months (MAM + JJA) over the summer rainfall region of southern Africa (Tyson, 1986). Only a small area of the south-western part of the subcontinent receives winter rainfall. Unless the models project marked changes in rainfall seasonality, any projected changes in winter rainfall over the summer rainfall region will have little meaning climatologically. For example, a 50% increase or decrease in a winter rainfall total of only 10 mm over the summer rainfall region will not affect the annual rainfall cycle greatly. Area-averaged seasonal rainfall totals for summer (SON + DJF) and winter (MAM + JJA), expressed as a percentage of the annual rainfall total, are illustrated for both the summer and winter rainfall regions (Tables 7.1a and 7.1b, respectively). Both types of model simulate rainfall seasonality in both the summer and winter rainfall regions with some accuracy. In addition, neither the fully-coupled or mixed-layer models project any change in rainfall seasonality over either the summer and winter rainfall regions.

For both fully-coupled and mixed-layer models, the magnitude of projected changes in summer rainfall is seldom greater than 20 per cent (Fig. 7.7). Rainfall decreases are projected by both types of models during winter over most of the subcontinent. However, as stated above, such changes are not expected to have a meaningful impact on the annual rainfall cycle. During summer (SON and DJF), the fully-coupled models project small increases in rainfall over the tropical regions and along the eastern coast of Africa during SON (Fig. 7.7a). Largest percentage increases and decreases are juxtaposed along the west African coast and reflect the much lower rainfall totals (causing percentage changes to be more marked) in that region. Over the oceans south of 45°S, the fully-coupled models simulate small (0-10 per cent) increases in rainfall. During summer and especially DJF (Fig. 7.7f) the mixed-layer models project that rainfall will increase over more widespread and homogeneous regions than the fully-coupled models. However, relatively small decreases in rainfall (< 10 per cent) are projected in several regions, particularly during SON (Fig. 7.7e).

The extent to which both types of models display agreement in terms of the sign of projected rainfall change is an important measure of the degree of confidence that can be placed in the projections. Projected changes in regions where agreement amongst models of the same type is high can be interpreted with confidence. Both types of models display good agreement for rainfall increases over the mid- and high-latitude oceans (Fig. 7.8).

However, over the subcontinent where changes in rainfall will impact directly on human activity, almost no agreement in the sign of rainfall changes is achieved amongst either group of models during summer. The lack of any broad-scale inter-model agreement over the subcontinent during summer suggests that the average changes illustrated in Figure 7.7 are strongly dependent on which individual models are selected in order to calculate average changes as shown in Figure 7.7. Hence, in regions where inter-model agreement is poor, little confidence may be expressed in the average projection.

The Reliability of Projections

Present Climate Performance and Inter-Model Consensus

Surface air temperature

All projections of temperature change resulting from either an instantaneous doubling or gradual increase of atmospheric CO_2 indicate a general warming throughout the subcontinent and throughout the year. Given differences in experimental design, projected warming from the transient climate change experiments (fully-coupled models) is considerably lower than from the equilibrium climate change experiments (mixed-layer models).

Differences in warming projected during DJF and JJA are largest over the central interior south of 15°S (Fig. 7.1). In general, projected warming by both mixed-layer and fully-coupled models is approximately 0.5°C higher in winter (JJA) than in summer (DJF). The implication of this pattern of warming is a reduction in the amplitude of the annual cycle of surface air temperature over much of the central interior of southern Africa. Over the Kalahari, the mixed-layer models exhibit a tendency to under-estimate the present day annual cycle in temperatures (cf. Fig. 5.7). The fully-coupled models (with the exception of CSIROC) provide a more realistic representation of the annual cycle. Given the fact that differences in warming projected by the mixed-layer models between DJF and JJA are larger than the coupled models (Fig. 7.1), the reduction in an already smaller than observed annual cycle may be more significant for the mixed-layer models.

Table 7.1 Observed (Hulme *et al.*, 1996) and projected seasonal rainfall totals expressed as a percentage of annual rainfall; averaged for all models and area-averaged for a) the summer and b) the winter rainfall regions and. For simulations, the summer rainfall region extends from 20°E to 30°E and from 20°S to 30°S. The winter rainfall region extends from 10°E to 20°E and from 30°S to 40°S. For observations, the winter rainfall region land grid points only.

a) Summer rainfall region

	Summer Season (SON + DJF)	Winter Season (MAM + JJA)
Observed	73	27
Fully-coupled Models		
1 x CO_2	72	28
Time of CO_2 doubling	72	28
Mixed layer Models		
1 x CO_2	70	30
2 x CO_2	71	29

b) Winter rainfall region

	Summer Season (SON + DJF)	Winter Season (MAM + JJA)
Observed	34	66
Fully-coupled Models		
1 x CO_2	40	60
Time of CO_2 doubling	39	61
Mixed layer Models		
1 x CO_2	36	64
2 x CO_2	36	64

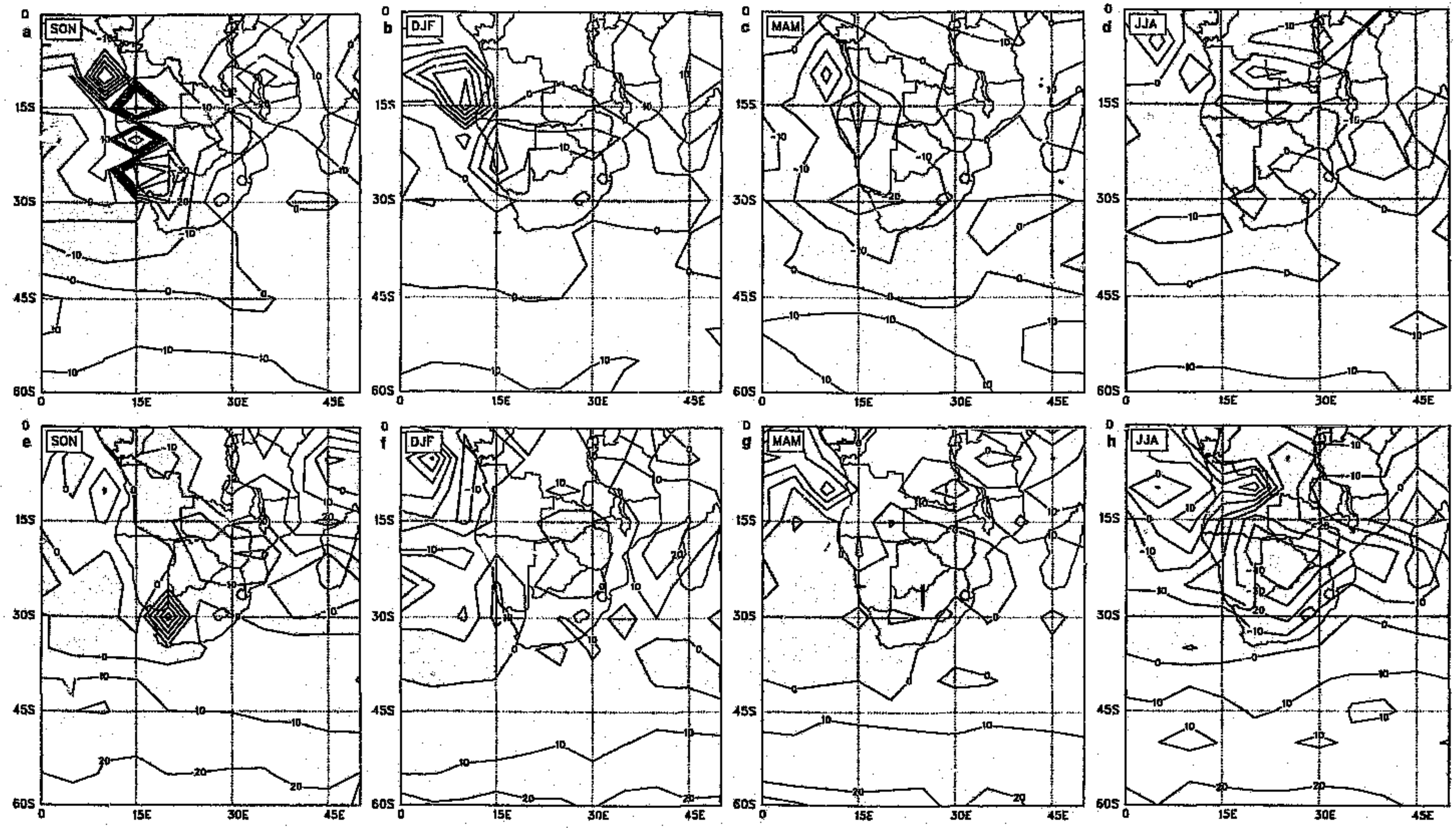

Figure 7.7. Average change in rainfall (expressed as a percentage) projected by all fully-coupled (*a-d*) and mixed-layer models (*e-h*) under enhanced greenhouse conditions. Results are presented for the four seasons defined in Figure 5. Shading indicates regions of projected decrease in rainfall.

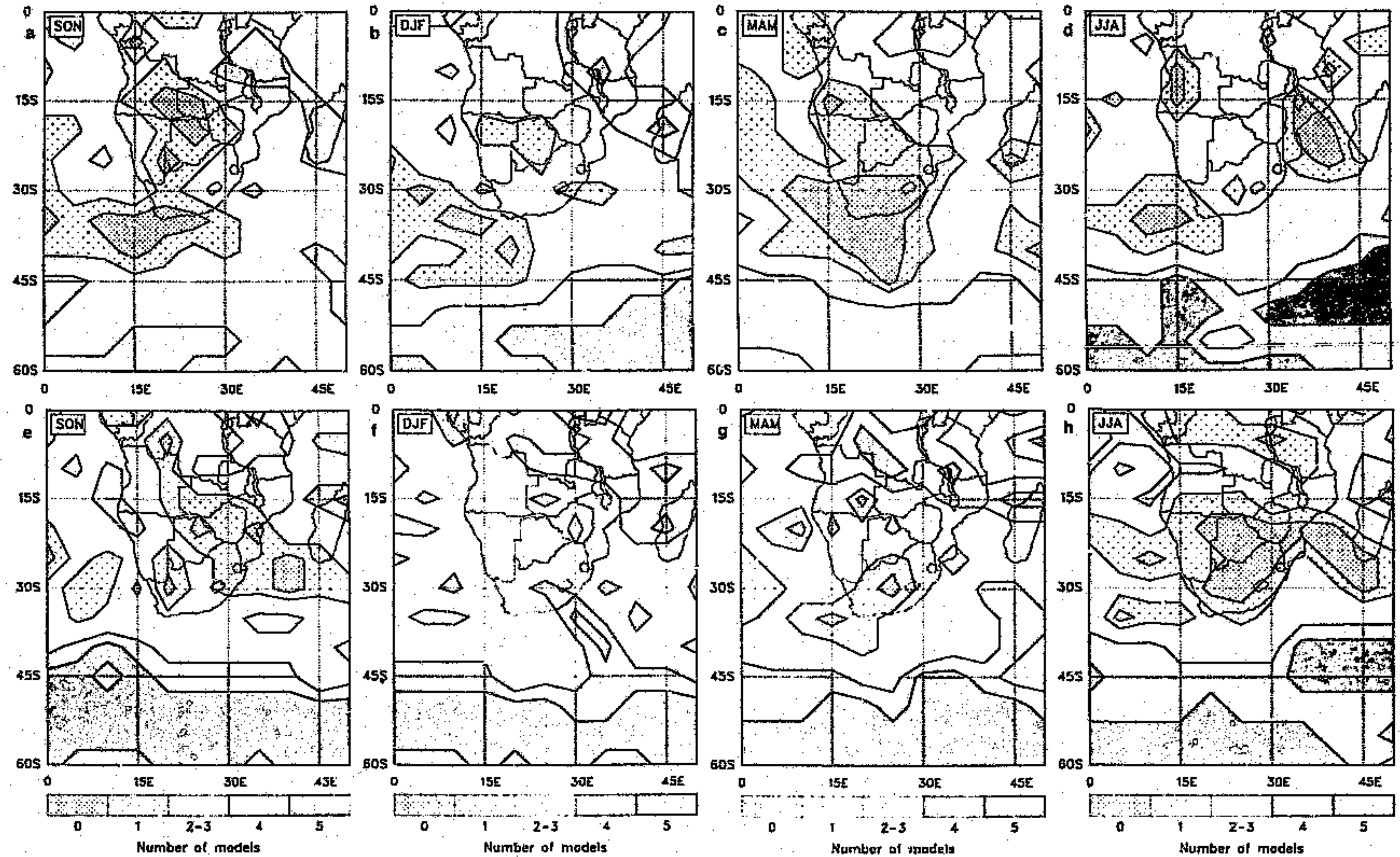

Figure 7.8. The number of fully-coupled (*a-d*) and mixed-layer models (*e-h*) at each grid point which simulate an increase in rainfall under enhanced greenhouse conditions during the four seasons defined in Figure 7.5. Shading as for Figure 7.6. In MAM and SON, a total of four fully-coupled models are considered (*c,d*). For all other plots, the total number of models is five.

Mean sea-level pressure

While both mixed-layer and fully-coupled models display little agreement with observations in terms of the magnitude of present-day mean sea-level pressures (Figs. 5.5 and 5.6), all of the models simulate the observed pressure distribution and seasonal adjustment in the distribution reliably (Chapter 5). Over the tropical and subtropical oceans and the subcontinent, there is good agreement amongst both types of model that pressures will decrease by as much as 1 hPa. Note that the magnitude of projected changes in pressure is often smaller than the simulation error defined in Chapter 5.

In combination with expected temperature increases throughout the region, however, the projected change in pressure may imply an intensified tropical easterly circulation extending further south than under present conditions. Over the subcontinent the projections must be interpreted with caution as the use of mean sea-level pressure changes to estimate changes in circulation at 900 hPa - 850 hPa over the plateau (where altitudes are generally above 1000 m) may be misleading. The small magnitude of projected changes over the subcontinent are of similar magnitude to observed pressure anomalies associated with both seasons and years of above- and below-average rainfall over southern Africa. Averaged over seasons or longer, observed mean pressure anomalies of the order of 1 hPa are indicative of considerable adjustments in atmospheric circulation at the surface and in the upper atmosphere (Tyson, 1986). Hence, while in themselves projected changes in pressure are small, they may be associated with marked changes in circulation patterns over the southern African region.

Circulation adjustments over the oceans to the south of southern Africa also have important implications for inter-annual rainfall variability over the subcontinent south of 20°S. As a consequence, projected changes in pressure over the southern oceans have implications for changes in circulation and rainfall over southern Africa. While the models display greatest agreement with observations in the mid-latitudes, almost no agreement in terms of the sign of projected changes in pressure in the mid-latitudes exists between either the fully-coupled or mixed-layer model groups. Over the oceans south of 50°S, the fully-coupled models display agreement for a decrease in pressure, whereas mixed-layer models display agreement for a pressure increase. In both cases, the range in projected values

values (maximum-minimum) amongst models from both model groups is largest over the high latitude southern oceans.

Rainfall

Neither the fully-coupled nor mixed-layer models project any significant change in rainfall seasonality under enhanced greenhouse conditions over either the summer or winter rainfall regions. In addition, both types of models display acceptable skill in simulating the pattern of rainfall seasonality over much of the subcontinent (Fig. 5.10). As a consequence projections of as much as a 40 per cent decrease in winter rainfall over the central interior are unlikely to have a significant impact on the annual rainfall cycle as almost no rainfall occurs during winter in that region. During summer, projected changes in rainfall are on average no greater that 10-20 per cent. However, changes of this magnitude may have important implications over the summer rainfall regions where inter-annual rainfall variability is high. Within the tropics, both types of models project increases in rainfall which are physically consistent with projected increases in temperature and intensified tropical circulation patterns. However, over much of southern Africa, the projected decreases in rainfall are not consistent with similar projected changes in pressure and temperature. This is particularly the case for the fully-coupled models. Whilst projected increases in temperature are notably smaller than from mixed-layer models, pressures are expected to decrease over almost all of southern Africa south of 15°S. These results may point to a thermodynamic limitation on the relationship between increased temperatures and increased moisture availability associated with an intensified tropical easterly circulation. While this relationship is strongly non-linear, the much-diminished warming in the fully-coupled models may result in a much weaker role for temperature increases in controlling moisture availability over the subcontinent during summer. In addition, projected rainfall changes over much of the subtropical subcontinent are at least similar in magnitude to the simulation error defined in Chapter 5.

In the final analysis, the inability of all models to simulate the magnitude of rainfall events at individual grid points (cf. Fig. 5.12) represents an important restriction on the use of grid point rainfall estimates to develop projections of rainfall changes. This problem is again highlighted by the absence of any broad-scale consensus between the models in terms of the sign of projected rainfall changes. For these reasons, the projected changes in rainfall presented above cannot be interpreted with as much confidence as those for surface air temperature and mean sea-level pressure.

The Reliability of Fully-Coupled Models

The lack of agreement in the sign of the rainfall changes projected by both fully-coupled and mixed-layer models over much of the subcontinent has been identified in other regions in the southern hemisphere (Whetton *et al.*, 1996b). While the lack of agreement is most obvious over southern Africa, similar disagreements exist in regions of southern South America and Australia. Noting that the use of either fully-coupled or mixed-layer models to estimate future rainfall conditions resulted in markedly different projections of rainfall change for some regions of Australia, Whetton *et al.*(1996b) were prompted to investigate whether there is any specific benefit by using either one or the other type of model to develop scenarios of future climate change. They suggest that at least one source of the disagreement between fully-coupled and mixed-layer models in the sign of projected rainfall change is the diminished warming in the southern oceans observed in the fully-coupled models. Recent evidence has shown that the pattern of warming projected by the fully-coupled models in the southern hemisphere could be misleading. In particular, south of 50°S the ocean models in many contemporary fully-coupled models sequester heat from the atmosphere too rapidly and significantly over-estimate vertical mixing and convective overturning (England *et al.*, 1994; England, 1995). As a consequence, Whetton *et al.* (1996b) suggest that the pattern of projected rainfall changes in the fully-coupled models are apparently also linked to the diminished pattern of warming and therefore could also be unreliable. They conclude that the fully-coupled models currently used to provide estimates of transient climatic change may be unreliable for deriving regional climatic change scenarios.

For southern Africa, neither fully-coupled nor mixed-layer models provide reliable estimates of future rainfall conditions. In future, more reliable estimates of regional rainfall changes will depend on improvements in the representation of rainfall processes in GCMs.

Improvements in GCMs will affect directly the success with which nested modelling or downscaling techniques can be used to develop high-resolution projection of rainfall changes. In southern Africa there is no evidence to support the exclusive use of the current fully-coupled model simulations to the exclusion of their mixed-layer model counterparts. The goal of developing reasonable estimates of regional climate change is currently best served by considering projections from both transient climate change experiments using fully-coupled models *and* equilibrium climate change experiments using mixed-layer models.

Synthesis

All mixed-layer and fully-coupled models project increased temperatures throughout the southern African region resulting from increased anthropogenic forcing of climate. As may be expected due to the differences in experimental design, the transient response to gradually increasing levels of atmospheric CO_2 is smaller than the equilibrium response to an instantaneous doubling of CO_2. Average predictions from the fully-coupled models are 1°-2°C over the subcontinent (at around the time of CO_2 doubling), in comparison with 3°-4°C from the mixed-layer models (with doubled-CO_2). Both types of models project slightly larger temperature increases in winter than in summer. A slight decrease in the amplitude of the annual cycle of temperatures over the subcontinent is likely to follow. Differences between mixed-layer and fully-coupled models are most evident over the southern oceans, where the fully-coupled models project a markedly diminished warming in comparison to the mixed-layer models.

Both types of models simulate small (~1hPa) decreases in mean sea-level pressure over the tropical and subtropical regions of the subcontinent. Such changes, considered in conjunction with projected increases in temperature, are consistent with an intensified tropical easterly circulation. However, projected changes in mean pressure are of at least similar magnitude (if not smaller than) errors in the present climate performance of these models defined in Chapter 5, suggesting that it is difficult to distinguish clearly between the signal and the noise introduced by model error. Caution must also be exercised in interpreting mean sea-level pressure changes over the interior plateau region which is as more than 1000 m above sea-level. Despite their relatively small magnitude, the changes in pressure which may occur in future are similar in magnitude to known circulation adjustments associated with major inter-annual rainfall variability and the occurrence of wet and dry spells over the subcontinent in the past. They may have similarly important consequences in the future. Over the mid-latitudes and high southern oceans, neither the mixed-layer nor the fully-coupled models display inter-model agreement in terms of the sign of pressure changes. The result suggests that little confidence can be placed in projected changes over these regions.

Neither mixed-layer nor fully-coupled models suggest any changes in rainfall seasonality over the southern Africa subcontinent in future. Projected changes in the amount of winter rainfall over the summer rainfall region of the interior of the subcontinent are not expected to impact significantly on the annual rainfall cycle. Over much of the summer rainfall region, projected changes of a 10-15 per cent decrease in rainfall are indicated by the fully-coupled models, and over more restricted regions by the mixed-layer models. The projected changes are at least similar in magnitude, if not considerably smaller than the simulation errors defined in Chapter 5. While projected changes of 10-15 % in summer rainfall may have important consequences over the summer rainfall region (which experience high rainfall variability), very little inter-model consensus exists in terms of the sign of projected changes. For these reasons, little confidence may be placed in grid point projections of regional rainfall changes over southern Africa. Alternative approaches for obtaining more reliable estimates of future rainfall will have to be developed.

****

Projections of regional climate change from both fully-coupled and mixed-layer models have been presented for southern Africa. In addition, an estimate of the level of confidence that can be placed in the projected changes has been provided. While all models project increased temperatures over southern Africa, warming projected by the fully-coupled transient climate change experiments is lower than estimates of equilibrium temperature change using mixed-layer models. While there is some indication that summer rainfall may decrease, very little inter-model agreement exists in terms of projected rainfall changes. Projections of transient climate change are considered in the following chapter.

CHAPTER EIGHT

RECENT FULLY-COUPLED MODEL ESTIMATES OF FUTURE CLIMATE

Introduction

Projections of both equilibrium and transient change in mean climate were considered in Chapter 7. The impact of a climate-change scenario based on gradually-increasing anthropogenic forcing as opposed to an instantaneous doubling of CO_2 is most notable in the projections of temperature change presented in the previous chapter. Projections of transient climate change using fully-coupled models are considered in greater depth in the current chapter. Until very recently, all climate change scenarios used in climate modelling studies were based on an equilibrium response to doubling of CO_2 or equivalent CO_2, representing forcing by greenhouse gas changes only. Projections using the Second Hadley Centre fully-coupled ocean atmosphere model (HADCM2) include the direct effects of sulphate aerosols in addition to greenhouse gas forcing and projected changes in mean temperature and diurnal temperature range are considered below.

In Chapter 6, the simulation of contemporary mean sea-level pressure variability by both the Hadley Centre and the CSIRO fully-coupled models control integrations was assessed. In general, both models were shown to be capable of reproducing the observed features of inter-annual variability, although the simulated inter-annual variability was weaker than observed. Projected changes in inter-annual in the transient climate change integrations from both modelling groups are considered below.

Almost all climate change scenarios include a projection of change in rainfall or rainfall-producing systems (as presented in Chapter 7). Over southern Africa, however, fine-weather anticyclonic conditions (by definition, synoptic systems which inhibit rainfall production) persist throughout winter and represent an important component of the climatology of the region (e.g. Tyson, 1986; Cosijn and Tyson, 1996). Recent analyses have shown that persistent fine-weather conditions represented by anticyclonic circulation throughout the lower troposphere play a significant role in determining the transport and recirculation of aerosols and trace gases from southern Africa (e.g. Tyson *et al.*, 1996a). Possible changes in the position or intensity of the continental anticyclone could have important implications for aerosol and trance gas transport off southern Africa and subsequently throughout the southern hemisphere. In this chapter, a scenario of projected changes in the synoptic systems responsible for fine weather conditions during the winter season as well as changes in divergence at 700 hPa associated with the system is presented.

Greenhouse Gas and Sulphate Aerosol Forcing of Temperature Change

Recent transient climate change experiments which include anthropogenic forcing from both greenhouse gases and sulphate aerosols have demonstrated a reduction in both the magnitude and rate of global average warming (IPCC, 1995; Hasselmann *et. al.*, 1995; Mitchell *et. al.*, 1995a; Mitchell and Johns, 1996; Santer *et al.*, 1995). Simulations of present climate variability over southern Africa using both the greenhouse gas only (GHG) and combined greenhouse and sulphate aerosol (SUL) experiments of the Hadley Centre fully-coupled model (Johns *et al.*, 1996; Tett *et al.*, 1996) were examined in Chapter 5. Annual mean temperature simulations for southern Africa between 1961 and 1990 were shown to be statistically indistinguishable from observed conditions. The representation of present regional climate variability in the model is therefore considered sufficiently reliable to place some confidence in projections of possible future temperature change.

The direct effects of sulphate aerosol forcing in addition to greenhouse gas forcing have been parameterised in the Hadley Centre model by simply increasing surface the albedo, thereby inducing localised cooling. Over southern Africa, sulphate aerosol forcing has been included over much of tropical central southern Africa (see Fig. 2.1).

Changes in Annual Mean Temperature

Based on a 1% per annum compounded increase, CO_2-doubling occurs 70 years after the start of both the greenhouse gas only and sulphate aerosol transient climate change experiments in 1990 (i.e. in 2059). Because both experiments utilise gradually increasing forcing, the coupled model is not in equilibrium at the time of CO_2 doubling. Area-averaged decadal mean anomalies for the 24 decades between 1860 and the end of the transient integration in 2099 are shown in Figure 8.1. *Regional* southern African temperatures in the greenhouse gas only integration increase by 3.7°C in the decade starting in 2050, relative to the decadal average for 1990-1999. In the combined greenhouse gas and sulphate aerosol experiment, warming over the same period is projected to be 2.1°C, with both models simulating less warming over southern Africa than the *global* temperature change of approximately 2.5°C and 1.75°C for the respective models (Mitchell *et. al.*, 1995a).

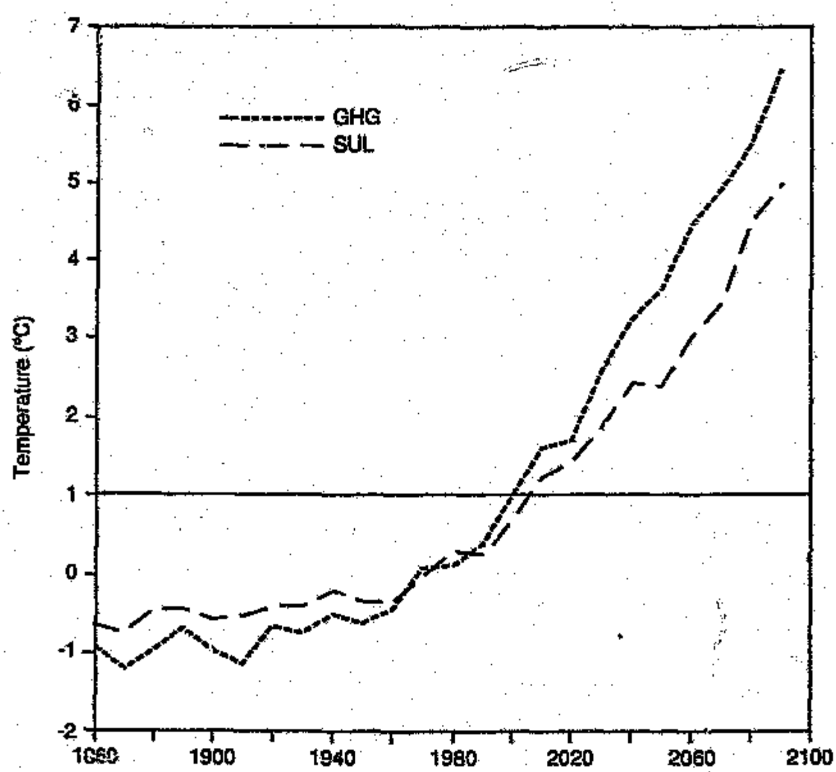

Figure 8.1. Changes in area-averaged decadal mean temperatures relative to the respective 1961-1990 means for GHG (dotted curve) and SUL (dashed curve). Area averages as calculated in Figure 5.8.

The average rate of regional warming for the 7 decades between 1990 and 2059 is expected to be 0.47°C per decade in the greenhouse gas experiment and 0.3°C per decade in the combined greenhouse gas and sulphate aerosol experiment. Respectively, these rates of warming are higher than the globally-averaged rates of warming of 0.3°C and 0.2 °C per decade for the two experiments (Mitchell *et. al.*, 1995a).

The pattern of warming averaged over the 30-year period 2035-2064 for the southern African subcontinent in both experiments is expressed relative to the Hadley Centre control integration (CON), and illustrated in Figure 8.2. Differences between the greenhouse gas only and sulphate aerosol experiments are marked over the subcontinent. For greenhouse gas only (Fig. 8.2a), projected warming exceeds 5°C over the central interior near 20°S. This is also the region for which surface albedo has been modified to represent forcing by sulphate aerosols. Over the oceans adjacent to the subcontinent, projected warming is expected to between 1.5 and 2.5°C. With the inclusion of sulphate aerosols in addition to greenhouse gases (Fig 8.2b), warming is generally 1.5°-2°C lower than with greenhouse gases only. Warming exceeding 3°C is restricted to a small region over the central subcontinent between 10°S and 25°S.

Changes in Diurnal Temperature Range

Globally, increases in minimum temperatures over the land-surface since 1950 have been approximately twice those of maximum temperatures (IPCC, 1992; Karl *et. al.*, 1993, Horton, 1995). An important effect of anthropogenically-induced climate change over recent decades as a consequence has been a reduction in the globally-averaged diurnal temperature range. An increasing number of equilibrium climate change studies suggest that decreases in diurnal temperature range will continue to occur and are associated with increased evaporative cooling as a result of climate warming (Cao *et. al.*, 1992; Hansen *et. al.*, 1995). The changes are expected to vary regionally and seasonally, and from model to model (e.g. Cao *et. al.*, 1992; Cubasch *et. al.*, 1995; Hansen *et. al.*, 1995; Mearns *et. al.*, 1995; Mitchell *et. al.*, 1995a). The effect of aerosol forcing is likely to reduce the diurnal range further as a consequence of a reduction in the amplitude of the diurnal cycle of insolation (IPCC, 1995).

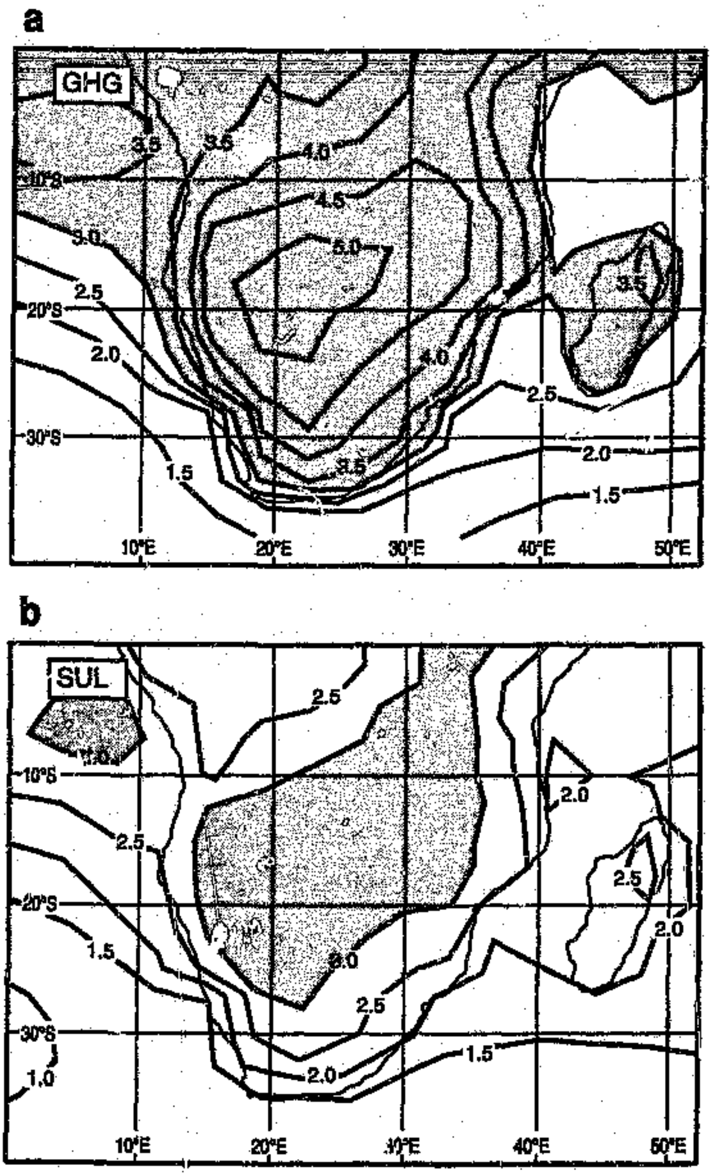

Figure 8.2. Annual mean changes in (a) GHG and (b) SUL, averaged over 2035-2064, relative to the control integration. Contours are every 0.5°C and shading indicates regions where predicted changes exceed 3°C.

Fully-coupled model studies which have included sulphate aerosol forcing have shown that the influence of sulphate aerosols on global climate is not simple. The tendency towards a reduction in diurnal temperature range exhibited by most equilibrium climate change studies can be counter-acted by other feedbacks. For example, the cooling which occurs as a result of sulphate aerosol forcing can result in a reduction of evaporative cooling and therefore an increase in the global mean diurnal range (Hansen *et. al.*, 1995; Mitchell *et. al.*, 1995a). This is in direct opposition to the effect observed in the equilibrium studies. Most models do, however, project decreases in diurnal temperature, particularly over the mid-latitude continents of the Northern Hemisphere, but these changes still differ regionally and with the seasons (IPCC, 1995).

Over South Africa, Mühlenbruch-Tegen (1992) examined trends in mean maximum and minimum temperature between 1940 and 1989. Trends in minimum and maximum temperature were shown to differ seasonally and also do not necessarily follow trends in mean temperature. During summer, trends in maximum temperature over the eastern half of the country and coastal areas were small or negative, while trends in minimum temperature were positive; implying a decrease in the diurnal temperature range. During autumn, the diurnal temperature range has increased strongly over the interior due to a statistically significant decreasing trend in minimum and increasing trend in maximum temperatures. During winter, trends in minimum temperature were positive over the central and western parts, as well as over the north-eastern parts. Almost no trend in maximum temperature was observed in these regions, suggesting a decrease in the diurnal temperature range (Mühlenbruch-Tegen, 1992).

Changes in diurnal temperature range in both Hadley Centre fully-coupled model experiments are expressed relative to the 1961-1990 mean in the control integration (CON). For both the greenhouse gas only and sulphate aerosol experiments, average changes are calculated for the 2035-2064 and for the summer (DJF), autumn (MAM), winter (JJA) and spring (SON) seasons. Changes in diurnal temperature range are larger in the greenhouse gas experiment than in the experiment which includes sulphate aerosols (Fig. 8.3). This is likely to be a consequence of a reduction in the amplitude of the diurnal cycle of insolation due to the inclusion of sulphate aerosol forcing over much of the region. Within the tropics, both experiments project a decrease in the diurnal temperature range (as far as 10°S) throughout the year. Decreases exceed 2°C over northern Angola and eastern tropical Africa in summer.

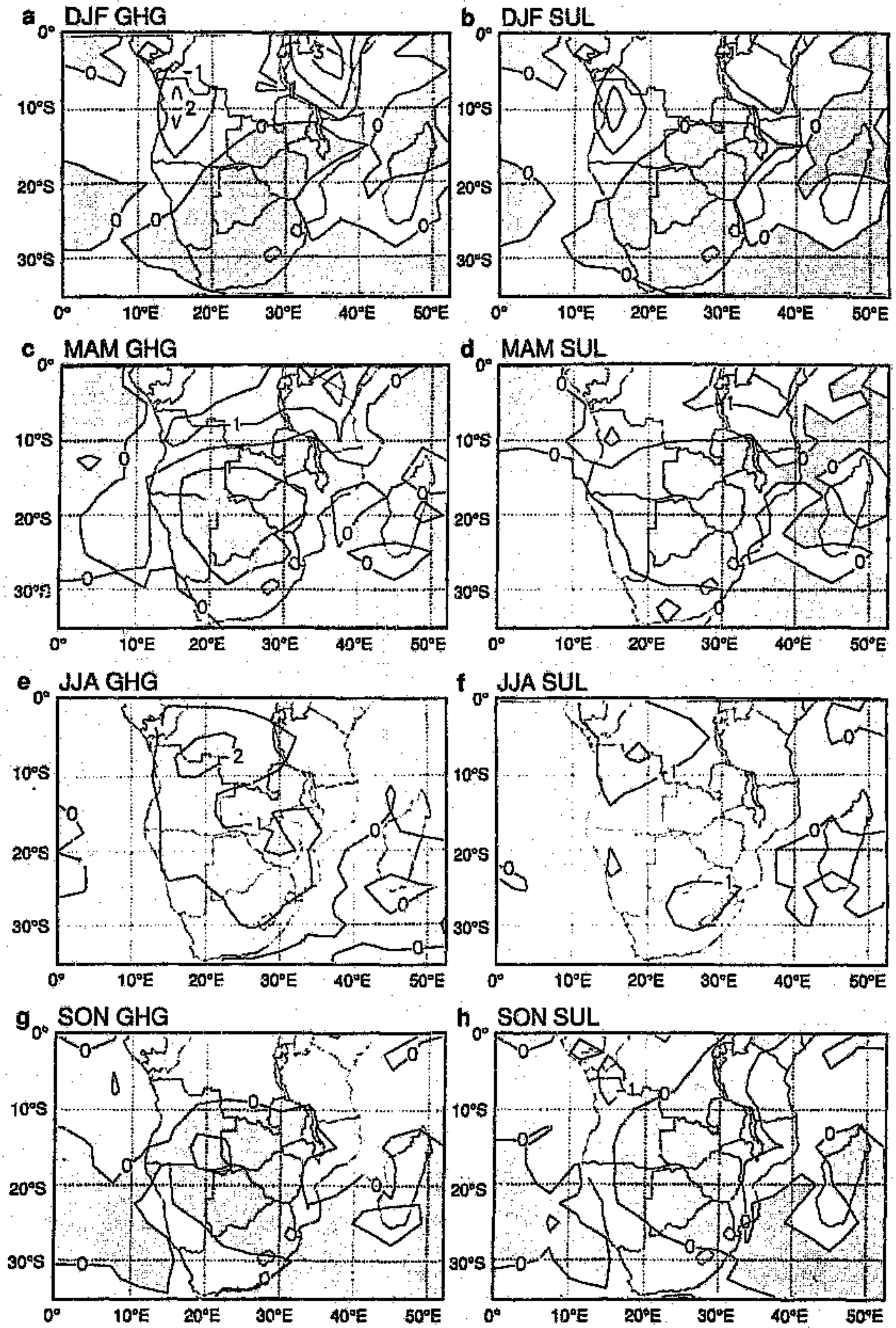

Figure 8.3. Changes in seasonal-mean diurnal temperature range (difference between maximum and minimum temperature) for GHG and SUL (in °C). Changes are calculated for the 2035-2064 period and expressed relative to the 1961-1990 averaged for the control integration (CON). Increases in the diurnal temperature range are shaded.

Over land areas south of 10°C, changes in diurnal temperature range are markedly seasonally-dependent. In the summer and autumn seasons (SON, DJF, and MAM), both experiments simulate an increase in the diurnal temperature range. For the greenhouse gas only experiment, the diurnal temperature range increases by approximately 1°C in both spring and summer (Fig. 8.3a,g). Larger increases over the central interior of southern Africa occur in the autumn, where increases in diurnal temperature range exceed 1°C over a large region (Fig. 8.3c). For the experiment which includes sulphate aerosol forcing, changes in diurnal temperature range throughout summer and autumn are also positive, but are smaller than the changes simulated by the greenhouse gas only experiment, not exceeding 1°C.

The expected increases in the summer and autumn are in contrasted to the changes projected during winter (JJA). In both experiments (Fig. 8.3e,f) the diurnal temperature range is expected to decrease throughout the subcontinent. Decreases are largest over northern Angola / southern Zaire and the central interior of South Africa. Changes projected by the sulphate aerosol experiment are smaller by approximately 1°C than the greenhouse gas experiment, but for both experiment the decreases are 1°-2°C over most areas. As observed in the global land-surface changes over recent decades, changes in diurnal temperature range in both Hadley Centre model experiments during winter are due to a larger increase in minimum temperatures relative to the increases observed in maximum temperatures (not shown).

When interpreting changes in diurnal temperature range, it is important to note that only in regions of maximum aerosol loading can decreases in diurnal temperature range be explained by a reduction in the amplitude of solar heating due to the presence of aerosols (Hansen *et. al.*, 1995, Mitchell *et. al.*, 1995a). Increases in CO_2 and aerosols alone cannot explain the decrease in diurnal temperature range globally, and other physical changes such as increases in cloud cover and changes in soil hydrology are also important mechanisms (Hansen *et al.*, 1995). The role of increasing cloud cover and/or changes in soil hydrology as a mechanism to explain the projected changes in diurnal temperature range over southern Africa is unknown. However, there is some evidence to indicate a reduction in soil moisture during summer over the subtropical land-masses in the Hadley Centre model

(Johns, *personal communication*). It could be postulated that a reduction in soil moisture, combined with (to date, unknown) changes in cloud cover (possibly also decreases) could give rise to increases in diurnal temperature range observed during the summer and autumn. A similar argument could be invoked, postulating increases in soil moisture and cloud cover to explain the decreases in diurnal temperature range during winter. The nature of projected changes in soil moisture and cloud cover, and possible feedbacks between the land surface and the atmosphere remain be examined for southern Africa. It is likely, though, that these elements play an important role in controlling the response of surface temperatures and diurnal temperature ranges to increases in anthropogenic forcing.

Changes in Mean Sea-Level Pressure Variability

In this section, projected changes in inter-annual mean sea-level pressure variability in two fully-coupled models will be examined using principal components analysis. The ability of the CSIRO and Hadley Centre fully-coupled models to simulate observed variability in surface circulation has been examined and both models were shown to perform adequately. A Procrustes Target Rotation procedure was used in order to test formally the ability of the models to reproduce the observed features of variability. Results suggest that the models tend to over-emphasise the importance of the annual cycle in sea-level pressures and consequently under-estimate the amplitude of observed inter-annual variability. Overall, however, the simulated features of mean sea-level pressure variability in both models is robust.

The analysis to follow is a model-sensitivity study only. In other words, no further consideration is given to the ability of the respective models to reproduce the observed features of variability and the representation of observed variability by the respective model control runs is assumed to be accurate. As discussed above, this assumption appears justified. Projected changes in inter-annual variability of mean sea-level pressure *only* are considered. In all cases, therefore, mean sea-level pressure data are de-seasonalised prior to analysis. Principal components are calculated using a correlation matrix and are rotated using the varimax criteria. Only the first six principal components are retained for rotation.

Both spatial and temporal aspects of the changes in variability described using principal components analysis have been analysed. In general, spectral analysis of principal component scores reveals that neither of the models exhibit significant low-frequency (spectral peaks at longer than 5-year intervals) variability in de-seasonalised principal component scores (not shown). The spatial characteristics of the principal modes of inter-annual variability in both the CSIRO and Hadley Centre transient climate change experiments are described below.

Changes in Spatial Characteristics

CSIRO model control and transient climate change experiments

Principal component loading patterns of the first six principal components of the CSIRO control integration (CM8) and transient (gradual) climate change experiment (TX8) are shown in Figure 8.4. All of the individual loading patterns present in the control integration are also present in the transient climate change integration. By implication, therefore, all of the modes of inter-annual variability which are present in the control integration are unchanged in the transient experiment, indicating that no change in the principal modes of inter-annual variability around southern Africa are projected by the model. In addition, the cumulative total of variance explained by the first six principal components changes by less than 0.5% between control and the climate change simulations (Table 8.1). However the contribution of individual modes to the overall variance appears to change more noticeably. As a consequence, the principal components for the climate change experiments are not arranged sequentially, but are arranged to illustrate the correspondence in the loading patterns with control run (Fig. 8.4). Changes in the contribution of individual modes to the overall variance explained is illustrated below with reference to the loading patterns.

Maximum loadings on PC 1 of the control run (Fig. 8.4a) are located between 40°S and 60°S and centred on approximately 70°E and appear to reflect a feature of inter-annual variability in cyclogenesis in the mid-latitudes. The mid-latitude Indian Ocean is a region of preferred cyclogenesis in association with strong sea-surface temperature gradients and hence the transfer of oceanic baroclinicity to the atmosphere (Sinclair, 1994). The location of cyclogenesis is slightly poleward of the subtropical jet stream (cf. Trenberth, 1991). Mid-latitude cyclones are typically found in close association with the enhanced divergence and baroclinicity associated with upper-tropospheric jet streams (Palmén, 1951; Sinclair, 1994). The loading pattern associated with control run PC 1 is associated with PC 5 of the climate change experiment (Fig. 8.4b). The contribution to the overall variance in mean sea-level pressures from the two components differs by about 1% (Table 8.1).

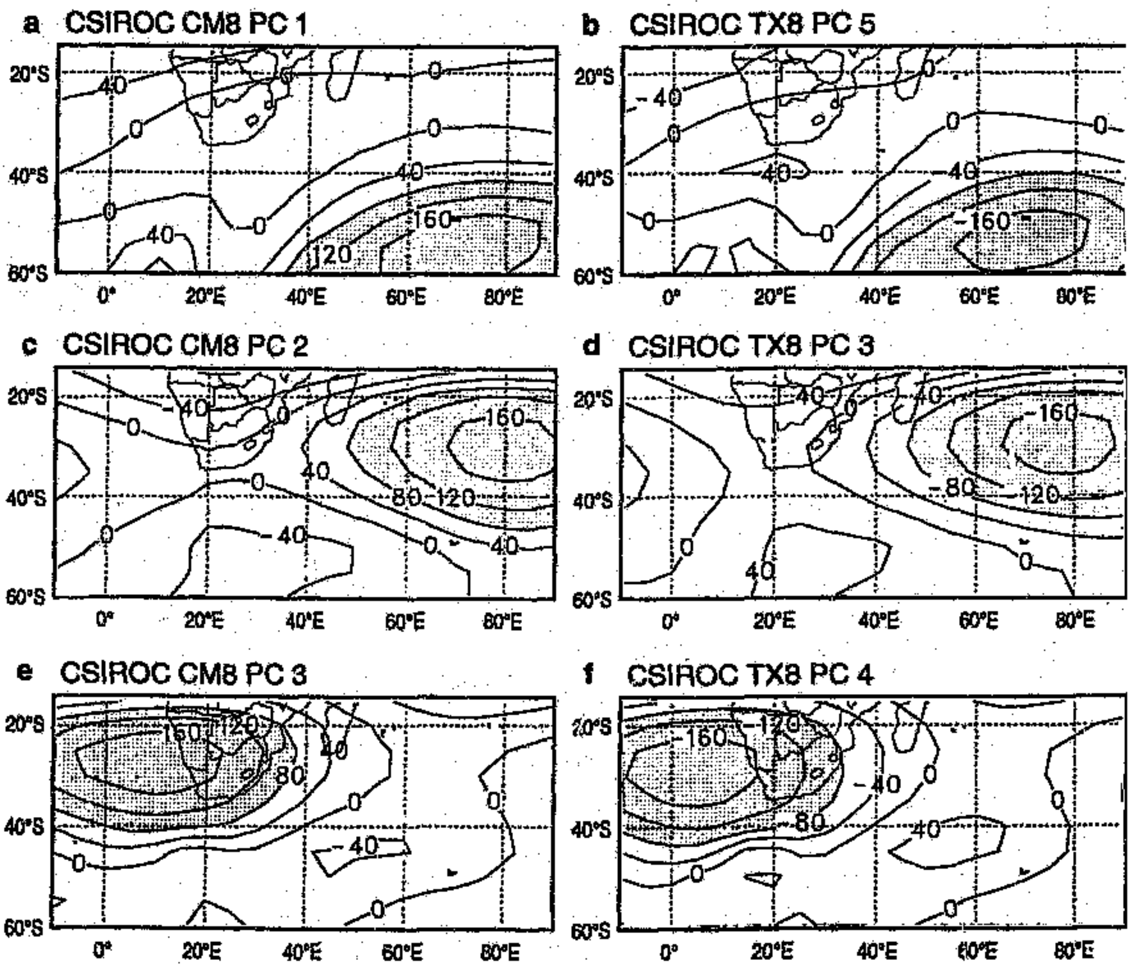

Figure 8.4. Rotated principal component loading patterns for the CSIRO control integration (CM8) and transient climate change integration (TX8). TX8 Loading patterns are arranged in order of correspondence with the loading patterns of CM8. While the sign of the loadings is arbitrary, strongest loadings (of both sign) are indicated by grey-shading.

Control run PC 2 and PC 3 are associated with inter-annual variability in the South Indian and South Atlantic Anticyclones, respectively (Figs. 8.4c,e). Inter-annual variability is greater over the subtropical Indian Ocean than at similar latitudes in the Atlantic Ocean (Dyer, 1981). Anomalously weaker pressures in the South Indian Anticyclone are associated with diminished easterly inflow of atmospheric moisture over the east coast and hence below-average rainfall (Matarira, 1990; Jury, 1996; D'Abreton and Lindesay, 1993; D'Abreton and Tyson, 1995). This feature of inter-annual circulation variability is well captured by the control run and is still present in the future climate simulation but associated with PC 3 (Fig. 8.4d). Similarly, control run PC3 is associated with PC 4 in the climate change experiment (Fig. 8.4f). In both cases, the change in variance accounted for by these two modes is less than 0.5% (Table 8.1).

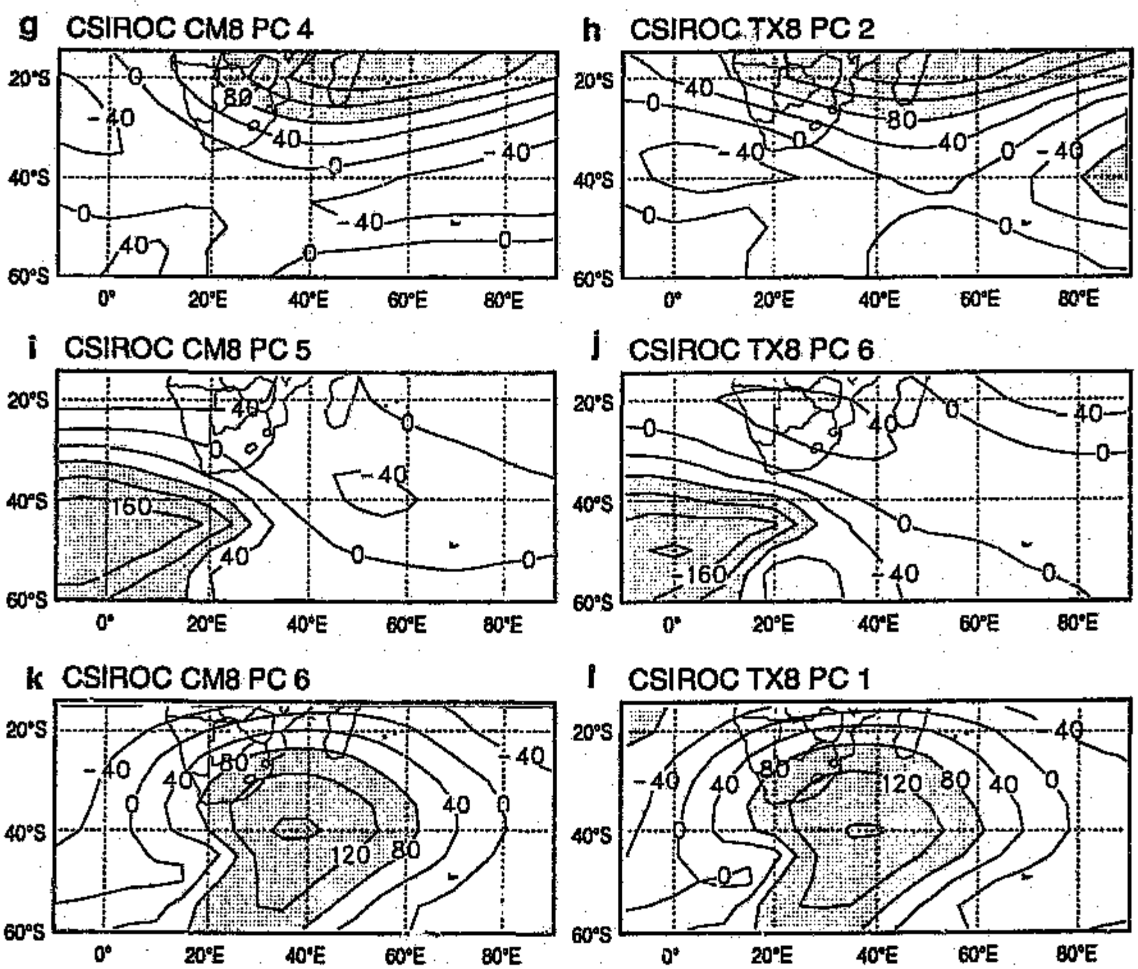

Figure 8.4. (continued)

The maximum loading patterns for control run PC 4 (Fig. 8.4g) are located in the western tropical Indian Ocean and are associated with loadings of opposite sign (the sign itself is arbitrary) in the mid-latitudes. The loading pattern appears to indicate a mode of inter-annual variability associated with mass overturning in the Hadley Cell. Over the east coast of southern Africa, and the western tropical Indian Ocean, overturning in the Hadley cell increases during dry years (Lindesay, 1988; Lindesay and Jury, 1991; Jury and Pathack, 1993; Jury, 1996). There is also evidence for a reversal of a Walker cell between wet and dry years (Jury *et al.*, 1994; Shinoda and Kawamura, 1996). In the climate change experiment, this mode of inter-annual variability is associated with PC 2 (Fig. 8.4h), suggesting an increase in importance of the contribution from this mode to the overall variance. However, from Table 8.1, there is almost no difference in the percentage variance explained by this mode between the control run and transient climate change experiment.

Table 8.1. The percentage of total variance explained by the first six principal components for the CSIRO control (CM8) and transient climate change (TX8) integrations. Principal components were rotated using the varimax criteria. TX8 principal components are arranged in the order of correspondence of their loading patterns shown in Fig. 8.4.

CSIRO control integration (CM8)		CSIRO transient climate change integration (TX8)	
Principal Component	Percentage of Total Variance	Principal Component	Percentage of Total Variance
PC 1	11.19	PC 5	12.56
PC 2	14.07	PC 3	14.36
PC 3	12.46	PC 4	12.86
PC 4	10.05	PC 2	10.18
PC 5	10.76	PC 6	8.99
PC 6	15.94	PC 1	15.57
Total	74.47		74.52

The maximum loading patterns for control run PC 4 (Fig. 8.4g) are located in the western tropical Indian Ocean and are associated with loadings of opposite sign (the sign itself is arbitrary) in the mid-latitudes. The loading pattern appears to indicate a mode of inter-annual variability associated with mass overturning in the Hadley Cell. Over the east coast of southern Africa, and the western tropical Indian Ocean, overturning in the Hadley cell increases during dry years (Lindesay, 1988; Lindesay and Jury, 1991; Jury and Pathack, 1993; Jury, 1996). There is also evidence for a reversal of a Walker cell between wet and dry years (Jury *et al.*, 1994; Shinoda and Kawamura, 1996). In the climate change experiment, this mode of inter-annual variability is associated with PC 2 (Fig. 8.4h), suggesting an increase in importance of the contribution from this mode to the overall variance. However, from Table 8.1, there is almost no difference in the percentage variance explained by this mode between the control run and transient climate change experiment.

Table 8.1. The percentage of total variance explained by the first six principal components for the CSIRO control (CM8) and transient climate change (TX8) integrations. Principal components were rotated using the varimax criteria. TX8 principal components are arranged in the order of correspondence of their loading patterns shown in Fig. 8.4.

CSIRO control integration (CM8)		CSIRO transient climate change integration (TX8)	
Principal Component	Percentage of Total Variance	Principal Component	Percentage of Total Variance
PC 1	11.19	PC 5	12.56
PC 2	14.07	PC 3	14.36
PC 3	12.46	PC 4	12.86
PC 4	10.05	PC 2	10.18
PC 5	10.76	PC 6	8.99
PC 6	15.94	PC 1	15.57
Total	74.47		74.52

Loadings on control run PC 5 (Fig. 8.4i) are greatest in the region of Gough Island, indicating a mode of inter-annual variability associated with anticyclonic ridging. Over southern Africa, periods of above-average rainfall are associated with ridging in the vicinity of Gough Island (Taljaard 1981, Tyson 1981, Miron and Tyson, 1984). Ridging is indicative of larger amplitude westerly waves with a trough over the west coast (Hofmeyr and Gouws, 1964, Taljaard 1986) and result in conditions favourable for the formation of tropical-temperate troughs (Harrison, 1986). In the climate change experiment, this mode of variability is associated with PC6 (Fig. 8.4j). In this case, PC6 in the climate change experiment accounts for almost 2% less of the overall variance in mean sea-level pressure than it's equivalent in the control run i.e. PC 5 (Table 8.1).

PC 6 of the control run indicates a mode of inter-annual variability associated with Marion Island blocking (Fig. 8.4k). Marion Island blocking is associated with above normal rains in summer over much of southern Africa and persistent westerly disturbances over the subcontinent in winter (Tyson, 1984, 1986). In the climate change experiment, this mode is associated with PC 1 (Fig. 8.4l). Again however, only very small differences in the percentage of variance explained by the two PCs is indicated (Table 8.1).

Hadley Centre model control and transient climate change experiments

Principal component loading patterns for the Hadley Centre fully-coupled model control run (CON), as well as two transient climate change integrations are shown in Figures 8.5 and 8.6. Two climate change experiments are based on increasing greenhouse gases only (GHG), and the combined effects of greenhouse gases and sulphate aerosols (SUL), respectively. As with the CSIRO fully-coupled model, the modes of inter-annual variability are realistic and can be related to known features of variability in circulation. The loading patterns observed in the Hadley Centre model simulations are very similar to those observed in the CSIRO simulations. Most modes of variability observed in the control integration are present in both of the transient climate change integrations.

Hadley Centre control run PC 1 (Figs. 8.5a, 8.6a) is similar to CSIRO control run PC 2 and represents variability in the Indian Ocean Anticyclone. The mode is also present in the greenhouse gas only experiment as PC 1 (Fig. 8.5b) and in the sulphate aerosol experiment as PC 2 (Fig. 8.6b). The percentage of total variance accounted for by this mode is higher in both climate change experiments than in the control run (Table 8.2), but never by more than 2%. The Hadley Centre model control run PC 5 (Figs. 8.5i, 8.6i) is similar to CSIRO control run PC 1 and indicates a mode of inter-annual variability associated with cyclogenesis in the mid-latitude Indian Ocean. In both Hadley Centre climate change experiments, the mode is again associated with PC 5 (Figs. 8.5j, 8.6j). Similarly, control run PC 6 (see CSIRO control run PC 4) which describes inter-annual variability in Hadley cell overturning in the western Indian Ocean and subtropics south of Madagascar (Figs. 8.5k, 8.6k), is present in the greenhouse gas experiment as PC 2 and in the sulphate aerosol experiment as PC 3 (Figs. 8.5l, 8.6l). As with Hadley Centre control run PC 1, the percentage of total variance explained by the two climate change experiment modes (GHG and SUL) is larger than for the control integration, although not by more than 1% (Table 8.2). In the case of control run PC 6, the difference is larger, with for example the sulphate aerosol climate change experiment PC 3 accounting for slightly more than 2% more of the total variance. Overall, simulated features of inter-annual variability throughout the tropical, subtropical and mid-latitude Indian Ocean are present in the Hadley Centre fully-coupled model and remain largely unchanged in terms of their contribution to the overall variance in mean sea-level pressures.

In the subtropics between 0°E and 40°E, including the southern African subcontinent (control run PC 3, Figs. 8.5e, 8.6e), the subtropical Atlantic Ocean (control run PC 4, Figs. 8.5g, 8.6g), and the oceanic region south of the subcontinent (control run PC 2, Figs. 8.5c, 8.6c), larger changes in the principal component loading patterns are observable within the subtropics. Control run PCs 3 and 4 are associated with anticyclonic circulation variability in the Atlantic Ocean Anticyclone as well as over the subcontinent itself. In both the greenhouse gas and sulphate aerosol transient climate change experiments, there is only one mode of variability in the subtropical Atlantic Ocean; as PC 4 in both experiments (Figs. 8.5h, 8.6h). The mode in both experiments is similar to control run PC 4, and little change is evident in the contribution to the overall variance (Table 8.2).

A larger change is evident in control run PC 3 (Fig. 8.5e). The loading pattern on this mode exhibits a secondary loading of opposite sign in the south-western corner of the region (roughly south of Gc land). This pattern becomes the dominant mode in both the greenhouse gas experiment as PC 6 (Fig. 8.5f) and the sulphate aerosol experiment as PC 6 (Fig. 8.6f). Following the interpretation for the CSIRO model (CSIRO control run PC 5), this mode is associated with high pressure ridging in the region of Gough Island. The change in the percentage of variance explained by any individual mode is most marked in the case of PC 6 in both experiments, which both explain slightly more than 4% less of the total variance than Hadley Centre model control run PC 3 (Table 8.2).

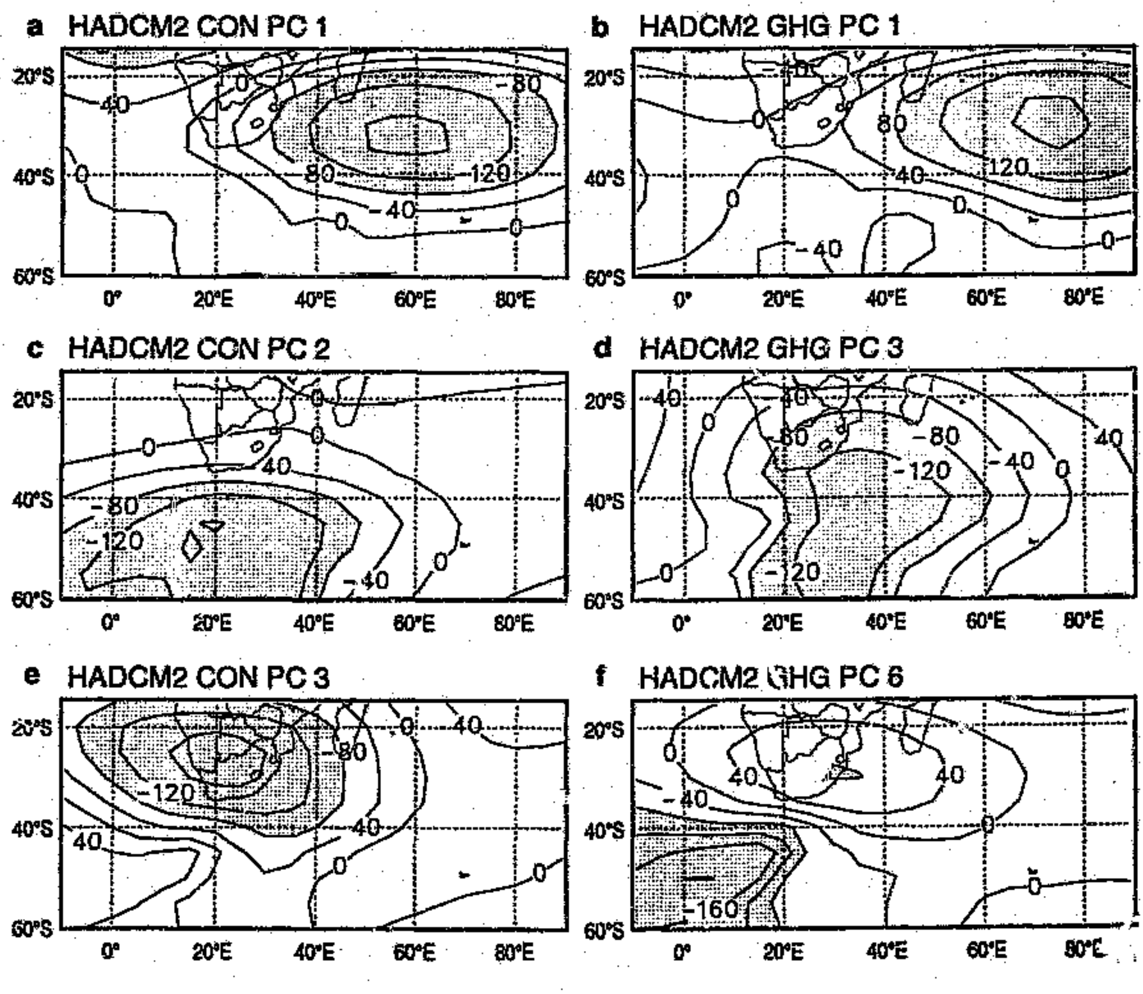

Figure 8.5. Rotated principal component loading patterns for the Hadley Centre model (HADCM2) control integration (CON) and the greenhouse gas only (GHG) transient climate change experiment. PCs are arranged in a similar manner as in Fig. 8.4, and shading is also as in Fig. 8.4.

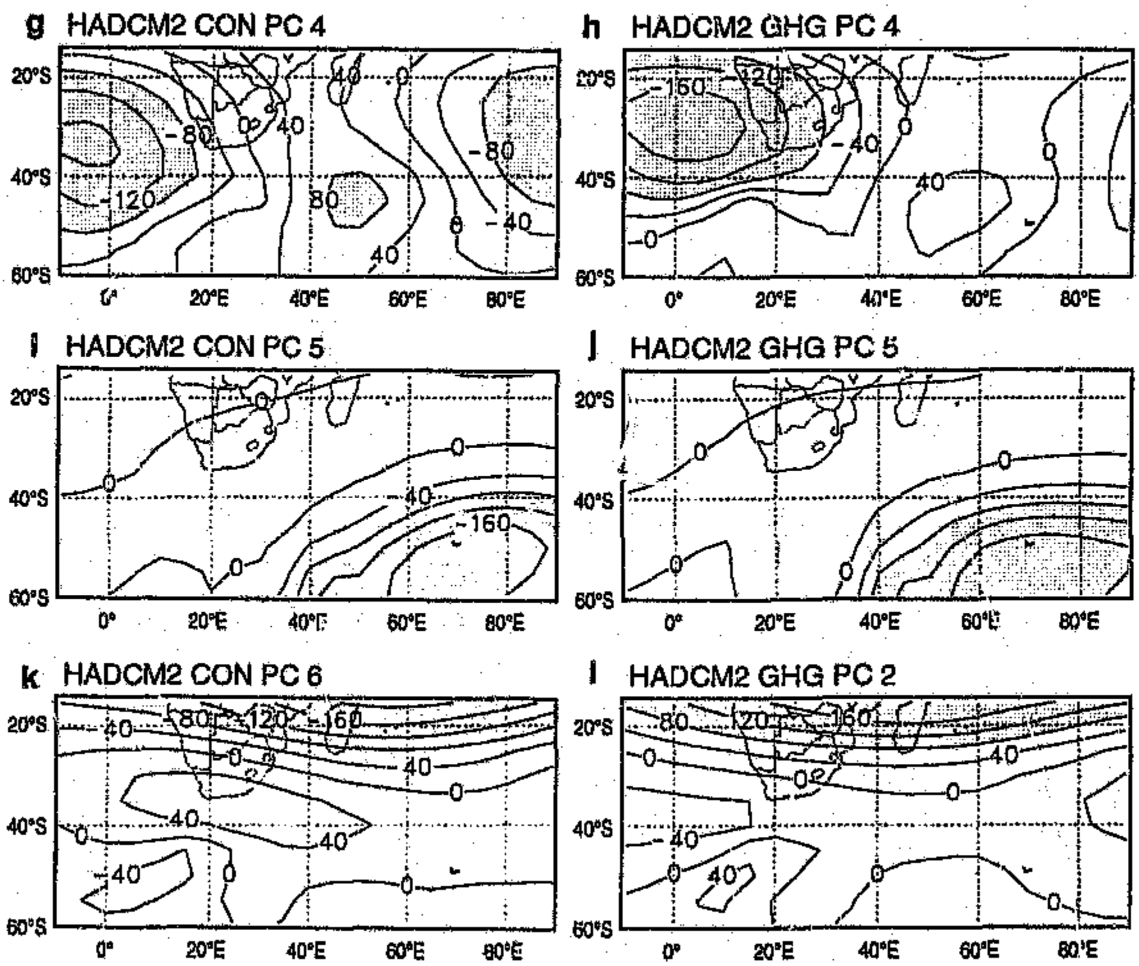

Figure 8.5. (continued)

Changes in loading patterns on control run PC 2 (Fig. 8.5c) are smaller than for control run PC 3. Loading patterns for the greenhouse gas experiment PC 3 (Fig. 8.5d) and sulphate aerosol experiment PC 1 (Fig. 8.6d) are both slightly smaller in spatial extent than in the control integration, but both explain more of the total variance than in the control integration (Table 8.2).

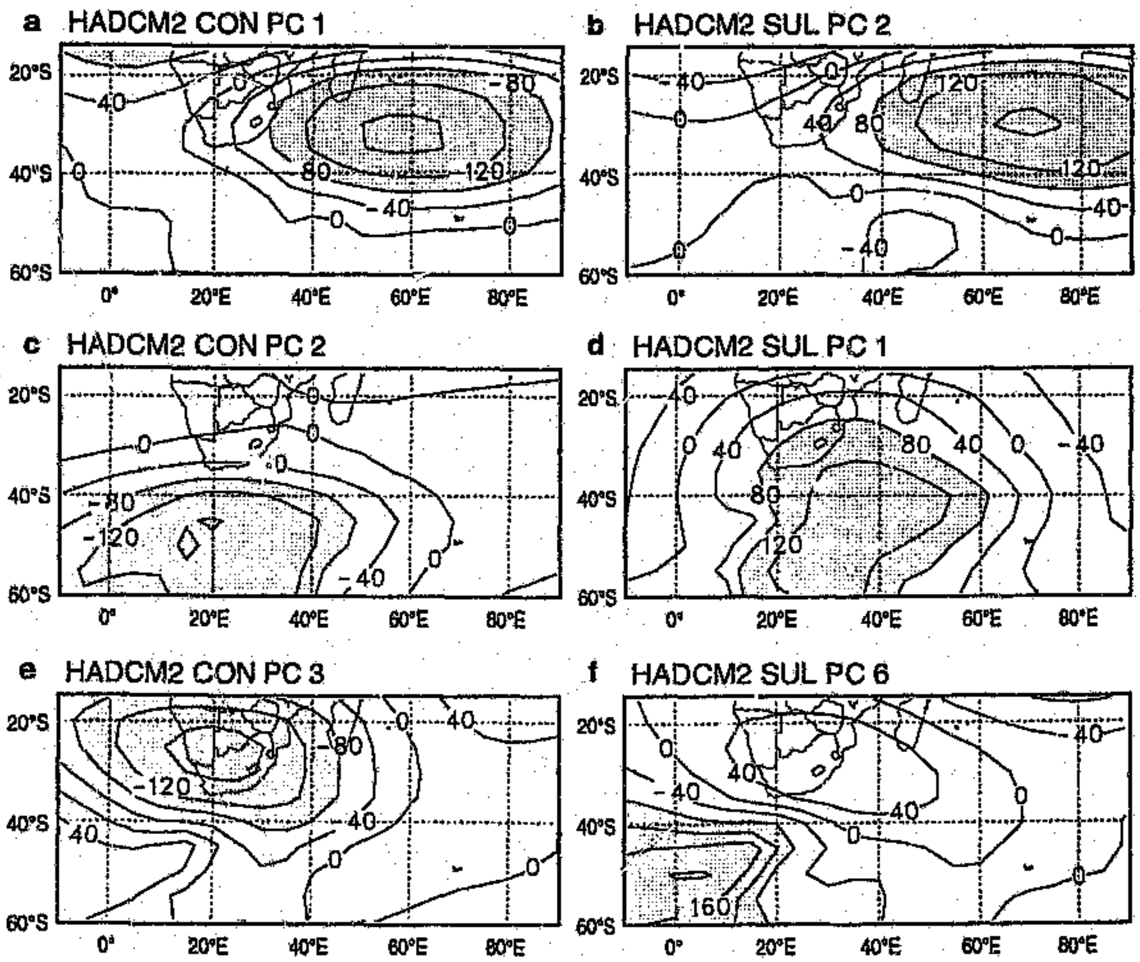

Figure 8.6. Rotated principal component loading patterns for the Hadley Centre model (HADCM2) control integration (CON) and the combined greenhouse gas and sulphate aerosol (SUL) transient climate change experiment.

Overall the first six principal modes of inter-annual variability in mean sea-level pressure in the greenhouse gas only and sulphate aerosol transient climate change experiments explain approximately 3% more of the total variance in simulate mean sea-level pressure than in the control integration (Table 8.2). This difference is larger than in the CSIRO integrations. Over the Indian Ocean, modes of inter-annual variability present in the control integrations are both present in the two climate change experiments, and only very small changes in their contributions to the overall variance is indicated. Largest differences occur over the southern Atlantic Ocean, where modes of inter-annual variability in the control run appear to be consolidated into a single mode of variability in both climate change experiments.

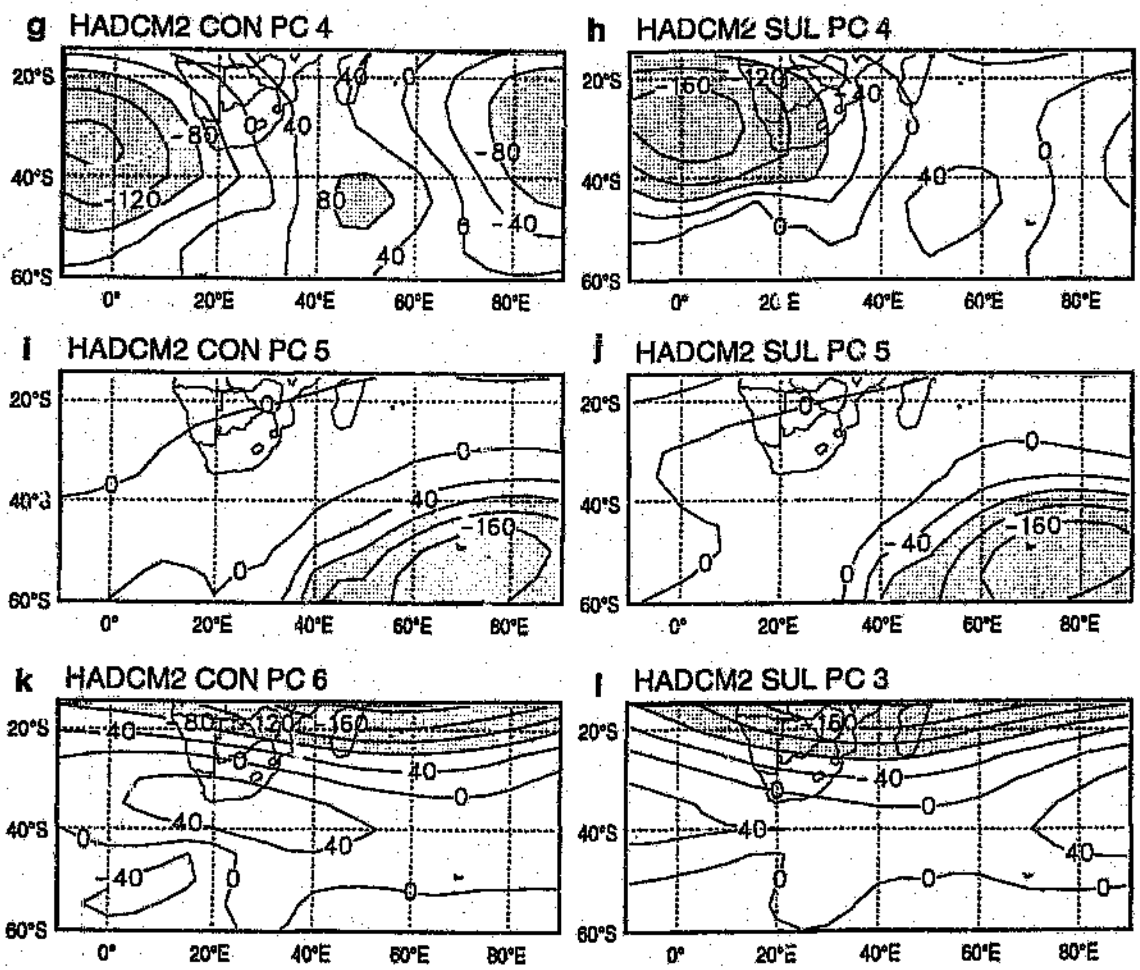

Figure 8.6. (continued)

Table 8.2. The percentage of total variance explained by the first six principal components for the Hadley Centre fully-coupled model (HADCM2) control (CON), greenhouse gas (GHG) and greenhouse gas and sulphate aerosol (SUL) transient climate change integrations.

HADCM2 CON		HADCM2 GHG		HADCM2 SUL	
Principal Component	Percentage of Total Variance	Principal Component	Percentage of Total Variance	Principal Component	Percentage of Total Variance
PC 1	15.17	PC 1	16.27	PC 2	16.63
PC 2	12.89	PC 3	15.62	PC 1	15.14
PC 3	13.83	PC 6	9.65	PC 6	9.56
PC 4	12.75	PC 4	13.05	PC 4	13.20
PC 5	9.87	PC 5	10.23	PC 5	10.69
PC 6	8.40	PC 2	10.56	PC 3	10.06
Total	72.91		75.38		75.28

Are the changes in contribution to the overall variance in mean sea-level pressure indicated in Figs. 8.4 and 8.5 real? The changes in the percentage of variance accounted for by individual principal components summarised in Tables 8.1 and 8.2 are small and suggest that this may not be the case. No attempt has been made here to determine the statistical significance of the changes summarised in the Tables. Possibly, therefore, the more important conclusion to reach is that no change in the six most important modes of variability occur in either the CSIRO or the HADCM2 fully-coupled models. The possibility that changes may occur in the contribution of these individual modes to the overall variance remains to be demonstrated as statistically robust.

Changes in Fine Weather Systems

The frequency of occurrence of anticyclones over the subtropical subcontinent reaches a maximum during the winter months of June and July (Vowinckel, 1956; Tyson *et. al.*, 1996a) although anticyclonic conditions in the lower troposphere prevail throughout the year (Cosijn and Tyson, 1996). Anticyclonic circulation is associated with stable conditions and subsidence over the subcontinent, resulting in a sequence of elevated stable layers throughout the troposphere. The first of these elevated stable layers occurs at an altitude of approximately 3 km (~700 hPa) (Preston-Whyte and Tyson, 1977; Garstang *et. al.*, 1996) but they are also present at ~500 and ~300 hPa (Cosijn and Tyson, 1996). Stable layering of the atmosphere over South Africa on no-rain days occurs with a frequency in excess of 80%, and displays little seasonal variation (Cosijn and Tyson, 1996). Such conditions exert and important control on the horizontal and vertical transport of aerosols and trace gases in the troposphere around and off the subcontinent (Garstang *et. al.*, 1996; Tyson *et. al.*, 1996a,b).

Any change in the location or intensity of the continental anticyclone due to anthropogenically-induced climate change, particularly during winter, could have important implications for the transport and recirculation of aerosols and trace gases from the subcontinent. Projected changes in tropospheric circulation at 700 hPa by the Second Hadley Centre fully-coupled model (HADCM2) are examined below. The 700 hPa level was chosen as representative of the level of the first elevated stable layer over southern Africa. Projected changes are derived from the Hadley Centre transient climate change integration, which includes increasing forcing from both greenhouse gases and sulphate aerosols (SUL).

700 hPa Circulation

At 700 hPa, anticyclonic circulation is prevalent throughout the year. The circulation streamline in the lower troposphere derived from the Hadley Centre model climate change experiment indicate that this feature is successfully reproduced (Fig. 8.7). The streamlines at 700 hPa are calculated from u- and v-wind component data as 30-year monthly deviations from the annual mean for each year and then averaged over two 30-year periods (1961-1990 and 2035-2064). The second 30-year period between 2035 and 2064 is chosen to include the year in which CO_2 doubles (2059). The 1961-1990 period will be used as a reference against which to compare the results for 2035-2064. By using deviations from the annual mean, the streamlines represent those features of the circulation which are unique to each month of the year.

The circulation patterns simulated by the Hadley Centre model sulphate aerosol experiment closely resemble the observed circulation patterns (cf. Tyson *et. al.*, 1996a). For the reference period (1961-1990), the circulation south of 20°S is anticyclonic throughout the year (Fig. 8.7). In January, cyclonic vorticity over south-eastern Angola is indicative of the position of the Zaire Air Boundary (Fig. 8.7a). Between April and December the anticyclonic circulation intensifies and gradually moves north-eastwards from a position over the Northern Province of South Africa in April (Fig. 8.7c) to a position over south-eastern Zimbabwe in December (Fig. 8.7h). During this period the anticyclonic feature expands longitudinally and extends equatorward beyond 10°S. The anticlone is most clearly defined in July (Fig. 8.7e) when it is located over south-eastern Botswana. Off the west coast of South Africa, a westerly wave is also most clearly defined during July. In the mid-latitudes, westerlies predominate throughout the year.

In future, anticyclonic conditions at 700 hPa between 20°S and 30°S are likely to remain the dominant feature of the general circulation over southern Africa throughout the year (Fig. 8.7b,d,f,h). The seasonal displacement of the feature to the north-east between summer and winter is likely to continue. No long-term intensification or weakening of the 700 hPa anticyclone circulation over southern Africa is likely to occur with gradually-increasing anthropogenic forcing.

Divergence at 700 hPa

Subsidence is a persistent feature of the semi-permanent subtropical anticyclone over southern Africa. This may be illustrated by the divergence which occurs at 700. The Hadley Centre model simulates a region of strong divergence (shaded) along the leading edge of the westerly wave over the west coast of South Africa hPa (Fig. 8.8). The boundary between the region of convergence and divergence over southern Africa marks the south-western extreme of the continental anticyclone. Divergence is therefore associated with airflow around the anticyclone at 700 hPa which is removed rapidly by the westerly wave and transported eastwards off the subcontinent. Recent analyses have shown that significant proportions of air leaving the subcontinent in this manner are re-circulated back over the subcontinent by the anticyclone (e.g. Tyson *et. al.*, 1996a).

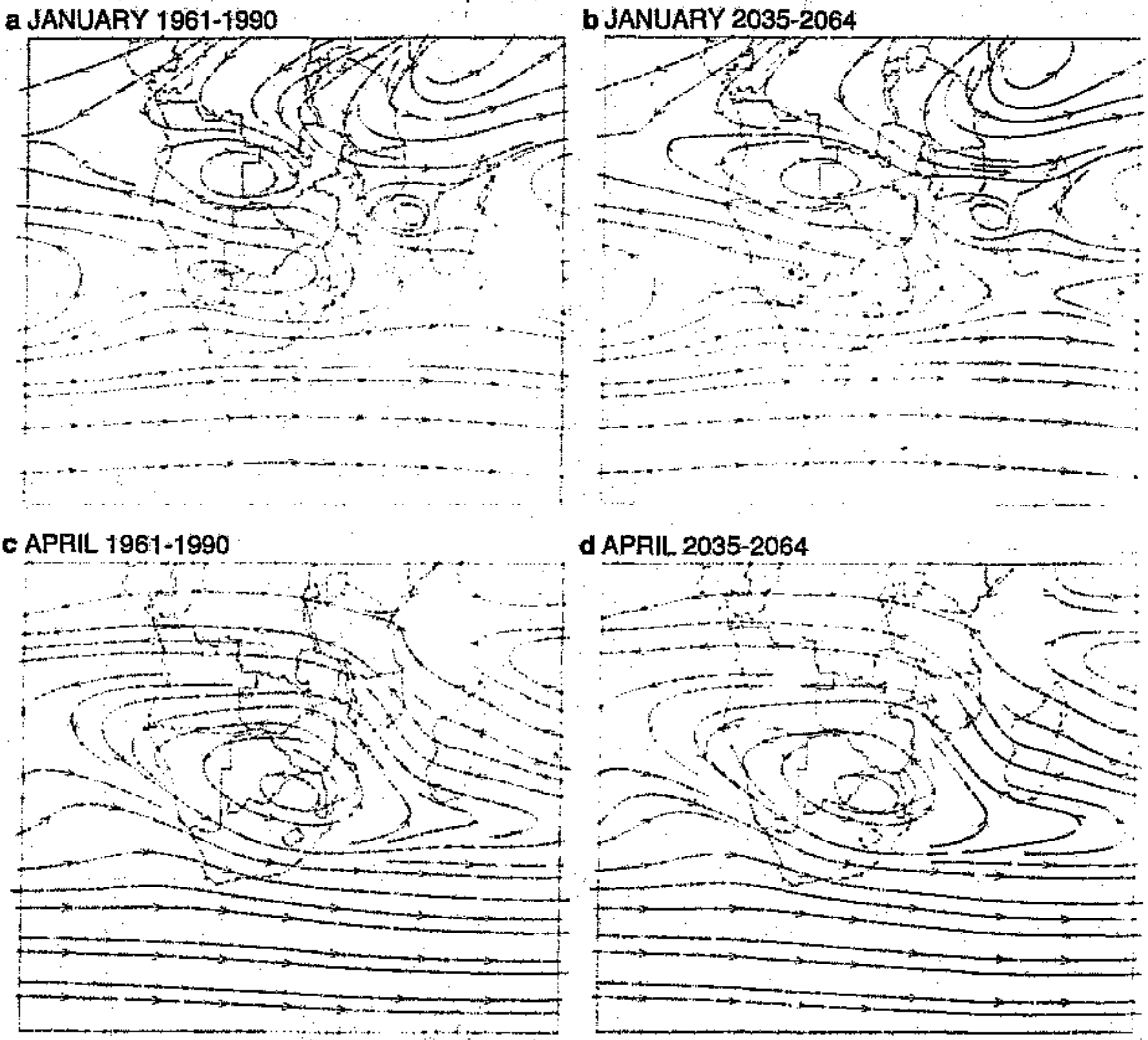

Figure 8.7. Streamlines at 700 hPa simulated by the HADCM2 SUL integration for January (a,b), April (c,d, July (e,f) and October (g,h). A 30-year reference period for model years 1961-1990 (a,c,e,g) is contrasted against a 30-year period between 2034 and 2064 (b,d,f,h) which incorporates the year that CO_2 doubles (2059).

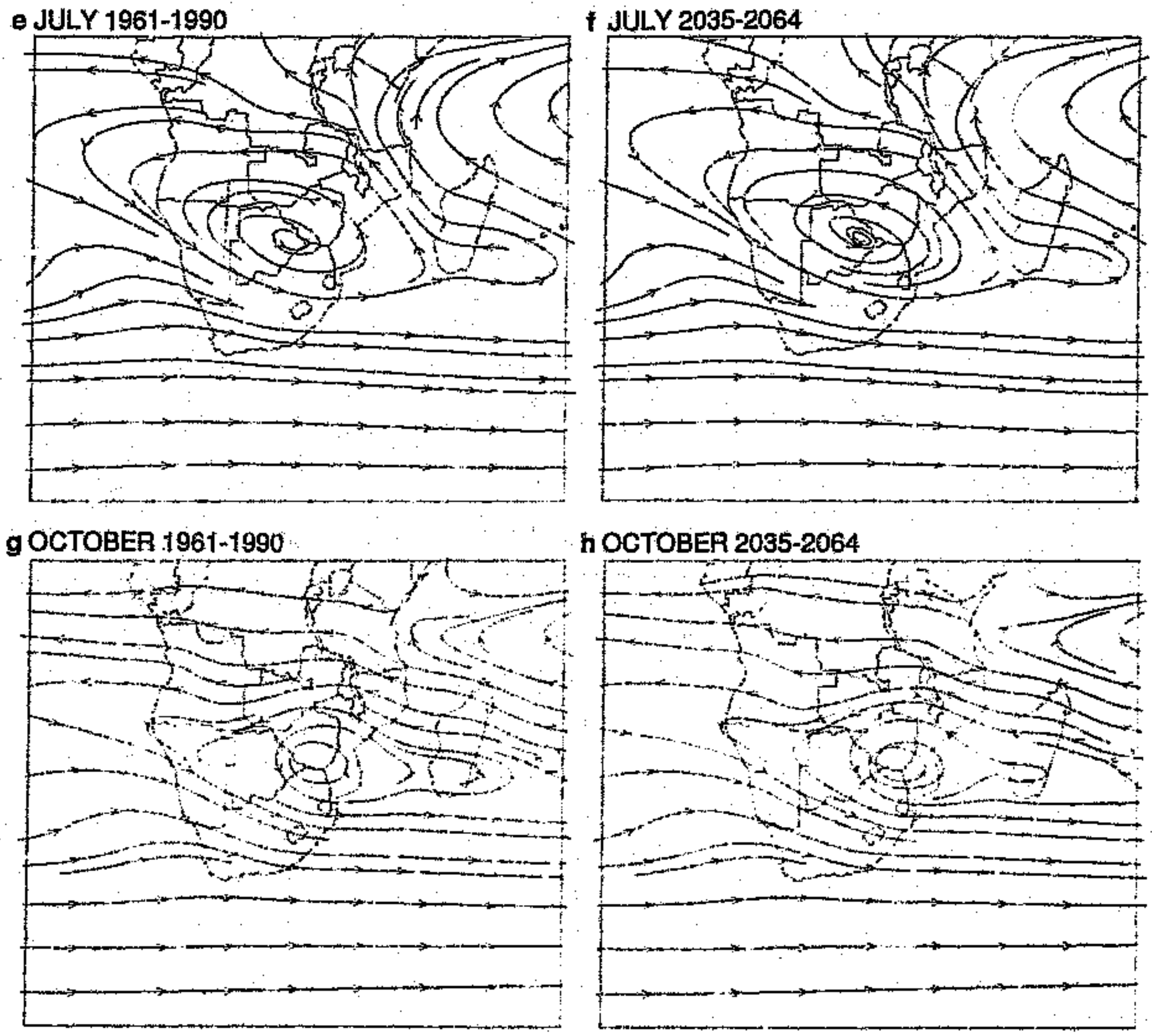

Figure 8.7. (continued)

The pattern of a region of divergence oriented north-west to south-east over south-western southern Africa, with a band of convergence located east of that and also oriented north-west to south-east, persists throughout the year. In January over the 1961-1990 period, the Hadley Centre model simulates divergence of between $0.2 \times 10^{-5}s^{-1}$ and $0.6 \times 10^{-5}s^{-1}$ over the west coast (Fig. 8.8a). The strength of convergence over the central interior is smaller in magnitude at -0.2 x $10^{-5}s^{-1}$ to -0.4 x $10^{-5}s^{-1}$. In July (Fig. 8.8c), the magnitude of both divergence and convergence increases, and the boundary between the region of convergence and divergence shifts eastwards. Magnitudes of divergence over the west coast approach 1.0 x $10^{-5}s^{-1}$ during winter. Divergence at 700 hPa occurs over much of the tropics during summer in association with surface convergence and shifts northwards in winter as the ITC migrates seasonally.

Little change in the patterns and magnitude of the divergence field over southern African is evident from the simulation of future conditions (Fig. 8.8b,d). A slight eastward shift in the location of the boundary between the regions of divergence and convergence between January (Fig. 8.8b) and July (Fig. 8.8d) occurs between the 2035-2064 and 1961-1990 periods. Changes in the strength of divergence over the west coast are 0.2-0.4 x $10^{-5}s^{-1}$. The changes are of the same order as the inter-annual variability in the region and are not likely to be either statistically or physically significant. Over the remainder of the tropical subcontinent, changes in 700 hPa divergence simulated by The Hadley Centre climate change experiment are similarly small.

Synthesis

Scenarios for transient climate change based on two recent fully-coupled model simulations of future climate have been presented for the southern Africa region. The changes in climate are based on gradually-increasing concentrations of greenhouse gases. One experiment using the Hadley Centre fully-coupled model incorporates the direct effects of sulphate aerosols in addition to greenhouse gases.

The inclusion of sulphate aerosols in addition to greenhouse gases in the Hadley Centre model results in a decrease in both the magnitude and rate of warming over southern Africa in comparison to the experiment based on increasing concentrations of greenhouse gases only. For the greenhouse gas only experiment, area-averaged warming for the decade 2050-2059 expressed relative to 1900-1990 is 3.7°C compared with 2.1°C for experiment which includes both greenhouse gases and sulphate aerosols. The decadal average rate of warming over the same period in the greenhouse gas experiment is 0.47°C per decade and 0.3°C per decade in the sulphate aerosol experiment. For both the magnitude and rate of warming, the projected changes for southern Africa are larger than the global average. Based on the accurate performance of the model described in Chapter 5, these estimates of future temperature changes are considered reliable.

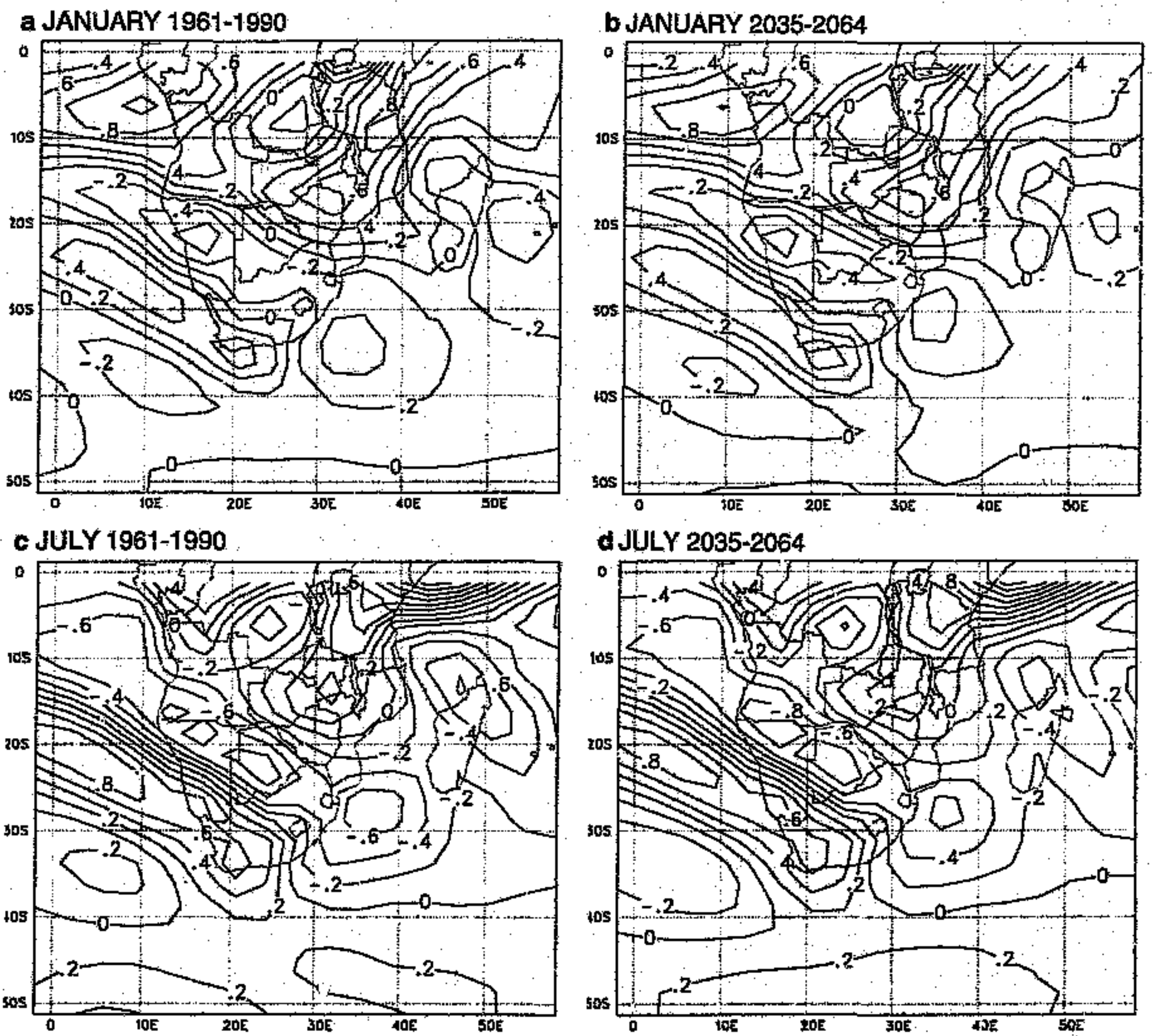

Figure 8.8. Divergence at 700 hPa simulated by the HADCM2 SUL integration for January (a,b) and July (c,d) and for two 30-year periods 1961-1990 (a,c) and 2034-2064 (b,d). All values are multiplied by $10^{-5}s^{-1}$. Contours are every 0.2 x $10^{-5}s^{-1}$. Regions of divergence are shaded.

Changes in the diurnal temperature range projected by the Hadley Centre greenhouse gas only experiment are larger than the combined sulphate aerosol and greenhouse gas experiment. The inclusion of sulphate aerosols leads to a reduction in the amplitude of the diurnal cycle of insolation and hence in changes in diurnal temperature range. Changes in diurnal temperature range are seasonally dependent. Increases in diurnal temperature range in both summer seasons (SON and DJF) and the autumn (MAM) are in contrast to projected decreases in diurnal temperature range in winter (JJA). The seasonal dependence in the projected changes is found in both climate change experiments using the Hadley Centre model, indicating that the result is not due to the inclusion of sulphate aerosols alone.

Possible mechanisms to explain the changes include changes in surface hydrology (soil moisture, evapotranspiration) and cloud cover, and must include interactions and feedbacks between the various components of the land-surface and lower-atmosphere. One hypothesis to explain the projected increases in diurnal temperature range in summer and autumn would be that increases in summer drying of the soil surface and consequent decreases in cloud cover would cause the increases that the model projects. A similar mechanism (with opposing changes) could be invoked to explain the decreases in diurnal temperature range projected during winter. It is interesting to note that the seasonal dependence of the changes mimics the seasonally-dependent changes over South Africa observed from the observational record (Mühlenbruch-Tegen, 1992).

While little confidence can be placed in estimates of a 10-15% decrease in summer rainfall among fully-coupled models (Chapter 7), the decreases in soil moisture and cloud cover suggested by the increase in diurnal temperature in the Hadley Centre model during summer lend credence to the simulated rainfall changes. Similarly, the decreased diurnal temperature during winter and implied increases in soil moisture and cloud cover are reflected in simulated increases in winter rainfall. Simulated interactions in fully-coupled models between surface hydrology, cloud cover and the lower atmosphere over southern Africa remain to be examined in greater detail.

Transient climate change experiments from both the Hadley Centre and CSIRO fully-coupled models have been used to examine projected changes in inter-annual mean sea-level pressure variability around southern Africa. Both models reproduce the same features of inter-annual variability as observed over southern Africa, although simulate lower-amplitude variability than observed (Chapter 6). All three transient climate change experiments considered demonstrate the same set of principal component loading patterns as observed in their respective control integrations. The result suggests that no change in the principal modes of inter-annual variability around southern Africa is expected in a future climate influenced by gradually-increasing greenhouse gas and sulphate aerosol concentrations. While both indicates indicate that the relative contribution from individual modes to the over-all variance may change. However, these changes are generally very small (only 1-2% of the total variance) and no attempt has been made to assess the statistical significance of the changes and they are not expected to be robust.

Subsidence and stable layering of the atmosphere associated with anticyclonic circulation represents and important control on the vertical and horizontal transport of aerosols and trace gases over southern Africa (Cosijn and Tyson, 1996; Garstang *et. al.*, 1996; Tyson *et. al.*, 1996a,b). The Hadley Centre combined greenhouse gas and sulphate aerosol experiment has been used to investigate possible changes in the position and intensity of the anticyclone at 700 hPa, the level of the first elevated stable layer. The model simulates anticyclonic circulation over the subtropics south of 20°S throughout the year, as observed. The north-easterly seasonal migration and longitudinal expansion of the cyclone (strengthening in winter) is also well-captured by the model. As such, the simulated features of 700 hPa circulation over southern Africa are highly realistic and are closely related to the observed features. In the transient climate change integration, the model does not simulate any change in either the position or intensity of the continental anticyclone. Indeed, the pattern of divergence and convergence over southern Africa also changes very little in either magnitude or position. In conclusion then, it can be stated that the representation of observed features of 700 hPa circulation is highly realistic. In addition, the atmospheric circulation which controls the transport of aerosols and trace gases off southern Africa in contemporary climate is likely to remain constant in terms of both position and intensity, suggesting that similar mechanisms which operate in the present atmosphere will operate in the atmosphere in the future.

****

Projections of transient climate change by two century-scale fully-coupled model integrations have been considered. The inclusion of sulphate aerosol in addition to greenhouse gas forcing of climate change results in a decrease of both the magnitude and rate of warming over southern Africa. For both, projected changes over southern Africa are greater than the global average. Projected changes in diurnal temperature range are seasonally-dependent, with increases in summer and autumn and decreases in winter. Both the Hadley Centre and CSIRO fully-coupled model simulate no change in the principal modes of inter-annual variability of mean sea-level pressure around southern Africa. The Hadley Centre model also simulates no change anticyclonic circulation at 700 hPa responsible for fine-weather conditions. The summary and conclusions of this thesis are presented in Chapter 9.

SECTION IV

SUMMARY AND CONCLUSIONS

CHAPTER NINE

SUMMARY AND CONCLUSIONS

Evidence is mounting to support the contention that increasing emissions of greenhouse gases and aerosols due to human activity are resulting in anthropogenically-induced climate change. This process may be expected to continue into the next century and have lasting impacts on the Earth's climate. Complex and sophisticated models of the global climate system have been developed to understand the processes which drive the system and hence project the future impacts of anthropogenic climate change. Climate models which incorporate all of the components of the climate system (atmosphere, ocean, land, ice) have been developed and are capable of representing the cumulative effects of gradually-increasing concentrations of greenhouse gases (and more recently) tropospheric aerosols.

At global and hemispheric scales, climate models display acceptable skill in reproducing observed features of contemporary climate. At these scales, projected climate changes are considered to be realistic. However, the need to represent several small-scale processes which are often not well understand at GCM grid-scales requires the use of parameterisations. Most of the uncertainties associated with climate model projections of future climate are related to the representation of physical processes in this way. At regional spatial scales, the effect of such uncertainties is stronger and consequently present climate simulations and projections of regional climate change are less reliable.

The ability of a wide range of different types of climate models to simulate the features of present climate and variability over southern Africa has been evaluated. Implicit in this process is the assumption that adequate representation of present climate is a necessary although not exclusive pre-requisite for reliable projections of future climate. All of the projections of regional climate change have been assessed in terms of the ability of the model in question to represent present climate. Results from both atmospheric GCMs linked to simple, non-dynamic mixed-layer oceans (referred in this thesis as mixed-layer models) and fully-coupled ocean-atmosphere GCMs (fully-coupled models) have been considered.

Results of the evaluations of present climate performance and projections of future climate are summarised below.

Simulations of Present Climate

1. No single model accurately simulates *all* features of present southern African climate. The performance of individual models is both regionally- and seasonally-dependent.

2. Present climate performance over southern Africa is *dependent on model resolution*. Models which incorporate horizontal grid resolutions of at least ~250 km of latitude by ~400 km longitudes (~2.5° by 3.75° or spectral resolution truncated at T30 or T42) perform better than lower-resolution models. Similarly, models with vertical resolution of 18 or more levels provide more accurate simulations of near-surface and tropospheric circulation features.

3. The atmospheric GCMs linked to mixed-layer oceans incorporate higher spatial resolution than the current fully-coupled ocean-atmosphere models. As a consequence, the present climate performance of the mixed-layer models is generally superior to the performance of the fully-coupled models. Simulation errors among the fully-coupled models are similar to errors calculated for earlier, coarser-resolution mixed-layer models over southern Africa.

4. Mixed-layer models forced by both observed and mean sea-surface temperatures provide accurate simulations of the features of observed mean circulation at both the surface and in the troposphere. Near the surface, features of the circulation which are well-captured include the intensity and seasonal location of the subtropical anticyclones, the depth of the circumpolar trough and the meridional

pressure gradient in the mid-latitudes. In the troposphere, the 850 hPa zonal wind profile, 500 hPa zonal asymmetries and 500 hPa planetary wave structure are well simulated.

5. Of the mixed layer models tested, the UKHI model provides the best overall performance over the southern African region. The model performs better in summer than in winter. The MPI, BMRC and CSIRO models also provide accurate simulations of mean southern African circulation.

6. Among the fully-coupled models which have been assessed, the UKTR model performs best over southern A ,a.

7. While both the mixed-layer and fully-coupled models accurately simulate the major features of surface circulation around southern Africa, grid-point simulation errors in mean sea-level pressure within the tropics and subtropics are larger than the observed inter-annual variability and agreement with observations is poor. The number of both types of models which display agreement with observed mean values is greatest in the mid-latitudes. The result is more indicative of a larger observed inter-annual variability and hence range of acceptable values, than an improvement in model performance.

8. Higher-resolution atmospheric GCMs forced by observed sea-surface temperatures over the 1979-1988 period (the AMIP models) simulate correctly the observed large-scale circulation adjustments in the vicinity of southern Africa associated with inter-annual rainfall variability over the subcontinent.

9. The magnitude of AMIP simulated anomalies in both circulation and rainfall are smaller than observed, suggesting a weaker than observed response to imposed sea-surface temperature anomalies and weaker simulated inter-annual variability than observed.

10. Both the CSIRO and Hadley Centre fully-coupled models simulate the observed principal modes of intra- and inter-annual variability in mean sea-level pressure around southern Africa accurately. The models simulate stronger intra-annual, and weaker inter-annual variability than observed.

11. The pattern of rainfall seasonality, with a pronounced summer maximum over the central interior of the subcontinent, is well reproduced by almost all of the models. Both types of models display substantial errors in terms of simulated rainfall totals over the subcontinent. *Little confidence* may be placed in simulated rainfall *totals* at individual grid-points.

12. The Hadley Centre fully-coupled model simulations forced by greenhouse gases only, and combined greenhouse gas and sulphate aerosol forcing provide accurate simulations of observed annual mean temperatures and diurnal temperature ranges over the subcontinent.

13. The inclusion of *sulphate aerosols* in addition to greenhouse gas forcing of present climate in the Hadley Centre model *does not result in a statistically significant improvement* in it's ability to simulate regional temperature variability over recent decades.

Projections of Future Regional Climate

1. All of the mixed-layer and fully-coupled models project *increased temperatures* throughout southern Africa under enhanced greenhouse conditions.

2. Temperature changes of *3°-4°C* over the subcontinent based on an *equilibrium* response to an instantaneous doubling of CO_2 are projected by the mixed-layer models. Fully-coupled models simulate the *transient* response of the climate system to gradually-increasing anthropogenic forcing and project changes over southern Africa of *1°-2°C*. The different magnitudes of warming are due to the difference

between the equilibrium and a transient response to imposed forcing and reflect the inclusion of the thermal inertia of the oceans in the fully-coupled models.

3. Differences in warming projected by the mixed-layer and fully-coupled models are marked over the southern oceans. Fully-coupled models simulate almost no warming at all, whereas the mixed-layer models simulate warming in excess of 6°C. The difference in the pattern of warming at these latitudes affects the simulation of changes in other variables by the two types of models.

4. Fully-coupled models simulate greater warming relative to the global average over southern Africa than mixed-layer models. Similarly, warming simulated by the mixed-layer models over the southern oceans is higher than the global average and greater than the warming expected from the fully-coupled models.

5. Including the direct effects of *sulphate aerosols* in addition to forcing by greenhouse gases in the Hadley Centre fully-coupled model results in *a decrease of both the magnitude and rate of warming* that can be expected over southern Africa.

6. In an experiment forced by greenhouse gas increases only, the Hadley Centre model simulates a decadally-averaged warming of 3.7°C between the decade starting in 1990 and the decade starting in 2050. The corresponding warming that may be expected from an experiment which includes both greenhouse gas and sulphate aerosol forcing is 2.1°C.

7. The expected rate of warming over the seven decades between 1990 and 2059 is 0.47°C per decade in the greenhouse gas only experiment, and 0.3°C per decade in the combined greenhouse gas and sulphate aerosol experiment. *For both experiments, the rate of warming expected over southern Africa is higher than the global average.*

8. Changes in diurnal temperature range over the subcontinent simulated by the Hadley Centre model reflect a response to changes in soil moisture, evapotranspiration and cloud cover, and not only changes in maximum and minimum temperature. The effect of including sulphate aerosols is to reduce the magnitude of diurnal temperature ranges due to a reduction in the diurnal cycle of insolation.

9. Changes in diurnal temperature range simulated by the Hadley Centre model over the subcontinent south of 15°S are *seasonally-dependent*. During *summer*, an *increased* diurnal temperature range of 1°C is projected by the greenhouse gas only simulation. Increases in diurnal temperature range in the combined greenhouse gas and sulphate aerosol experiment are lower than in the greenhouse gas only experiment. The expected changes imply a reduction soil moisture and cloud cover in the model during summer.

10. During *winter*, the diurnal temperature range over the southern subcontinent is expected to *decrease* by 1°-2°C as minimum temperatures increase faster than maximum temperatures. In contrast to the changes expected during summer and winter, the simulated changes during winter imply an increase in soil moisture and cloud cover.

11. Throughout the southern African region, simulated changes in mean sea-level pressure simulated by both the mixed-layer and fully-coupled models are small (~1 hPa) but are similar in size, or smaller than the present-day simulation errors calculated for both types of models. Observed sea-level pressure anomalies of the same magnitude as the simulated changes are known to accompany major large-scale circulation adjustments associated with extended wet and dry spells over the subcontinent. The simulated changes may therefore have a significant impact on circulation over the southern African region.

12. Neither the CSIRO nor the Hadley Centre fully-coupled models simulate any significant change in the principal modes of inter-annual variability in mean sea-

level pressure over the southern African region. The most important modes of observed variability in contemporary climate are well-captured by the models and not expected to change in the future.

13. *No change in rainfall seasonality* over the subcontinent is simulated by either the mixed-layer or fully-coupled models. Given the small contribution of winter rainfall to the annual total over much of the central interior, simulated changes in winter rainfall in that region are not expected to have an impact on the annual rainfall cycle.

14. *Little confidence* may placed in projected changes seasonal rainfall *totals* over the southern African region. Simulated changes are of smaller magnitude than the simulation errors observed in the present climate simulations of both the mixed-layer and fully-coupled models. In addition, both types of model display a lack of inter-model consensus in terms of the simulated sign of rainfall changes over much of the subcontinent. Nonetheless, the 10-15% decrease in summer rainfall (on average) simulated by the fully-coupled models and increases in winter rainfall simulated by both types of models are in agreement with the expected changes in diurnal temperature range and implied changes soil moisture and cloud cover simulated by the Hadley Centre model.

15. The Hadley Centre model which includes combined greenhouse gas and sulphate aerosol forcing provides a realistic representation of circulation at 700 hPa. The model does not project any change in either the seasonal location or intensity of anticyclonic circulation and the associated pattern of divergence and convergence over subtropical southern Africa. The contemporary atmospheric circulation in the lower troposphere responsible for controlling the transport of aerosols and trace gases off southern Africa may be expected to persist in a future climate.

16. The existence at high southern latitudes of systematic errors in the ocean component of current fully-coupled models, and the absence of a clear improvement in the simulation of contemporary southern African climate by such

models, means that currently they cannot be considered to the exclusion of high-resolution mixed-layer models when estimating possible future climates over the southern African region.

Climate models represent the best available tools for estimating the response of the global climate system to increasing anthropogenic forcing. For regional climates, uncertainties associated with the representation of physical processes at the coarse spatial scales, mean that less confidence can be placed in estimates of future climate. For the southern African region, the ability of a range of atmospheric GCMs linked to simple mixed-layer oceans, as well as fully-coupled ocean-atmosphere models has been assessed in order to provide confidence in their projections of future climates over the region.

All models are able to reproduce the major features of southern African circulation reliably. Model performance over southern Africa is influence by model resolution. Models with higher spatial resolution are better able to reproduce features of regional circulation. Both mixed-layer models forced by observed sea-surface temperatures, and fully-coupled models are capable of reproducing the observed features of intra- and inter-annual circulation variability in the vicinity of southern Africa. While considerably less confidence exists in the ability of the models to simulate present-day rainfall totals, the models' ability to simulate the large-scale circulation adjustments associated with extended periods of above and below-average rainfall over the subcontinent is indicative of the correct response in the models to those processes which are associated with inter-annual rainfall variability.

Future southern African climate can be expected to be between 1°C and 4°C warmer than the present. The upper limit of that range is defined by the simulated equilibrium response of the mixed-layer models to an instantaneous doubling of CO_2. The lower limit of that range is defined by the transient response of fully-coupled models to gradually-increasing anthropogenic forcing. If the direct forcing effect of sulphate aerosols is considered in addition to greenhouse gases, temperatures may be expected to increase on average by approximately 0.3°C per decade over the next 70 years; a warming of slightly more than 2°C.

Less confidence can be placed in estimates of regional rainfall totals, although expected changes in mean rainfall are not expected to exceed 20% of the current mean summer rainfall. Nonetheless, changes of 20% in mean rainfall may have important implications for surface hydrology and the occurrence of extreme rainfall events. No change in rainfall seasonality over the subcontinent is expected. Decreases in summer rainfall totals and increases in winter rainfall totals projected by most fully-coupled models are consistent with projected changes in diurnal temperature range in the Hadley Centre fully-coupled model. Changes in diurnal temperature range reflect changes in soil moisture, evapotranspiration and cloud cover and are indicative of important interactions between surface hydrology, land surface processes and the lower atmosphere, which are currently poorly understood.

Finally, despite the uncertainties associated with the use of climate models at regional scales, meaningful estimates of regional climate change over southern Africa have been derived. The simulations of present and future climate have provided valuable insights into the physical processes, circulation dynamics and synoptic-scale meteorology and climatology which influence the climate of the southern African region. In future, the need to provide high-resolution estimates of future climate over southern Africa which incorporate the effects of interactions between the land surface, vegetation and atmospheric components of the regional climate system will have to be addressed.

APPENDICES

1 LIST OF ABBREVIATIONS

AMIP	Atmospheric Model Intercomparison Project
ANN	Artificial Neural Network
ANOVA	Analysis of Variance
BMRC	Australian Bureau of Meteorology Research Centre used here to refer to the atmospheric general circulation model (Colman *et al.*, 1994)
CCC	Canadian Climate Centre used here to refer to the AMIP atmospheric general circulation model (Boer *et al.*, 1992b)
CRU	Climate Research Unit, University of East Anglia
CSIRO	Commonwealth Scientific and Industrial Research Organisation used here to refer to the 9-level atmospheric general circulation model (McGregor *et al.*, 1993)
CSIROC	CSIRO fully-coupled ocean-atmosphere general circulation model (Gordon and O'Farrell, 1996)
CSIROC CM8	CSIROC control integration
CSIROC TX8	CSIROC transient climate change integration
ECMWF	European Centre for Medium-Range Weather Forecasts
ENSO	El Niño / Southern Oscillation event
ERBE	Earth Radiation Budget Experiment
GCM	General Circulation Model
GFDL	Geophysical Fluid Dynamics Laboratory used here to refer to the atmospheric general circulation model (Wetherald *et al.*, 1991)
GFDLC	GFDL fully-coupled ocean-atmosphere general circulation model (Manabe *et al.*, 1991)
GMT	Greenwhich Mean Time

HADCM2	Second Hadley Centre for Climate Prediction and Research fully-coupled ocean-atmosphere GCM (Johns *et al.*, 1996)
HADCM2 CON	HADCM2 control integration (Johns *et al.*, 1996)
HADCM2 GHG	HADCM2 transient climate change integration forced by increasing concentrations of greenhouse gases only (Mitchell *et al.*, 1995a)
HADCM2 SUL	HADCM2 transient climate change integration forced by increasing concentrations of greenhouse gases and sulphate aersosols (Mitchell *et al.*, 1995a)
IPCC	Intergovernmental Panel on Climate Change
IS92	IPCC emission scenario IS92a (IPCC, 1994)
ITC	InterTropical Convergence Zone
MPI	Max Planck Istitüt für Meteorologie used here to refer to the atmospheric general circulation model (DKRZ, 1992)
MPILC	MPI fully-coupled ocean-atmosphere general circulation model. MPILC includes the LSG ocean formulation (Cubasch *et al.*, 1993)
MPIOC	MPI fully-coupled ocean-atmosphere general circulation model. MPIOC includes the OPYC ocean formulation (Lunkeit *et al.*, 1994)
NCAR	National Centre for Atmospheric Research used here to refer to the AMIP atmospheric general circulation model simulation (Hack *et al.*, 1994)
PCA	Principal Components Analysis
PC	principal component
SAO	semi-annual oscillation
UKMO	United Kingdom Meteorological Office used here to refer to the AMIP atmospheric general circulation model integration using the UKMO Unified Model (Cullan, 1993)
UKHI	UKMO Hadley Centre high-resolution atmospheric general circulation model (Gregory and Mitchell, 1995)
UKTR	First Hadley Centre fully-coupled atmosphere-ocean general circulation model (Murphy, 1995)
WMO	World Meteorological Organisation

REFERENCES

Adler, R.F., 1975: A comparison of the general circulations of the Northern and Southern Hemispheres based on satellite, multi-channel radiance data, *Monthly Weather Review*, 103, 52-60.

Barnett, T.P., 1995: Monte Carlo climate forecasting, *Journal of Climate*, 8, 1005-1020.

Barnett, T.P., Bengtsson, L., Arpe, K., Flugel, M., Graham, N., Latif, M., Ritchie, J., Roeckner, E., Schlese, U., Schulzwieda, U. and Tyree, M., 1994: Forecasting global ENSO-related climate anomalies, *Tellus*, 46A, 381-397.

Boer, G.J., Arpe, K., Blackburn, M., Déqué, M., Gates, W.L., Hart, T.L., Le Treut, H., Roeckner, E., Sheinin, D.A., Simmonds, I., Smith, R.N.B., Tokioka, T., Wetherald, R.T. and Williamson, D., 1992a: Some results from an intercomparison of the climates simulated by 14 atmospheric general circulation models, *Journal of Geophysical Research*, 97, 12771-12786.

Boer, G.J., McFarlane, N.A. and Lazare, M., 1992b: Greenhouse gas-induced climate change simulated with the CCC second-generation general circulation model, *Journal of Climate*, 5, 1045-1077.

Boville, B., 1991: Sensitivity of simulated climate to model resolution, *Journal of Climate*, 4, 469-485.

Brankovic, C., Palmer, T.N. and Viterbo, P., 1990: Seasonal simulations with the ECMWF NWP model, *WMO Programme on Long-Range Forecasting Research Report 14*.

Brankovic, C., Palmer, T.N. and Ferranti, L., 1994: Predictability of seasonal atmospheric variations, *Journal of Climate*, 7, 217-237.

Bryan, K., 1969: Climate and the ocean circulation III: The ocean model, *Monthly Weather Review*, 97, 806-827.

Bryan, K. and Spelman, M.J., 1985: The ocean's response to a CO_2-induced warming, *Journal of Geophysical Research*, 90, 11679-11688.

Bryan, K., Manabe, S. and Spelman, M.J., 1988: Interhemispheric asymmetry in the transient response of a coupled ocean-atmosphere model to a CO_2 forcing, *Journal of Physical Oceanography*, 18, 851-867.

Burgos, J.J., Ponce, H.F. and Molion, L.C.B., 1991: Climate change predictions for South America, *Climatic Change*, 18, 223-239.

Campbell, G.G., Kittel, G.F., Meehl, G.A. and Washington, W.M., 1995: Low-frequency variability and CO_2 transient climate change. Part 2: EOF analysis of CO_2 and model-configuration sensitivity, *Global and Planetary Change*, 10, 201-216.

Cao, H.-X., Mitchell, J.F.B. and Lavery, J.R., 1992: Simulated diurnal range and variability of surface temperature in a global climate model for present and doubled-CO_2 climates, *Journal of Climate*, 5, 920-943.

Cess, R.D., Ghan, S.J., Randall, D.A., Schlese, U., Potter, G.L., Riches, M.R., Roeckner, E., Kiehl, J.T., Yagai, I., Wetherald, R.T., Blanchet, J.P., Boer, G.J., Li, Z.-X., Liang, X.-Z., Le Treut, H., Morcrette, J.-J., Mitchell, J.F.B., Taylor, K.E., Slingo, A. and Washington, W.M., 1989: Interpretation of cloud-climate feedback as produced by 14 atmospheric general-circulation models, *Science*, 245, 513-516.

Cess, R.D., Potter, G.L., Blanchet, J.P., Boer, G.J., Del Genio, A.D., Déque, M., Dymnikov, V., Galin, V., Gates, W.L., Ghan, S.J., Kiehl, J.T., Lacis, A.A., Le Treut, H., Li, Z.-X., Liang, X.-Z., McAvaney, B.J., Meleshko, V.P., Mitchell, J.F.B., Morcrette, J.-J., Randall, D.A., Rikus, L., Roeckner, E., Royer, J.F., Schlese, U., Sheinin, D.A., Slingo, A., Sokolov, A.P., Taylor, K.E., Washington, W.M., Wetherald, R.T., Yagai, I. and Zhang, M.-H., 1990: Intercomparison and interpretation of climate feedback processes in 19 atmospheric general circulation models, *Journal of Geophysical Research*, 95, 16601-16615.

Cess, R.D., Zhang, M.-H., Ingram, W.J., Potter, G.L., Alekseev, V., Barker, W., Cohen-Solal, E., Colman, R.A., Dazlich, D.A., Del Genio, A.D., Dix, M.R., Dymnikov, V., Esch, M., Fowler, L.D., Fraser, J.R., Galin, V., Gates, W.L., Hack, J.J., Kiehl, J.T., Le Treut, H., Lo, K.K.-W., McAvaney, B.J., Meleshko, V.P., Morcrette, J.-J., Randall, D.A., Roeckner, E., Royer, J.F., Schlesinger, M.E., Sporyshev, P.V., Timbal, B., Volodin, E.M., Taylor, K.E., Wang, W. and Wetherald, R.T., 1996: Cloud feedback in atmospheric general circulation models: An update, *Journal of Geophysical Research*, 101, 12791-12794.

Clarke, G.M. and Cooke, D., 1983: *A Basic Course in Statistics. Second Edition*, Arnold, London.

Colman, R.A., McAvaney, B.J., Fraser, J.R. and Power, S.B., 1994: Annual mean meridional energy transport modelled by a general circulation model for present and 2 x CO_2 equilibrium climates, *Climate Dynamics*, 10, 221-229.

Cosijn, C. and Tyson, P.D., 1996: Stable discontinuities in the atmosphere over South Africa, *South African Journal of Science*, 92, 381-386.

Cox, M.D., 1984: A primitive equation, three dimensional model of the ocean, *GFDL Ocean Group Technical Report No. 1*, Princeton, NJ, USA, 143pp.

Cubasch, U., Hasselmann, K., Hock, H., Maier-Reimer, E., Mikolajewicz, U., Santer, B.D. and Sausen, R., 1992: Time-dependent greenhouse warming computations with a coupled ocean-atmosphere model, *Climate Dynamics*, 8, 55-69.

Cubasch, U., Hasselmann, K., Höck, H., Mikolajewicz, U., Santer, B.D. and Voss, R., 1995: A climate simulation starting in 1935, *Climate Dynamics*, 11, 71-84.

Cullan, M.J.P., 1993: The Unified forecast / climate model, *Meterological Magazine*, 122, 81-94.

D'Abreton, P.C. and Lindesay, J.A., 1993: Water vapour transport over southern Africa during wet and dry early and late summer months, *International Journal of Climatology*, 13, 151-170.

D'Abreton, P.C. and Tyson, P.D., 1995: Divergent and non-divergent water vapour transport over southern Africa during wet and dry conditions, *Meteorology and Applied Physics*, 55, 47-59.

Del Genio, A.D., Yeo, M.-S., Kovari, W. Jr. and Lo, K.K.-W., 1995: A prognostic cloud water parameterization for global climate models, *Journal of Climate*, 9, 270-304.

Deutches Klimarechenzentrum (DKRZ) Modelbetreungs-Gruppe, 1992: The ECHAM3 atmospheric general circulation model, *DKRZ Tech. Report No. 6, ISSN 0940-9237*, Deutches Klimarechenzentrum, Hamburg, Germany, 184pp.

Dignon, J. and Hameed, S., 1989: Global emissions of Nitrogen and Sulphur oxides from 1860 to 1980, *Journal of the Air and Waste Management Association*, 39, 180-186.

Druyan, L.M., Shah, K.P., Lo, K.-W.K., Marengo, J.A. and Russell, G., 1995: Impacts of model improvements on general circulation model sensitivity to sea-surface temperature forcing, *International Journal of Climatology*, 15, 1061-1086.

Dyer, T.G.J., 1975: The assigment of rainfall stations into homogeneous groups: an application of principal components analysis, *Quarterly Journal of the Royal Meteorological Society*, 101, 1005-1013.

Dyer, T.G.J., 1981: The apparent absence of the quasi-biennial oscillation in sea-level pressure in the South Indian Ocean and South Atlantic Ocean, *Quarterly Journal of the Royal Meteorological Society*, 107, 461-467.

England, M.H., 1995: Using chlorofluorocarbons to assess ocean models, *Geophysical Research Letters*, 22, 3051-3054.

England, M.H., Garcon, V. and Minster, J., 1994: Chlorofluorocarbon uptake in a World Ocean Model 1. Sensitivity to the surface gas forcing, *Journal of Geophysical Research*, 99, 25212-25233.

Ferranti, L., Hoskins, B.J., Palmer, T.N. and Slingo, J.M., 1995: Relations between interannual and intraseasonal monsoon variability as diagnosed from AMIP integrations, *Proceedings of the First International AMIP Scientific Conference*, WCRP-92, WMO/TD-732, 149-154.

Flohn, H., 1969: *Climate and Weather*, Weidenfeld and Nicholson, London, 253pp.

Fowler, L.D. and Randall, D.A., 1996: Liquid and ice cloud microphysics in the CSU general circulation model. Part 2: Simulations of the Earth's Radiation Budget, *Journal of Climate*, 9, 530-560.

Garstang, M., Tyson, P.D., Swap, R. and Edwards, M., 1996: Horizontal and vertical transport of air over southern Africa, *Journal of Geophysical Research*, 101, 23721-23736.

Gates, W.L., 1992: AMIP: The Atmospheric Model Intercomparison Project, *Bulletin of the American Meteorological Society*, 73, 1962-1970.

Gates, W.L., 1995: An overview of AMIP and preliminary results. *Proceedings of The First International AMIP Scientific Conference*, WCRP-92, WMO/TD-No. 732, Geneva, 1-8.

Giambelluca, T.W. and Henderson-Sellers, A., (Eds.) 1996: *Climate Change. Developing Southern Hemisphere Perspectives*, John Wiley & Sons, Chichester, 475pp.

Giorgi, F. and Mearns, L.O., 1991: Approaches to the simulation of regional climate change: A review, *Reviews of Geophysics* 29, 191-216.

Giorgi, F., Marinucci, M.R. and Visconti, G., 1990: Use of a limited-area model nested in a general circulation model for regional climate simulation over Europe, *Journal of Geophysical Research*, 95, 18413-18431.

Giorgi, F. Brodeur, C.S. and Bates, G.T., 1994: Regional climate change scenarios over the United States produced with a nested regional climate model, *Journal of Climate*, 7, 375-399.

Gordon, H.G. and O'Farrell, S.P., 1996: Transient climate change in the CSIRO coupled model with dynamic sea ice, *Monthly Weather Review*, in press.

Gordon, H.B., Whetton, P.H., Pittock, A.B., Fowler, A.M. and Haylock, M.R., 1992: Simulated changes in daily rainfall intensity due to the enhanced greenhouse effect: Implications for extreme rainfall events, *Climate Dynamics*, 8, 83-102.

Green, B.F., 1952: The orthogonal approximation of an oblique structure in factor analysis, *Psychometrika*, 17, 429-440.

Gregory, J.M., 1993: Sea level changes under increasing atmospheric CO_2 in a transient coupled ocean-atmosphere GCM experiment, *Journal of Climate*, 6, 2247-2262.

Gregory, J.M. and Mitchell, J.F.B., 1995: Simulation of daily variability of surface temperature and precipitation over Europe in the current and 2 x CO_2 climates using the UKMO high-resolution climate model, *Quarterly Journal of the Royal Meteorological Society*, 121, 1451-1476.

Grotch, S.L., and MacCracken, M.C., 1991: The use of general circulation models to predict regional climate change, *Journal of Climate*, 4, 286-303.

Hack, J.J., Boville, B.A., Kiehl, J.T., Rasch, P.J. and Williamson, D.L., 1994: Climate statistics from the NCAR Community Climate Model (CCM2), *Journal of Geophysical Research*, 9 [illegible])785-20813.

Hameed, S. and Dignon, J., 1992: Global emissions of Nitrogen and Sulphur oxides in fossil fuel combustion, 1970-1986, *Journal of the Air and Waste Management Association*, 42, 159-163.

Hansen, J.E., Sato, M. and Ruedy, R., 1995: Long-term changes of the diurnal temperature cycle: Implications about mechanisms of global climate change, *Atmospheric Research*, 37, 175-209.

Harangozo, S.A. and Harrison, M.S.J., 1983: On the use of synoptic data in indicating the presence of cloud bands over southern Africa, *South African Journal of Science*, 79, 413-414.

Harrison, E.F., Minnis, P., Barkstrom, B.R., Ramanathan, V., Cess, R.D. and Gibson, G.G., 1990: Seasonal variation of cloud radiative forcing derived from the Earth Radiation Budget Experiment, *Journal of Geophysical Research*, 95, 18687-18703.

Harrison, M.S.J., 1986: A synoptic climatology of South African rainfall variations, Unpublished PhD Thesis, University of the Witwatersrand, 341pp.

Hasselmann, K., Bengtsson, L., Cubasch, U., Hegerl, G.C., Rodhe, H., Roeckner, E., von Storch, H., Voss, R. And Waszkewitz, J., 1995: Detection of anthropogenic climate change using a fingerprint method, in Ditlevsen, P., (Ed.), *Proceedings of "Modern Dynamical Meteorology", Symposium in honor of Aksel Wiin-Nielsen, 1995*, ECMWF Press, 1995.

Henderson-Sellers, A. and Hanson, A.-H., 1995: *Climate Change Atlas: Greenhouse Simulations from the Model Evaluation Consortium for Climate Assessment*, Kluwer Academic Publishers, Dordrecht, The Netherlands.

Henderson-Sellers, A., McGuffie, K. and Gross, C., 1995: Sensitivity of global climate simulations to increased stomatal resistance and CO_2 increases, *Journal of Climate*, 8, 1738-1756.

Hennessey, K.J., Gregory, J.M. and Mitchell, J.F.B., 1995: Changes in daily precipitation under enhanced greenhouse conditions, *Climate Dynamics*, in press.

Hewitson, B. C. and Crane R. G., 1992: Regional-scale climate prediction from the GISS GCM, *Palaeogeography, Palaeoclimatology, Palaeoecology (Global and Planetary Change Section)*, 97, 249-267.

Hewitson, B. C. and Crane, R. G. (Eds.), 1994: *Neural Nets: Applications in Geography*, Kluwer Academic Publishers, Dordrecht, The Netherlands.

Hewitson, B.C. and Crane, R.G., 1996: Climate downscaling: Techniques and application, *Climate Change*, in press.

Hofmeyr, W.L. and Gouws, V., 1964: A statistical and synoptic analysis of wet and dry conditions in northwestern Transvaal, *Notos*, 12, 37-48.

Horton, E.B., 1995: Geographical distribution of changes in maximum and minimum temperatures, *Atmospheric Research*, 37, 102-117.

Hulme, M., 1994: Validation of large-scale precipitation fields in General Circulation Models, in Desbois, M. and Désalmand, F. (Eds.), *Global Precipitation and Climate Change*, Springer-Verlag, Berlin, 387-405.

Hulme, M., Conway, D., Jones, P.D., Jiang, T., Barrow, E.M. and Turney, C., 1995: Construction of a 1961-1990 climatology for Europe for climate change impacts and modelling applications, *International Journal of Climatology*, 15, 1333-1363.

Hulme, M., Joyce, A., Conway, D. and Mulenga, H., 1996: A 1961-1990 climatology for Africa south of the equator and a comparison of potential evapotranspiration estimates, *South African Journal of Science*, 92, 334-343.

Hurley, J.R. and Cattell, R.B., 1962: The Procrustes program: Producing direct rotation to test a hypothesized factor structure, *Behavioural Science*, 7, 258-262.

Hurrell, J.W. and van Loon, H., 1994: A modulation of the atmospheric annual cycle in the southern hemisphere, *Tellus*, 46A, 325-338.

Intergovenmental Panel on Climate Change (IPCC), 1990: *Climate Change, The IPCC Scientific Assessment*, (Eds.) J.T. Houghton, G.J. Jenkins and J.J. Ephraums, Cambridge University Press, Cambridge, UK, 365pp.

Intergovenmental Panel on Climate Change (IPCC), 1992: *Climate Change, The Supplementary Report to the IPCC Scientific Assessment*, (Eds.) Houghton, J.T., Callander, B.A. and Varney, S.K., Cambridge University Press, Cambridge, UK, 198pp.

Intergovenmental Panel on Climate Change (IPCC), 1994: *Climate Change 1994: Radiative Forcing of Climate Change and an Evaluation of the IPCC IS92 Emission Scenarios*, (Eds.) Houghton, J.T., Meira Filho, L.G., Bruce, J., Hoesung

Lee, Callander, B.A., Haites, E., Harris, N., and Maskell, K., Cambridge University Press, Cambridge, UK, 339pp.

Intergovernmental Panel on Climate Change (IPCC), 1995: *Climate Change 1995. The Science of Climate Change. Contribution of Working Group I to the Second Assessment Report of the Intergovernmental Panel on Climate Change,* (Eds.) Houghton, J.T., Meira Filho, L.G., Callander, B.A., Harris, N., Kattenberg, A. and Maskell, K., Cambridge University Press, Cambridge, UK, 572pp.

Jenkins, G.S., and Barron, E.J., 1996: General circulation model and coupled regional climate model simulations over the eastern United States: GENESIS and RegCM2 simulations, *Global and Planetary Change*, in press.

Jenkins, G.M. and Watts, D.G., 1968: *Spectral Analysis and its Applications*, Holden-Day, San Francisco, USA, 525pp.

Jenkinson, A.F., 1977: A powerful elementary method of spectral analysis for use with monthly, seasonal and annual meterological time series, Meterological Offfice 13, Branch Memo No. 57, Bracknell, 23pp.

Johns, T.C., Carnell, R.E., Crossley, J.F., Gregory, J.M., Mitchell, J.F.B., Senior, C.A., Tett, S.F.B. and Wood, R.A., 1996: The second Hadley Centre coupled model ocean-atmosphere GCM: Model description, spinup and validation, *Climate Dynamics*, in press.

Jones, P.D., 1991: Southern Hemisphere sea-level pressure data: An analysis and reconstruction back to 1951 and 1911, *International Journal of Climatology*, 11, 585-607.

Jones, P.D., 1994: Hemispheric surface air temperature variability - a reanalysis and an update to 1993, *Journal of Climate*, 7, 1794-1802.

Jones, R.G., Murphy, J.M. and Noguer, M., 1995: Simulation of climate change over Europe using a nested regional-climate model. I: Assessment of control climate, including sensitivity to location of lateral boundaries, *Quarterly Journal of the Royal Meteorological Society*, 121, 1413-1450.

Joubert, A.M., 1994: Simulations of southern African climatic change by early-generation General circulation models, *WaterSA*, 20, 315-322.

Joubert, A.M., 1995: Simulations of southern African climate by early generation general circulation models, *South African Journal of Science*, 91, 85-91.

Joubert, A.M., 1996: AMIP simulations of atmospheric circulation over southern Africa, *International Journal of Climatology*, in press.

Joubert, A.M. and Hewitson, B.C., 1996: Simulating present and future climates of southern Africa using general circulation models, *Progress in Physical Geography*, in press.

Joubert, A.M. and Tyson, P.D., 1996: Equilibrium and fully-coupled GCM simulations of future southern African climates, *South African Journal of Science*, 92, 471-484.

Joubert, A.M., Mason, S.J. and Galpin, J.S., 1996: Droughts over southern Africa in a doubled-CO_2 climate, *International Journal of Climatology*, 16, in press.

Jury, M.R., 1996: Regional teleconnection patterns associated with summer rainfall over South Africa, Namibia and Zimbabwe, *International Journal of Climatology*, 16, 135-153.

Jury, M.R. and Pathack, B.M.R., 1993: Composite climatic patterns associated with extreme modes of summer rainfall over southern Africa: 1975-1984, *Theoretical and Applied Climatology*, 47, 137-145.

Jury, M.R., McQueen, C. and Levey, K., 1994: SIO and QBO signals inthe African region, *Theoretical and Applied Climatology*, 50, 103-115.

Karl, T.R., Jones, P.D., Knight, R.W., Kukla, G., Plummer, N., Razuvayev, V., Gallo, K.P., Lindesay, J., Charlson, R.J. and Peterson, T.C., 1993: A new perspective of recent global warming: Asymmetric trends of daily maximum and minimum temperature, *Bulletin of the American Meteorological Society*, 74, 1007-1023.

Karoly, D.J. and Oort, A.H., 1987: A comparison of Southern Hemisphere circulation statistics based on GFDL and Australian analyses, *Monthly Weather Review*, 115, 2033-2059.

Katz, R.W. and Brown, B.G., 1992: Extreme events in a changing climate: Variability is more important than averages, *Climatic Change*, 21, 289-302.

Katz, R.W. and Acero, J.G., 1994: Sensitivity analysis of extreme precipitation events, *International Journal of Climatology*, 11, 505-513.

Kinter, J.L., III, Shukla, J., Marx, L. and Schneider, E.K., 1988: A simulation of the winter and summer circulations with the NMC global spectral model, *Journal of the Atmospheric Sciences*, 45, 2486-2522.

Kitoh, A., 1994: Tropical influence of the South Pacific double jet variability, *Proc. NIPR Symposium on Polar Meteorology Glaciology*, 8, 34-45.

Kitoh, A., Yamazaki, K. and Tokioka, T., 1990: The double jet and semi-annual oscillations in the southern hemisphere simulated by the Meteorological Research Insititute general circulation model, *Journal of the Meteorological Society of Japan*, 68, 251-264.

König, W., Sausen, R. and Sielmann, F., 1993: Objective identification of cyclones in GCM simulations, *Journal of Climate*, 6, 2217-2231.

Langner, J., and Rodhe, H., 1991: A global three-dimensional model of the tropospheric sulphur cycle, *Journal of Atmospheric Chemistry*, 13, 225-263.

Le Marshall, J.F., Kelly, G.A.M. and Karoly, D.J., 1985: An atmospheric climatology of the Southern Hemisphere based on ten years of daily numerical analyses (1972-1982), *Australian Meteorological Magazine*, 33, 65-85.

Legates, D.R. and Willmott, C.J., 1990: Mean seasonal and spatial variability in guage-corrected, global precipitation, *International Journal of Climatology*, 10, 111-128.

Lindesay, J.A., 1988: The Southern Oscillation and atmospheric circulation changes over southern Africa, Unpublished PhD Thesis, University of the Witwatersrand, 284pp.

Lindesay, J.A., 1992: Modelling the influence of sea surface temperature anomalies on summer rainfall in southern Africa, paper presented to the International Geographical Union Commission on Climatology, Pennsylvania State University, 3-7 August 1992.

Lindesay, J.A. and Jury, M.R., 1991: Atmospheric circulation controls and characteristics of a flood event in central South Africa, *International Journal of Climatology*, 11, 609-627.

Lindesay, J.A. and Smith, I.N., 1993: Modelling southern African rainfall responses to SST anomalies in the South Atlantic and Indian Oceans, *Preprints of the 4th International Conference on Southern Hemisphere Meterology and Oceanography*, American Meteorological Society, Boston, 526-527.

Livezey, 1990: Variability of skill of long-range forecasts and implications for their use and value, *Bulletin of the American Meteorological Society*, 71, 300-309.

Lorenz, E.N., 1963: Deterministic nonperiodic flow, *Journal of the Atmospheric Sciences*, 20, 130-141.

Lorenz, E.N., 1984: Irregularity: A fundamental property of the atmosphere, *Tellus*, 36A, 98-110.

Lorenz, E.N., 1990: Can chaos and intransitivity lead to interannual variability?, *Tellus*, 42A, 378-389.

Lunkeit, F., Sausen, R. and Oberhuber, J.M., 1994: Climate simulations with the global coupled atmosphere-ocean model ECHAM/OPYC. Part I: Present-day climate and ENSO events, *MPI Report No. 132*, Max Planck Institute for Meteorology, Hamburg, Germany.

McAvaney, B.J. and Colman, R.A., 1993: The AMIP experiment: The BMRC AGCM configuration, *BMRC Research Report No. 38*, Bureau of Meterology Research Centre, Melbourne, Australia, 231pp.

McGee, O.S. and Hastenrath, S.L., 1966: Harmonic analysis of the rainfall over South Africa, *Notos*, 15, 79-90.

McGregor, J.L., Gordon, H.B., Watterson, I.G. and Dix, M.R., 1993: The CSIRO 9-level atmospheric general circulation model, *CSIRO Division of Atmospheric Research Technical Paper. No. 26*, CSIRO DAR, Mordialloc. 55pp.

Malone, R.C., Pitcher, E.J., Blackmon, M.L., Puri, K. and Bourke, W., 1984: The simulation of stationary and transient geopotential height eddies in January and July with a spectral general circulation model, *Journal of the Atmospheric Sciences*, 41, 1394-1419.

Manabe, S. and Stouffer, R.J., 1988: Two stable equilibria of a coupled ocean-atmosphere model, *Journal of Climate*, 1, 841-866.

Manabe, S. and Stouffer, R.J., 1994: Multiple-century response of a coupled ocean-atmosphere model to an increase of atmospheric carbon dioxide, *Journal of Climate*, 7, 5-23.

Manabe, S., Stouffer, R.J., Spelman, M.J. and Bryan, K., 1991: Transient responses of a coupled ocean-atmosphere model to gradual changes of atmospheric CO_2 Part I: annual mean response, *Journal of Climate*, 4, 785-818.

Manabe, S., Spelman, M.J. and Stouffer, R.J., 1992: Transient responses of a coupled ocean-atmosphere model to gradual changes of atmospheric CO_2 Part II: seasonal response, *Journal of Climate*, 5, 105-126.

Mason, S.J., 1995: Sea-surface temperature-South African rainfall associations, 1910-1989, *International Journal of Climatology*, 15, 119-135.

Mason, S.J. and Joubert, A.M., 1996: Simulated changes in extreme rainfall over southern Africa, *International Journal of Climatology*, in press.

Mason, S.J., Lindesay, J.A. and Tyson, P.D., 1994: Simulating drought in southern Africa using sea surface temperature variations, *WaterSA*, 20, 15-22.

Matarira, C.H., 1990: Drought over Zimbabwe in a regional and global context, *International Journal of Climatology*, 10, 609-625.

Mearns, L.O., Katz, R.W. and Schneider, S.H., 1984: Extreme high-temperature events: Changes in their probabilities with changes in mean temperature, *Journal of Climate and Applied Meteorology*, 23, 1601-1613.

Mearns, L.O., Schneider, S.H., Thompson, S.L. and McDaniel, L.R., 1990: Analysis of climate variability in general circulation models: Comparison with observations and changes in variability in 2 x CO_2 experiments, *Journal of Geophysical Research*, 95, 20469-20490.

Mearns, L.O., Giorgi, F., McDaniel, L. and Shields, C., 1995: Analysis of variability and diurnal range of daily temperature in a nested regional climate model: Comparison with observations and doubled-CO_2 results, *Climate Dynamics*, 11, 193-209.

Meehl, G.A., 1990: Development of global coupled ocean-atmosphere general circulation models, *Climate Dynamics*, 5, 19-33.

Meehl, G.A., 1991: A reexamination of the mechanism of the semiannual oscillation in the Southern Hemisphere, *Journal of Climate*, 4, 911-926.

Meehl, G.A., 1995: Global coupled general circulation models, *Bulletin of the American Meteorological Society*, 76, 951-957.

Meehl, G.A., 1996: Climate Modelling, in Karoly, D.J. and Vincent, D. (Eds.) *Meteorology of the Southern Hemisphere*, American Meteorological Society, in press.

Meehl, G.A. and Albrecht, B.A., 1988: Tropospheric temperatures and southern hemisphere circulation, *Monthly Weather Review*, 116, 953-960.

Meehl, G.A. and Albrech, B.A., 1991: Response of a GCM with a hybrid convection scheme to a tropical Pacific sea surface temperature anomaly, *Journal of Climate*, 4, 672-688.

Meehl, GA., Washington, W.M. and Karl, T.R., 1993a: Low-frequency variability and CO_2 transient climate change, *Climate Dynamics*, 8, 117-133.

Meehl, G.A., Branstator, G.W. and Washington, W.M., 1993b: Tropical Pacific interannual variability and CO_2 climate change, *Journal of Climate*, 6, 42-63.

Meehl, G.A., Wheeler, M. and Washington, W.M., 1994: Low-frequency variability and CO_2 transient climate change. Part 3: Intermonthly and interannual variability, *Climate Dynamics*, 10, 277-303.

Miron, O. and Tyson, P.D., 1984: Wet and dry conditions and pressure anomaly fields over South Africa and the adjacent oceans, 1963-1979, *Monthly Weather Review*, 112, 2127-2132.

Mitchell, J.F.B. and Ingram, W.J., 1992: Carbon dioxide and climate: Mechanisms of changes in cloud, *Journal of Climate*, 5, 5-21.

Mitchell, J.F.B. and Johns, T.C., 1996: On the modification of global warming by sulphate aerosols, *Journal of Climate*, in press.

Mitchell, J.F.B., Wilson, C.A. and Cunnington, W.M., 1987: On CO_2 climate sensitivity and model dependence of results, *Quarterly Journal of the Royal Meteorological Society*, 113, 293-322.

Mitchell, J.F.B., Johns, T.C., Gregory, J.M. and Tett, S.F.B., 1995a: Climate response to increasing levels of greenhouse gases and sulphate aerosols, *Nature*, 376, 501-504.

Mitchell, J.F.B., Davis, R.A., Ingram, W.J. and Senior, C.A., 1995b: On surface temperature, greenhouse gases, and aerosols: Models and Observations, *Journal of Climate*, 8, 2364-2386.

Mo, K.C. and van Loon, K., 1984: Some aspects of the interannual variation of mean monthly sea level pressure in the Southern Hemisphere, *Journal of Geophysical Research*, 89, 9541-9546.

Mühlenbruch-Tegen, A., 1992: Long-term surface temperature variations in South Africa, *South African Journal of Science*, 88, 197-205.

Mullan, A.B., and Renwick, J.A., 1990: Climate change in the New Zealand region inferred from general circulation models, *New Zealand Meteorological Office Report*, 142pp.

Mullan, A.B. and McAvaney, B.J., 1995: Validation of high latitude tropospheric circulation in the Southern Hemisphere (Subproject 9), in *Proceedings of the First AMIP Scientific Conference*, WCRP-92, WMO/TD-No. 732, Geneva, 205-210.

Murphy, J.M., 1995: Transient response of the Hadley Centre coupled ocean-atmosphere model to increasing carbon dioxide. Part I: Control climate and flux adjustment, *Journal of Climate*, 8, 36-56.

Murphy, J.M. and Mitchell, J.F.B., 1995: Transient response of the Hadley Centre coupled ocean-atmosphere model to increasing carbon dioxide. Part II: Spatial and temporal tructure of response, *Journal of Climate*, 8, 57-80.

Murray, R.J. and Simmonds I., 1991: A numerical scheme for tracking cyclone centres from digital data. Part 2: application to January and July general circulation model simulations, *Australian Meteorological Magazine*, 39, 167-180.

Oreskes, N., Shrader-Frechette, N. and Belitz, K., 1994: Verification, validation and confirmation of numerical models in the Earth sciences, *Science*, 263, 641-646.

Overall, J.E. and Klett, C.J., 1972: *Applied Multivariate Analysis*, McGraw-Hill, New York.

Palmén, E., 1951: The aerology of extratropical disturbances, *Compendium of Meteorology*, American Meterological Society, 599-620.

Palmer, T.N., 1993: Extended-range atmospheric prediction and the Lorenz model, *Bulletin of the American Meteorological Society*, 74, 49-65.

Palmer, T.N. and Anderson, L.T., 1994: The prospects for seasonal foecasting, *Quarterly Journal of the Royal Meteorological Society*, 120, 755-793.

Palmer, T.N., Brankovic, C., Moletini, F., Tibaldi, S., Ferranti, L., Hollingsworth, A., Cubasch, U. and Klinker, E., 1990: The European Centre for Medium-Range Weather Forecasts (ECMWF) programme on extended-range forecasting, *Bulletin of the American Meteorological Society*, 71, 1317-1330.

Parrish, T.R., Bromwich, D.H. and Tzeng, R.-Y., 1994: On the role of the Antarctic continent in forcing large-scale circulations in the high southern latitudes, *Journal of the Atmospheric Sciences*, 51, 3566-3579.

Phillips, T.J., 1994: A Summary Documentation of the AMIP Models, *PCMDI Report No. 18*, PCMDI, LLNL, April 1994.

Physick, W.L., 1981: Winter depression tracks and climatological jet streams in the Southern Hemisphere during the FGGE year, *Quarterly Journal of the Royal Meteorological Society*, 107, 883-898.

Pollard, D. and Thomspon, S.L., 1995: The effect of doubling stomatal resistance in a global climate model, *Global Planetary Change*, 10, 1-4.

Portman, D.A., Wang, W.-C. and Karl, T.T., 1992: Comparison of general circulation model and observed regional climates: Daily and seasonal variability, *Journal of Climate*, 5, 343-353.

Preston-Whyte, R.A., Diab, R.D. and Tyson, P.D., 1977: Towards an inversion climatology of southern Africa. Part II: Non-surface inversions in the lower atmoshere, *South African Geographical Journal*, 59, 45-59.

Ramanathan, V., Cess, R.D., Harrison, E.F., Minnis, P., Barkstrom, B.R., Ahmad, E. and Hartman, D., 1989: Cloud-radiative forcing and climate: Results from the Earth Radiative Budget Experiment, *Science*, 243, 57-63.

Rayner, J.N., 1971: *An Introduction to Spectral Analysis*, Pion Limited, London.

Richman, M.B., 1986: Rotation of principal components, *Journal of Climatology*, 6, 293-335.

Richman, M.B. and Easterling, W.E., 1988: Procrustes Target Analysis: A multivariate tool for identification of climate fluctuations, *Journal of Geophysical Research*, 93, 10989-11003.

Roeckner, E., Rieland, M. and Keup, E., 1990: Modelling of clouds and radiation in the ECHAM model. *Proceedings of the ECMWF/WCRP Workshop on Clouds, Radiation, and the Hydrological Cycle*, ECMWF, Reading, UK, 199-222.

Ropelewski, C.F. and Halpert, M.S., 1986: North American precipitation and temperature patterns associated with the El Niño/Southern Oscillation (ENSO), *Monthly Weather Review*, 114, 2352-2362.

Santer, B.D., Taylor, K.E., Wigley, T.M.L., Penner, J.E., Jones, P.D. and Cubasch, U., 1995: Towards the detection and attribution of an anthropogenic effect on climate, *Climate Dynamics*, 12, 77-100.

Sausen, R., Barthel, K. and Hasselmann, K., 1988: Coupled ocean-atmosphere models with flux correction, *Climate Dynamics*, 2, 145-163.

Schönemann, P.H., 1966: A generalized solution of the orthogonal Procrustes problem, *Psychometrika*, 31, 1-10.

Schulze, B.R. 1984: Climate of South Africa: Part 8: General Survey, *WB28*, South African Weather Bureau, 5th edition, 330pp.

Senior, C.A. and Mitchell, J.F.B., 1993: CO_2 and climate: The impact of cloud parameterisation, *Journal of Climate*, 6, 393-418.

Shepard, D., 1968: A two-diimensional interpolation function for irregularly-spaced data, *Proceedings - 1968 ACM National Conference*, 517-524.

Shinoda, M. and Kawamura, R., 1996: Relationships between rainfall over semi-arid southern Africa, geopotential heights, and sea-surface temperatures, *Journal of the Meteorological Society of Japan*, 74, 21-36.

Sinclair, M.R., 1994: A climatology of cyclogenesis for the Southern Hemisphere, *Monthly Weather Review*, 123, 1601-1619.

Slingo, A., 1990: Sensitivity of the Earth's radiation budget to changes in low clouds, *Nature*, 343, 49-51.

Smith, R.N.B., 1990: A scheme for predicting layer clouds and their water content in a general circulation model, *Quarterly Journal of the Royal Meteorological Society*, 116, 435-460.

Stouffer, R.J., Manabe, S. and Bryan, K., 1989: Interhemispheric asymmetry in climate response to a gradual increase of atmospheric CO_2, *Nature*, 342, 660-662.

Swanson, G.R. and Trenberth, K.E., 1981: Interannual variability in the Southern Hemisphere troposphere, *Monthly Weather Review*, 109, 1890-1897.

Taljaard, J.J., 1972: Synoptic meteorology of the Southern Hemisphere, inNewton, C.W., (Ed.), *Meterology of the Southern Hemsiphere*, Meteorological Monographs, 35, American Meteorological Society, 139-213.

Taljaard, J.J., 1981: The anomalous climate and weather systems of January to March 1974, *South African Weather Bureau Technical Paper 9*, 92pp.

Taljaard, J.J., 1986: Contrasting atmospheric circulation during wet and dry summers in South Africa, *South African Weather Bureau Newsletter*, 445, 1-5.

Taljaard, J.J., van Loon, H., Crutcher, H.L. and Jenne, R.L., 1969: Climate of the upper air: Part I - Southern Hemisphere. Vol I Temperatures, dew points and heights at selected pressure levels, *NAVAIR 50-IC-55, Chief Naval Operations*, Washington, D.C., 135pp.

Taylor, K.E. and Penner, J.E., 1994: Response of the climate system to atmospheric aerosols and greehouse gases, *Nature*, 369, 734-737.

Tett, S., 1995: Simulation of El Niño-Southern Oscillation-like variability in a global AOGCM and its response to CO_2 increase, *Journal of Climate*, 8, 1473-1502.

Tett, S.F.B., Johns, T.C. and Mitchell, J.F.B., 1996: Global and regional variability in a coupled AOGCM, *Climate Dynamics*, in press.

Trenberth, K.E., 1979: Inter-annual variability of the 500 mb zonal flow in the southern hemisphere, *Monthly Weather Review*, 107, 1515-1524.

Trenberth, K.E., 1980: Planetary waves at 500 mb in the southern hemisphere, *Monthly Weather Review*, 108, 1378-1389.

Trenberth, K.E., 1981: Observed Southern Hemisphere eddy statistics at 500 hPa: Frequency and spatial dependence, *Journal of the Atmospheric Sciences*, 38, 2585-2605.

Trenberth, K.E., 1983: Interactions between orographically and thermally forced planetary waves, *Journal of the Atmospheric Sciences*, 40, 1126-1153.

Trenberth, K.E., 1991: Storm tracks in the Southern Hemisphere, *Journal of the Atmospheric Sciences*, 48, 2159-2178.

Trenberth, K.E. and Mo, K.C., 1985: Blocking in the Southern Hemisphere, *Monthly Weather Review*, 113, 3-21.

Triegaardt, D.O., Terblanche, D.E., van Heerden, J. and Laing, M.V. 1988: The Natal flood of 1987, *South African Weather Bureau Technical Paper Number 19*, Republic of South Africa, 62pp.

Tyson, P.D., 1981: Atmospheric circulation variations and the occurrence of extended wet and dry spells over southern Africa, *Journal of Climatology*, 1, 115-130.

Tyson, P.D., 1984: The atmospheric modulation of extended wet and dry spells over South Africa, 1958-1978, *Journal of Climatology*, 4, 621-635.

Tyson, P.D., 1986: *Climate Change and Variability in Southern Africa*, Oxford University Press, Cape Town, 220pp.

Tyson, P.D., 1990: Modelling climatic change in southern Africa: A review of available methods, *South African Journal of Science*, 86, 318-330.

Tyson, P.D., 1991: Climatic change in southern Africa: Past and present conditions and possible future scenarios, *Climatic Change*, 18, 241-258.

Tyson, P.D., 1993: Recent developments in the modelling of the future climate of southern Africa, *South African Journal of Science*, 89, 494-505.

Tyson, P.D., Garstang, M., Swap, R., Kållberg, P. and Edwards, M., 1996a: An air transport climatology for subtropical southern Africa, *International Journal of Climatology*, 16, 265-292.

Tyson, P.D., Garstang, M., Swap, R., Browell, E.V., Diab, R.D. and Thompson, A.M., 1996b: Transport and vertical structure of ozone and aerosol distributions over southern Africa, in Levine, J., (Ed.), *Biomass Burning and Global Change*, MIT Press, Cambridge, Mass., 403-421.

van Loon, H., 1967: The half-yearly oscillation in middle and high southern latitudes and the coreless winter, *Journal of the Atmospheric Sciences*, 24, 472-486.

van Loon, H., 1972: Pressure in the Southern Hemisphere, in Newton, C.W., (Ed.), *Meterology of the Southern Hemsiphere*, Meteorological Monographs, 35, American Meteorological Society 59-86.

van Loon, H., 1980: Transfer of sensible heat by transient eddies in the atmosphere of the southern hemisphere. An appraisal of the data before and during 1980, *Monthly Weather Review*, 108, 1774-1781.

van Loon, H. and Jenne, R.L., 1972: The zonal harmonic standing waves in the Southern Hemisphere, *Journal of Geophysical Research*, 77, 992-1003.

van Loon, H., Jenne, R.L., Taljaard, J.J. and Crutcher, H.L., 1968: An outline of the yearly and half-yearly components in the zonal mean temperature and wind between the surfac and 100 mb in the Southern Hemisphere, *Notos*, 17, 53-62.

van Loon, H., Kidson, J.W. and Mullan, A.B., 1993: Decadal variation of the annual cycle in the Australian dataset, *Journal of Climate*, 6, 1227-1231.

Vogel, C.H., 1994: (Mis)management of droughts in South Africa: past, present and future, *South African Journal of Science*, 90, 4-5.

Vines, R.G., 1980: Analyses of South African Rainfall, *South African Journal of Science*, 76, 404-409.

von Storch, H., Zorita, E. and Cubasch, U., 1993: Downscaling of global climate change estimates to regional scales: An application to Iberian rainfall in wintertime, *Journal of Climate*, 6, 1161-1171.

Vowinckel,E., 1955: Southern Hemisphere weather map analysis: Five year mean pressures, *Notos*, 4, 17-50.

Vowinckel, E., 1956: Ein Beitrag zur Witterungsklimatologie des suedlichen Mozambiquekanals. Miscelanea Geofisica Publicada Pelo Servico Meteorologico de Angola em Comemoracao do X Aniversario do Servico Meteorologico Nacional, Luanda, 68-86.

Wallace, J.M., 1983: The climatological mean stationary waves: Observational evidence, in Hoskins, B. and Pearce, R. (Eds.), *Large-Scale Dynamical Processes in the Atmosphere*, Academic Press, London, 55-94.

Washington, W.M. and Meehl, G.A., 1989: Climate sensitivity due to increased CO_2: Experiments with a coupled atmosphere and ocean general circulation model, *Climate Dynamics*, 4, 1-38.

Washington, W.M. and Meehl, G.A., 1991: Characteristics of coupled atmosphere-ocean CO_2 sensitivity experiments with different ocean formulations. In: Schlesinger, ME (Ed.) *Greenhouse-Gas-Induced Climatic Change: A Critical Appraisal of Simulations and Observations.* Elsevier, Amsterdam. 79-110.

Washington, W.M. and Meehl, G.A., 1996: High-latitude climate change in a global coupled ocean-atmosphere-sea ice model with increased atmospheric CO_2, *Journal of Geophysical Research*, 101, 12795-12801.

Watterson, I.G., Dix, M.R., Gordon, H.B. and McGregor, J.L., 1996: The CSIRO 9-level atmospheric general circulation model and its equilibrium present and doubled CO_2 climates, *Australian Meteorological Magazine*, 44, 111-125.

Wetherald, R.T. and Manabe, S., 1988: Cloud feedback processes in a general circulation model, *Journal of the Atmospheric Sciences*, 45, 1397-1415.

Wetherald, R.T., Ramaswamy, V. and Manabe, S., 1991: A comparative study of the observations of high clouds and simulations by an atmospheric general circulation model, *Climate Dynamics*, 5, 135-143.

Whetton, P.H. and Pittock, A.B., 1991: Australian region intercomparison of the results of some general circulation models used in enhanced greenhouse experiments, *CSIRO DAR Technical Paper No. 21*, Mordialloc, 73pp.

Whetton, P.H., Fowler, A.M., Haylock, M.R. and Pittock, A.B., 1993: Implications of climate change due to the enhanced greenhouse effect on floods and droughts in Australia, *Climatic Change*, 25, 289-318.

Whetton, P.H., Rayner, P.J., Pittock, A.B. and Haylock, M.R., 1994: An assessment of possible climate change in the Australian region based on an intercomparison of general circulation modelling results, *Journal of Climate*, 7, 441-463.

Whetton, P.H., Pittock, A.B., Labraga, J.C., Mullan, A.B. and Joubert, A., 1996a: Southern Hemisphere Climate: Comparing Models with Reality, in Henderson-Sellers, A. and Giambelluca, T.W. (Eds.), *Climate Change. Developing Southern Hemisphere Perspectives*, John Wiley & Sons, Chichester, 89-130.

Whetton, P.H., England, M., O'Farrell, S., Watterson, I. and Pittock, A.B., 1996b: Global comparison of the regional rainfall results of enhanced greenhouse coupled and mixed-layer ocean experiments: Implications for climate change scenario development. *Climatic Change*, 33, 497-519.

Wigley, T.M.L. and Raper, S.C.B., 1990: Natural variability of the climate system and detection of the greenhouse effect, *Nature*, 344, 324-327.

Wigley, T.M.L., Jones, P.D., Briffa, K.R. and Smith, G., 1990: Obtaining sub-gridscale information from coarse-resolution general circulation model output, *Journal of Geophysical Research*, 95, 1943-1953.

Willmott, C.J., Rowe, C.M. and Philpot, W.D., 1985: Small-scale climate maps: A sensitivity analysis of some common assumptions associated with grid-point interpolating and contouring, *The American Cartographer*, 12, 5-16.

Wilson, C.A. and Mitchell, J.F.B., 1987: A doubled CO_2 climate sensitivity experiment with a global climate model including a simple ocean, *Journal of Geophysical Research*, 92, 13315-13343.

WMO, 1988: *Modelling the Sensitivity and Variations of the Ocean-Atmosphere System (Report of Workshop)*, WMO/TD No. 254, World Meteorological Society, Geneva, 289pp.

Xu, J.-S., von Storch, H. and van Loon, H., 1990: The performance of four spectral GCMs in the southern hemisphere: The January and July climatology and the semiannual wave, *Journal of Climate*, 3, 53-70.

Yang, S. and Gutowski, W.J. Jr., 1994: GCM simulations of the three-dimensional propagation of stationary waves, *Journal of Climate*, 7, 414-433.

Zwiers, F.W., 1995: Inter-annual variability in an ensemble of AMIP climate simulations conducted with the CCC GCM2, *Proceedings of the First International AMIP Scientific Conference*, WCRP-92, WMO/TD-732, 239-244.